Comparison of design methods for quay walls

Based on measured deformations in Eemshaven Groningen

Master's Thesis

A.A. (Arnoud) Theunisse

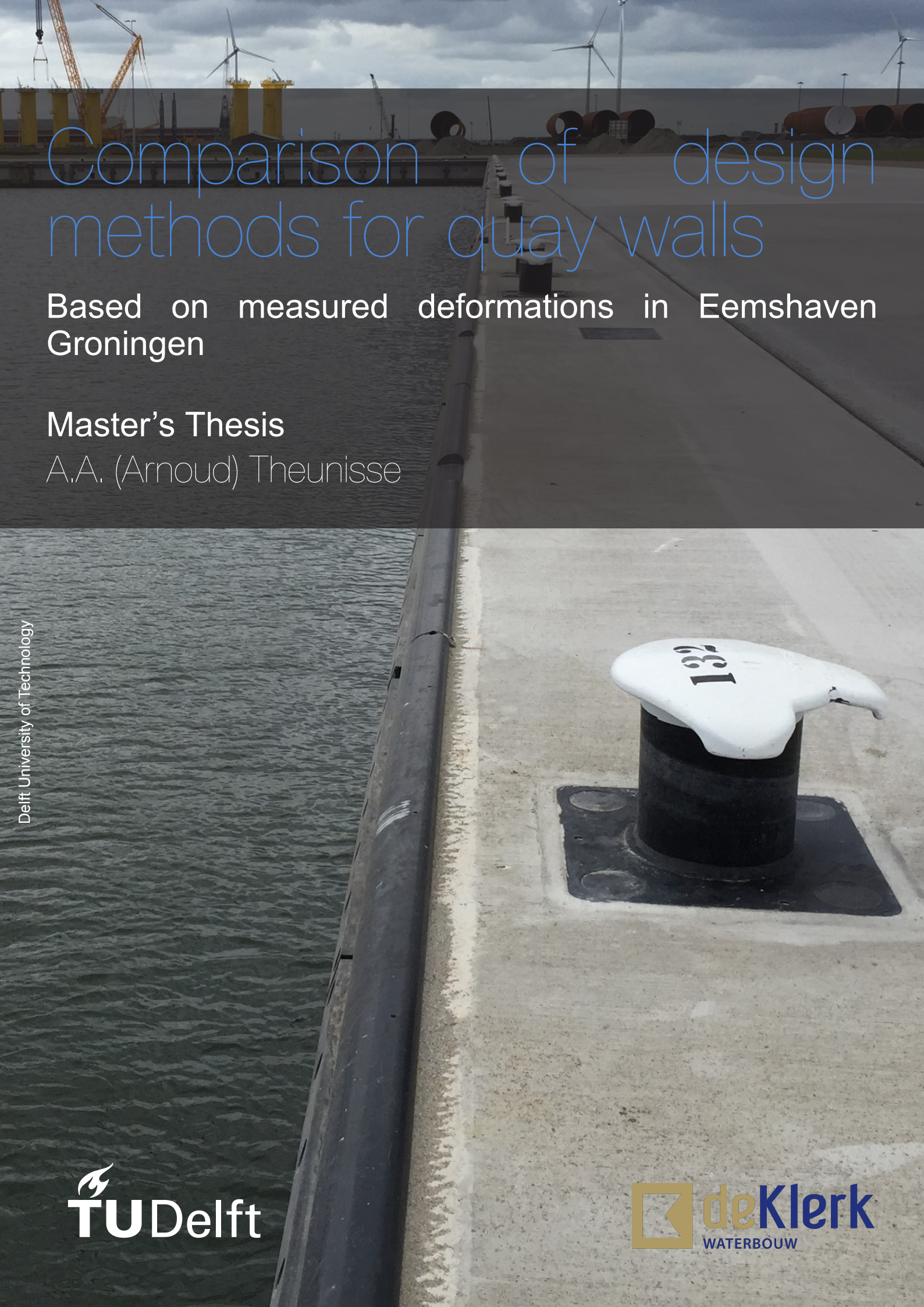

Delft University of Technology

TU Delft

deKlerk WATERBOUW

Comparison of design methods for quay walls

Based on measured deformations in Eemshaven Groningen

by

A.A. (Arnoud) Theunisse

to obtain the degree of Master of Science
at the Delft University of Technology,
to be defended publicly on Wednesday April 5, 2023 at 3:00 PM.

Student number: 4700422
Project duration: December 14, 2021 – April 5, 2023

Chairman:	Dr. ing. M. Z. Voorendt,	TU Delft, Hydraulic Engineering
Thesis committee:	Dr. ir. J.G. de Gijt,	TU Delft, Hydraulic Engineering
	Dr. ir. M. Korff	TU Delft, Geoscience & Engineering
	Ing. A. J. Tanis,	De Klerk BV
	Prof. dr. ir. R.D.J.M. Steenbergen	TNO

TU Delft

deKlerk WATERBOUW

Preface

This report describes my thesis to obtain the Master degree of science in Hydraulic Engineering at the TU Delft. This research was performed at the De Klerk BV, located in Werkendam.

I would like to express my gratitude to the graduation committee for their useful feedback, encouragement and guidance during this research. Dr. ing. M.Z. Voorendt for the valuable and extensive feedback on the report every time and for being the chairman of this committee. Dr. ir. J.G. de Gijt for proposing this subject and for the encouragement during the project. Also thanks to prof. dr. ir. R.D.J.M. Steenbergen and dr. ir. M. Korff for their valuable feedback during the meetings. Especially, I would like to thank my supervisor at De Klerk, Hans Tanis, who was involved as a designer during the construction of this quay wall. One question often led, due to his experience and excellent memory about the project, to a load of valuable suggestions that I could continue with when things were unclear or when I was out of options.

After doing an interesting internship at De Klerk, I got the opportunity to perform the thesis at this company as well, for which I am very grateful. Also special thanks to my colleagues for keeping me company and for providing a pleasant and enjoyable working environment.

Finally, I would like to thank my family and friends for their support in multiple ways not only during this research but during my entire study at TU Delft. Also many thanks to Rien Boer for reviewing my report in detail at the end of the process.

A.A. (Arnoud) Theunisse
Delft, March 2023

Summary

Over the years, the complexity and dimension of quay walls increased due to an increase in vessel dimensions and freight load. Different methods are available to design these quay walls which differ in applicability and conservativity. The aim of this research is to investigate which design method results in the best approximation of the deformations of a quay wall consisting of an anchored combined wall with relieving platform, looking at the elastoplastic method and the finite element method. The elastoplastic method is performed with the program D-Sheet Piling and the program Plaxis is used as a finite element method. Measurements on a quay wall in Eemshaven Groningen are used to analyse which design method results in the best approximation of the real deformation. This quay wall was constructed in 2014-2015 by contractor De Klerk and deformation measurements have been done during and after construction.

First, the input parameters for Plaxis and D-Sheet are determined for this wall. The soil parameters are based on available CPTs where the mean values are determined by averaging the low and high characteristic values in NEN-EN1997 and CUR166, with the assumption that these mean values are a good estimate of the real values. Other input parameters such as properties of the structural elements are based on the available design reports.

From the available measurements, only the inclinometer results of the three tubular piles TP38, TP68 and TP78 appeared to be useful, where TP38 is situated in the middle of the wall length and TP68 and TP78 are situated at the end of the quay wall near the shore. Inclinometer measurements were done in 2014 and 2015 (during construction) and repeated in 2022. The relative measured deformation between 2022 and 2014 is compared to the relative calculated deformation between 2022 and 2014 in the following steps.
The D-Sheet model, after some adaptations in the calibration, gives a relative good approximation of the deformations of TP38 with a deviation of the maximum deformation at NAP -10.70 m of 1.3%. A large part of the curve is within the range of the measurement error. This is not the case for TP68 and TP78 where the deviation of the maximum displacement at NAP -9.50 m is still 10 to 34%. For all three piles, the top displacement is strongly deviating from the measured one. This deviation is for all three 100 to 113%, see the results in Figure 1. The main cause of this large deviation in top displacement is probably that the relieving platform can not be modelled properly in D-Sheet. The platform works as a support that prevents or resists movement to the land and does not prevent movement to the harbour basin. This can not be modelled in D-Sheet.

The calculation with Plaxis is done with the same input as D-Sheet in the last calibration step. This results in a good approximation of the deformation with a deviation from the measurement of only several mm. The largest deviation appears at the toe where Plaxis calculates a smaller rotation than measured. The calculated deformations of the calibrated models in D-Sheet and Plaxis are plotted in Figure 1 together with the inclinometer measurements.

Comparing the results of both methods shows a large difference in top deformation. D-Sheet calculates approximately 0 mm top displacement, while Plaxis results in a top displacement of 30 mm, see Figure 1. Two possible explanations for this large difference are investigated. The first explanation is that the modelling limitations of D-Sheet lead to different results. A simplified Plaxis model simulating these limitations has resulted in a top displacement of 17 mm. Secondly, the difference in the input of the soil stiffness between both models is investigated by linking both stiffness parameters E and k_h to each other using the relation of Ménard. A D-Sheet model with adjusted values for k_h results in only a small change in the top deformation. The remaining differences in results are attributed to the difference in calculation method.

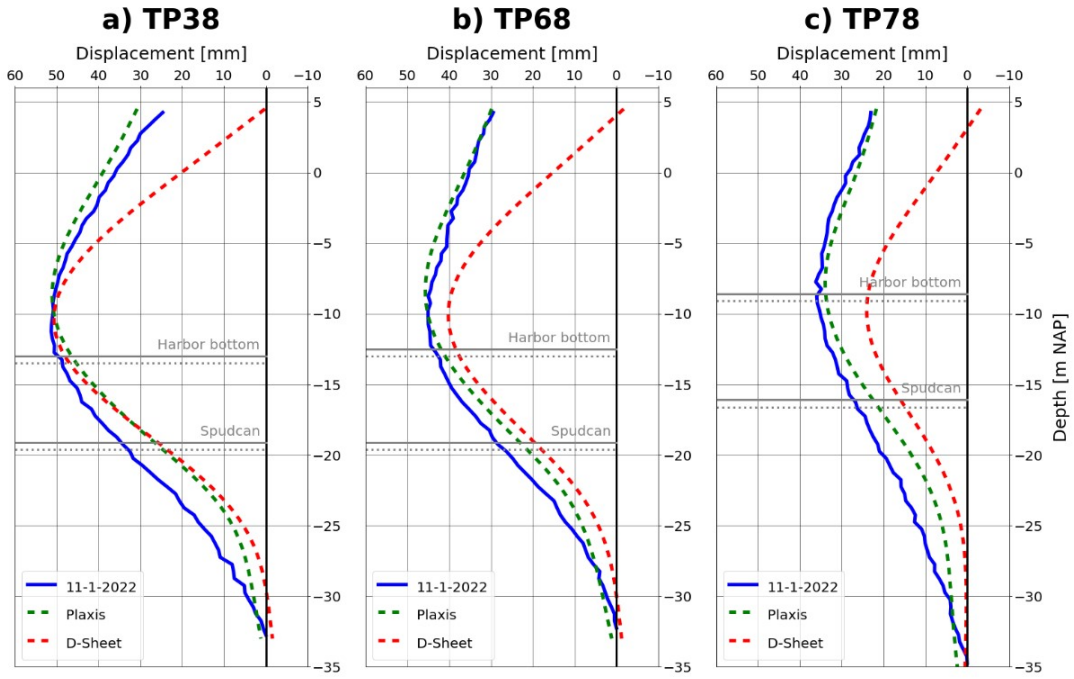

Figure 1: Calculated deformations from D-Sheet and Plaxis with the inclinometer measurements of 2022

Several variations are performed in a sensitivity analysis to investigate to which extent different input parameters would have led to different results. The following variations are made:

1. Variation in phasing: Excluding intermediate phases between the construction and the stage of the measurement of 2022 results in smaller deformations. Exchanging the two intermediate stages *Spudcan (7)* and *Lowest water level (8)* however results in an increase of 20% of the maximum displacement.
2. Variation in modelling piles: Replacing the embedded beams with fixed-end piles or node-to-node piles results in an increase of the maximum wall displacement of respectively 25% and 50%.
3. Variation of soil model: The use of the Linear Elastic soil model results in a decrease of the displacement by 28%. The use of Hardening Soil and Mohr-Coulomb model increases the maximum displacement by respectively 125% and 140%.
4. Variation of surcharge load: Halving the load Q on the platform decreases the displacement by 8% and halving the load q behind the platform decreases it by only 2%.
5. Variation of sea water level (tide): Including a tidal water level variation in the final calculation stage results in only a change of 0.5 mm in the max wall displacement.
6. Variation of soil parameters: Calculating the deformations with low characteristic strength and stiffness parameters results in a maximum deformation that is 209% and 127% of the measurement for Plaxis and D-Sheet respectively. Applying high characteristic values for strength and stiffness results in a maximum deformation of 78% of the measurement for both Plaxis and D-Sheet.

Based on the results in this case study, it is concluded that Plaxis results in a better approximation of the measured deformation than D-Sheet. Considering the three cross-sections, the calculated deformation at the top deviates by up to 114% from the measurement in D-Sheet and 25% in Plaxis. For the maximum field deformation, D-Sheet deviates by up to 34%, while this is 6% for the results from Plaxis. The Finite Element Method Plaxis thus results in a better approximation than the elastoplastic method D-Sheet, especially for calculating deformations at the top.

Contents

Preface i

Summary ii

1 Introduction 1
- 1.1 Motivation . . . 1
- 1.2 Problem analysis . . . 2
  - 1.2.1 Types of quay walls . . . 2
  - 1.2.2 Classical design methods . . . 3
  - 1.2.3 Elastoplastic model . . . 4
  - 1.2.4 Finite element methods . . . 5
  - 1.2.5 Comparison of FEM and Elastoplastic method . . . 6
  - 1.2.6 Research on design methods . . . 7
  - 1.2.7 Problem statement . . . 8
- 1.3 Objective . . . 8
- 1.4 Scope . . . 8
- 1.5 Research questions . . . 9
- 1.6 Methodology and report layout . . . 9

2 Case description 10
- 2.1 Project overview . . . 10
- 2.2 Construction stages . . . 12
- 2.3 Soil characteristics . . . 16
- 2.4 Water levels . . . 16
- 2.5 Structural elements . . . 16
  - 2.5.1 Combined sheet pile wall . . . 16
  - 2.5.2 Anchor . . . 17
  - 2.5.3 Relieving platform . . . 19
- 2.6 Loads . . . 19
  - 2.6.1 Permanent loads . . . 19
  - 2.6.2 Terrain loads . . . 20
  - 2.6.3 Loads of ships . . . 20
  - 2.6.4 Drainage system . . . 20
  - 2.6.5 Jack-up barges . . . 21
  - 2.6.6 Soil- and top load . . . 21

3 Measurements 23
- 3.1 Inclinometer measurement set-up . . . 23
  - 3.1.1 Location of the inclinometers . . . 23
  - 3.1.2 Usability . . . 24
  - 3.1.3 Accuracy . . . 24
- 3.2 Top displacement in X and Z direction . . . 25
  - 3.2.1 Availability of data . . . 25
  - 3.2.2 Combining top displacement with inclinometer data . . . 27
- 3.3 Conclusion . . . 28

4 Calculation of quay wall deformation in D-Sheet 29
- 4.1 Modelled stages . . . 29
- 4.2 Challenges . . . 30
  - 4.2.1 Modelling the stiffness of the grout anchor . . . 30
  - 4.2.2 Modelling the relieving platform . . . 30

4.3 Results . . . 31
4.4 Model calibration . . . 32
4.4.1 Influence of strain condition on strength parameter φ . . . 32
4.4.2 Lowering the modulus of subgrade reaction k_h . . . 34
4.4.3 Combining loads on bollards and spudcans . . . 35
4.4.4 Summary of adaptations . . . 36
4.5 Causes of difference between calculation and measurements . . . 37
4.5.1 Addition of the anchor test stage . . . 37
4.5.2 Effect of pile driving on soil characteristic . . . 39
4.5.3 Using apparent tendon free length L_{app} . . . 39
4.5.4 Slipping of anchor . . . 40
4.5.5 Construction of RoRo jetty . . . 41
4.5.6 Modelling relieving platform in DSheet . . . 41
4.5.7 Uncertainty in measurements . . . 41
4.6 Conclusion . . . 42

5 Calculation of quay wall deformation in Plaxis 43
5.1 Soil model selection for FEM . . . 43
5.1.1 Available soil models . . . 43
5.1.2 Applicability of the soil models . . . 44
5.1.3 Selection of soil model . . . 44
5.2 Model input . . . 45
5.2.1 Relieving platform . . . 45
5.2.2 Additional soil parameters . . . 46
5.3 Results . . . 47
5.4 Model calibration . . . 49
5.4.1 Adaptation of connection piles-platform . . . 49
5.4.2 Adaptation of connection platform-wall . . . 50
5.5 Conclusion . . . 52

6 Comparing results of calculation methods 53
6.1 Comparing calculated deformations . . . 53
6.2 Explanations for difference in results . . . 54
6.2.1 Limitations in D-Sheet Piling . . . 54
6.2.2 Difference in input soil stiffness . . . 55
6.3 Conclusion . . . 59

7 Sensitivity analysis of the Finite Element Method 60
7.1 Variation in phasing . . . 60
7.2 Variation in modelling bearing piles . . . 61
7.3 Variation of soil model . . . 64
7.3.1 Sensitivity analysis on small strain parameters . . . 65
7.4 Variation of surcharge loads . . . 66
7.4.1 Surcharge load Q on platform . . . 67
7.4.2 Surcharge load q behind the platform . . . 68
7.5 Variation of soil parameters . . . 69
7.6 Variation of water level (tidal variation) . . . 70
7.7 Conclusion . . . 70

8 Discussion 72
8.1 Use of 2D or 3D model . . . 72
8.2 Model input . . . 73
8.2.1 Soil model selection . . . 73
8.2.2 Determination of plain strain φ . . . 73
8.2.3 Determination of soil parameters . . . 73
8.3 Accuracy of calculation results and measurements . . . 75
8.4 Applicability to other quay walls . . . 75
8.5 Results compared to earlier design calculations . . . 76

9 Conclusions and recommendations **77**
9.1 Conclusions . . . 77
9.1.1 Answering sub-questions . . . 77
9.1.2 Answering the main research question . . . 79
9.2 Recommendations . . . 80
9.2.1 Recommendations related to measurements . . . 80
9.2.2 Recommendations related to modelling . . . 80
9.2.3 Recommendation for further research . . . 80

References **83**

A Drawings **84**
A.1 Cross section . . . 84
A.2 Overview . . . 84

B Deformation measurements **87**
B.1 XZ-top deformations . . . 87
B.2 Inclinometer . . . 95

C Soil characteristics **98**
C.1 Selection of CPT's . . . 98
C.2 Determination of soil parameters . . . 100
C.2.1 Modulus of subgrade reaction . . . 106
C.3 CPT's before and after driving of the piles . . . 107
C.4 Additional soil parameters for FEM . . . 110

D Combined wall properties **111**

E Anchors **113**
E.1 Anchor tests . . . 113
E.2 Calculation of anchor stiffness . . . 114

F Results of D-Sheet and Plaxis **117**
F.1 Deformation results D-Sheet Piling . . . 117
F.1.1 Version 1 . . . 117
F.1.2 Version 2 . . . 118
F.1.3 Version 3 . . . 118
F.1.4 Version 4 . . . 119
F.2 Deformation results Plaxis . . . 119
F.3 Bending moment, shear force and displacement in final stage . . . 120
F.3.1 TP38 . . . 120
F.3.2 TP68 . . . 120
F.3.3 TP78 . . . 121

G Results of sensitivity analysis **122**
G.0.1 Variation in phasing . . . 123
G.0.2 Variation in modelling bearing piles . . . 124
G.0.3 Variation of soil model . . . 125
G.0.4 Variation of surcharge loads . . . 126

1 Introduction

1.1. Motivation

Quay walls form important structures in ports. From the earliest days, quay walls are used to provide berthing places for seagoing and inland vessels. The main functions of a quay wall are (CUR211, 2014):

- Provide berthing facilities for the vessels.
- To provide bearing capacity to carry loads, freight storage facilities and cranes.
- To retain soil behind the quay wall.
- To serve as water retaining structures in case of high water level in the harbour.

These four functions are important during the design phase. Especially the requirements for the first two are subject to change, caused by increasing ship sizes, as shown in Figure 1.1. This directly leads to different requirements for the first function, but larger ships carry more load, which changes the demands for the bearing capacity fo the quay wall.

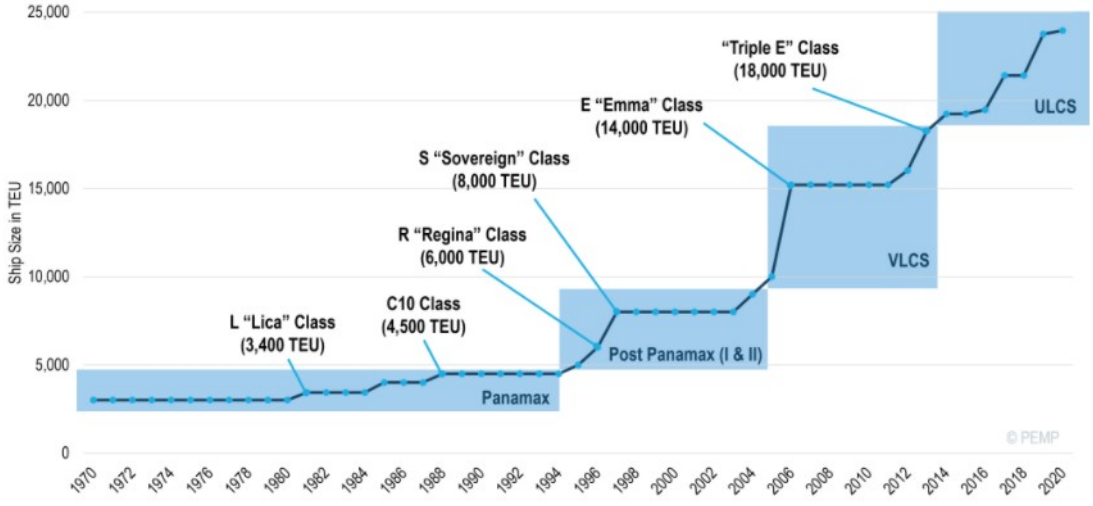

Figure 1.1: Increase of ships cargo capacity over time (Notteboom et al., 2022)

Bigger and heavier cranes are needed to load and unload the ships and the storage of the freight load on the quay wall is increasing. Besides that, the bollard forces on the quay walls become larger. Throughout the years more complex quay wall structures have been designed to be able to resist these loads. For this design, several methods are used, with different degrees of applicability and

conservatism. Applying a design method in the wrong way can result in unsafe designs. It is therefore important to evaluate and compare the different design methods available to design such quay walls. This research will provide a comparison of the most commonly used design methods.

1.2. Problem analysis

During the 20th century, several design methods were developed to calculate the required depth and cross-section of the retaining sheet pile wall. Before the commercial use of computers, the methods used were only classical methods which could be performed by hand. After 1990, computer models became available such as the finite element methods and the elastoplastic models.

1.2.1. Types of quay walls

The applied construction methods applied in the Netherlands can be subdivided into four main types (CUR211, 2014):

- Gravity walls: This type of wall obtains its stability by the self-weight of the structure and the weight of the soil when this is situated on top of the structure, see Figure 1.2a.
- Sheet pile walls: It obtains its retaining function from the soil pressure in front of the wall in combination with the anchoring system in case of an anchored quay wall. In case of a clamped wall, the passive soil under the rotation point at the back of the wall will also contribute to the retaining function, see Figure 1.2b.
- Structures with relieving platforms: This is a sheet pile wall with a relieving platform to reduce the horizontal loads on the retaining wall from the surcharge load, see Figure 1.2c.
- Open berth quays: This type of quay wall has no function of retaining soil or water. The load-bearing structure is provided by a deck that is constructed on piles extended over a slope, see Figure 1.2d.

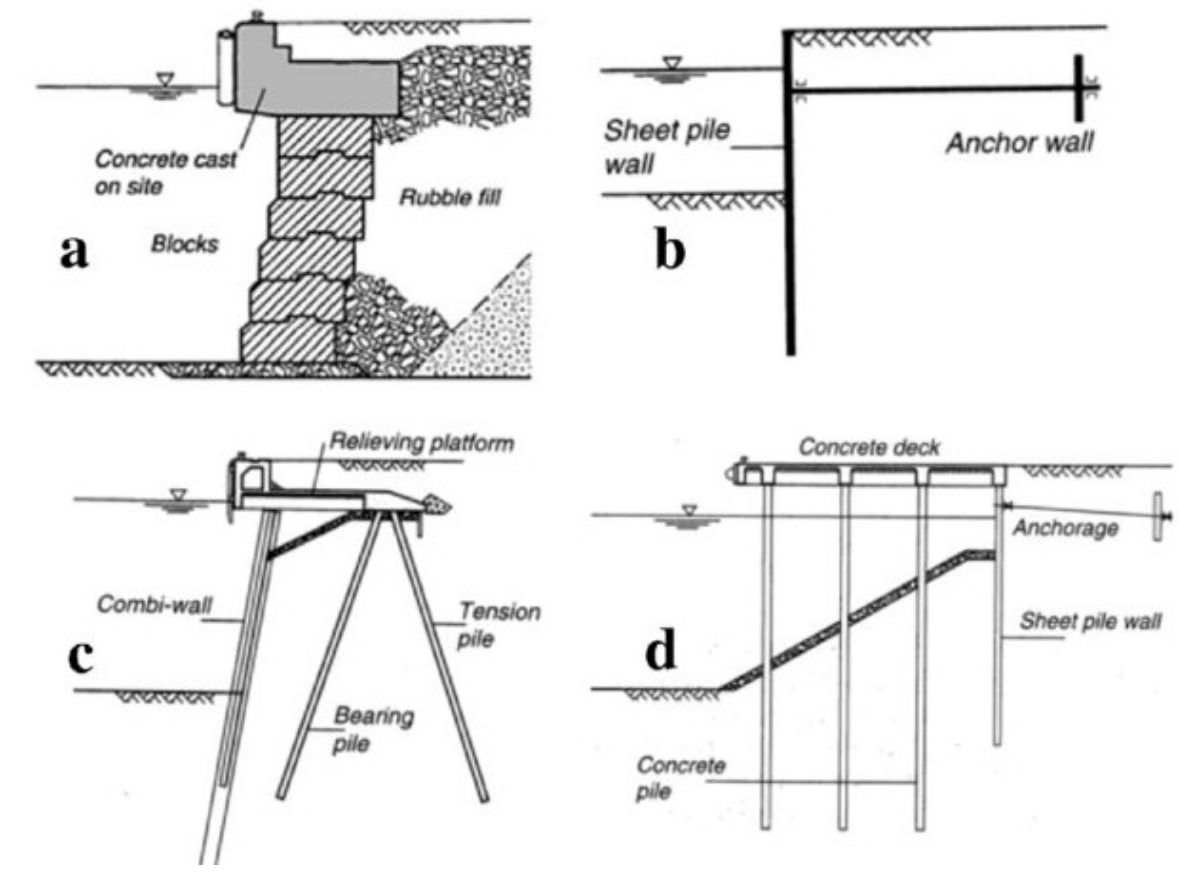

Figure 1.2: Different type of quay walls (Nguyen et al., 2021)

1.2.2. Classical design methods

Classical calculation methods are based on the assumption that the soil resistance is fully developed where the retaining wall is deforming, either active or passive. The loading on the sheet pile wall is thus dependent on the assumed deformed shape. The deformation behaviour is highly dependent on the type of support condition at the base of the wall. A difference is made between a simply supported wall and a fully fixed wall, see Figure 1.3 (Sheet Piling Handbook, 2008). Sometimes this is called a free earth support and fixed earth support (ARBED, 1991).

Different schematisations

Figure 1.3 shows four different schematizations of an anchored sheet pile with increasing depth. The first schematization (Figure 1.3a) shows the minimum depth needed to gain horizontal equilibrium. The toe is able to displace with an amount Δ and rotate with an angle α. This free earth support is the concept of the American method. For increasing depth, the passive earth pressure develops further, the displacement Δ becomes zero, and the rotation angle finally becomes zero, see Figure 1.3d. This last schematization is the concept for the European method and is called the fixed support (TU Delft Manual Hydraulic Structures, 2020). The schematization in between is called the partially fixed support where the rotation angle is not equal to zero yet, but the displacement of the toe is zero.

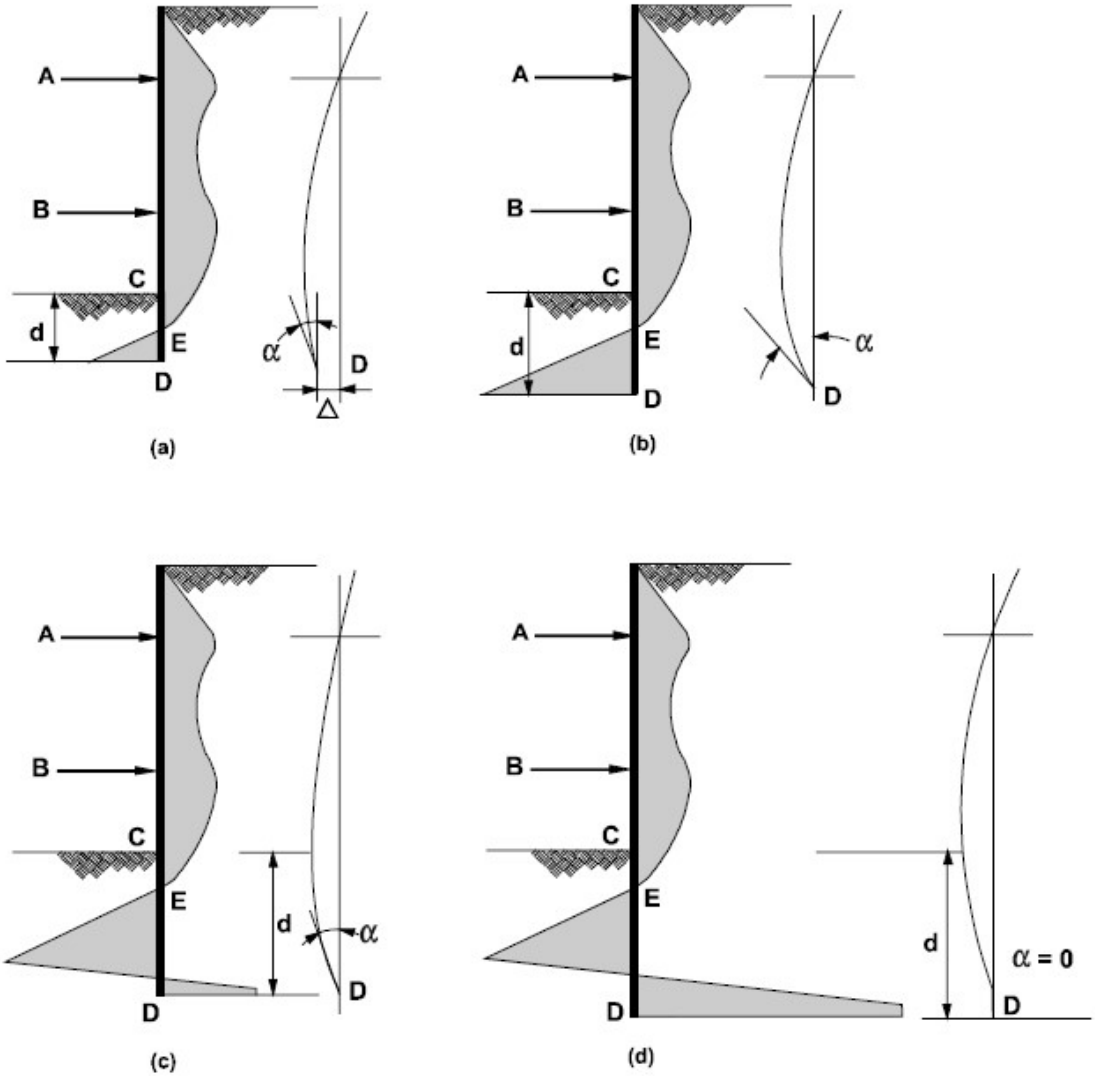

Figure 1.3: Wall deformation and stress distribution with different support conditions (FHWA, 1999)

In general, for the fixed earth support or fully fixed wall, a larger embedded depth is needed while the internal forces and the deformations are lower than for the simply supported wall or wall with free earth support. Hermann Blum (1931) simplified the schematization of the fully fixed wall and developed a graphical method as well as an analytical method to calculate the embedded depth and the internal forces with the deformations. This method is mostly used in Europe and is therefore sometimes called the European method. The free earth support is mostly used in America, Brazil, and the United Kingdom and is therefore called the American method (Clayton et al., n.d.).

Fully fixed wall: European
In Europe, one of the most used design methods is the approach according to Blum. Up to 1990, all quay walls have been designed according to this approach. This classical method can relatively easy be performed by hand. Dr. Blum simplified the real soil pressure below the base of excavation by a triangular passive earth pressure diagram, see Figure 1.4b where the solid line represents the real soil pressure and the dashed line the simplified triangular distribution. The added triangular soil pressure on the right above the rotation point is now replaced by an equivalent force C acting at the rotation point, see Figure 1.3 c.

The theoretical depth is the depth until this rotation point. In case of a cantilever wall, this depth is found by taking the moment equilibrium around the rotation point and the equivalent force C is found by the horizontal equilibrium. In case of an anchored wall, an extra equation is needed to calculate the anchor force. In that case, one should use the condition that the displacement at the anchor is equal to zero. To ensure that the passive earth pressure below the rotation point is developed, the theoretical embedded depth should be multiplied by a factor ranging from 1.05 to 1.30, depending among others on the retaining height (Blum, 1931).

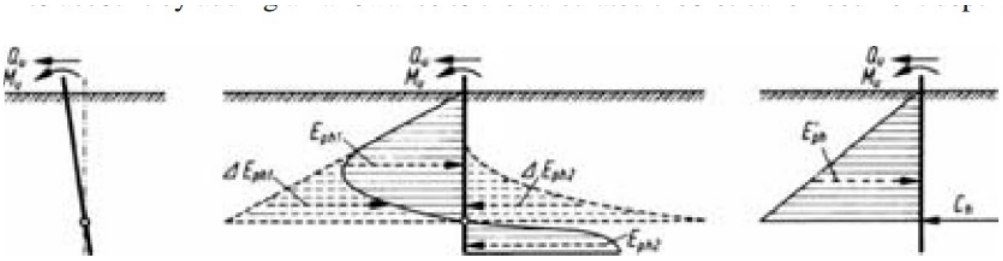

Figure 1.4: Simplification according to Blum. (Weissenbach, 2001)

Simply supported: American
This method uses the schematization of the free earth support. This results in the minimum embedded depth possible at which failure of the sheet pile wall due to horizontal movement of the base is prevented. It is assumed that the sheet pile is infinitely stiff and that the wall is rotating around its anchor point when it fails (Clayton et al., n.d.). The embedded depth is found by taking the moment equilibrium around the anchor point. By means of safety, some of the manuals state that the calculated theoretical depth from moment equilibrium should be multiplied by 20% (ARBED, 1991).

The assumption that the wall is rotating about its anchor point implies that this method only can be used for anchored walls, which is one of the disadvantages of this method. Another disadvantage is that there is no redistribution capacity during extreme load situation, which is however the case in the anchored fully fixed support. As stated before, also the bending moments with the American method are higher than that of the European method. On the other hand, the free earth support results in a very economical design and a minimum depth can be desired when there are high driving risks (Quay Walls, 2014).

1.2.3. Elastoplastic model
The elastoplastic method is one of the computer models that can be used. This method is based on the relation between displacements and the soil pressures acting on the retaining wall by the modulus of

subgrade reaction. The sheet pile is modelled as a beam on multiple elastic supports, see Figure 1.5. The behaviour of these springs is prescribed by the spring characterstics with an elastic and plastic regime. In the calculation procedure, the program gives the wall an initial displacement. Because of the stiffness, the wall bounces back. Iterations are made until the wall displacement corresponds with the calculated earth pressures (Visschedijk, 2005). This results in a better approximation of the soil displacements than the classical methods, because the soil is not assumed fully plastic but can behave partially elastic. The disadvantage with respect to the earlier mentioned classical method is that more soil parameters should be known. Another disadvantage that also holds for the classical methods is that the springs are uncoupled, which means that the arching effect in non-cohesive soils is not taken into account resulting in a larger bending moment (Quay Walls, 2014). D-Sheet Piling is a well-known computer program in the Netherlands that is using this method.

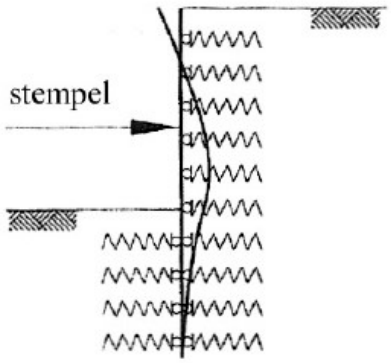

Figure 1.5: Elastoplastic model (Vanhoutte and Verstrynge, 2007)

1.2.4. Finite element methods

First, the main principle of finite element methods will be explained, after which several existing methods will be mentioned.

Main principle of finite element methods

A finite element method (FEM) is a method where the stresses and deformations in the soil and the structural elements can be calculated. The equilibrium of stresses and deformations of the soil and the bending behaviour of the structural elements are described by a coupled system of partial and ordinary differential equations. This system is solved numerically using a FEM resulting in the deformed shape of the structure where there is equilibrium (CUR166, 2012).

The soil is divided into small pieces, the finite elements. Each element has several nodes which connect the elements with each other. The mutual displacement of the nodes in one element then determines the stress state in the elements. The sheet pile wall is divided into several line elements with several nodes. The interface elements connect the soil elements with the structural line elements and are able to model the sliding behaviour between the wall and the soil.

Coupling the equations of all the elements results in a system of algebraic equations with the node displacements as unknowns. The solution thus defines the displacement of the nodes and thereby determines the deformed shape, see Figure 1.6. From the displacement, the soil stresses and internal forces in the structural elements can be derived. The FEM can be used to solve both two-dimensional and three-dimensional problems .

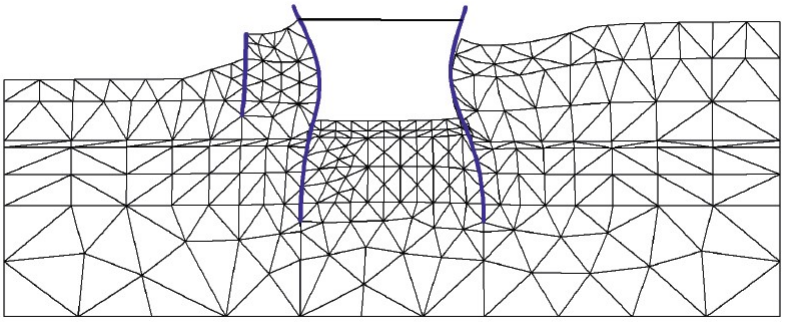

Figure 1.6: Deformed elements in FEM (CUR166, 2012)

The reliability of the outcome of a FEM calculation depends on the way the relationship between stresses and deformations is described. For the construction elements, such as the sheet pile wall and the anchor elastic models are used. For the sheet pile wall, this relation is described with the bending equation and for the anchor, this is described with the force-elongation relation. For the soil elements, these elastic relations are however not sufficient and this is where partial differential equations are needed.

There are several FEM's that model the construction elements properly, but only a few that also can model the soil accordingly.

PLAXIS
PLAXIS is designed especially for the analysis of soil and rock deformation and stability, as well as soil-structure interaction, groundwater, and heat flow (Bentley Advancing Infrastructure, 2021). This has been the FEM that is used most often for geotechnical problems. There are several soil models available in PLAXIS varying in degrees of accuracy.

DIANA
DIANA is a FEM that is used for many kinds of structures and focuses more on structural aspects. DIANA however also has a geotechnical model so it can also be used to solve geotechnical problems such as quay walls (DIANA FEA, n.d.). DIANA has about twenty models available to describe the behaviour of soils and rocks, which is more than PLAXIS (DIANA, 2021). Not all of these models will be elaborated on in detail here because most of these models are the same as the earlier mentioned models in PLAXIS.

1.2.5. Comparison of FEM and Elastoplastic method

It was mentioned in Section 1.2.3 that the main disadvantage of the elastoplastic model with respect to the classical model was that more soil input parameters are needed for the elastoplastic model. This applies in general for all computer models, especially for FEM. In this section, the two explained computer models are compared.

The schematization used in the spring-supported beam design model or elastoplastic model is relatively simple and only takes into account the soil-structure interaction of the front wall. The soil is modelled by horizontal uncoupled springs, which means that relieving platforms and inclined walls are difficult to model correctly. With a finite element model, stresses and deformations of both soil and all structural elements and their interaction can be calculated in a fundamental way. Another advantage of FEM is that it does not require a prescription of a failure plane, whereas a prescription of a curved or straigh failure plane is required in the elastoplastic model. Besides that, with FEM it is possible to predict the soil settlement behind the wall. With the different soil models available in FEM it is also possible to model undrained behaviour, which can be useful when considering different construction phases. With the spring-supported beam model, this modelling of undrained behaviour is generally not included.

The elastoplastic model such as used in D-Sheet Piling is however user-friendly and not time-consuming. In finite element modelling a lot of steps have been taken to increase user-friendliness. However, both building and calculating the model is still rather complicated and time-consuming . Due to its fast calculation and simple use, the elastoplastic method is very easy to adjust in different design steps. Another advantage is that the spring-supported beam model incorporates the full safety approach.

Based on these considerations, the CUR211(2014) recommends using the spring-supported beam model for relatively simple quay wall structures or for complex structures in a draft design only. More complex quay walls with relieving platforms, inclined walls or combined walls where the arching effect plays a role, can modelled more accurate in FEM.

1.2.6. Research on design methods

Various thesis studies have been done comparing several design methods for different types of quay walls. In the previous century, Vorm (1993) already compared the method of Blum with the then available program TILLY for mooring dolphins. Tilly is one of the first finite element models where the dolphin is modelled as a bending beam divided into finite elements. The soil is modelled with three parallel elastoplastic springs and a viscous damper, see Figure 1.7a. The three springs are approximating the p-y curve for the soil layer that is modelled, see Figure 1.7b. Finite element models such as Diana and Plaxis were not available at that time.

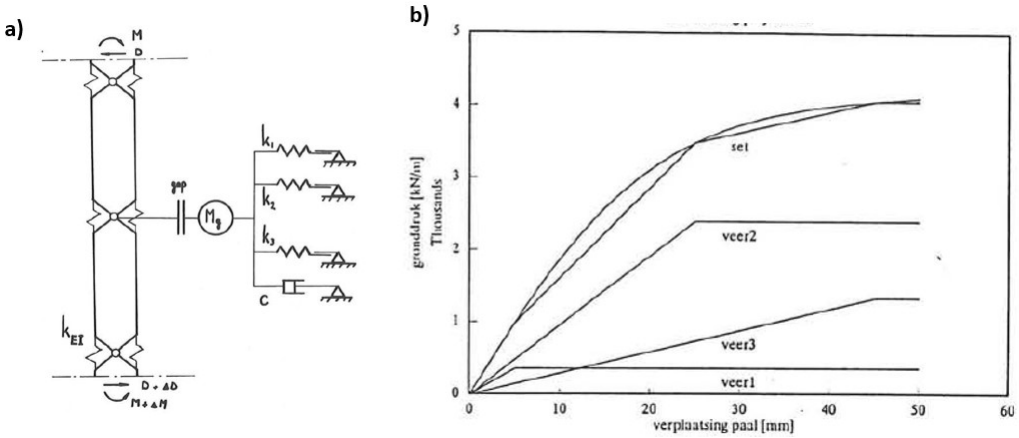

Figure 1.7: Dolphin schematisation in TILLY (a) and approximation of p-y curve with three springs (b) (van der Vorm, 1993)

Conclusions about the calculation results were that TILLY could give a reduction of the bending moment up to 20% and that in general the calculated maximum forces are 25% lower than calculated with Blum.

Vanhoutte and Vertstrynge (2007) included the finite element methods in a study for simple sheet pile walls. The design methods of Blum, the elastoplastic method and the finite element method Plaxis for a cantilever wall were compared. The result of this study was that the bending moment calculated with Blum is 18% higher than the one calculated with Plaxis. The elastoplastic method resulted in a 3% lower bending moment compared to Plaxis. For an anchored wall, the American method was compared with the Elastoplastic method and Plaxis. The calculated bending moment with the American method was 6.46% lower and the anchor force was 2.64% higher than the results from Plaxis. The conclusion that Blum is relatively conservative is expected, however in this research, Blum was only used for a simple cantilever sheet pile wall. No conclusion can be drawn about a more complex wall with anchors and relieving platform.

Lopez Gumucio (2013) compared the spring-supported beam model (D-Sheet) with the finite element model (Plaxis) for an anchored quay wall with and without a relieving platform with a parametric study. This showed that both methods for the structure with and without relieving platform result in comparable bending moments. The calculated anchor force in D-Sheet is generally lower than that of the Plaxis model, but for a structure with relieving platform, this difference in anchor force is larger. This can be

a factor of 1.24 to 1.5, depending on the length of the platform. The research of Vanhoutte and Verstrynge (2007) and Gumucio (2013) both are an evaluation of methods based on mutual results and not based on measured data.

A comparative study that was based on measured data was done by Weringh (2018). The methods Blum, D-Sheet and the FEM Plaxis 2D were compared for two quay walls in Rotterdam (Amazonehaven and SIF). Both are structures with a combined sheet pile wall with relieving platform. The differences between the results of Blum, D-Sheet and Plaxis could be explained by the assumptions that were needed to make the methods compatible with the structure, so only the deformations of the Plaxis model were compared with real measured data for the SIF quay wall. This showed that the calculated displacement was a factor 2 larger than the measured displacement. This large difference was attributed to the way in which the field measurements were performed and the fact that characteristic soil parameters were used. This is however not confirmed with additional measurements.

Another research with measured data on quay walls was done on the Gevelco quay wall in Rotterdam by Grotegoed (2010). The Gevelco quay wall is a combined sheet pile wall with relieving platform anchored with an anchor wall. This structure was modelled in M-Sheet and Plaxis to investigate the causes of the deformations. It could be concluded that the increase in deformations in time was caused by a combination of cyclic loading and the position and magnitude of the surcharge loading. The design methods Plaxis and M-Sheet were in this research only used to investigate causes of the deformations but no conclusion could be drawn about the performance of the methods compared to each other.

For structures with relieving platforms, it is recommended to use a FEM and with the currently available soil models in Diana, Diana can, besides Plaxis, also be used to design such structures. The studies that include a finite element model are always making use of Plaxis, and none of these is comparing the FEM Diana with the conventional methods or comparing Diana with Plaxis. There is a comparison between Diana and Plaxis for tunnel design, done by Kunst (2017), which is also a geotechnical issue. However, most of the conclusions made in this report are about modelling the tunnel lining. One conclusion concerning soil modelling is that Diana is not very suitable for modelling consolidation phases where the excess pore pressures can dissipate.

1.2.7. Problem statement

The literature study showed that there are only a few comparative studies of quay walls with relieving platforms making use of real measured data of displacements and that the one making use of these data do not give a satisfying conclusion about the cause of the large difference in results. Therefore it is not known which method is the most reliable, so quay walls are potentially designed either unsafe or too conservative.

1.3. Objective

The aim of this research is to investigate which design method results in the most realistic deformations of a quay wall consisting of an anchored combined wall with relieving platform, looking at the elastoplastic method and the finite element method.

1.4. Scope

The calculation with the elastoplastic method will be performed with the program D-Sheet Piling, developed by Deltares. This program is commonly used in the Netherlands for designing retaining structures. The program Plaxis will be used as the finite element method. Measured deformations on an existing quay wall will be used to judge which method results in the most realistic deformations. These measurements are performed on an anchored quay wall with relieving platform in Eemshaven Groningen. This quay wall was constructed in 2014-2015 by the contractor De Klerk and deformation measurements were done during and after construction. De Klerk was also involved in the design of the quay wall, so a lot of information about the design and the construction process is available, which is of importance when modelling the quay wall and comparing it with the measurements.

1.5. Research questions

The main research question to reach this objective is formulated as follows:

Which design method approximates the measured deformation best for the quay wall with relieving platform in Eemshaven Groningen, considering the elastoplastic method D-Sheet and the finite element method Plaxis?

In order to answer this main research question, the following sub-questions are formed:

1. Which modelling choices in the elastoplastic method D-Sheet lead to the best possible approximation of the measured deformation?
2. What causes the difference between measured deformation and the result of the best possible approximation with D-Sheet?
3. Which modelling choices in the finite element method Plaxis lead to the best possible approximation of the measured deformation?
4. What causes the difference between measured deformation and the result of the best possible approximation with Plaxis?
5. What are the differences between the calculated deformation in Plaxis and D-Sheet and can this be explained based on the difference in calculation procedure?
6. How does the calculated deformation change due to changes in model input or modelling choices?

Note: The term 'best possible approximation' used in subquestions 1 to 4 means a calculation resulting in deformations with the smallest deviation from the measurements.

1.6. Methodology and report layout

The methodology that will be followed is divided into the following steps with each step covered in a separate chapter:

1. Determine the soil parameters based on soil investigations done during the design phase of the quay wall in the Beatrixhaven. In this project, the design was made with a D-Sheet Piling model, so not all soil parameters needed for the finite element models are known. The unknown parameters will be estimated based on the literature.
   The loads that have been applied to the quay wall or the surrounding soil depend on the different execution phases and the duration of these phases. This information can be obtained by contacting the manager of the harbour, which is Groningen Seaports. Other loads come from the water level variations in the period that the construction started until the moment that the measurement takes place. This information can be obtained from the website of the Department of Waterways and Public Works (Rijkswaterstaat). **(Chapter 2)**
2. Analyse the usability of the measurements on the quay wall. Based on the reliability and usability of the data along the quay wall, a decision can be made on which part of the wall should be modelled in the next steps. **(Chapter 3)**
3. Model the quay wall in D-Sheet Piling and compare the resulting deformations with the measured deformations. Possible explanations for differences between measurements and results can lead to different and better modelling choices to calibrate the model. In this way, subquestions 1 and 2 are answered iteratively. Give explanations for the remaining differences to complete the answer to question 2. **(Chapter 4)**
4. Model the quay wall in Plaxis and compare the resulting deformations with the measured deformations. Possible explanations for differences between measurements and results can lead to different and better modelling choices to calibrate the model. In this way, questions 3 and 4 are answered iteratively. Give explanations for the remaining differences to complete the answer to question 4. **(Chapter 5)**
5. Compare the calculated deformations from D-Sheet and Plaxis and explain the difference based on the difference in calculation method to answer question 5. **Chapter 6**
6. Perform a sensitivity analysis on the calculation methods to investigate whether different input parameters or other modelling choices would have led to large changes in results and thereby different conclusions. This answers question 6. **(Chapter 7)**

2

Case description

This chapter gives a description of the project used for the validation of the models including the way of execution. Together with the local conditions and the loads during and after construction, this covers the first step of the methodology. For parameters that are depending on the cross-section, only parameters for sections at piles 38, 68 and 78 are given. This is because these locations will be modelled in the next steps. The reason for selecting these locations is based on the available measurements and will be elaborated in Chapter 3.

2.1. Project overview

The quay wall that is used in this research is situated in the Eemshaven Groningen. Approximately one-third of the produced energy in the Netherlands is produced in the Eemshaven with new power stations and with the Dutch largest wind farms. Besides that, the port plays an important role in development and maintenance of wind farms on sea (Groningen Seaports, n.d.). The considered quay wall is in the Beatrixhaven, which is situated in the northern part of the Eemshaven, see Figure 2.1. This Beatrixhaven was developed in different phases. In the latest phase (phase 5) the harbour was extended to the west with new quay walls. In this phase, on the western side, a quay wall consisting of a combined sheet pile wall with a high relieving platform for high surcharge loads was constructed.

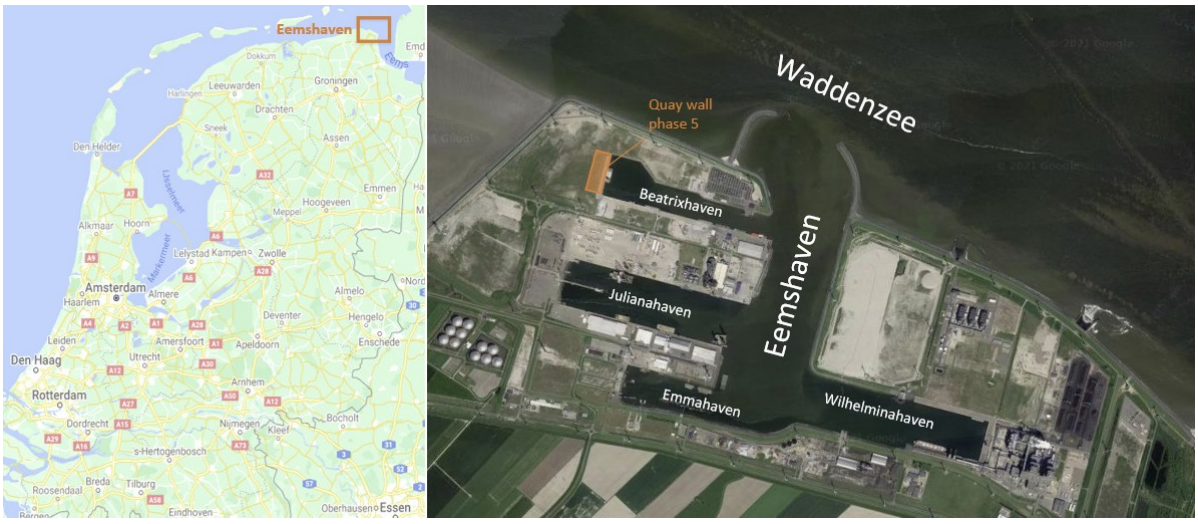

Figure 2.1: Overview of Eemshaven with quay wall

The quay wall is designed especially for loading and unloading of heavy loads such as wind turbines. With a design load of 300 kN/m^2, this is one of the quay walls with the largest bearing capacity in the Netherlands. To resist these large loads, the wall is designed with a relieving platform founded on

screwed piles with a length of 24 meters. The quay wall has a length of 290 m and a retaining height of approximately 16 m (from NAP -11.40 m till NAP +4.50 m). The retaining wall is a combined sheet pile wall with tubular piles with a diameter of 1829 mm embedded till NAP -33.00 m and sheet piles embedded till NAP -24.00 m. This wall is anchored with screwed injection anchors with the injection from NAP -22.80 m. A cross-sectional drawing is given in Figure 2.2. The full drawing including all dimensions can be found in Appendix A.

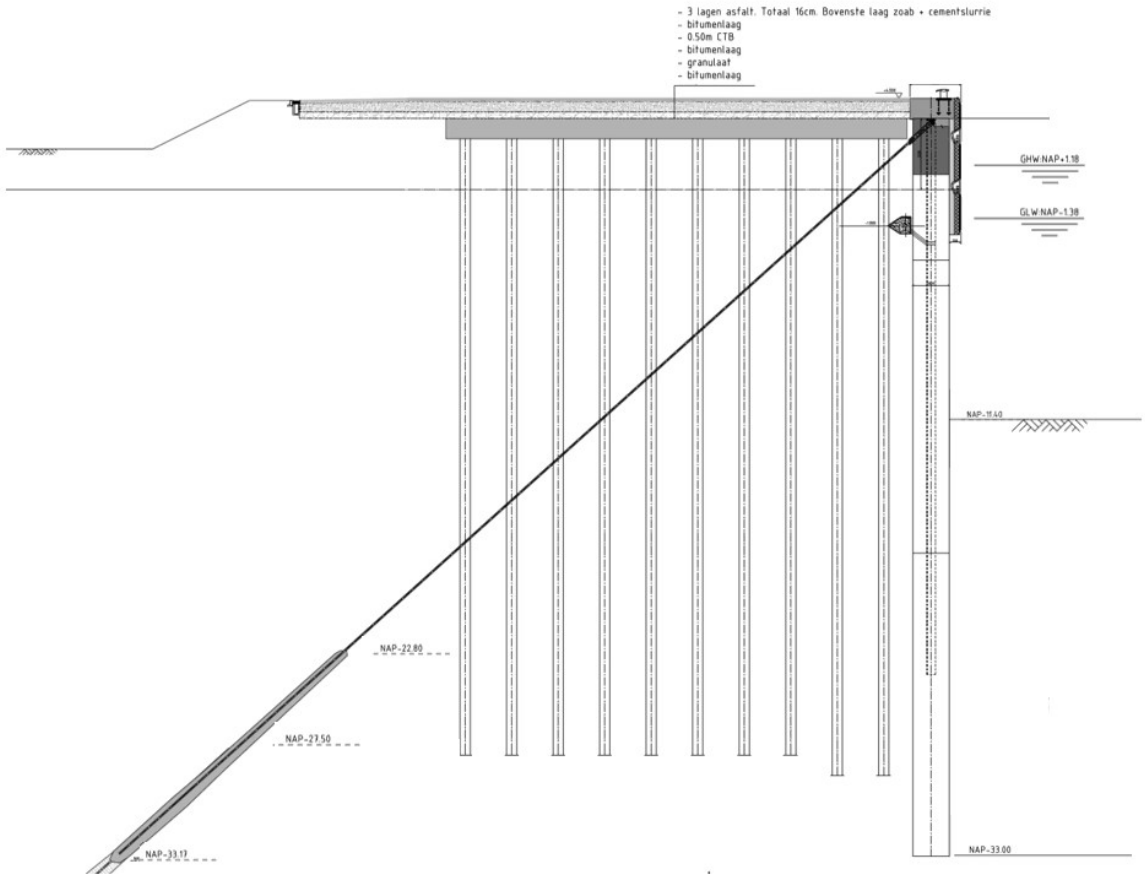

Figure 2.2: Cross section of quay wall Beatrixhaven (by De Klerk BV)

An important feature of this quay wall is that there is no bed protection in front of the quay wall. In this way, the self-elevating units or jack-up vessels can berth by using their own spudcans and use their own cranes to unload and load the freight. Soundings are made every month to monitor the influence of these spudcans on the harbour bottom. Figure 2.3 shows an example of a sounding where the holes and the hilly bottom are clearly visible. The lowest level in this sounding is approximately NAP -13 m due to the spudcan. In §2.6.5 it is shown how this is implemented in the model.

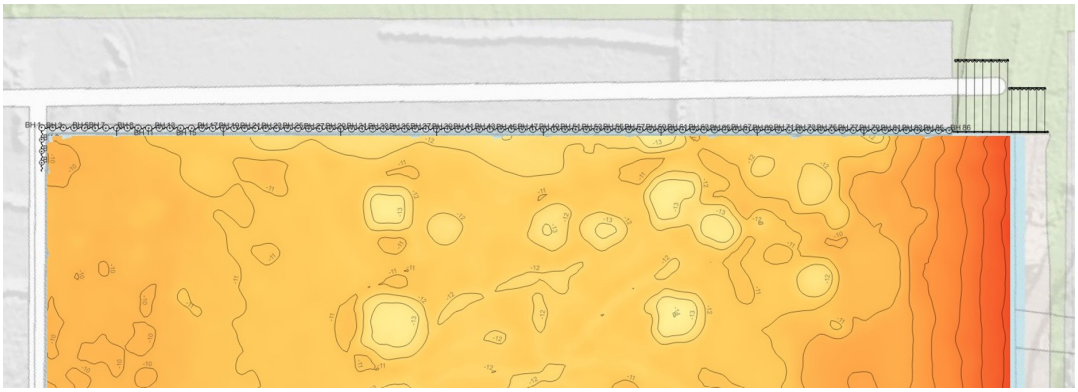

Figure 2.3: Sounding of harbour bottom on 18-1-2022. Data received from Groningen Seaports (2022) and processed in QGIS.

2.2. Construction stages

The quay wall is built for a large part in dry conditions. The quay wall was constructed before the extension of the harbour was excavated. During the installation of the combined sheet pile wall and the anchoring, the dry conditions were maintained by a first embankment situated at a large distance from the quay wall. During this stage, the ground levels on both sides were equal. Once the wall was installed, a second embankment was made closer to the wall and the soil in front of the wall was excavated to a lower level, maintaining dry conditions by a drainage pump. In this way, it was possible to construct the fender systems. The construction sequence can be described and visualised in the following six steps:

Stage 1: Installation of combined wall

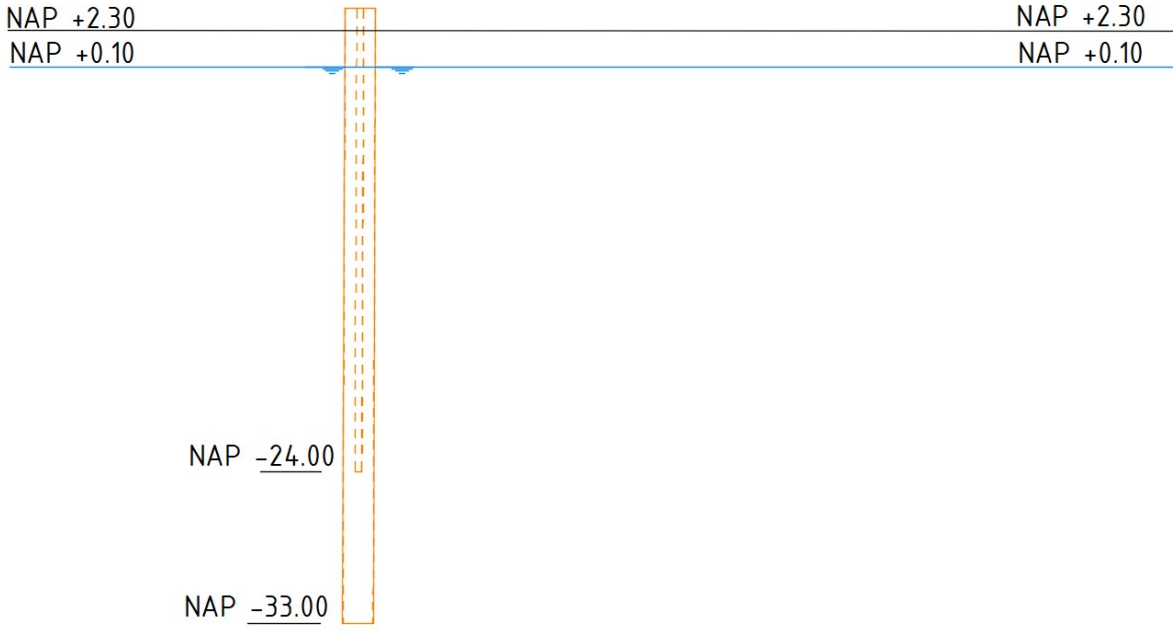

The tubular piles of the combined wall are installed by vibration. The last few meters were done with a hammer. After that, the sheet piles in between are installed by vibration until a depth of NAP -24.00 m.

Stage 2: Concrete plug and back-fill

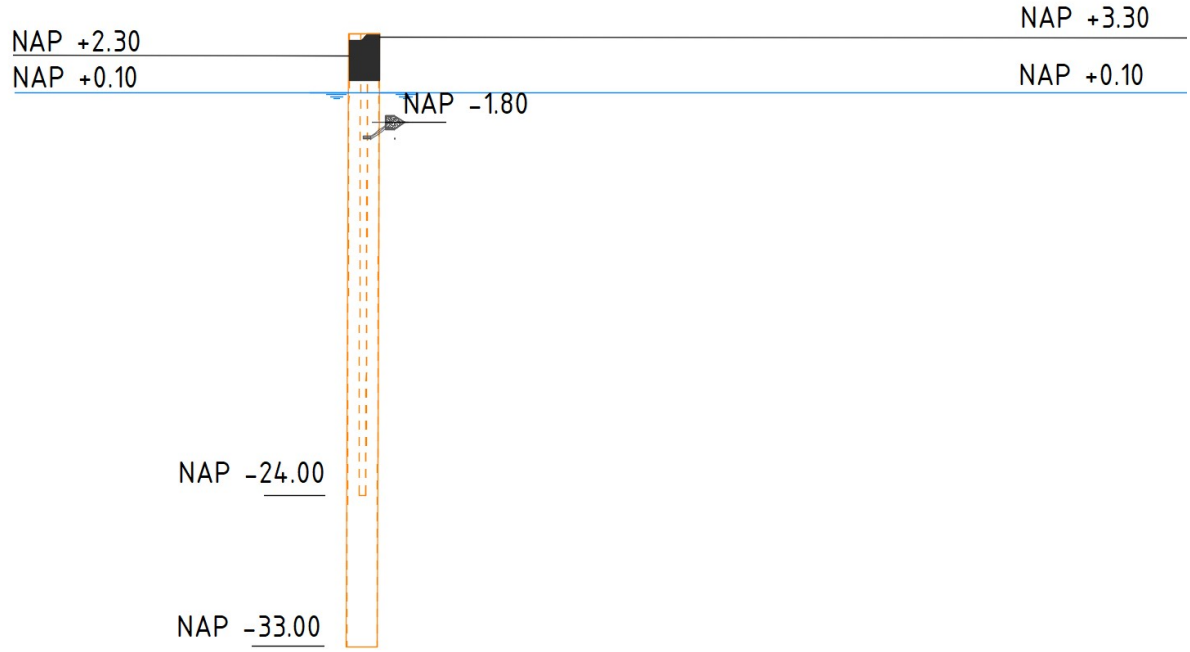

The top of the tubular piles is filled with a reinforced concrete plug to create an anchor point. The drainage system in the form of a gravel case and drainage tube is installed at a level of NAP -1.80 m. This drainage system is meant to decrease the head water difference over the wall when the outside water level is fluctuating. After that, the soil on the landside is raised by one meter.

Stage 3: Anchoring and prestressing

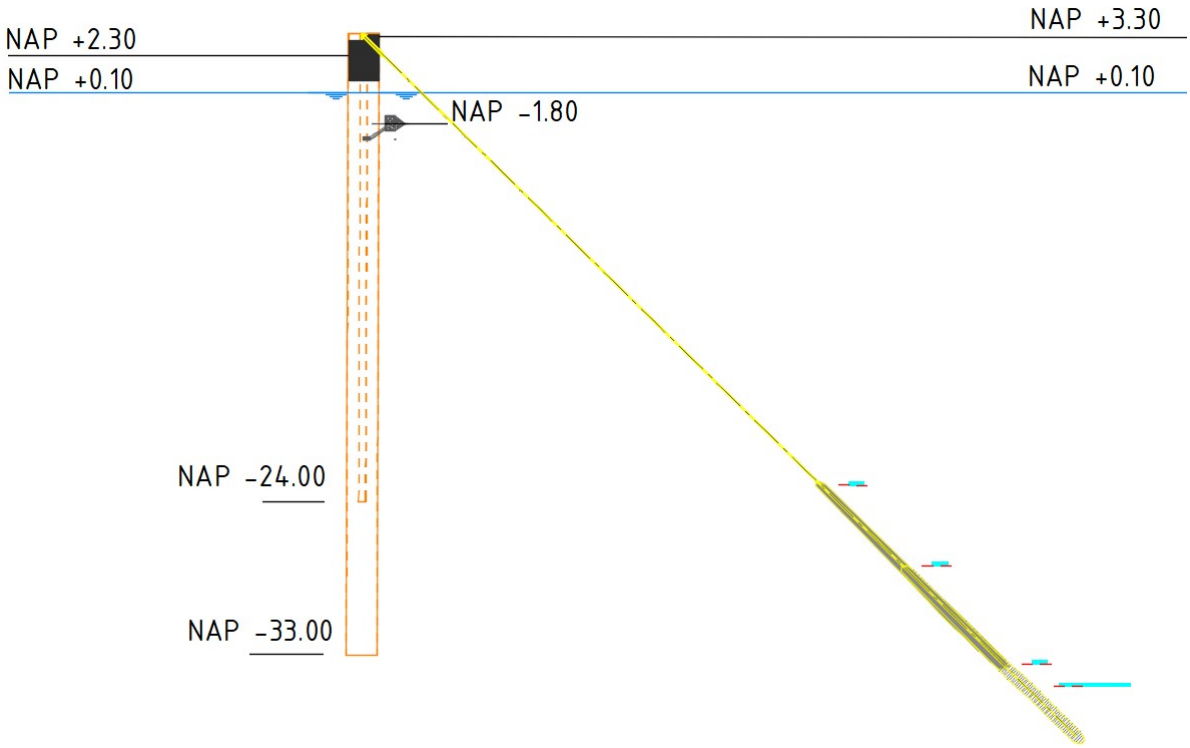

One screw injection anchor per tubular pile is installed under an inclination angle of 42 °. The anchors have a grout body that starts at NAP -22.80 m and extends to NAP -32.17 m. This can differ, depending on the location of the anchors. After that, the anchors are prestressed to the prescribed level.

Stage 4: Dry excavation NAP -1.65 m

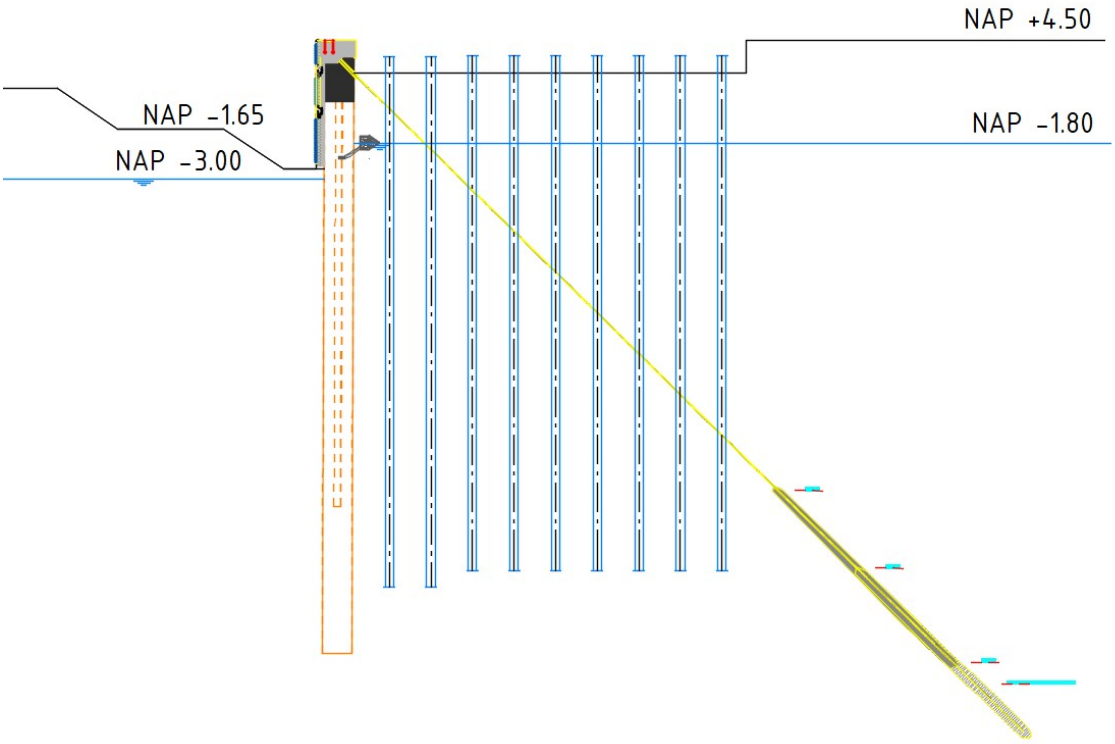

The soil in front of the wall is excavated to a level of NAP -1.65 m with the deepest point at NAP -2.50 m to install the fender systems on the combined wall. The excavation is kept dry by drainage pumps that lower the water level to approximately NAP -3.00 m. The gravel drainage system results in a lowered groundwater level on the landside to NAP -1.80 m. With the fender systems installed, the space between the fender systems and the combined wall is filled with concrete. Subsequently, the bollards are positioned on the reinforcement of the capping beam after which the capping beam is poured. In the meantime, the bearing piles under the relieving platform are screwed into the soil.

Stage 5: Dry excavation NAP -5.00 m

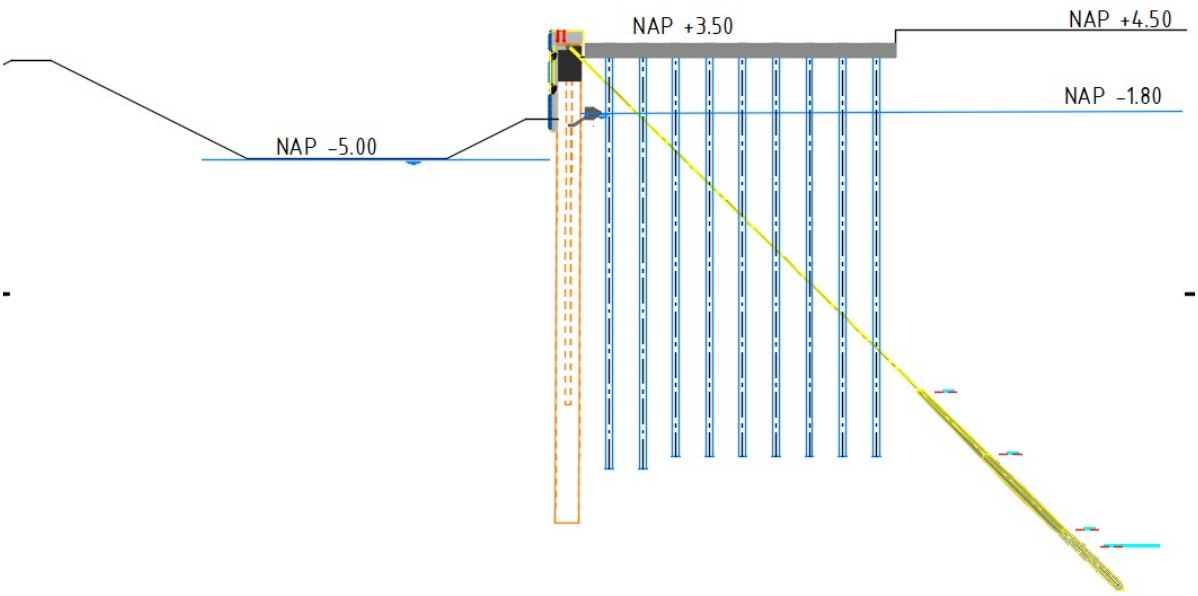

The dry excavation is deepened and the water level is lowered further by extra drainage pumping. This level of NAP -5.00 m was the maximum allowable dry excavation level in this phase of construction. The relieving platform with a thickness of 1 meter is poured in the meantime.

Stage 6: Final stage

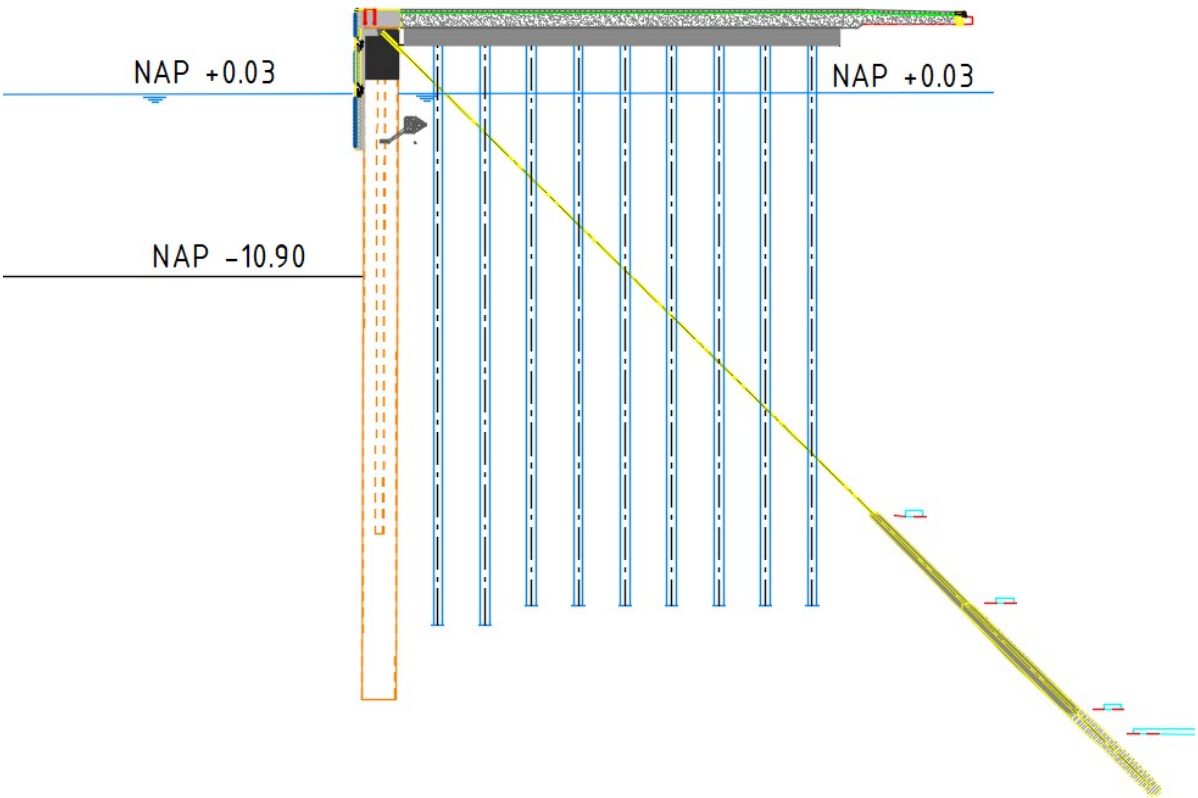

In the final stage, the road pavement above the relieving platform is placed. This consists of several layers of bitumen with granulate in between and the top is finalized with three layers of asphalt. The dam of the dry excavation is removed and the harbour is excavated to its final level, which is NAP -10.90 m. The water level NAP +0.03 m is the average sea water level that is now in front of the wall.

2.3. Soil characteristics

The soil characteristics are determined with the available CPTs at the site. Unfortunately, these CPTs are the only soil investigation available and therefore the only way to determine the soil characteristic. Table 2b of NEN-EN 1997-1 is used to obtain values for the main soil parameters based on the cone resistance q_c. This table presents low and high characteristic values, but the values can also lie outside these characteristic values. Based on the soil investigation, no estimate could be made. Therefore it is assumed that the mean values represent the values for the soil of interest. The detailed interpretation with the used parameters can be found in Appendix C. The soil characteristic is determined at three locations along the quay wall: tubular piles 38, 68 and 78.

2.4. Water levels

Description	Water level in m NAP	
During construction	+0.01	
During dry excavation NAP-1.65 m	-3.00	
During dry excavation NAP-5.00 m	-5.00	
Mean low tide	-1.40	
Average water level	+0.03	
Lowest water level	-2.83	1-3-2018

Table 2.1: Water levels

2.5. Structural elements

The structural elements consist of the combined sheet pile wall, anchors and relieving platform with bearing piles.

2.5.1. Combined sheet pile wall

The wall is a combination of tubular piles with an outer diameter of 1829 mm and PU22 sheet piles. One repeating system consists of a tubular pile with two PU22 sheet piles. The wall thickness of the tubular pile is varying over the height to make it stiffer at the place of the highest bending moment. This results in three different sections, see Figure 2.4. The sheet piles are also shorter than the tubular piles, so in total four sections. Corrosion can lead to a reduction of the stiffness, but this is not accounted for in this research as it is only 8 years ago that the quay wall is built. Furthermore, the steel qualities, in reality, are probably higher than the qualities used in this model which were guaranteed by the manufacturer. The properties are summarised in Table 2.2. The detailed calculation can be seen in Appendix D .

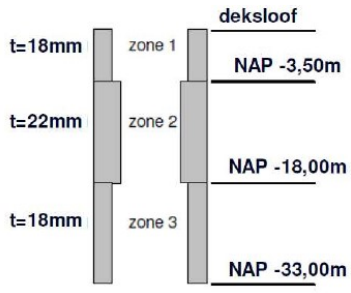

Figure 2.4: Wall thicknesses tubular pile (De Klerk B.V., 2014)

Description	Symbol	Value	Unity
Tubular pile			
Outer diameter	D	1829	mm
Wall thickness max	t	22	mm
Wall thickness min	t	18	mm
Steel quality	-	X70	-
Tip level	-	-33.00 (-36.00 for TP78)	m NAP
Sheet pile			
Type	-	PU 22	-
Steel quality	-	S240GP	-
Quantity	-	2	-
Tip level	-	-24.00	m NAP
System			
Width	B_{system}	3089	mm
Moment of inertia (t=22mm)	I_{system}	1650454	cm^4/m'
Moment of inertia (t=18mm)	I_{system}	1375996	cm^4/m'
Moment of inertia (t=18mm)	I_{pile}	1359292	cm^4/m'
Bending stiffness (t=22mm)	EI_{system}	3.50E+06	kNm^2/m'
Bending stiffness (t=18mm)	EI_{system}	2.89E+06	kNm^2/m'
Bending stiffness (t=18mm)	EI_{pile}	2.85E+06	kNm^2/m'

Table 2.2: Properties combined wall

2.5.2. Anchor

On every tubular pile in the combined wall, a screw injection anchor is applied under an angle of $42°$, consisting of a steel rod and a grout body.

Steel rod

The rod is a 117/64 steel anchor rod with a cross-sectional area of 6989 mm^2 and a length varying from 36 to 48 m, depending on the position along the wall. Tension tests were done in the design phase to calculate the exact modulus of elasticity E and to determine the yield force. This is very useful in this research as this gives the most reliable results. The resulting force-displacement diagram is shown in Figure 2.5. The force where the yielding is 0.2% of the anchor length is taken as the yield force, resulting in $F_{yield;0.2}$ = 4450 kN. The tubular piles and thus the anchors have a centre-to-centre distance of 3.09 m, so the yield force per meter is 4450/3.09 = 1440 kN/m'. At this point, the yielding already started, but this is taken as the yielding point because only one elastic branch can be modelled. Taking a lower yield force would therefore result in large plastic deformations.

Calculating the modulus of elasticity from this graph gives E = 190.442 kN/m^2. The exact calculation is given in Appendix E. The properties of the anchor rod are summarised in Table 2.3.

	TP38	TP68	TP78	
Total anchor length	56	60	56	m
Modulus of elasticity E	1.90E08			kN/m^2
Prestressing force	568.3			kN/m'
Level	3.30			m NAP
Yield force	1440			kN/m'
Cross section	2.262E-03			m^2/m'

Table 2.3: Properties of the anchor rod

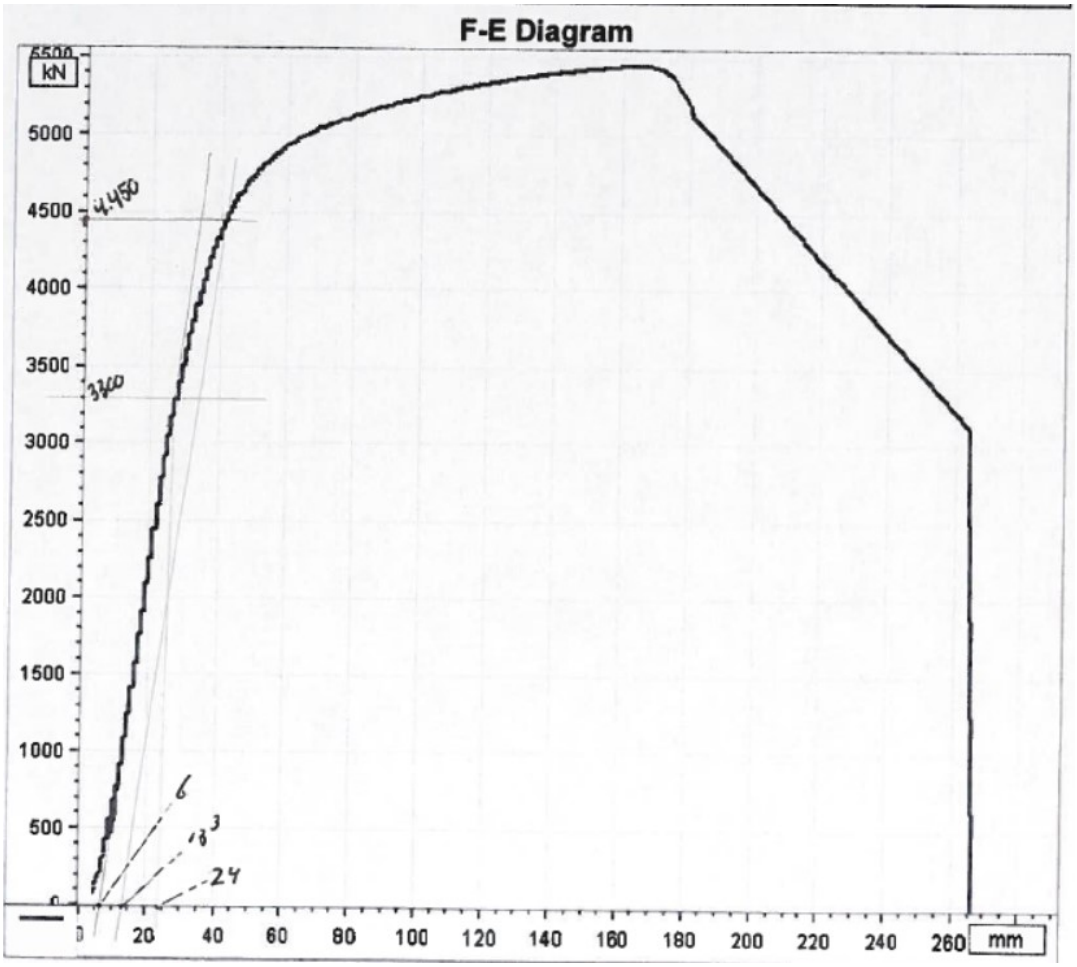

Figure 2.5: Force-displacement diagram of anchor tension test (Mennens Dongen B.V., n.d.)

Grout body

The grout body has a length of 15 m on all anchors and a diameter of 370 mm. The stiffness of the grout body is determined with available anchor tests that were done after installation. These tests resulted in force-displacement graphs which is an indication of the total stiffness k_{tot} of the anchor rod and grout body. The graphs can be found in Appendix E. The anchor test shows the increases in elongation with an increasing load. The spring stiffness k_{tot} can be determined:

$$k_{tot} = \frac{\Delta F}{\Delta L} \tag{2.1}$$

Where:

k_{tot}	:	Stiffness of anchor system	[kN/m]
ΔF	:	Difference in load from initial load P_i to the prestressing level P_{prestr}	[kN]
ΔL	:	Elongation	[m]

The stiffness of the grout body is then determined based on the relation of the stiffnesses of springs in series:

$$\frac{1}{k_{tot}} = \frac{1}{k_{rod}} + \frac{1}{k_{grout}} \tag{2.2}$$

Where the stiffness k_{rod} is the stiffness which is known from the previously determined E-modulus:

$$k_{rod} = \frac{E_{rod} \cdot A_{rod}}{L_{rod}} \tag{2.3}$$

The unknown k_{grout} can thus be determined for the anchors at piles 38, 68 and 78. The resulting E-modulus of the grout body E_{grout} follows from the same formula for the grout body as Formula 2.3 with

$A_{grout} = 0.25 \cdot \pi \cdot 0.370^2 = 0.108$ m^2 and $L_{grout} = 15$ m. The input for the calculation and the calculated E-modulus E_{grout} can be found in Table 2.4.

TP	P_i [kN]	P_{prestr} [kN]	ΔL [mm]	k_{tot} [kN/m]	E_{rod} [kN/m^2]	L_{rod} m	k_{rod} [kN/m]	k_{grout} [kN/m]	E_{grout} [kN/m^2]
38	322	3219*	103.78	2.79E+04	1.90E+08	41	3.25E+04	1.99E+05	2.78E+07
68	100	1756	76.85	2.15E+04	1.90E+08	45	2.96E+04	7.94E+04	1.11E+07
78	100	1756	73.69	2.25E+04	1.90E+08	41	3.25E+04	7.30E+04	1.02E+07

* This is not the prestressing level, but the force during the anchor test. This is used instead of the prestressing force because this line in the diagram is more linear.

Table 2.4: Calculation input and results of grout body stiffness

2.5.3. Relieving platform

The relieving platform has a thickness of 1 meter and its bottom is constructed at NAP +2.5 m. The relieving platform is founded on a total of 850 screw injection piles called Terr-econ injection piles (Terracon Funderingstechniek, n.d.). This Terr-econ pile is a soil-displacing pile which is cast in situ. A temporary tubular pile with a diameter of 560 mm is placed on a separate drill tip with a diameter of 670 mm. The pile and the drill tip are then screwed into the ground, after which the reinforcement is placed in the empty pile. The pile is poured with concrete while the temporary pile is pulled out of the soil. The drill tip is left in the soil. Removing the temporary pile creates a pile with a large skin resistance and large bearing resistance due to its rough skin.

The top of the platform is at NAP +3.5 m and the remaining 1 meter above the platform is filled with a layer of granulate (0.32m), Cement-Treated Base (CTB) (0.52m) and a layer of asphalt (0.16m) with the properties specified in Table 2.5.

Layer	Thickness [m]	E [Mpa]	ν [-]	γ [kN/m3]
Asphalt	0.16	4500	0.35	24.5
CTB	0.52	6000	0.15	21
Granulate	0.32	400	-	17

Table 2.5: Elastic properties of fill above relieving platform

2.6. Loads

This section gives an overview of the different loads on the quay wall which are both permanent and variable loads.

2.6.1. Permanent loads

The permanent loads consist of the weight of the capping beam, the concrete plug and the concrete fill between the combined wall and fender system (from now on called concrete fill). The capping beam has a width of 2.245 m and a height of 1.05 m. The concrete plug inside the pile has a height of 2.75 m with a diameter of 1.793 m and the concrete fill has a volume of 5.38 m^3/m'. With a volumetric weight of 25 kN/m^3, the total vertical permanent load is:

$$(2.245 \cdot 1.05 + (2.75 \cdot \frac{1}{4} \cdot \pi \cdot 1.793^2)/3.09 + 5.38) \cdot 25 = 249.3 \text{ kN/m'}$$

The concrete fill has an eccentricity with respect to the tubular pile of 0.836 m resulting in a bending moment of:

$$5.38 \cdot 25 \cdot 0.836 = 112.4 \text{ kNm/m'}$$

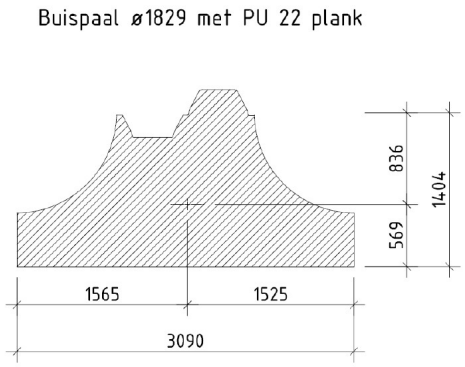

Figure 2.6: Eccentricity of concrete fill (De Klerk B.V., 2014)

2.6.2. Terrain loads

The relieving platform is designed for a terrain load of 300 kN/m^2, however, this is not the load that occurred over the period since the construction. In December 2017, a Noise Mitigation System of 460 tons in total was assembled on the quay wall, see Figure 2.7. This resulted in a maximum ground bearing pressure under the crane of 176 kN/m^2. This is the maximum load on the relieving platform of the quay wall. In the past period, several loading and offloading projects were done with a ground-bearing pressure of 80-150 kN/m^2. These pressures are very local and therefore a uniform surcharge load of 100 kN/m^2 is assumed. These loads from loading and unloading projects were done on the relieving platform. Behind the relieving platform, a surcharge load of 20 kN/m^2 is assumed, which can be due to a mobile crane of 60 tons on a surface of 9 m^2.

Figure 2.7: Assembling of the NMS 8800 in December 2017 (Groningen Seaports, n.d.)

2.6.3. Loads of ships

The quay wall is equipped with 2 bollards per 20 m with a design load of 600 kN per two bollards. This results in a maximum bollard load of $2 \cdot 600/20 = 60$ kN/m'. The bollard load can act at a height of 0.4 m above the top of the wall resulting in an additional bending moment of $60 \cdot 0.4 = 24$ kNm/m'. This is the maximum design load on the bollard.

2.6.4. Drainage system

At NAP -1.80 m, a drainage system in the form of a gravel case is constructed to reduce the water head differences over the quay wall. According to the CUR166, a water level difference of at least 0.5m should be taken into consideration to account for the possibility that the drainage system is clogged. There are two scenarios where the water level outside is below this level. The first one is when the

water level outside is at NAP -5.00 m during the construction of the fender systems. In this stage, the drainage system is just constructed, so the groundwater level is assumed to be at the level of the drainage NAP -1.80 m. The second scenario is during the lowest sea water level since the construction. This was on 1 March 2018 with a water level of NAP -2.83 m. In this case, the groundwater level is assumed as NAP -1.80 + 0.5 m = NAP -1.30 m.

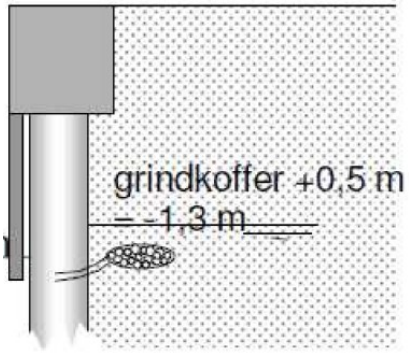

Figure 2.8: Drainage system (De Klerk B.V., 2014)

2.6.5. Jack-up barges

The design made by the contractor and the engineering consultant used a spudcan with a maximum load of 12.315 kN and an area of 3.25 m^2. The engineering consultant *Witteveen en Bos* used a safety factor of 1.5 on this load and calculated the penetration depth based on the CPT resulting in a penetration depth to NAP -20.1 m. Without the safety factor this results in a penetration to NAP -19.1 m. It is assumed that the holes will be filled with loosely packed soil. This does not give horizontal resistance to the wall, so this is modelled as a surcharge load on the lowered ground level, see Figure 2.9. In this situation, the retaining height thus becomes 24.60 m instead of 16 m (De Klerk B.V., 2014).

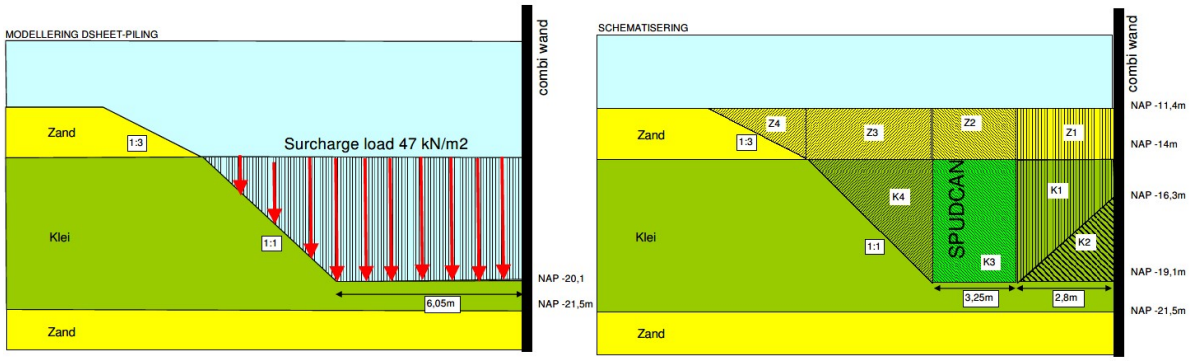

Figure 2.9: Influence area of spudcans (De Klerk B.V., 2014).
*Penetration depth of left figure should be to NAP -19.1 m instead of NAP -20.1 m

2.6.6. Soil- and top load

The top of the relieving platform is 1 meter below the ground level at NAP +3.50 m. In the design, the ground fill above the platform has a prescribed volumetric weight $\gamma = 25$ kN/m^3 and an internal friction angle $\varphi = 45°$. It is impossible to model the relieving platform in DSheet, so a lower ground level of NAP +2.50 m is assumed as the normal ground level is NAP +4.50 m and the fill and the platform have a thickness of 1 m. The loads from the soil fill above the platform are implemented in the model as horizontal loads. This consists of the load from the soil fill itself and the load from the top load. With a neutral earth pressure coefficient $K_0 = 1 - sin(\varphi) = 0.29$, the horizontal pressure from the soil fill is:

$$\sigma_{h,soil} = \gamma \cdot h \cdot K_0 = 25 \cdot 1 \cdot 0.29 = 7.25 \text{ kN/m}^2$$

The maximum top load is the design load of 300 kN/m^2, but this did not occur over the past time. As mentioned, the average uniform surcharge load is 100 kN/m^2, resulting in a horizontal soil pressure of:

$$\sigma_{h,topload} = 100 \cdot K_0 = 100 \cdot 0.29 = 29 \text{ kN/m}^2$$

Both pressures act on half the height above the platform, so this results in two horizontal loads at NAP +4.00 m: $F_{soil} = 7.25 \cdot 1 \cdot 0.5 = 3.63$ kN/m' and $F_{topload} = 29 \cdot 1 = 29$ kN/m'.

3

Measurements

This chapter describes the measurements that were done on the quay wall. Based on the reliability and usability of the measurements a decision will be made on which part of the wall will be modelled in D-Sheet Piling and Plaxis. This is step 2 of the main methodology. These measurements will be compared to the computed deformations in Chapters 4 and 5.

3.1. Inclinometer measurement set-up

During the construction in 2014 and 2015, measurements were done with inclinometers at 8 points along the 290 m long quay wall. This section describes the availability and usability of these measurements.

3.1.1. Location of the inclinometers

The pipes used for the inclinometer are rectangular casings installed inside the tubular piles of the combined wall over the full length from NAP +4.50 m to the toe at NAP -33.00 m. These tubes are accessible from the top of the quay wall where the probe can be lowered. The casing is a rectangular pipe installed such that one diagonal is perpendicular to the quay wall and one diagonal is in the line of the wall. The probe is lowered inside the casing with its guiding wheels in the corners of the casing. In this way, both the deformation perpendicular and in-line are measured. The perpendicular deformation is called the A-direction, and the in-line is the B-direction. The inclinometer measures the slope variation over the height of the tubular piles with an interval of 0.5 m. The deformation is then calculated by multiplying the measured inclination with the interval between two readings, which is usually 0.5m.

The first two measurements took place on 12-11-2014 and 08-01-2015 during the construction of the quay wall at 8 tubular piles. These moments are placed on a timeline based on the construction stages in Figure 3.1.

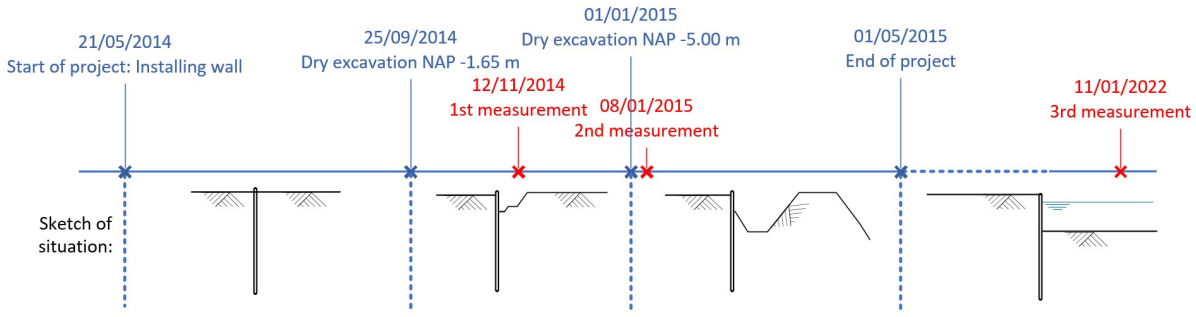

Figure 3.1: Timeline with moments of measurement and sketches of the situation

The exact same measurement was repeated on 11-01-2022 for the benefit of this research. In the meantime the quay wall was multiple times used for loading and unloading ships, and mooring with spudcans.

All three measurements were absolute measurements where it is assumed that the displacement at the toe is zero. Therefore the measurement of 2014 is taken as the reference measurement. The 8 measured points are displayed in Figure 3.2.

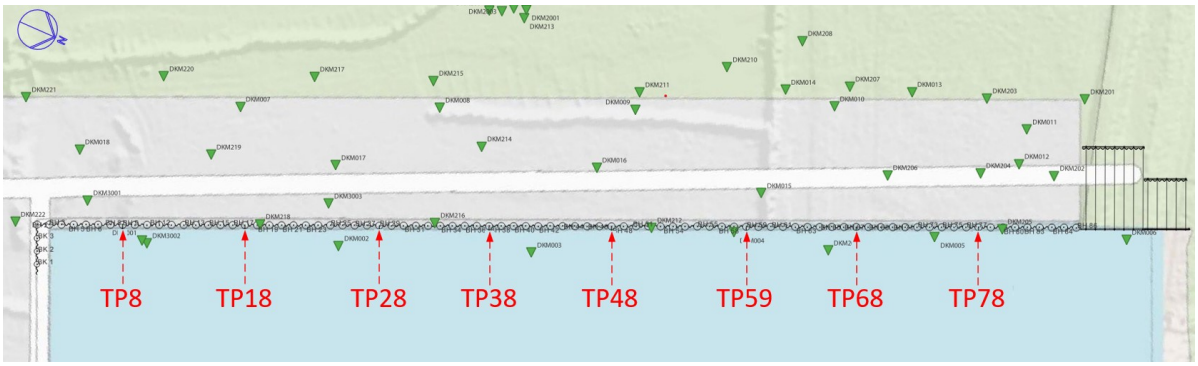

Figure 3.2: Location of tubular piles measured with an inclinometer, indicated in red.

3.1.2. Usability

Unfortunately, there is not a complete measurement set (2014, 2015 and 2022) available for all 8 points. In Table 3.1 for every measured pile, the availability per year is indicated with a V or X.

	TP	8	18	29**	38	48**	59	68	78
2-11-2014 (reference)		V*	V*	V	V	X	X	V	V
1-8-2015		V	V	V	V	X	V	V	V
22-1-2022***		X	X	X	V	X	V	V	V

Table 3.1: Overview usability of measurements
*Measurement is done only till halfway the pile, taking this as the basepoint
**Only the top 7 meters are measured because the tube was clogged.
***Several tubes were not accessible with the measurement in 2022

From this overview, it turns out that only the points at piles 38, 68 and 78 can be used in this research.

3.1.3. Accuracy

The precision of the inclinometer measurements depends on the accuracy of the material used such as the probe and sensors. Besides that, there also is a system field error which consists of random and systematic errors. Mikkelsen (2003) states that a random error is $\pm$ 0.16 mm for a reading interval. This accumulates with a rate of the square root of the number of reading intervals. The length of the casing is 37.5 m, and the interval between two readings is 0.5 m, which means that the total random error is $\sqrt{37.5 \cdot 2} \cdot 0.16 = \pm 1.39$ mm.

The systematic error is a collection of several errors such as the bias-shift error, sensitivity drift, rotation error and depth position error. The systematic error is about 0.13 mm per reading (Mikkelsen, 2007) which results in $37.5 \cdot 2 \cdot 0.13 = \pm 9.75$ mm over 37.5 m.

- **Bias-shift error:** The main type is the bias-shift error which is due to a small change in the bias of the probe over time. This can be corrected by repeating the measurement and rotating the probe 180 degrees. From the measurement company, it is known that this is done, so this error can be neglected.
- **Sensitivity drift:** This error is due to the change of the scale factor in the probe during the measurements. Due to this drift, some values are scaled with a larger amplifier than other values, resulting in deformations deviating from reality. Sensitivity drift is however difficult to recognize and is the least common error, so this will not be considered.

- **Rotation error:** This rotation error occurs when the casing is deviating from the vertical. The A-axis is slightly rotated to the B -axis, so the measured deformation in A-direction also is partly due to inclination in B-direction, see Figure 3.3.

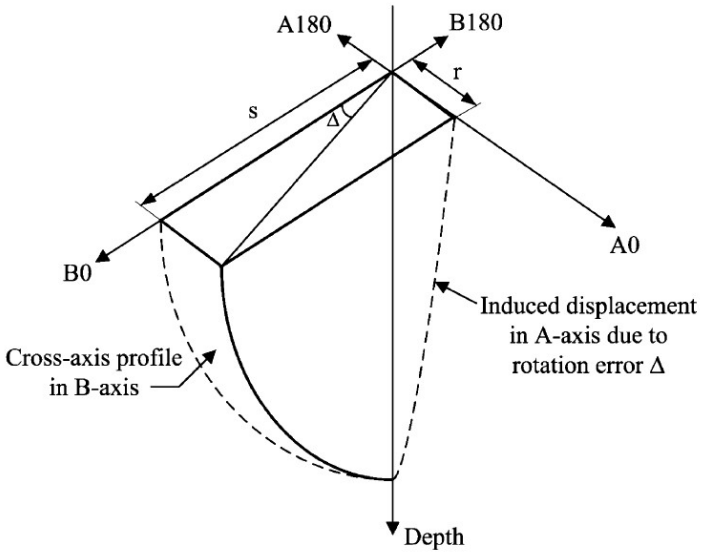

Figure 3.3: Illustration of rotation error (Mikkelsen, 2003)

The rotation error can be expressed as (Stark & Choi, 2008):

$$\Delta = sin^{-1}(\frac{r}{s}) \tag{3.1}$$

Where:

Δ	:	Rotation error angle	[°]
r	:	Induced displacement in A-axis due to rotation error Δ	[mm]
s	:	Induced displacement in B-axis due to rotation error Δ	[mm]

This rotation error can be observed when the casing is out of vertical alignment or when the measurements in A and B show the same shape. The vertical alignment is, in this case, difficult to verify, but from the data it can be seen that the graph in A and B direction shows a resemblance which could indicate that the rotation error is occurring. This error can only be corrected when special software is available, which is not the case.

- **Depth positioning error:** The last type of systematic error is the depth positioning error that occurs when the probe is not lowered to the bottom of the casing. However, this is not the case because all data sets of measurements that reached the bottom had the same length.

It can be concluded that the random error and the rotation and sensitivity error can still occur. The random error was quantified, however, the rotation and sensitivity error can not be quantified separately. Therefore the total systematic error is divided by two to get an estimate. This results in a total error of $1.39 + 9.75/2 = \pm 6.27$ mm over 37.5 m.

3.2. Top displacement in X and Z direction

The top displacement was measured by measuring horizontal and vertical displacements of bolts on the capping beam of the quay wall.

3.2.1. Availability of data

From 2017, the top displacement was measured yearly at 14 points along the quay wall. The full report with the measured data is added in Appendix B. The last measurement was in April 2021. The

14 points (61 to 75) represent the bolts placed in the capping beam on top of the piles. The available data shows for every year the horizontal distance between a defined measurement line and the bolt. This measurement line is a fictitious line between two points in RD coordinates. Unfortunately, the exact location of these bolts on the quay wall is not known, so only displacements relative to the first measurement, which is February 2017, are known.

The horizontal top displacements are shown in Figure 3.4. It is remarkable that in 2018 and in 2020 the top of the quay wall apparently moved to the land side. At first sight, this may seem very unlikely because of the large relieving platform that is constructed just below ground level. Also, the relatively high anchor point at NAP +3.30 m makes it hard to believe that the top at NAP +4.50 m is moving inland. However, there are several reasons why this is still possible:

1. Because the relieving platform is not connected with the combined wall. Some Tempex or EPS elements are installed between the platform and the combined wall to ensure that the combined wall can rotate and move away freely from the platform. These EPS elements with relatively low stiffness can also be compressed when the wall is moving inland.
2. This inland moving can also be due to loading and unloading of the quay wall. When the measurement in 2017 was done with a high surcharge load and the measurement in 2018 without a surcharge load, this could result in a relative movement landward in 2018.

Figure 3.4 shows that the profile stays approximately the same, so the inland moving is a displacement over the whole quay wall. The second mentioned reason about change in surcharge loads is therefore less conceivable, because this quay wall is mainly used for surcharge loads concentred at a part of 10 to 100 m.

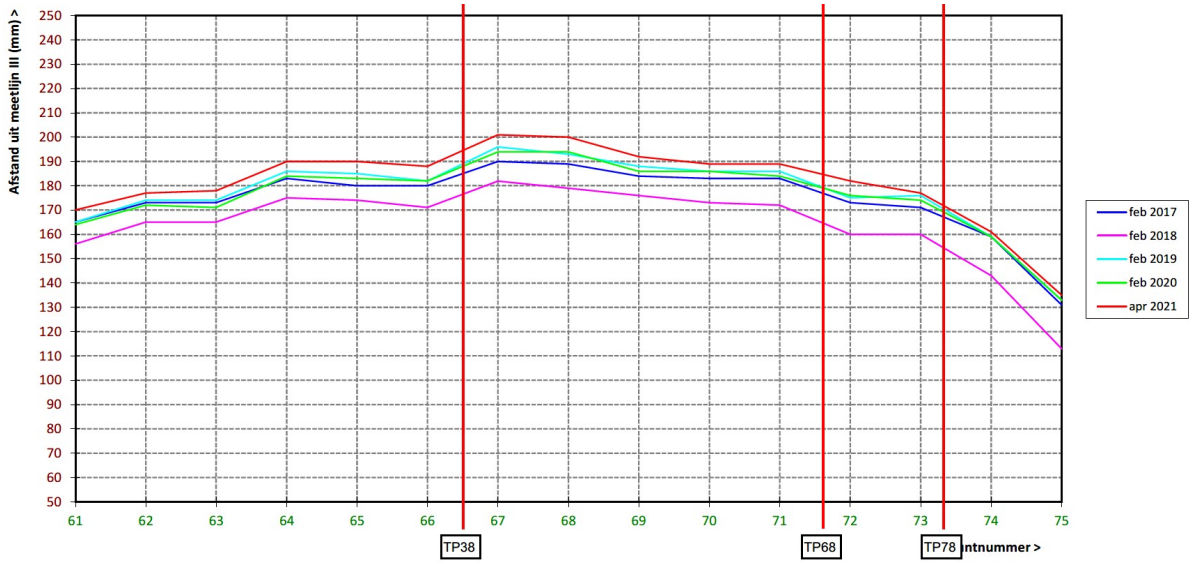

Figure 3.4: Horizontal top displacements in mm. The locations of piles 38, 68 and 78 are indicated with red vertical lines.

The vertical top displacements are shown in Figure 3.5. These are also measured yearly from 2017 until 2021 for each point and recorded with respect to NAP. A jump can be seen between the measurements of 2018 and 2019. This is mainly because the reference bolt 0A4042 was lowered 17 mm that year. The subsidence in the region of the Eemshaven is approximately 5 mm/year (SkyGeo, 2023). Apparently, the reference bolt was corrected in 2018 for this subsidence resulting in this jump.

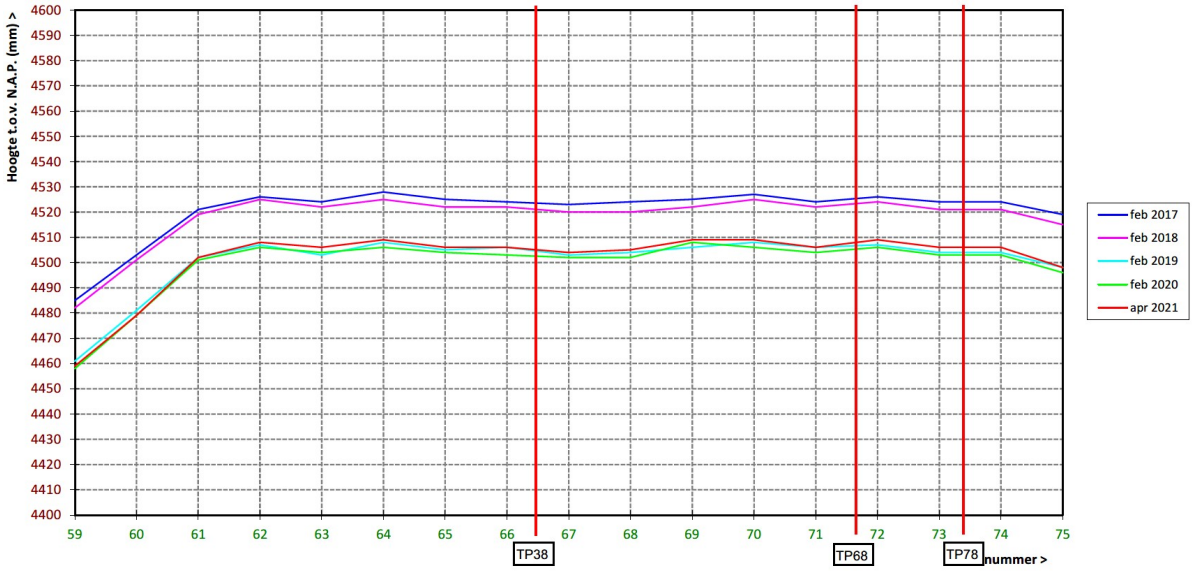

Figure 3.5: Vertical top displacements in mm. The locations of piles 38, 68 and 78 are indicated with red vertical lines. Points 59 and 60 are located in the wall perpendicular to the new wall to connect with the existing wall.

3.2.2. Combining top displacement with inclinometer data

The inclinometer assumes that the deformation at the toe is always zero. This can be true but is most likely not the case. It is expected that there will be a displacement of the toe to the waterside to mobilize the passive resistance. Starting the deformation graph at zero thus results in a top displacement which is not the actual top displacement as it does not imply the toe displacement. For the inclinometer the measurement of 2014 is taken as the reference, and the measurement of 2015 is the first relative deformation measurement. However, the first known relative top displacement is that of 2018, taking 2017 as the reference.

	Point	Feb 2017	Apr 2021	Relative (2021-2017)	
TP38	*66*	180	188	+8	+9.5
	67	190	201	+11	
TP68	*71*	183	189	+6	+8
	72	173	182	+9	
TP78	*73*	171	177	+6	+4.7
	74	159	161	+2	

Table 3.1: Measured horizontal top displacement with respect to a reference line of 2017 and 2021. Values in mm. Positive = to the water

For the three piles, the relative top displacement in X direction is shown in Table 3.1. This is the relative top displacement of 2017 until 2021. This value, together with the displacement from 2014 to 2017 ($X_{2014-2017}$), the toe displacement (X_{Toe}) and the displacement between April 2021 and January 2022 ($X_{2021-2022}$) should result in the deformation at the top according to the inclinometer. The absolute and relative inclinometer results for TP38 are shown in Figure 3.6, so a relative top displacement of 25 mm. The 9.5 mm from Table 3.1 is a part of this, together with the other unknown displacements:

$$25 = X_{2014-2017} + 9.5 + X_{2021-2022} + X_{Toe}$$

Unfortunately, this means that the toe displacement is still unknown.

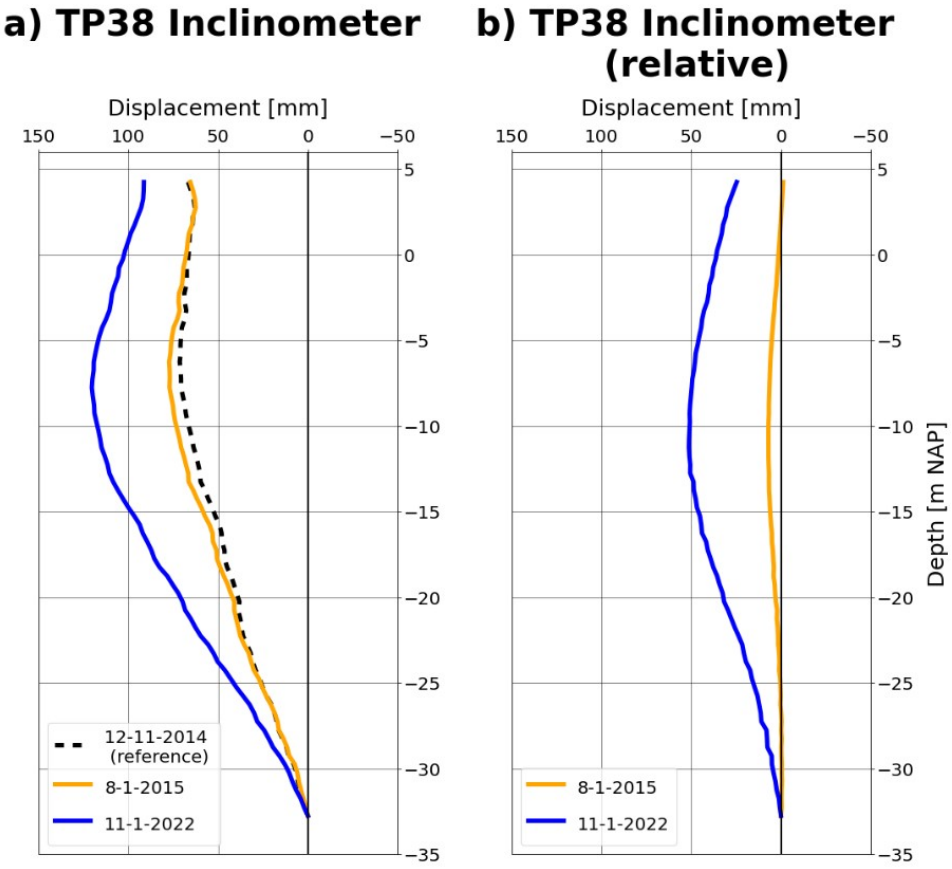

Figure 3.6: Measured deformations for TP38. A positive displacement means displacement to the waterside.

The graphs for the other measured points TP68 and TP78 can be found in Appendix B.

3.3. Conclusion

From the inclinometer data only TP38, TP68 and TP78 appeared to have useful data (§3.1.2). The measurement of 2014 is the reference, so the relative deformation in 2015 and 2022 is known by subtracting the reference data. Based on a literature study, the total error is determined as $\pm$6.27 mm over 37.5 m (§3.1.3).

The assumption of zero toe displacement in the inclinometer results in a top displacement that is not the real displacement. Therefore the measurement of top displacement in X-direction should be used. However, this is only known in 2021 relative to 2017 (§3.2.1), while the inclinometer measurement in 2022 is relative to 2014. This means that the value of toe displacement is not known and the top displacement from the inclinometer is probably not the reality (§3.2.2). Measuring the top displacement in X-direction and the inclinometer simultaneously would have prevented this problem.

4

Calculation of quay wall deformation in D-Sheet

This chapter describes the set-up of the model in D-Sheet Piling and compares the resulting deformations with the measured deformations. The model input was given in Chapter 2. Different modelling options will be shown to get a better estimate of the deformations and causes will be given to explain the remaining differences between measurements and computed deformations. This is step 3 of the main methodology.

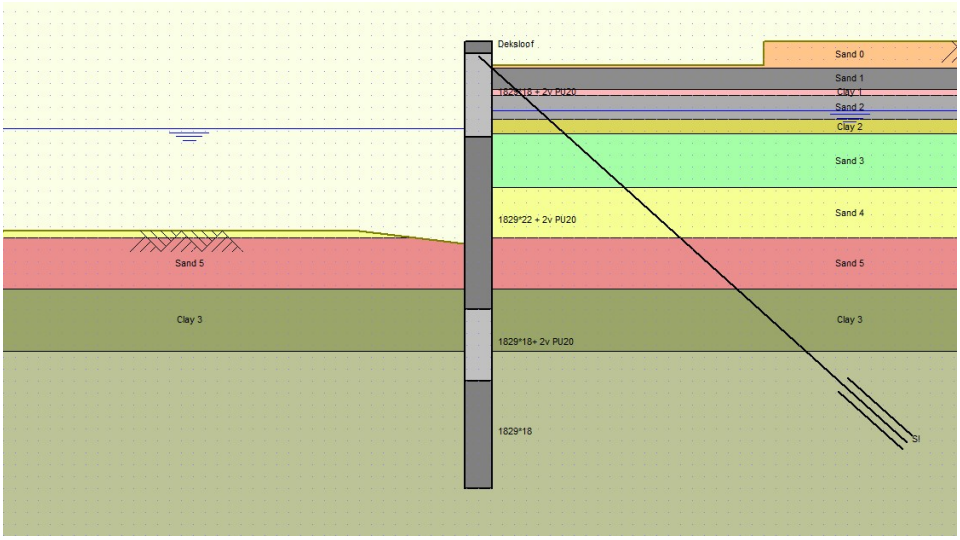

Figure 4.1: Model in D-Sheet Piling

4.1. Modelled stages

Figure 4.2 shows an overview of the modelled stages in D-Sheet Piling. This includes the main construction phases and the moments of doing the inclinometer measurements to get an accurate comparison between the measured and calculated deformations.

Stage	1	2	3	4	5	6	7	8	9	10
Description	Installing combiwall	Fil lto NAP +3.30	Anchoring	Prestressing	Dry excavation NAP -1.65m	Dry excavation NAP -5.00m	Dredged with ship loads	Lowest seawater 1-3-2018	Spudcan	Measurement
Inclinometer	-	-	-	-	12-11-2014	8-1-2015	-	-	-	11-1-2022
Water level										
- left	0.10	0.10	0.10	0.10	-3.00	-5.00	-1.40	-2.83	-1.40	0.03
- right	0.10	0.10	0.10	0.10	-1.80	-1.80	-1.40	-1.30	-1.40	0.03
Surface level										
- left	2.30	2.30	2.30	2.30	-1.65/-2.50	-5.00	-10.90	Sounding 6-4-2018	-19.10	Sounding 18-1-2022
- Right	2.30	3.30	3.30	3.30	+2.50/4.50	+2.50/4.50	+2.50/4.50	+2.50/4.50	+2.50/4.50	+2.50/4.50
Permanent loads										
-Capping beam	x	x	x	x	x	x	v	v	v	v
-Fender and concrete fill	x	x	x	x	v	v	v	v	v	v
Terrain load	x	x	x	x	x	x	v	x	v	x
Bollard load	x	x	x	x	x	x	v	x	x	x
Soil fill load	x	x	x	x	x	x	v	v	v	v
Top load	x	x	x	x	x	x	v	x	v	x
Spudcan	x	x	x	x	x	x	x	x	v	x

Figure 4.2: Overview of modelled stages in DSheet. A green "V" implies that this load is acting in this stage.

4.2. Challenges

Due to the limitations of the model, some adjustments on the input parameters as specified in Chapter 2 are needed.

4.2.1. Modelling the stiffness of the grout anchor

In §2.5.2, the E-modulus for the anchor rod and the grout body is calculated separately. However, in D-Sheet Piling it is only possible to model one anchor with one cross-section and stiffness. Therefore, an anchor is modelled with an equivalent stiffness to the total system. The total stiffness k_{tot} for each anchor is calculated in §2.5.2. This stiffness is applied to the anchors in D-Sheet by modelling an anchor with a cross-section A_{eqq} chosen such that it results in the same k_{tot}, according to the following relation:

$$k_{tot} = \frac{E_{rod} \cdot A_{eqq}}{L} \tag{4.1}$$

Where:

k_{tot}	:	Stiffness of anchor system	[kN/m]
E_{rod}	:	E-modulus of anchor rod (=1.90E08)	[kN/m^2]
A_{eqq}	:	Equivalent cross section	[m]
L	:	Length of modelled anchor (=rod length + 0.5 grout body)	[m]

TP	k_{tot}	L	A_{eqq}	
	[kN/m/m']	[m]	[m^2]	[m^2/m']
38	2.79E+04	48.5	7.11E-03	2.30E-03
68	2.15E+04	52.5	5.94E-03	1.92E-03
78	2.25E+04	48.5	5.72E-03	1.85E-03

Table 4.1: Properties of modelled anchor in D-Sheet

4.2.2. Modelling the relieving platform

In D-Sheet Piling it is impossible to model a relieving platform with bearing piles in D-Sheet Piling. The relieving platform has a width of 24 m, so the soil surface on the landside is lowered to NAP +2.5 m over a length of 24 m in the model. The weight of the platform is not added to the model as surcharge loads, because it is assumed that all the weight is taken by the bearing piles underneath. The disability to model the bearing piles will probably lead to larger calculated deformations than the measured deformations and the results from Plaxis because the shielding effect of the piles can not be taken into account.

4.3. Results

With the input as described in the previous sections, the resulting deformation for the three tubular piles is shown in Figure 4.3. Also, the measured deformations are plotted in this Figure with the range of the measurement error shown in the blue dotted lines. For the measurement in 2022, the range of the measurement error with inclinometer is plotted, which is 6.3 mm over a height of 37.5 m. The plotted measurement and calculation results are all relative values to the reference value in 2014. It will be clearly stated when the total displacement is plotted instead of the relative to 2014.

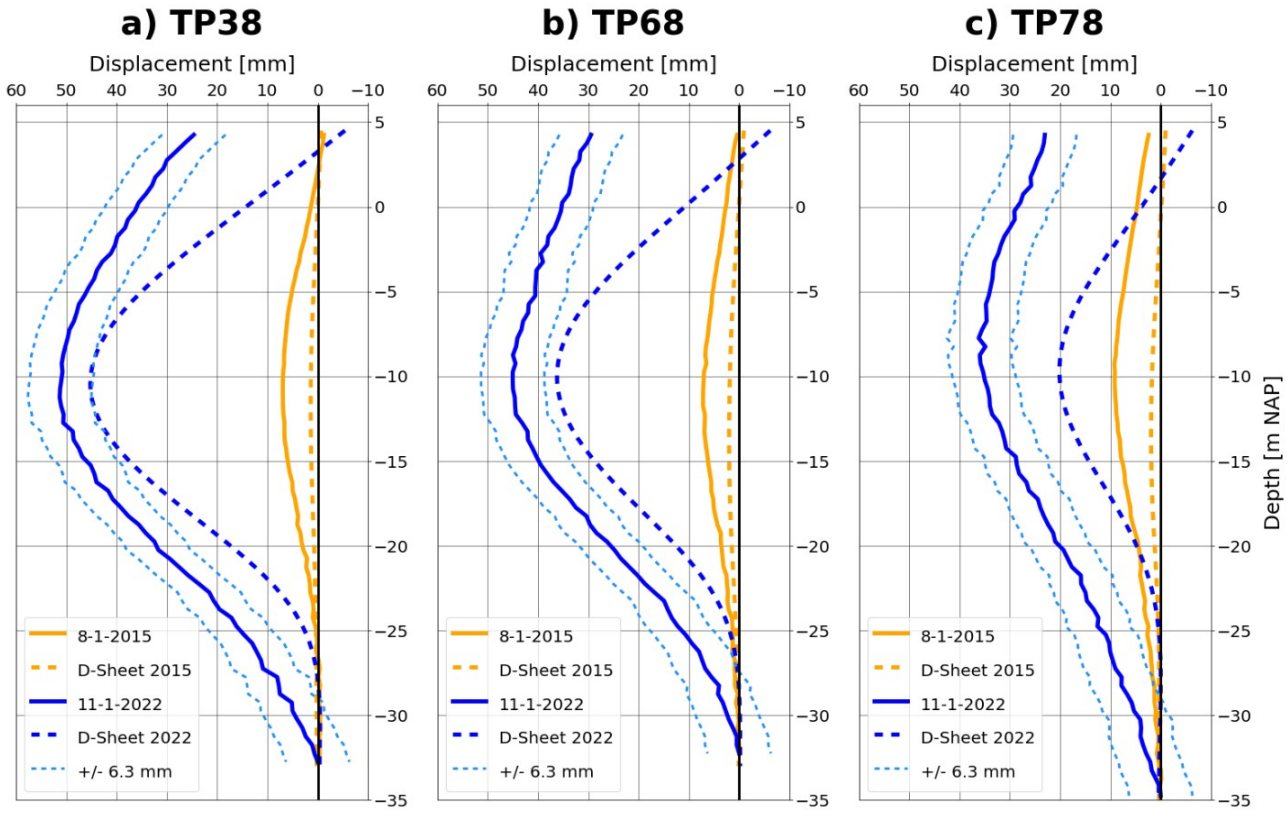

Figure 4.3: D-Sheet deformation results

Looking at the results, some general notes can be made:

- The measured deformation shows a gradual decrease of the maximum field- and top displacement when the tubular pile is located more to the end of the quay wall. TP38 is situated halfway the length of the quay wall and TP68 and TP78 are located at the end of the wall. TP78 is located inside the slope of the embankment perpendicular to the quay wall. This decrease is reasonable because of the reduced loads of spudcans and therefore less disturbance of the harbour bottom.
- The location of the calculated maximum deformation with respect to NAP corresponds with that of the measurements.
- The mismatch between measured and calculated displacements becomes larger for TP68 and TP78 for both the top displacement and the maximum field displacement.
- According to the calculated displacements for 2022, the top displacement is negative. In §3.2.1 it was explained that this can be the case for several reasons. However, between 2014 and 2022 the harbour was excavated which will result in a top displacement to the harbour basin, as the measurements also indicate.

The difference between measurement and calculation is relatively large, especially for the top displacement. With the largest deviation in top displacement of 122% for TP38 and a deviation of 44% in maximum displacement for TP78. Therefore, a model calibration will be done.

4.4. Model calibration

To get a deformation closer to the measured data, several adjustments are investigated. The displacements in 2015 have a maximum of $\pm$ 6-7 mm which is in the same order of magnitude as the error of the inclinometer. Therefore, from here on only the data from 2022 is used for all three tubular piles. The calibration steps involve the adjustment of φ, adjustment of k_h and a change in the modelled stages.

4.4.1. Influence of strain condition on strength parameter φ

Many soil problems involving shear strength, approximate a plain strain condition where the soil can move in one lateral direction. For example earth dams, foundation excavations, retaining walls and strip footings are design problems where the horizontal movement of the soil is only in one direction and restricted in the other direction, so using strength parameters based on plain strain conditions would result in more realistic results. Nowadays, for these plane strain problems the shear strength resistance is still determined with triaxial compression tests. Determining strength parameters with plane strain conditions will result in slightly higher values in some cases, making designs using triaxial conditions even more conservative (Lambe & Whitman, 1991). In the Netherlands, most often the soil parameters are determined using Table 2b from NEN-EN:1997-1 (2012) or Figure 3.22 of CUR166 (2012) with available CPTs where the strength parameters are based on triaxial conditions. Using strength parameters based on plain strain results in a slightly less conservative design, so the use of plain strain parameters becomes only beneficial for projects with large quantities of soil placed, such as earth dams.

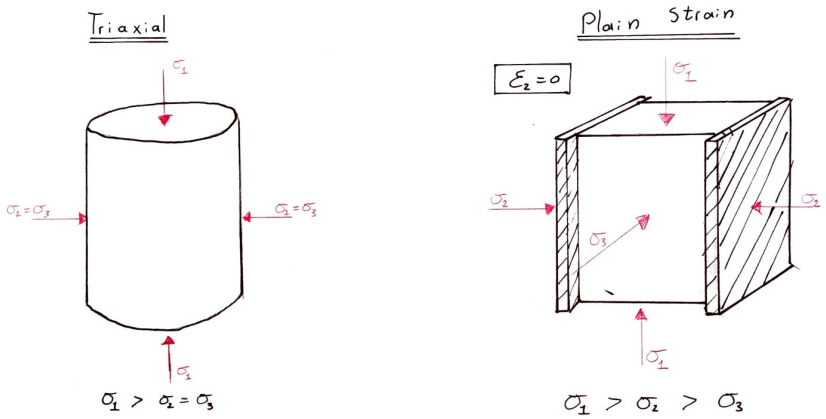

Figure 4.4: Left: Schematisation of a triaxial soil test. Right: Schematisation of plain strain test. σ_1 is the major principal stress which is increased during the test. σ_2 and σ_3 are respectively the intermediate and minor principal stresses (Own work).

In this research, it is important to calculate the deformation with the model input that corresponds the most to reality. The retaining wall is a problem that approximates a plain strain problem, and therefore the strength parameter φ can be more accurate when determined with plain strain tests. Unfortunately, the soil investigation for this project only consists of Cone Penetration Tests. However, Cornforth (1964) did some plain strain and triaxial compression tests for cohesionless soils with varying porosity. He found that the internal friction angle φ in plain strain can be $\frac{1}{2}$ to 4 $^\circ$ higher, depending on the porosity of the soil, see Figure 4.5. The cause for this increased resistance in plain strain conditions is possibly the reduced freedom of soil particles in plain strain tests. One lateral movement direction is fixed, so soil particles have less freedom to overcome the interlocking with the surrounding particles. This also explains that the difference in friction angle increases when the porosity is decreasing.

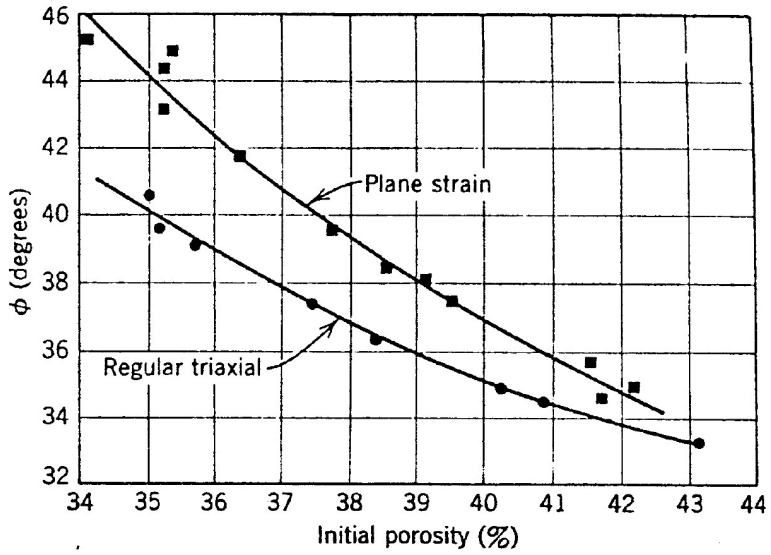

Figure 4.5: Relation between plain strain φ and triaxial φ (Cornforth, 1964).

It is difficult to determine the porosity of the soil with only the CPTs. The relative density can be calculated with empirical formulas using the vertical effective stress and the cone resistance, see Appendix C. However, this is only empirical and determining the porosity e from relative density Re also requires the minimum and maximum void ratio e_{min} and e_{max}, which are unknown:

$$Re = \frac{e_{max} - e}{e_{max} - e_{min}} \tag{4.2}$$

Therefore, in this case, the determined triaxial-φ from Table 2b from NEN-EN:1997-1 is taken as input in the graph of Figure 4.5. The difference between the triaxial-φ and plain strain-φ is only significant for a triaxial-φ of 33° or higher. Only values 35 and 37.5 are used as triaxial values. These values will be adapted to the plain strain conditions according to Figure 4.5:

$$\varphi = 35^\circ \rightarrow 37^\circ \tag{4.3}$$

$$\varphi = 37.5^\circ \rightarrow 40^\circ \tag{4.4}$$

After adjusting the φ for layers with a φ of 35 or 37.5 degrees, the results become as shown in Figure 4.6.

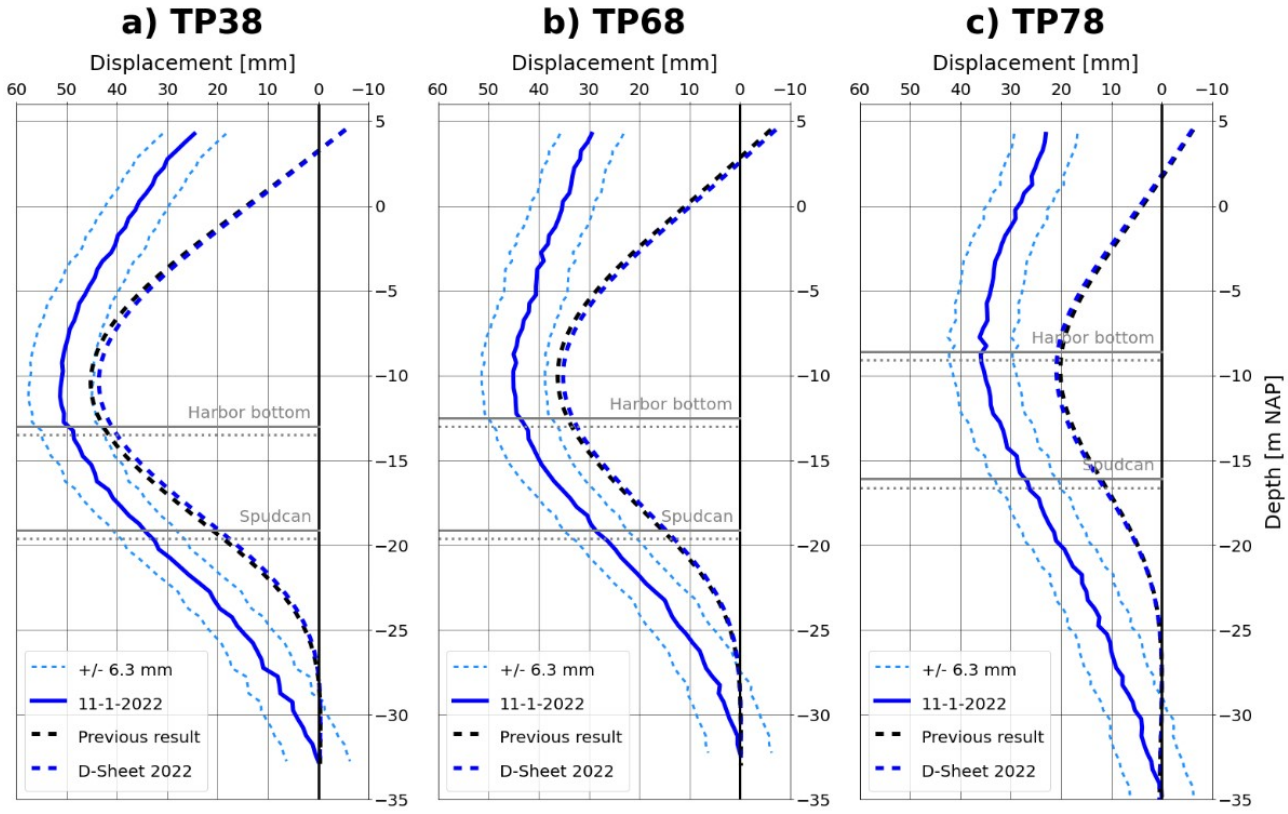

Figure 4.6: DSheet results version 2: After adapting the internal friction angle

Conclusion: For two out of the three cross-sections it increases the deviation from the measurement by approximately 3%, while for the last cross-section the deviation decreases with 1-2%. No conclusion can be made based on these ambiguous results.

4.4.2. Lowering the modulus of subgrade reaction k_h

The modulus of subgrade reaction is determined with Table C.3 from CUR166, see Appendix C. The high and low characteristic values in this table are obtained from various projects with a retaining height of 8-10 m, while the quay wall in Eemshaven has a retaining height of approximately 15 m. The subgrade reaction modulus is more or less inversely dependent on the length of the retaining wall, so the values from Table 3.10 of CUR166 should be divided by 2 in this case (CUR211, 2014). The results of this adaptation are shown in Figure 4.7.

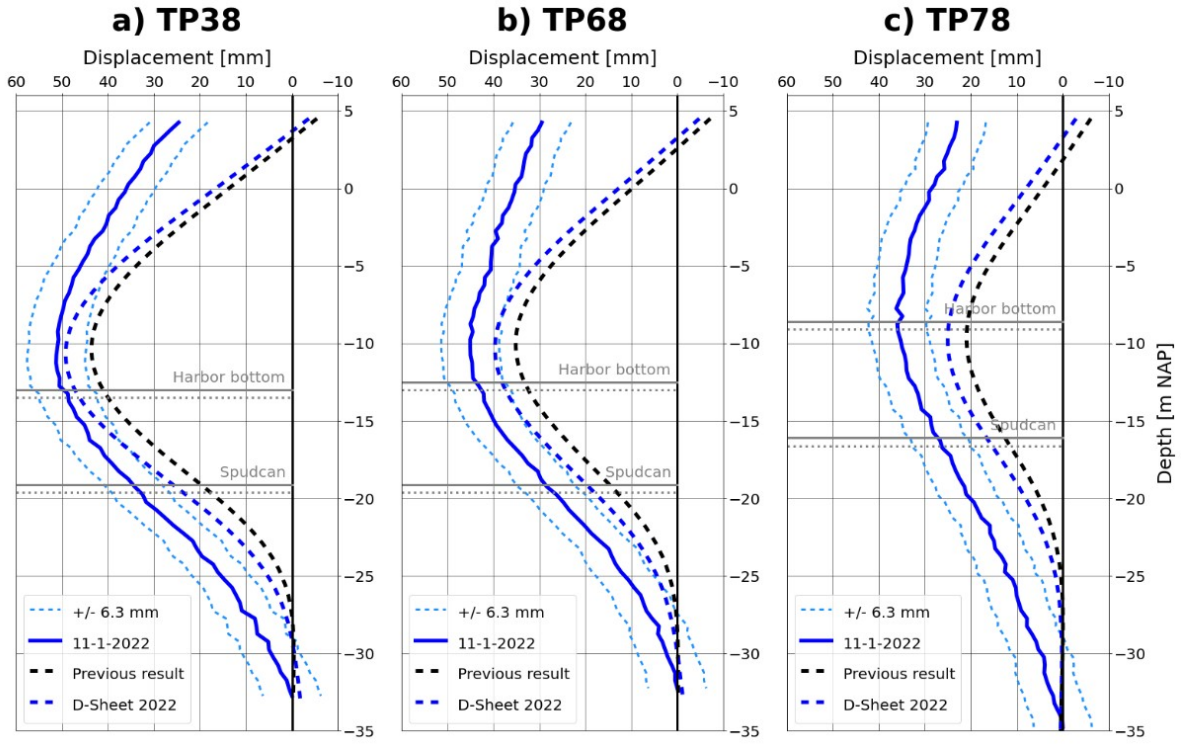

Figure 4.7: DSheet results version 3: After adjusting the modulus of subgrade reaction k_h.

The k_h gives a relation between horizontal soil pressure and displacement, however reducing this parameter with a factor 2, decreases the maximum displacement only with 5 mm, which is 10 to 20% of the maximum displacement. This is because the soil is already in its full active or passive state where the displacement has become independent from the subgrade reaction modulus.

Conclusion: Lowering the subgrade reaction modulus thus results in larger deformations in the final stage. This does improve the model because the deviation from the measurement decreases.

4.4.3. Combining loads on bollards and spudcans

Stage 7 is the stage where the ship loads on the bollards are modelled and stage 9 is the stage where loads of the spudcans are modelled. It is however realistic that loads of these stages occur simultaneously or shortly after each other. The disturbance of the soil after a ship used its spudcan is modelled as a lowered harbour level. Applying the bollard loads with this lowered level results in larger deformations. The result of this model is shown in Figure 4.8.

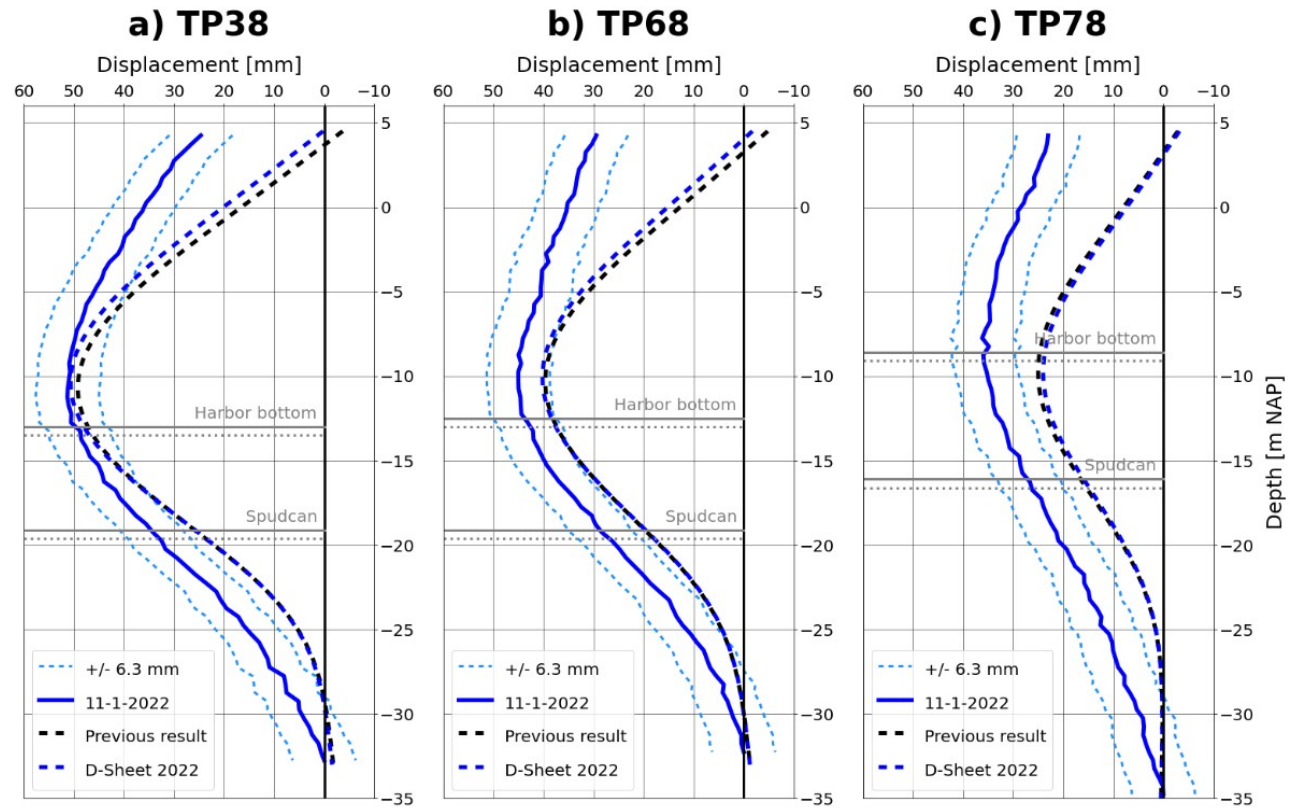

Figure 4.8: DSheet results version 4: After combining the stages of the ship loads with the stage of spudcans

Conclusion: Combining these leads to a reduction of the deviation of 1 to 10% for the cross-section TP38 and TP68. However, it increases the deviation of TP78 by 2.5%. This is probably because the spudcan load is not applied at the end of the quay wall near the shore where TP78 is situated, which can be observed at soundings. Based on these results it can be concluded that this adjustment improves the calculation results for the sections where the spudcan load applies.

No other calibration steps will be done because the large difference in top displacement is probably due to model limitations in D-Sheet. In the following section, some other reasons will be given.

4.4.4. Summary of adaptations

Tables 4.2, 4.3 and 4.4 give an overview of the results of each calibration step compared to the measurement.

TP38		**Top displacement [mm]**			**Max displacement [mm]**		
Version	*Adaptation*	*DSheet*	*Measured*	*Deviation [%]*	*DSheet*	*Measured*	*Deviation [%]*
1	-	-5.4	24.6	122.0	45.2	51.3	11.9
2	Plain Strain φ	-5.4		122.1	43.6		15.0
3	Lowering k_h	-3.7		115.0	49.2		4.1
4	Combining stages	0.2		99.1	50.7		1.3

Table 4.2: Overview of adaptations TP38

TP68		Top displacement [mm]			Max displacement [mm]		
Version	*Adaptation*	*DSheet*	*Measured*	*Deviation [%]*	*DSheet*	*Measured*	*Deviation [%]*
1	-	-6.2	29.5	121.0	36.2	45.0	19.6
2	Plain Strain φ	-7.2		124.3	35.1		22.0
3	Lowering k_h	-4.8		116.2	39.7		11.9
4	Combining stages	-1.7		105.8	40.2		10.7

Table 4.3: Overview of adaptations TP68

TP78		Top displacement [mm]			Max displacement [mm]		
Version	*Adaptation*	*DSheet*	*Measured*	*Deviation [%]*	*DSheet*	*Measured*	*Deviation [%]*
1	-	-6.3	23.0	127.4	20.1	36.2	44.4
2	Plain Strain φ	-6.1		126.5	20.9		42.2
3	Lowering k_h	-2.9		112.6	25.0		30.9
4	Combining stages	-3.2		114.0	24.0		33.7

Table 4.4: Overview of adaptations TP78

From these results, it becomes clear that the adaptation of the φ (version 2) results in a larger relative deviation than the reference (version 1) for all three cross sections. The second adaptation (version 3), lowering the k_h, results in smaller deviations from the measurements for both the top displacement and the maximum displacement. Also the last adaptation (version 4) results in a smaller deviation from the measurements, but not for the last cross-section TP78, which is at the end of the quay wall and near the shore.

The shear forces and bending moments of this calibrated model are shown in Appendix F.

4.5. Causes of difference between calculation and measurements

Some causes for the mismatch will be investigated in this section.

4.5.1. Addition of the anchor test stage

Before prestressing, the anchors were tested with the maximum design load after installation of the anchor while recording the elongation and shortening of the anchor. This test was done to verify that the grout body gives enough resistance. After the design load, the force is reduced to the initial load and prestressed to the prescribed level. The resulting force-displacement diagram for anchor 68 is shown in Figure 4.9 as an example. The force-displacement diagrams for anchors 38 and 78 can be found in Appendix E.

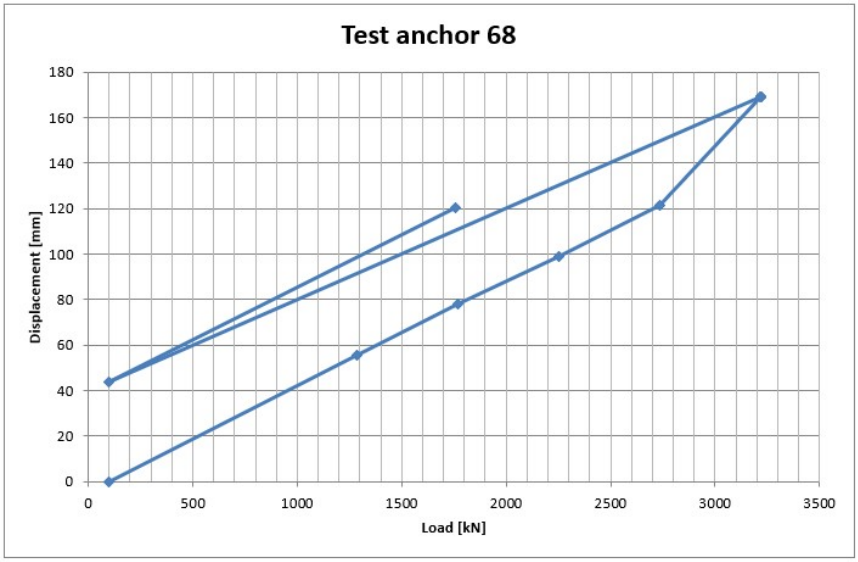

Force [kN]		Displacement [mm]
Pi	100	0
0.4Pd	1288	55.54
0.55Pd	1770	77.89
0.7Pd	2253	98.9
0.85Pd	2736	121.2
Pd	3219	168.89
Pd	3219	168.89
Pd	3219	168.89
Pd	3219	168.94
Pd	3219	169.09
Pi	100	43.54
Pprestr.	1756	120.39

Figure 4.9: Force-displacement diagram from the anchor test for anchor 68. Test performed by Geotech Foundation Solutions (2014).

Usually, this testing of the anchor is not modelled as a separate stage in D-Sheet Piling like the pre-stressing stage, but it might give an improvement of the calculated deformations considering the possible yielding of the anchor in this stage. Unfortunately, it is only possible to model the anchor with a linear elastic perfectly plastic model where the anchor reacts either plastic or elastic, see Figure 4.10. The maximum design load of 3219 kN used in the tests is lower than the yielding point modelled in DSheet, so DSheet will not give a plastic deformation of the anchor.

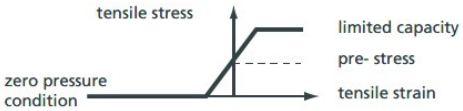

Figure 4.10: Stress-strain diagram of anchor in DSheet (Deltares, 2017)

However, the anchor tests also have an impact on the soil behind the combined wall. When the anchor test is modelled as a separate stage in DSheet, the passive zone at the anchor point is fully mobilised, meaning that there is plastic deformation of the soil, see Table 4.5. When the anchor in the next step is unloaded and prestressed to 1756 kN, some plastic deformation is still visible. This means that the model with the added anchor test stage results in a larger top displacement landwards after the prestressing than the model without the added stage.

Node number	Level	Left				Right			
	[m]	Effective Stress [kN/m²]	Water stress [kN/m²]	Stat*	Mob** [%]	Effective Stress [kN/m²]	Water stress [kN/m²]	Stat*	Mob** [%]
1	4,50	0,00	0,00	-		0,00	0,00	-	
1	4,00	0,00	0,00	-		0,00	0,00	-	
2	4,00	0,00	0,00	-		0,00	0,00	-	
2	3,50	0,00	0,00	-		0,00	0,00	-	
3	3,50	0,00	0,00	-		0,00	0,00	-	
3	3,30	0,00	0,00	-		0,00	0,00	-	
4	3,30	0,00	0,00	-		0,00	0,00	P	
4	3,00	0,00	0,00	-		38,63	0,00	P	
5	3,00	0,00	0,00	-		38,63	0,00	P	
5	2,50	0,00	0,00	-		101,95	0,00	3	99
6	2,50	0,00	0,00	-		101,95	0,00	3	99
6	2,30	0,00	0,00	-		117,69	0,00	3	91

Table 4.5: Soil reaction of DSheet in the stage of anchor test. The anchor is at NAP +3.30m.

The effect of this larger displacement landwards during prestressing on the deformation in the final stage can be investigated by adding this test stage before the prestressing stage in the D-Sheet model. However, these tests were not done on all anchors simultaneously so adding this stage in the 2D model D-Sheet will not represent the reality. The effect of adding this stage can be investigated in a 3D model but is not included in this 2D model.

4.5.2. Effect of pile driving on soil characteristic

Some extra CPT tests were done after the installation of the combined wall at the exact location of earlier CPTs in 2012. This makes it possible to compare these tests to investigate whether pile driving had a significant effect on loosening or compacting the soil. The extra CPTs were done in front of the combined wall approximately one month after installation. One was done near TP38 at a distance of 7.5 m normal to the wall. Another was done between TP68 and TP78 at a distance of 2.5 m normal to the wall. There are not very large differences in the CPTs. Some differences at the top layers can be observed, but these are probably due to construction activities. The only difference can be seen between the CPTs between TP68 and TP78, where the cone resistance dropped from 15 to 5 MPa between NAP -21.0 m and NAP -24.0 m, see Figure 4.11. The complete CPTs can be found in Appendix C.3.

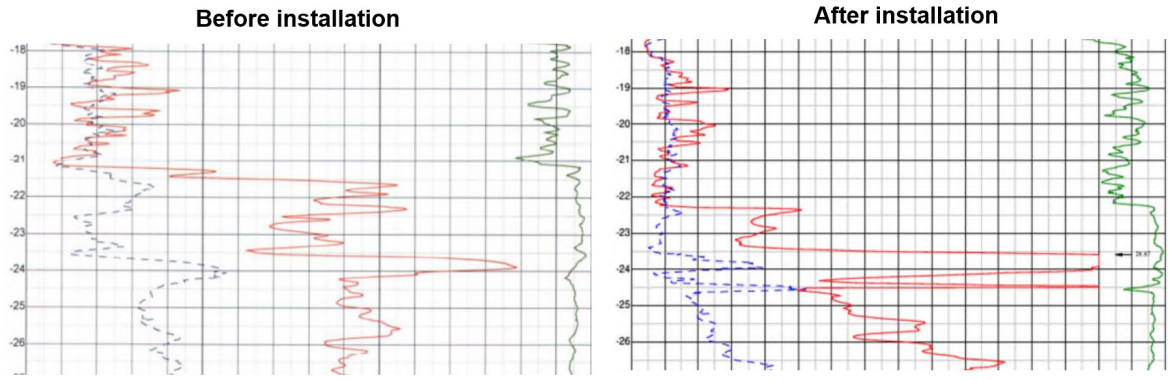

Figure 4.11: Part of CPT's before and after installation of tubular piles at a distance of 2.5 m perpendicular to the combined wall. Between TP68 and TP78. *Left:* Before installation *Right:* One month after installation

The soil parameters used in the model DSheet are from CPTs before the installation of the piles, so it could be that the loosening of this small layer causes larger deformations than the calculated ones. This effect would be especially above the toe which is at NAP -33.00 m. The fact that this loosening is only found around TP68 and TP78 can, to some extent, explain that the deviation of the calculations from the measurement is larger for these tubular piles than TP38. It should be noted that the normal distance of 7.5 m for TP38 is too large for witnessing possible loosening or compacting of the soil. It is however possible that the loosening found at TP68 and TP78 also occurred at other places along the wall.

4.5.3. Using apparent tendon free length L_{app}

In the unloading stage after the maximum design load is reached in the anchor tests, the apparent tendon free length L_{app} is calculated to ensure that the fictitious fixed anchor point is outside the active zone and within the grout body. If L_{app} is too short, the transfer of the load between anchor and soil is within the active slip surface that is moving when the retaining structure is moving horizontally. Therefore, an upper limit and a low limit are prescribed:

$$L_{app;lower} = 0.8 \cdot L_{tf} \tag{4.5}$$

$$L_{app;upper} = L_{tf} + 0.5 L_{tb} \tag{4.6}$$

The apparent anchor length is calculated with:

$$L_{app} = \frac{\Delta l \cdot EA}{P_d - P_i} \tag{4.7}$$

Where:

L_{app} : Apparent tendon free length
L_{tf} : Tendon free length
L_{tb} : Tendon bond length
Δl : Elongation of the anchor
EA : Normal stiffness of the anchor
P_d : Maximum design load of the anchor
P_i : Initial load during the anchor test

The calculated apparent tendon free lengths are listed in Table 4.5. The total length and grout length is different for each anchor.

Anchor	Total length L_{tot}	Grout length L_{tb}	Free length L_{tf}	Lower limit	L_{app}	Upper limit
38	56.00	18.00	38.00	30.40	39.52	47.00
68	60.00	15.00	45.00	36.00	52.04	52.50
78	56.00	15.00	41.00	32.80	42.15	48.50

Table 4.5: Apparent tendon free length

Using this calculated length might improve the resulting deformations. However, the L_{app} is determined with the tests that are done before the excavation started. With the excavation, the anchor force increases and the L_{app} also increases. The exact value of L_{app} is unknown, but it is assumed in the model that the anchor length is until halfway the grout body. When the load is increasing after excavation it might be possible that this assumption is not correct, especially for anchor 68, where the free tendon length already is at the upper limit, see Figure 4.12. When the real L_{app} is larger, this would result in a less stiff anchor and the calculated deformations thus might underestimate the deformations. Especially the top deformations.

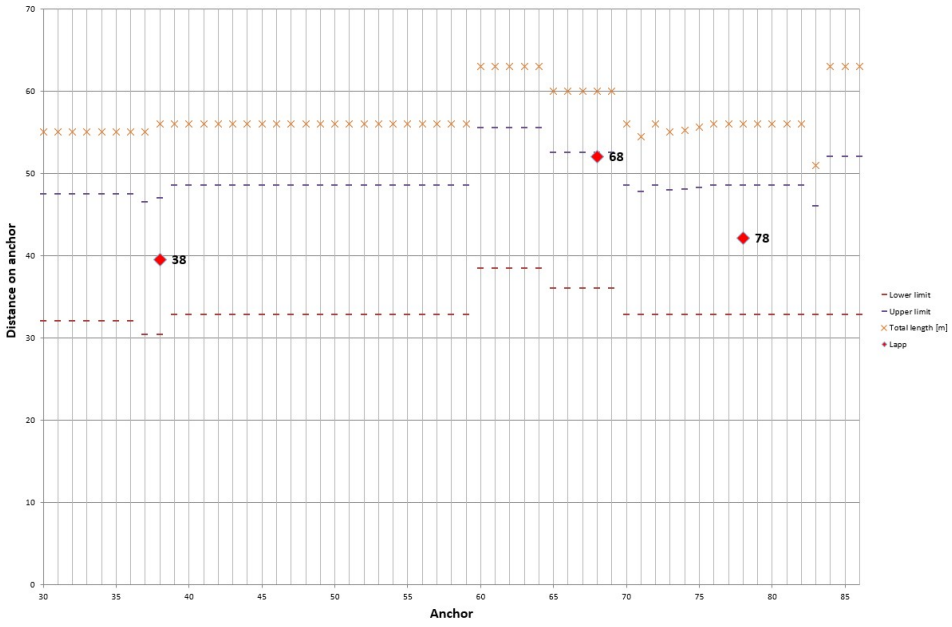

Figure 4.12: Apparent free tendon length of anchors 38, 68 and 78

4.5.4. Slipping of anchor

The minimum grip force of the anchors is calculated to investigate whether the testing of the anchor to the design load could have led to possible slipping of the anchor. The minimum grip force is calculated according to CUR166 part 2 (2012):

$$F_{r;A;gr;min} = \alpha_t \cdot q_{c;avg} \cdot O \cdot L_A \tag{4.8}$$

Where:

$F_{r;A;gr;min}$	:	Minimum grip force of the screw grout anchor
α_t	:	Friction factor (=1.5%)
$q_{c;avg}$	:	Average cone resistance in the embedded part of the grout body (=15 MPa)
O	:	Circumference of the grout body (D = 370 mm)
L_A	:	Length of the grout body (= 15m)

The friction factor of 1.5% is prescribed by the CUR166 and verified with anchors that were installed and tested at the construction site. This results in:

$$F_{r;A;gr;min} = \alpha_t \cdot q_{c;avg} \cdot O \cdot L_A = 0.015 \cdot 15 \cdot 10^3 \cdot \pi \cdot 0.370 \cdot 15 = 3923\text{kN} \tag{4.9}$$

This is much larger than the 3219 kN that was used in the tests. It can thus be concluded that it is not very reasonable that the anchor slipped significantly, although the grout body will move slightly with regard to the soil in order to develop body friction and mobilise the shear.

4.5.5. Construction of RoRo jetty

Recently, the construction of a RoRo jetty for the Holland Norway Lines started. This jetty is constructed at the end of the constructed quay wall, see Figure 4.13. The ferries can berth parallel to the quay wall and can load and unload with a floating bridge at the front of the ship, see Figure 4.14. This floating bridge was placed in March 2022 and the first departure of the ferry was in April 2022.

Figure 4.13: Top view of RoRo Holland Norway Lines (Boertjens, 2022)

Figure 4.14: RoRo bridge (Boertjens, 2022)

It is possible that the construction of this jetty made it necessary to excavate at the end of the quay wall. This then would explain the relatively large mismatch between the measurements and the calculated deformation with DSheet for TP68 and TP78. However, it is not known whether this excavation was done and whether it was done before or after the measurement date of 22-1-2022.

4.5.6. Modelling relieving platform in DSheet

From the calculated deformations, it is remarkable that the top displacement appears to be to the land side. This is unlikely because of the stiff relieving platform at 1 meter below ground level. Unfortunately, it is not possible to model this properly in DSheet. It is possible in DSheet to create a fixed point at the level of the platform, but this also prevents the movement of the wall to the waterside. The reality is that the platform does prevent movement to the land side, and does nothing when the wall is moving to the waterside because the capping beam and the platform are not connected. This disability of the model is possibly the main reason why the deformations at the top do not correspond with the measured ones.

4.5.7. Uncertainty in measurements

The previously mentioned causes are all related to the way of modelling and model input. However, not all differences can be related to the model. Based on literature it was concluded that this uncertainty has a range of $\pm$6.5 mm (§3.1.3). On top of that also the toe displacement is assumed to be zero in the measurement, which is probably not the case. This can be the reason for the mismatch at the toe.

4.6. Conclusion

The D-Sheet model including the adaptations in the calibration gives a good approximation of the deformations of TP38 with a relative deviation of the maximum deformation at NAP -10.70 m of 1.3%. Large parts of the curve lie within the range of the measurement error. This is not the case for TP68 and TP78 where the deviation of the maximum displacement at NAP -9.50 m is 10 to 34%. For all three piles, the top displacement is strongly deviating from the measured one. This deviation is for all three from 100 to 114%. The calculated top displacement is in many cases also negative, meaning that the top would be moving to the land side and pushing the relieving platform. Possible causes of the large deviation of the maximum deformation for TP68 and TP78 are the small effect of the pile driving on the soil (§4.5.2) or the construction and use of the RoRo jetty at this location(§4.5.5).

The disability of modelling the relieving platform properly in DSheet (§4.5.6) and not using the apparent tendon length (§4.5.3) can be the cause of the mismatch of the top displacement. The mismatch above the toe is probably because the toe displacement is not zero as assumed in this case (§4.5.7).

5

Calculation of quay wall deformation in Plaxis

This chapter describes the set-up of the model in Plaxis and compares the resulting deformations with the measured deformations. This is step 4 of the main methodology. First, the soil models will be selected based on literature. After that, the model input is specified. The resulting deformations are then compared to the measurements and the model will be calibrated.

5.1. Soil model selection for FEM

The available soil models are listed shortly below. After that, the applicability will be discussed.

5.1.1. Available soil models

The main soil models available in Plaxis are listed below (Bentley Advancing Infrastructure, 2022):

- **Linear Elastic model (LE):** The Linear Elastic model is the simplest available stress-strain relation and is based on Hooke's law of isotropic elasticity. Only two input parameters are needed, namely Young's modulus E and the Poisson ratio ν. This simple model is not accurate enough to describe the complex behaviour of soil, but it can be used to model stiff volumes such as concrete walls or bedrock.
- **Mohr-Coulomb model (MC):** The Mohr-Coulomb model is the linear elastic perfectly plastic model which is an extension of the Linear Elastic model. Additional input parameters needed to describe the plasticity are the internal angle of friction φ and the cohesion c. Also the angle of dilatancy ψ should be known. With this model it is possible to use a constant stiffness for the whole soil layer or a stiffness that increases linearly in depth. The Mohr-Coulomb model with a constant stiffness can be a fast first estimate of the expected deformations.
- **Hardening Soil model (HS):** The Hardening Soil model is a further advanced model compared to the Mohr-Coulomb model. The plastic limiting states described with the friction angle φ , cohesion c and dilatancy angle ψ are the same, but the soil stiffness is described with three different Young's Modules for three different types of loading. The stiffness is described with the triaxial loading stiffness E_{50}, the triaxial unloading stiffness E_{ur} and the oedometer stiffness E_{oed}.
  In addition, the model also accounts for stress-dependency of the stiffness meaning that all stiffnesses increase with pressure. Therefore, the three input parameters relate to a reference stress, which is usually 100 kPa. Also pre-consolidation can be taken into account in the initial stress generation.
- **Hardening Soil model with small-strain stiffness (HSsmall):** This model is a modification of the Hardening Soil model that accounts for the increased stiffness of soils at small strains. At low strain levels, most soils exhibit a higher stiffness than at engineering strain levels. The relation between stiffness and strain at this low level is also non-linear. This behaviour is described with two additional material parameters. G_o^{ref} is the small-strain shear modulus and $\gamma_{0.7}$ is the strain

level at which the shear modulus has reduced to 70% of the G_0^{ref}. This modification can be useful in dynamic applications to introduce hysteretic material damping.

- **Soft Soil model (SS):** The Soft Soil model is especially meant for compression of near normally-consolidated clay-type soils. The Hardening Soil model has most of its model capabilities, but the Soft Soil model is more capable to model the primary compression behaviour of soft soils.
- **Soft Soil Creep model (SSC):** This model is a modification of the Soft Soil model where the creep and stress relaxation can be taken into account. With this modification, also secondary compression can be modelled which is important for soft soils such as normally consolidated clays, silts and peat. As for the Hardening Soil Model, initial condition can be used to take into account the amount of consolidation.
- **Modified Cam-Clay model (MCC):** This model is added to PLAXIS because this is a well-known model from international soil modelling literature. It is meant to model near normally-consolidated clay soils.

5.1.2. Applicability of the soil models

As mentioned above, the Mohr-Coulomb model can only be used to get a first estimate but is not accurate enough to make a good comparison between FEM and methods such as D-Sheet and Blum which this research is about. A more advanced soil model is needed.

In general, a soil model is better as more aspects of soil behaviour are included in the model. Some of these aspects are specific to soft soils and some are more specific to stiff soils, which makes it a more advanced model. The Hardening Soil (HS), HSsmall, Soft Soil and Soft Soil Creep are the advanced models that can be applicable to model the quay wall in sandy and clayey layers. To choose between these four models, it is important to look at whether the model is able to describe the soil behaviour along the stress path that is followed (Brinkgreve, n.d.).

The Soft Soil model is a model that is applicable for weak soils, but not for every stress path. In unloading situations, the model behaves fully elastic which is the same as described in the Mohr-Coulomb model. Therefore, this model has no advantages when used in unloading situations. This also applies to situations where the deviatoric stress is increasing and the mean effective stress is decreasing, which is the case in excavation situations. This limitation of modelling in this stress path also applies to the Soft Soil Creep model. However, this model is able to include time-dependent behaviour. It therefore becomes a consideration which aspect is more important, the time-dependent behaviour or the correct modelling of the soil along the stress path.

The Hardening Soil model is an advanced model that does perform well for excavation problems. With the ability to input three different stiffnesses, it is possible to control the soil stiffness in different stress paths. The Hardening Soil model with small strain (HSsmall) results in an even more realistic deformation of the soil behind the quay wall as it is possible to model the high stiffness in the range of small strains (Brinkgreve, n.d.).

5.1.3. Selection of soil model

The determined soil characteristic shows that there are sand layers (stiff) and clay layers (soft). Based on the information about soil models in §5.1.1 and §5.1.2, a flow chart is made in Figure 5.1 to choose the right soil model.

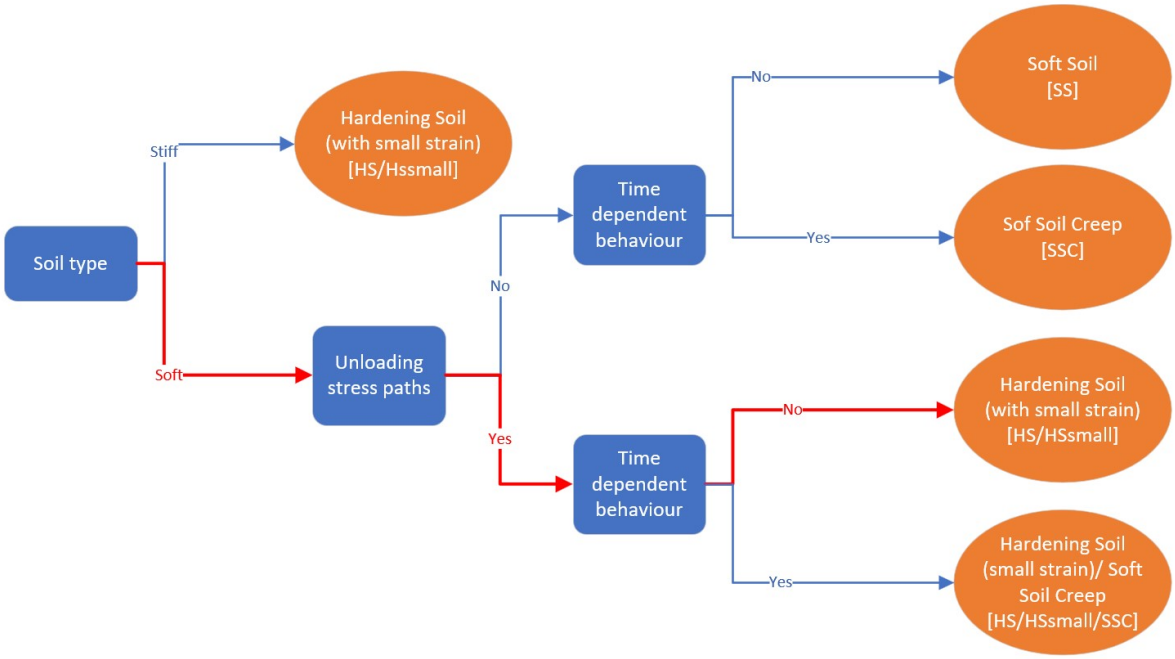

Figure 5.1: Flow chart of soil models in Plaxis. The red line represents the decisions on the soil model that is used.

The excavation problem is a situation where unloading and reloading stress paths change over time and in different regions. Therefore, the Hardening Soil with small strain is the most suitable model to use for both clay and sand layers. It is thereby assumed that the correct modelling of the clay in unloading stress paths is more important than including the time-dependent behaviour.

5.2. Model input

The model input is the same as the input in D-Sheet as described in Chapter 2. However, some additional parameters are needed regarding the relieving platform and the soil model that is used.

5.2.1. Relieving platform

The concrete platform and the 1 meter fill above are modelled with a linear elastic soil model with $E =$ 28 GPa and $\nu = 0.15$ for concrete. The soil fill above is divided into two layers. A layer of granulate with $E = 4$ GPa and $\nu = 0.20$ and a top layer of Asphalt/CTB with $E = 5$ GPa and $\nu = 0.20$. The concrete platform and the two layers on top are connected to the combined wall with interface elements.
The Terr-econ injection piles supporting the platform are modelled as embedded beams with a centre-to-centre distance of 3.09 m. The concrete platform is implemented as a polygon cluster structure, which makes it difficult to connect the embedded beams with the platform. Therefore, an elastic plate with very low stiffness is inserted on the bottom of the platform where the connection with the embedded beams takes place, see Figure 5.2. This low stiffness ensures that this plate will follow the deformations of the platform and does not affect the deformation of platform and piles.

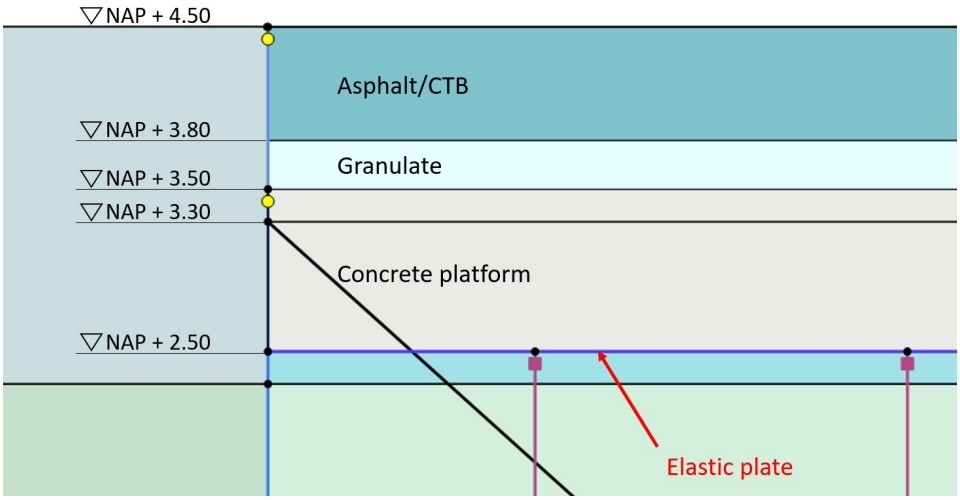

Figure 5.2: Detail of connection piles-platform and connection wall-platform

5.2.2. Additional soil parameters

Some additional soil parameters are needed for the modelling in a FEM with Hardening Soil small strain:

- ψ: Dilatancy angle. For quartz sands, the dilatancy angle can be estimated with $\psi = \varphi - 30$ (Bentley Advancing Infrastructure, 2022). For clays, the dilatancy angle is zero. Great care must be taken when using the drainage type Undrained(A) together with a positive dilatancy angle. This results in unlimited soil strength due to the generation of tensile pore pressures.
- R_{int}: Wall friction reduction factor. According to the Plaxis Reference (2022), this in the order of 2/3. Gouw (2014) specified this parameter more specifically per soil type: $R_{int} = 0.7$ for sand-steel interaction and $R_{int} = 0.5$ for a clay-steel interface. This factor results in a decreased strength and stiffness of the interface.
- m: Power for stress-level dependency of stiffness. Assumed 0.5 for sand and 1.0 for clays (Gouw Dr, 2014).
- E_{50}^{ref}: Secant stiffness in standard drained triaxial test. The secant stiffness modulus E_{50}^{ref} is defined for a reference minor principal effective stress of $p^{ref} = 100$ kPa (Bentley Advancing Infrastructure, 2022). The E_{100} from Table 2b (NEN-EN:1997-1, 2012) can be taken for this parameter as the E_{100} is also defined for an effective vertical soil stress of 100 kPa.
- E_{oed}^{ref}: Tangent stiffness for primary oedometer loading. The ratio $E_{50}^{ref}/E_{oed}^{ref}$ is equal to 1 for sand and 1.25 for clays (Bentley Advancing Infrastructure, 2022).
- E_{ur}^{ref}: Unloading/reloading stiffness from drained triaxial test. According to (Gouw Dr, 2014), the unloading/reloading stiffness can be 2 -5 times the E_{50}^{ref}. The default factor 3 according to PLAXIS is used.
- ν_{ur}: Poissons ratio for unloading-reloading. In the Hardening Soil small strain, this parameter is an elastic parameter which lies between 0.1 and 0.2, (Bentley Advancing Infrastructure, 2022). An average value of 0.15 is used.
- G_0^{ref}: Reference shear modulus at very small strains. This parameter is obtained from a relation between the static Young modulus E_s and dynamic Young modulus E_d, see Figure 5.3. Where the E_s is equal to the E_{ur} and E_d can be seen as the E_0 at very small strain. The shear modulus G_0^{ref} is calculated using the relation:

$$G_0 = \frac{E_0}{2(1+\nu_{ur})} = \frac{E_0}{2.3} \tag{5.1}$$

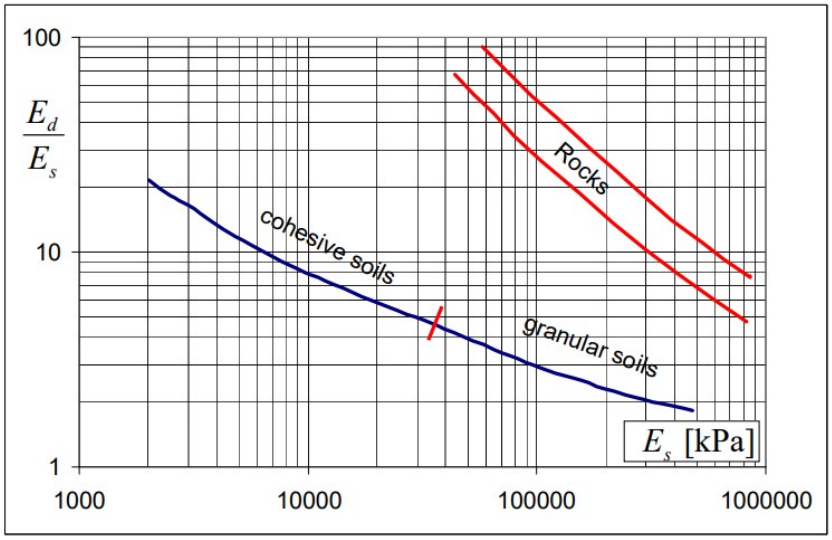

Figure 5.3: Relation between static Young modulus E_s and dynamic Young modulus E_d (Truty, 2008)

- $\gamma_{0.7}$: Threshold shear strain at which the secant shear modulus $G_s = 0.722G_0$. This is calculated with the following formula (Bentley Advancing Infrastructure, 2022):

$$\gamma_{0.7} = \frac{1}{9G_0^{ref}}[2c'(1 + cos(2\varphi')) - \sigma'(1 + K_0)sin(2\varphi') \tag{5.2}$$

All additional parameters for each soil layer are listed in Table 5.1 for TP38. The parameters for TP68 and TP78 are given in Appendix C.4.

Layer	φ [◦]	ψ [◦]	E_{oed}^{ref} [Mpa]	E_{50}^{ref} [Mpa]	E_{ur}^{ref} [Mpa]	m [-]	R_{int} [-]	E_0/E_s [-]	G_0^{ref} [Mpa]	K_0 [-]	σ' [kPa]	$\gamma_{0.7}$ [-]
Sand 0	32.5	2.5	62.5	62.5	187.5	0.5	0.7	2.3	187.5	0.46	7.31	5.7E-06
Sand 1	37.0	7.0	77.5	77.5	232.5	0.5	0.7	2.1	212.3	0.43	33.88	2.4E-05
Clay 1	25.0	0.0	5.6	7.0	21.0	1	0.5	6	54.8	0.58	60.39	2.3E-04
Sand 2	27.5	0.0	32.5	32.5	97.5	0.5	0.7	3	127.2	0.54	72.64	8.0E-05
Clay 2	25.0	0.0	6.0	7.5	22.5	1	0.5	5.6	54.8	0.58	88.89	3.1E-04
Sand 3	37.0	7.0	77.5	77.5	232.5	0.5	0.7	2.1	212.3	0.43	117.64	8.3E-05
Sand 4	32.5	2.5	62.5	62.5	187.5	0.5	0.7	2.3	187.5	0.46	159.27	1.3E-04
Sand 5	27.5	0.0	22.2	22.2	66.7	0.5	0.7	3.5	101.5	0.54	199.64	2.8E-04
Clay 3	21.3	0.0	4.8	6.0	18.0	1	0.5	6.5	50.9	0.64	237.95	6.4E-04
Sand 6	37.0	7.0	77.5	77.5	232.5	0.5	0.7	2.1	212.3	0.43	337.52	2.4E-04

Table 5.1: Additional soil parameters Plaxis for TP38

5.3. Results

The resulting deformed mesh in the final stage is shown in Figure 5.4 and the calculated deformation of the combined wall is plotted in Figure 5.5 together with the inclinometer measurement of 2022.

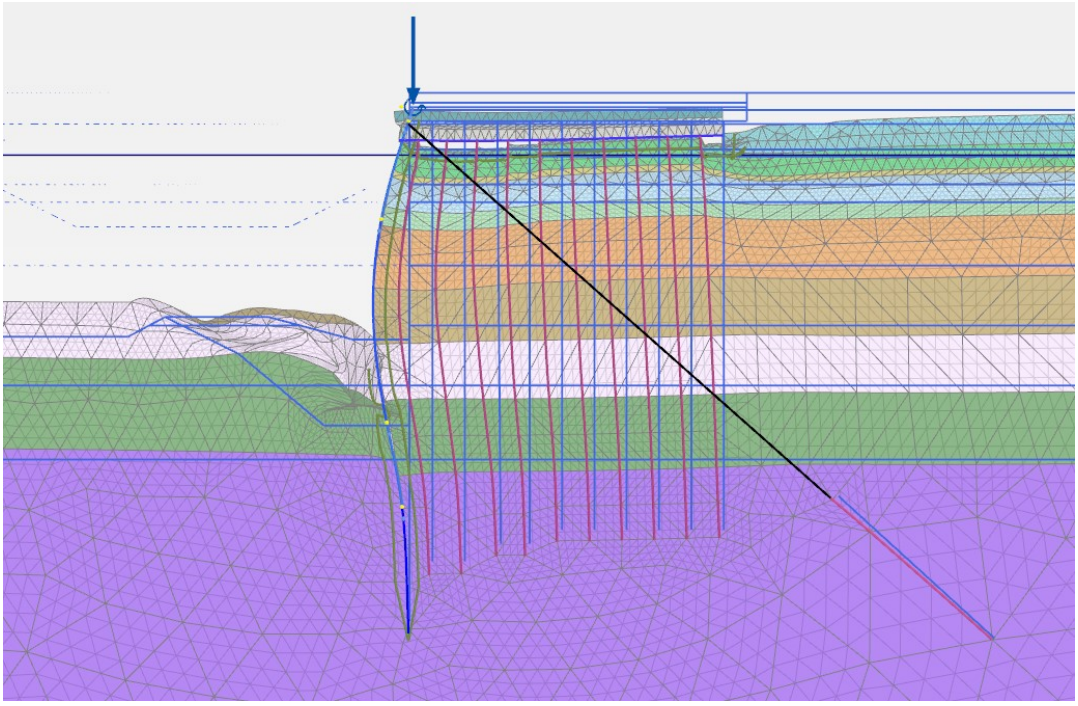

Figure 5.4: Deformed mesh for TP38 in final stage. Scaled up 50 times

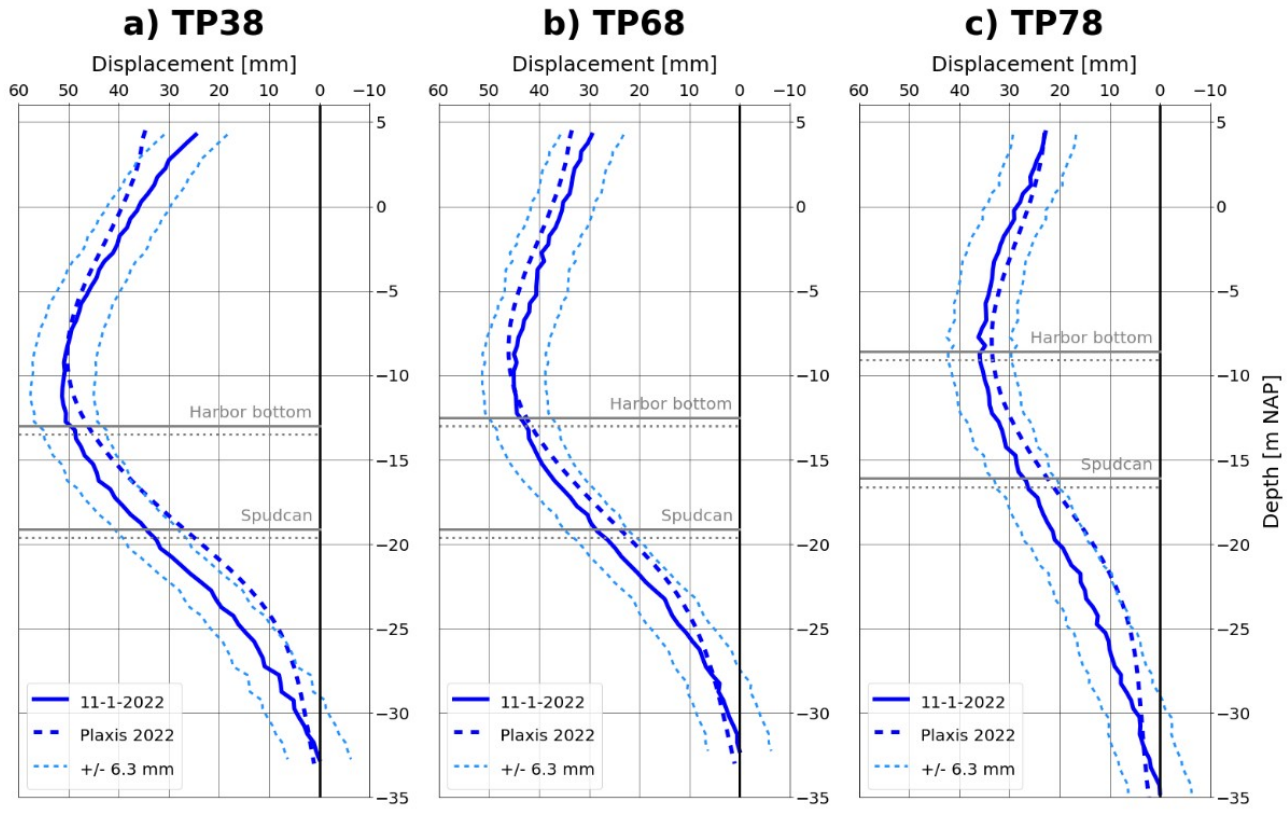

Figure 5.5: Calculated deformation with Plaxis plotted with the inclinometer measurement of 2022

These calculated deformations with Plaxis show a good fit with the inclinometer measurements for all three tubular piles. The maximum field displacement corresponds with the measured one and the

top displacement is inside the range of the measurement error, except for the model of TP38. Some differences are:

- The measurement shows a larger rotation at the toe than calculated.
- Plaxis shows a displacement of several mm at the toe to the waterside, which was expected to develop the passive resistance. In the inclinometer this was assumed to be zero.
- The overall shape corresponds to the measured deformation, however, the top displacement shows a deviation, especially for TP38. This is probably due to wrong choices in modelling the relieving platform.

The calculated deformation shows a satisfying fit over the entire height, except for the top displacement at some cross-sections. Therefore a model calibration will be done as a next step.

5.4. Model calibration

This model calibration focuses on changes in the model that can possibly decrease the deviation of the displacement at the top. This will be done by changing the modelling of the connection between combined wall and platform and the connection between piles and platform.

5.4.1. Adaptation of connection piles-platform

The connection between piles is modelled as embedded beams and the concrete platform is modelled as a rigid connection. In Plaxis it is possible to choose between a rigid, hinged or free connection at the top for embedded beams. With protruding bars of 400 to 750 mm into the concrete floor, this connection will in reality be a rotational spring with a certain rotational stiffness. Determination of this stiffness is difficult because it is influenced by the soil-structure interaction and little is known about the way this connection is constructed in reality. The real stiffness is somewhere between the limits of a hinged and a rigid connection and it is not known which choice represents reality the most. Therefore, in this calibration step the connection will be adjusted to hinged to investigate the influence of this uncertainty. Figure 5.6 shows the resulting deformations together with the measured deformations. Also the results of the previous calculation (with a rigid connection) are shown.

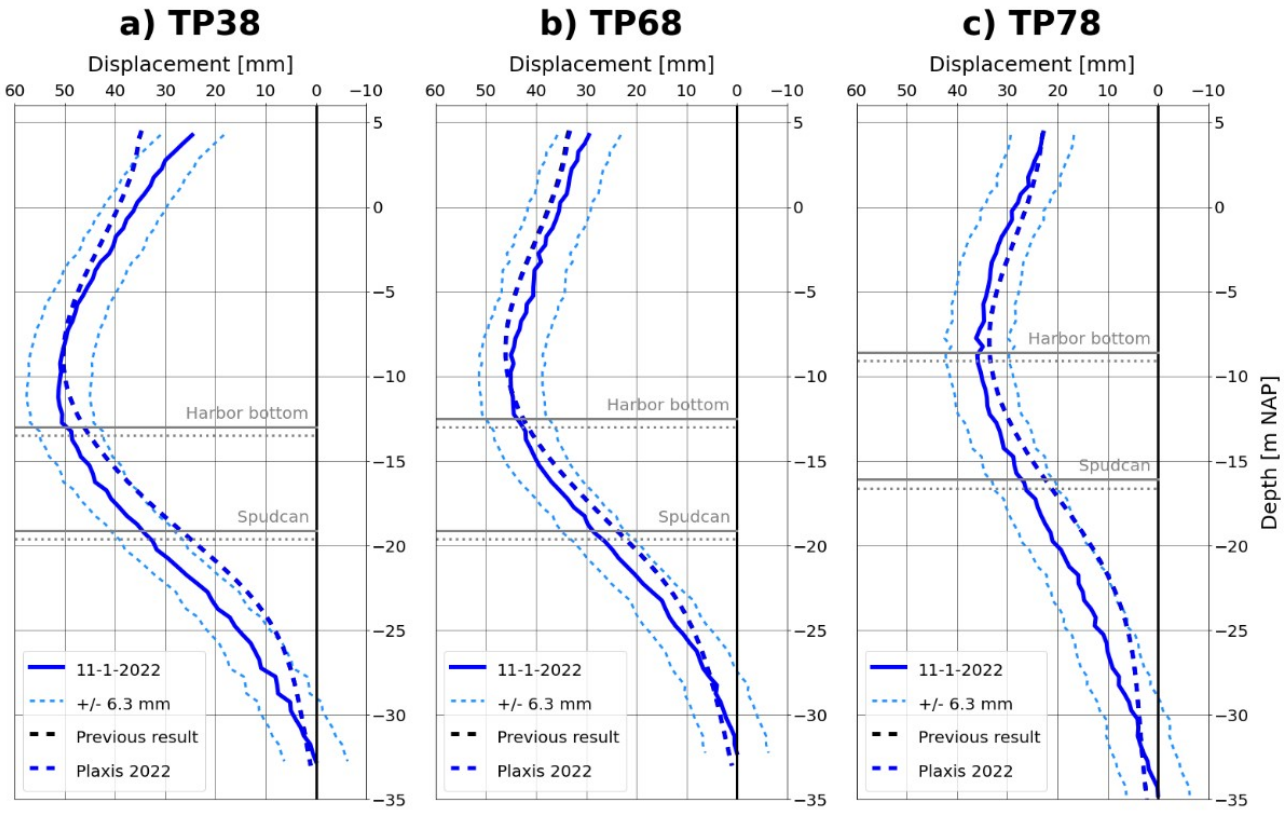

Figure 5.6: Deformation results of Plaxis after adapting the connection between piles and platform

Conclusion: It can be concluded that the adaptation of the connection between piles and platform from rigid to hinge has no significant influence on the resulting deformations.
Another calibration step will be done to improve the fit of the top displacement. This step will be performed with a rigid connection between piles and platform.

5.4.2. Adaptation of connection platform-wall

The connection of the platform and the wall is until now modelled with an interface element with an interface parameter $R_{inter} = 0.8$ for the concrete platform and the fill above. In this way, the wall is connected to the platform via the interface elements. However, in reality the platform is not directly connected but Tempex/EPS(Expanded Polystreen) elements were placed between the platform and the wall or the capping beam at the top, see Figure 5.8. These elements have low lateral stiffness and shearing resistance, so the wall can move to the land or to the water and move up and down without hindrance of the platform. This low resistance ensures that the wall can rotate around the anchor point which is at NAP +3.30m.

Unfortunately, little is known about the properties or the dimensions of the EPS that is used during construction, which leaves several options to model the connection wall-platform. Based on the resulting deformations compared to the measurements, it will be decided which is the best option to use. It is assumed that the elements have a thickness of 30 mm, see Figure 5.7. The following options in modelling this space will be investigated:

1. Gap of 30 mm: No material is modelled, so a gap of 30 mm is left between platform and wall. This is the situation where the platform has no influence on the top displacement of the wall and the wall can freely move. In reality this is not the case, because some material will be there, but this option is taken as the lower limit for the amount of interaction between platform and wall.
2. EPS100: The 30 mm is filled with EPS100, meaning that it has a compressive strength of 100 kPa. This material is modelled with the linear elastic soil model with a modulus of elasticity $E = 6$ MPa and a unit weight $\gamma = 0.25$ kN/m^3 (Stybenex, 2007).

3. EPS250: The 30 mm is filled with EPS250, which is stiffer than the EPS100. Modelled with the linear elastic soil model with $E = 12$ MPa and $\gamma = 0.40$ kN/m^3(Stybenex, 2007).

The available types of EPS range from EPS60 to EPS250, so options 2 and 3 are materials with respectively a low and a high stiffness.

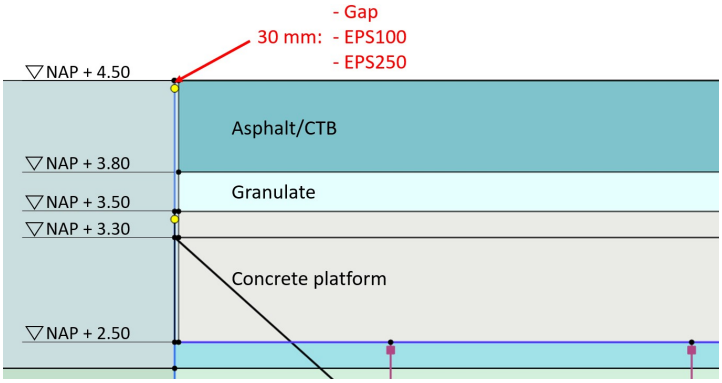

Figure 5.7: Detail of connection wall-platform

Figure 5.8: EPS elements during construction of the relieving platform

The results of these three options, together with the previous result and the measurement in Figure 5.9.

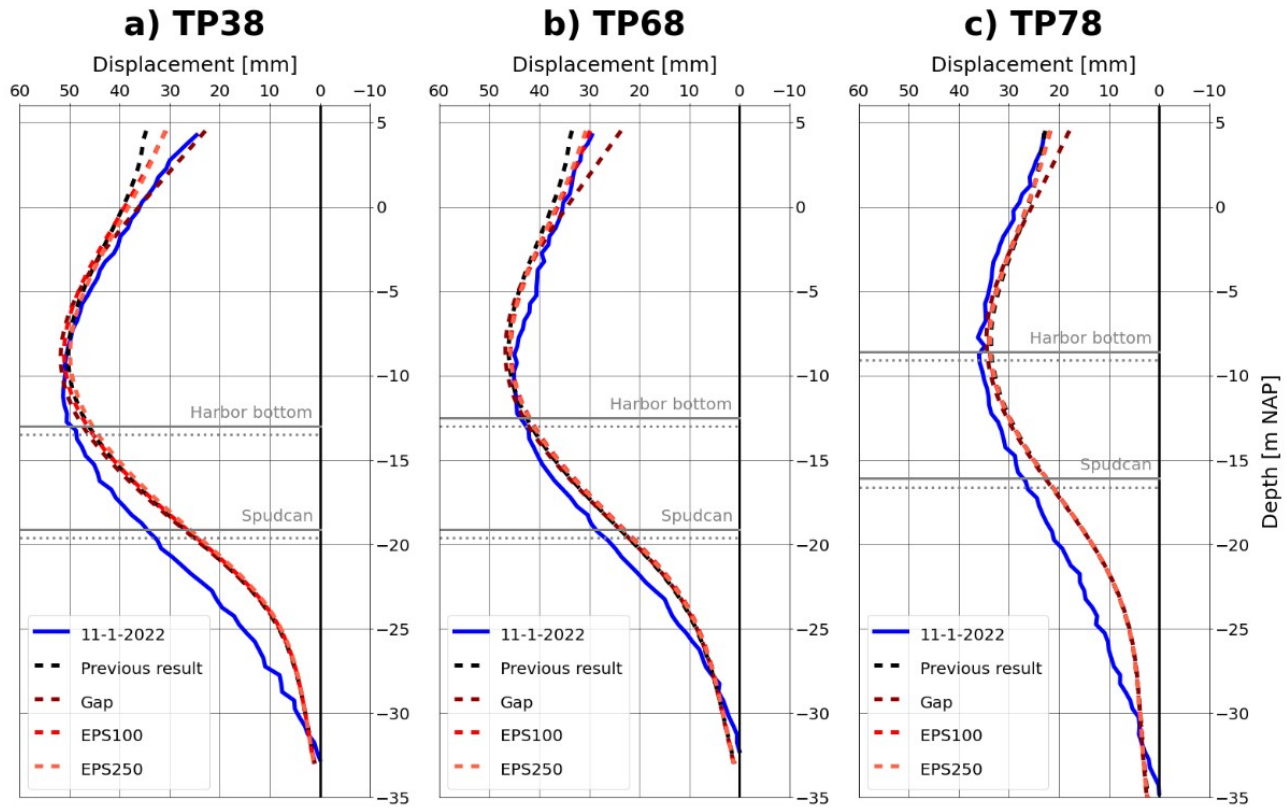

Figure 5.9: Calculated deformation for different variations of modelling the connection platform-wall. The results of the previous calibration step are plotted with the black dashed line.

It can be concluded that the three variations have only influence on the top displacement and very little on the maximum displacement. Apparently, the wall deformation is influenced by the existence of the relieving platform, because the results of the model with gap do not correspond with the measured top displacement. According to cross-sections TP68 and TP78, the model with EPS100 or EPS250 gives

the best fit with the measurements and thus models the interaction between wall and platform in a good way. The difference between the two types of EPS is very small and hardly visible, so either EPS100 or EPS250 can be used in the model. Only for TP38 the model with the gap (option 1) gives the best fit because the measurement of TP38 shows a slightly different shape at the top than the other two cross-sections. It is possible that this difference in shape is gradually changing over the length of the quay, where TP38 is in the middle of the quay wall and 68 and 78 at the end of the quay wall. However, measurements of more cross-sections are needed to confirm this.

Conclusion: Based on the two final cross-sections it is decided that modelling with EPS100 gives the most realistic deformation results. With this calibration step, the calculated deformations correspond well with the measurements and possible remaining difference are inside the measurement error range, so no extra calibration step is needed.

	TP38			**TP68**			**TP78**		
	Measured	*Calculated*	%	*Measured*	*Calculated*	%	*Measured*	*Calculated*	%
Top	24.6	30.8	25.2	29.5	29.8	1.0	23.0	21.7	-5.7
Max	51.3	51.0	-0.6	45.0	44.8	-0.4	36.0	33.9	-5.8

5.5. Conclusion

The Plaxis model gives, after the two calibration steps, a good approximation of the deformations for all three tubular piles. Changing the pile-platform connection from rigid to hinged in the first step has no significant influence on the difference (§5.4.1). In the second calibration step, the connection between wall and platform was adjusted by including an EPS with a thickness of 30 mm between the platform and wall. Variations with stiffnesses of this material concluded that using EPS100 with a modulus of elasticity $E = 6$ MPa and a unit weight $\gamma = 0.25$ kN/m^3 gives the best fit for the top displacement with the measurements (§5.4.2). The deviations of the maximum field displacement for the three cross-sections are 0.5 to 6%. The deviation of the top displacement for TP68 and TP78 is 1% and 6%. Only the top displacement for TP38 has a relatively large deviation of 25% from the measurements.

The small remaining differences between the measurements and calculations are a smaller rotation at the toe in the calculated deformation and a toe displacement larger than zero. The difference in toe displacement is probably due to the fact that the inclinometer does not measure the toe displacement.

6

Comparing results of calculation methods

The results of the D-Sheet model from Chapter 4 are compared with the results from Plaxis from Chapter 5 and possible differences are explained and investigated. This is step 5 of the methodology.

6.1. Comparing calculated deformations

Figure 6.1 shows the results of the calibrated models of Plaxis and DSheet together with the measurements. This section focuses on the differences between the model results. Differences between model results and measurements were already analysed in the preceding chapters.

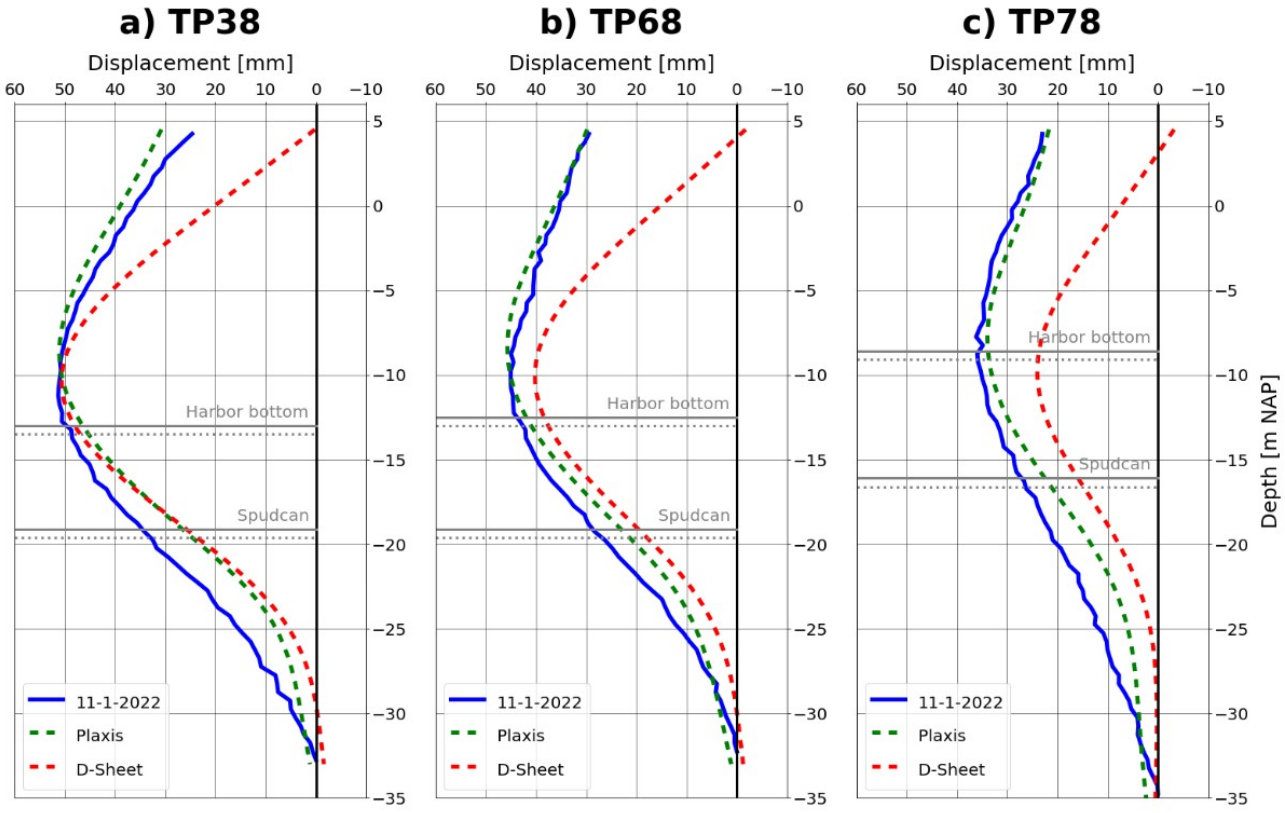

Figure 6.1: DSheet and Plaxis results with measurements of 2022

Some differences between Plaxis and D-Sheet results are:

- The Plaxis results show a large difference at the top with the calculation of D-Sheet, as was expected. This is probably due to the fact that the relieving platform can be modelled properly in Plaxis.
- The maximum field displacement with Plaxis is in all cases equal or larger than the one in D-Sheet. However, D-Sheet was expected to return larger deformations because the shielding effect of the bearing piles is not modelled.
- The toe displacement calculated with D-Sheet Piling is negative for TP38 and TP68, which means that it is moving inland with a rotation point at NAP -30m, while Plaxis shows a movement to the waterside of several mm.

The calculated shear force and bending moments are shown in Appendix F. An overview of the maxima is given in Table 6.1 together with the results from D-Sheet. From these maxima, the largest difference is in the anchor force, which is in the order of 10-15%. However, the shear force distribution in Appendix F shows a good resemblance between Plaxis and D-Sheet for the rest of the wall, except for the anchor point. The resulting bending moment from Plaxis is in all cases smaller than the one of D-Sheet.

		TP38			**TP68**			**TP78**	
		Plaxis	*Dsheet*		*Plaxis*	*Dsheet*		*Plaxis*	*Dsheet*
P_{anchor} [kN/m']		683.1	588.6		656.4	571.8		616.1	551.1
Q [kN/m']	Min	-392.1	-433.8		-368.3	-421.3		-353.5	-405.9
	Max	485.5	594.1		445.1	471.4		334.7	320.9
M [kNm/m']	Min	-2307.3	-2741.7		-2027.8	-2337.2		-1753.7	-1940.0
	Max	1560.2	1691.8		1220.7	1295.9		827.8	887.9

Table 6.1: Overview of calculated shear force Q, bending moment M and P_{anchor} with D-Sheet and Plaxis

6.2. Explanations for difference in results

Possible explanations for differences in calculated deformations are given. Two possible reasons will be investigated. First, the influence of the limitations in modelling this quay wall in D-Sheet will be investigated. After that, the influence of difference in input parameters is investigated.

6.2.1. Limitations in D-Sheet Piling

With a finite element model like Plaxis, stresses and deformations of both soil and all structural elements and their interaction can be calculated in a fundamental way. The schematization used in the elastoplastic model D-Sheet is relatively simple. The soil is modelled by horizontal uncoupled springs and the model thus only takes into account the soil-structure interaction of the front wall. This leads to some limitations in modelling more complex quay walls like the one in this case study. The main differences in model input due to these limitations are:

1. No relieving platform and bearing piles: The relieving platform with the bearing piles can not be modelled in D-Sheet, which means that the interaction between platform and the top of the wall is not taken into account. Also the shielding effect of the bearing piles on the wall is not included.
2. No calculation of vertical displacement: D-Sheet models the soil-structure interaction with horizontal uncoupled springs, so vertical displacement of the wall and vertical deformations of the wall are not included. It is expected that due to this vertical settlement, the wall will be pushed to the water at the top by the anchor and therefore resulting in a larger top displacement.
3. No grout body: The only soil-structure interaction included is between soil and wall, so it is not possible to model a structural element at a certain horizontal distance. Possible displacement of the grout body due to a high anchor force can thus not be calculated in D-Sheet.

It will be investigated whether these differences can be the reason for the difference in results of top displacement in D-Sheet and Plaxis.

To investigate the effect of each difference on the calculation of the top deformation, the Plaxis model will be simplified to simulate the geometry of the model in D-Sheet. This simplification will be done

only for the cross-section at TP68, as this is the section that shows the best fit with the measured deformation. The simplification is carried out in steps such that the effect of each adaptation can be distinguished.

1. The relieving platform and bearing piles are removed from the model leaving a lowered ground level at the place of the platform.
2. A fixed-end anchor at the toe is added to prevent the vertical displacement of the toe. Horizontal displacement of the toe is still possible.
3. The grout body is removed and the anchor rod is elongated to half the length of the grout body. The stiffness of this rod is adjusted to the k_{eqq} like in the D-Sheet model.

Figure 6.2 shows the resulting deformations for the different steps in the simplified Plaxis models. Relieving the bearing piles results in a larger maximum displacement as was expected. Also the top displacement reduces to 18 mm because of the absence of the platform. After adding a fixed toe in the second step, the top displacement will reduce further which is presumably because the wall is not pushed to the water by the anchor when the wall is settling. The final step, removing the grout body, does not have a significant influence on the deformation which indicates that the displacement of the grout body was not very large and that using k_{eqq} for the total system of grout and rod is an adequate modelling choice.

Despite the change in deformation results of the simplified Plaxis model, it still does not correspond with the results from D-Sheet, see the red line in Figure 6.2. The remaining difference is presumably because of the different calculation methods used in the different programs. This is investigated in the next section.

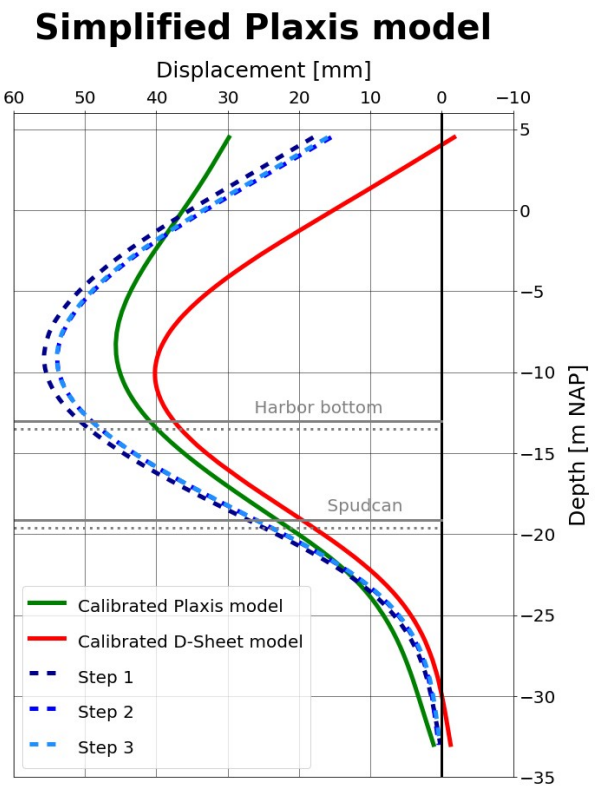

Figure 6.2: Calculated deformation after each step in simplifying the Plaxis model. Also the results of the calibrated D-Sheet and Plaxis models are plotted.

6.2.2. Difference in input soil stiffness

D-Sheet models the soil-structure interaction with elastic springs which requires the input of the subgrade reaction modulus k_h, why it is also called the Subgrade Reaction Method (SRM). This is different than Plaxis, where the stiffness is described by the three different Young's Moduli E: E_{50}^{ref}, E_{ur} and E_{oed} for the Hardening Soil model. Where E_{50}^{ref} is the secant modulus at 50 % of the maximum deviatoric stress at a reference pressure of 100 kPa, E_{ur} the stiffness during unloading and reloading and E_{oed} the oedometric stiffness. The values for k_h used in the D-Sheet model are determined with Table 3.10 from the CUR166 (2012) which is based on Dutch experience with excavations. For each type of soil, a spring characteristic with three branches was selected with three secant subgrade reaction moduli k_h at 50, 80 and 100% of $K_a - K_p$. These are respectively called k_{h1}, k_{h2} and k_{h3}. The values for the stiffness moduli E in Plaxis were obtained from Table 2b (NEN-EN:1997-1, 2012), where the average E_{100} from Table 2b is taken as input for E_{50}^{ref} because both parameters are normalized at a reference pressure of 100 kPa. The other two moduli E_{ur} and E_{oed} are related to this E_{50} with assumed ratios.

The inputted stiffness k_h from CUR66 and E from NEN-EN:1997-1 should somehow correspond to

each other and result in the same behaviour of the soil. To investigate this, a relation will be searched between the k_{h1} and E_{50}^{ref} while both parameters are defined as secant moduli at 50% of the maximum deviatoric strength.

The subgrade reaction modulus is a value that not only depends on the soil stiffness but also on various mechanical and geometric factors such as excavation depth and stiffness of the wall and anchors or struts. The influence of taking the mechanical factors (wall stiffness) into account in determining k_h was investigated by Monaco & Marchetti (2004) for a design of a diaphragm wall, where it was concluded that this does not improve the calculation of the deformations. The fact that k_h implicitly takes into account some characteristic length of the structure can also be recognized by looking at the dimensions of both parameters: $k_h \approx$ [kN/m^3] and $E \approx$ [kN/m^2]. A relation between these parameters should therefore include a length parameter. Based on experimental pressuremeter tests, Ménard derived the following expression (from CUR166 (2012)):

$$k_h = E_M(\alpha\frac{a}{2} + 13(9a \cdot 10^{-4})^{\alpha})^{-1} \tag{6.1}$$

Where:

k_h	:	Horizontal modulus of subgrade reaction	[kN/m^3]
E_M	:	The Young's Modulus according to Ménard	[kN/m^2]
α	:	Rheological coefficient (=2/3 for clay and 1/3 for sand for NC layers)	[-]
a	:	Length in meters which is equal to 2/3 D for a clamped wall and equal to D for a freely supported wall. D is the length of the sheet pile below the ground surface at the low side of the sheet pile wall.	[m]

This Ménard modulus E_M differs from the elastic modulus E mainly because of differences between the real soil behaviour and the conditions in the Ménard pressuremeter test. Sedran et all. (2019) modelled the pressuremeter tests in finite element analysis (FEA) with uniform values of E and back-calculated the values of E_M resulting in empirical relations between E and E_M at different stress levels, see Figure 6.3.

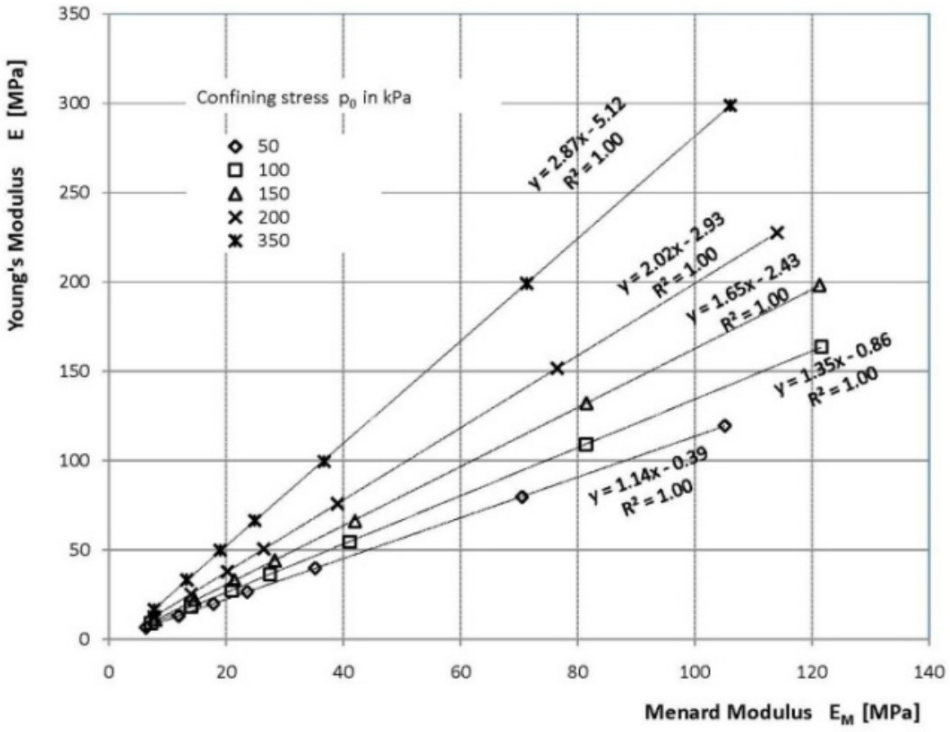

Figure 6.3: E_M and E correlation from parametric study (Sedran et al., 2019)

This relation is described as follows:

$$E = A + B \cdot E_M \tag{6.2}$$

With

$$A = 3.90 p_a - 0.16 p_0$$
$$B = 0.80 + 0.59 \frac{p_0}{p_a}$$

Where:

p_a	:	Atmosferic pressure (=100 kPa)	[kPa]
p_0	:	Initial effective horizontal stress(=$K_0 \cdot \sigma'_v$)	[kPa]
σ'_v	:	Vertical effective stress	[kPa]

This Young's Modulus E can now be related to the E_{50}^{ref} with the definition from the Plaxis Manual (2022):

$$E = \frac{2E_{50}^{ref}}{2 - R_f} (\frac{\sigma'_3}{p_a})^m \tag{6.3}$$

Where:

E	:	Young's Modulus	[kN/m^3]
E_{50}^{ref}	:	Soil stiffness at 50% of the maximum deviatoric stress at a reference stress level of 100 kPa	[kN/m^3]
R_f	:	Failure ratio(=0.9 as default value in Plaxis)	[-]
σ'_3	:	Horizontal effective soil stress	[kPa]
p_a	:	Atmosferic pressure (=100 kPa)	[kPa]
m	:	Power for stress-level dependency of stiffness (=0.5 for sand, 1.0 for clay)	[-]

With the three relations given in Equations 6.3, 6.2 and 6.1 it is thus possible to calculate the k_{h1} in D-Sheet from the inputted value of E_{50}^{ref} in Plaxis and investigate whether this calculated k_{h1} shows large deviations from the assumed values from the CUR166. It should be noted that this is only possible for the layers of sand because the relation between E and E_M by Sedran et all. (2019) is only given for cohesionless soils. The modulus of subgrade reaction for clay is therefore kept to its original value.

From the input parameters needed in the three equations, the horizontal effective stress σ'_3 in Equation 6.3 and the length parameter a in Equation 6.1 does not only depend on the type of soil but also on the construction stage and the side of the wall that is considered. This means that for each stage and side of the wall different values for k_{h1} can be calculated and adjusted in D-Sheet Piling. The procedure that is followed per stage is:

1. Determine the horizontal effective soil pressure σ'_3 with Plaxis on both sides of the wall.
2. Calculate the Young's Modulus E with Equation 6.3.
3. Calculate the Menard E_M with Equation 6.2 with the initial vertical effective stress as determined in Appendix C or from the initial phase in Plaxis to determine parameters A and B.
4. Calculate the new k_{h1} with Equation 6.1 where the length parameter a is varying per stage. Being 2/3 of the distance from toe to excavation level. a can also be seen as the distance over which the passive soil resistance is acting.
5. Add a new type of soil to the model in D-Sheet for each soil layer and for each side of the wall and calculate the resulting deformation.

Table 6.2 shows the input and results of the calculation of k_h for the final stage only according to this procedure. The calculated k_h is compared with the one from the CUR166 and the relative deviation is shown in the last column. This calculation is shown as an example only for the right side of the wall in the final stage.

	$E50_{ref}$ [kPa]	σ'_3 [kPa]	E [kN/m^3]	A [-]	B [-]	E_M [kN/m^3]	α [-]	k_h [kN/m^2]	k_h (CUR166) [kN/m^2]	*Deviation* [%]
Sand 0	62500	20	50820	0.26	0.85	59926	0.33	11353	9750	16.4
Sand 1	92500	50	118923	0.08	0.91	130313	0.33	24687	32500	-24.0
Clay 1	7000	40				4863			4875	
Sand 2	42500	55	57307	-0.23	1.03	55781	0.33	10567	16250	-35.0
Clay 2	7500	40				4924			4875	
Sand 3	77500	30	77179	-0.36	1.08	71618	0.33	13568	16250	-16.5
Sand 4	62500	50	80353	-0.81	1.24	64633	0.33	12244	9750	25.6
Clay 3	22235	90				23356			3250	
Sand 5	77500	100	140909	-1.41	1.47	96178	0.33	18220	16250	12.1
Clay 4	6500	175				11517			3250	
Sand 6	22500	185	55642	-2.28	1.79	31163	0.33	5904	16250	-63.7
Sand 7	77500	200	199276	-2.10	1.72	115912	0.33	21959	16250	35.1
									Average	**-6.2**

Table 6.2: Input and results of calculation of the k_h for the final stage on the right side of the wall

In Table 6.3, the average relative deviation of the calculated k_{h1} to the input in D-Sheet is for each stage of calculation, where a negative value means that the calculated value is lower than the input value in D-Sheet based on CUR166. Some gradual decrease in this deviation can be observed over the stages: the first stage (Fill to NAP +3.30 m) with -40 % and the last stage (Measurement 2022) with 1.1%. This is possibly because of the high values for the length parameter a in the formula of Ménard in the first stages where there is no excavation or a small excavation. a is defined as 2/3 of the distance from toe to the ground level at the low side of the wall for clamped walls but is practically the distance over which the passive soil acts. Using a lower value for a in the first construction stages might give larger k_h and thus smaller deviations from the input values in D-Sheet.

Construction stage	**Deviation [%]**	
	Left	Right
Fill to +3.30	-40.0	-42.7
Prestress	-46.8	-18.0
Dry NAP-.165	-16.9	-10.9
Dry NAP -5.00	-8.4	-9.7
Lowest water	6.8	-21.6
Spudcan	45.1	1.7
Measurement 3	1.1	-6.2

Table 6.3: Average deviation of the calculated k_h per stage

The D-Sheet model is adjusted with the calculated values for k_h, resulting in the deformation presented with the red dashed line in Figure 6.4. The change in deformation with respect to the calibrated D-Sheet model is relatively small despite the large changes in the subgrade reaction moduli. The top displacement shows a small improvement, but in the meantime, the maximum deformation decreases and deviates more from the measured displacement. The explanation for these small changes in displacement results given in §4.4.2 applies here. The resulting soil stresses from D-Sheet show that large parts of the active side are in fully active state, so the displacement becomes independent of k_h. Adjusting the k_h according to this procedure thus results in only small changes. Besides, this process of adjusting k_h is very time-consuming. It is therefore not recommended to follow this procedure in calibrating the model or in quay wall design.

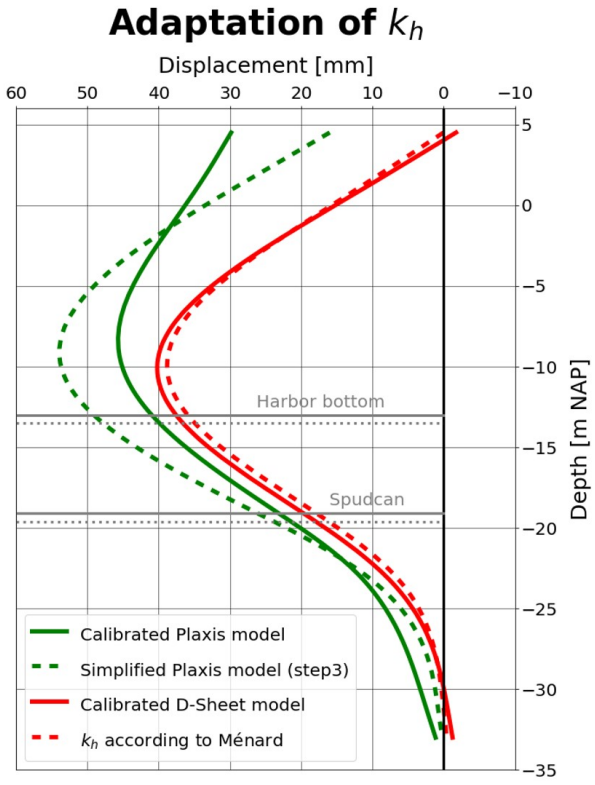

Figure 6.4: Resulting deformation after adjusting k_h according to Ménard equation

6.3. Conclusion

Comparing the resulting deformations from D-Sheet and Plaxis shows that the largest deviation is at the top displacement. D-Sheet calculates approximately 0 mm, while Plaxis results in a top displacement of 30 mm. The maximum wall deformation of Plaxis is in all three cross-sections equal or larger than that of D-Sheet (§6.1).

Two possible explanations for these differences were investigated. The first explanation is that the modelling limitations of D-Sheet lead to different results. These limitations are:

- No modelling of the relieving platform and piles
- No calculation of vertical displacement
- No modelling of the anchor grout body

A Plaxis model without relieving platform, piles and grout body and with a fixed toe was made to investigate the influence of these limitations on the resulting deformation. It turned out that this leads to a smaller top displacement of 17 mm, but still different from D-Sheet results (§6.2.1).

The second explanation investigated was searched in the difference of input of soil stiffness. D-Sheet requires the input of the subgrade reaction modulus k_h and Plaxis requires the input of three Young's Moduli. Based on, among others, the relation of Ménard, these two stiffness parameters could be linked to each other. These relations are used to calculate the k_h corresponding with the E_{50}^{ref} that was used as input in Plaxis. With these new values for k_h in D-Sheet the top displacement of D-Sheet increases with only 2 mm (§6.2.2).

These two explanations thus do not fully explain the difference in top displacement, because after adjusting both models, a difference of 15 mm still remains. More investigation is needed to explain this difference.

7

Sensitivity analysis of the Finite Element Method

This chapter covers a sensitivity analysis of the used finite element model in order to investigate whether different input parameters or other modelling choices would have led to large changes in results and thereby different conclusions. This analysis is only done for the Finite Element Method in Plaxis because the effect of difference in most input parameters in D-Sheet has already been investigated in the calibration of the model, see §4.4. Besides, Plaxis requires much more input parameters and thus much more variations are possible. The cross-section at TP68 will be used in this analysis because this cross-section gave the best fit with the measured deformations. This analysis includes variation in phasing, modelling of the bearing piles, soil model, surcharge load, sea water level and variation in soil parameters. This Chapter covers step 6 of the methodology and will give an answer to sub-question 8.

7.1. Variation in phasing

First, the influence of variations in phasing will be investigated by removing stages or by adjusting the order of the phases before the final stage. The reference measurement was during the first dry excavation of NAP -1.65 m and the measurement of 2022 is relative to this first measurement. Stages prior to this first measurement are the installation of the wall, the fill to NAP 3.30 and the anchor and prestressing stage. This is the order of construction and a relatively short time period, which therefore will not be changed in this sensitivity analysis. The time between the completion of the quay wall and the measurement of 2022 is however quite long and is only captured in two intermediate phases, namely the lowest water level and a phase with the spudcan, see Figure 7.1. This led to satisfying deformation results when compared with the measurements, but other choices about this uncertain period might have resulted in larger differences. Therefore, the following changes in phasing are investigated:

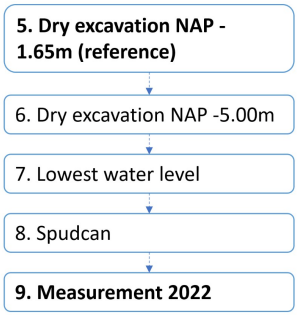

Figure 7.1: Intermediate phases

1. Excluding stages 6, 7 and 8 (no intermediate phases)
2. Excluding stages 7 and 8
3. Excluding stage 8
4. Excluding stage 6
5. Excluding stage 7
6. Exchange stages 7 and 8
7. Adding extra stage with spudcan

The resulting deformations and the relative changes in maximum displacement, bending moment and anchor force are shown in Figure 7.2. A graph with numerical values can be found in Appendix G.

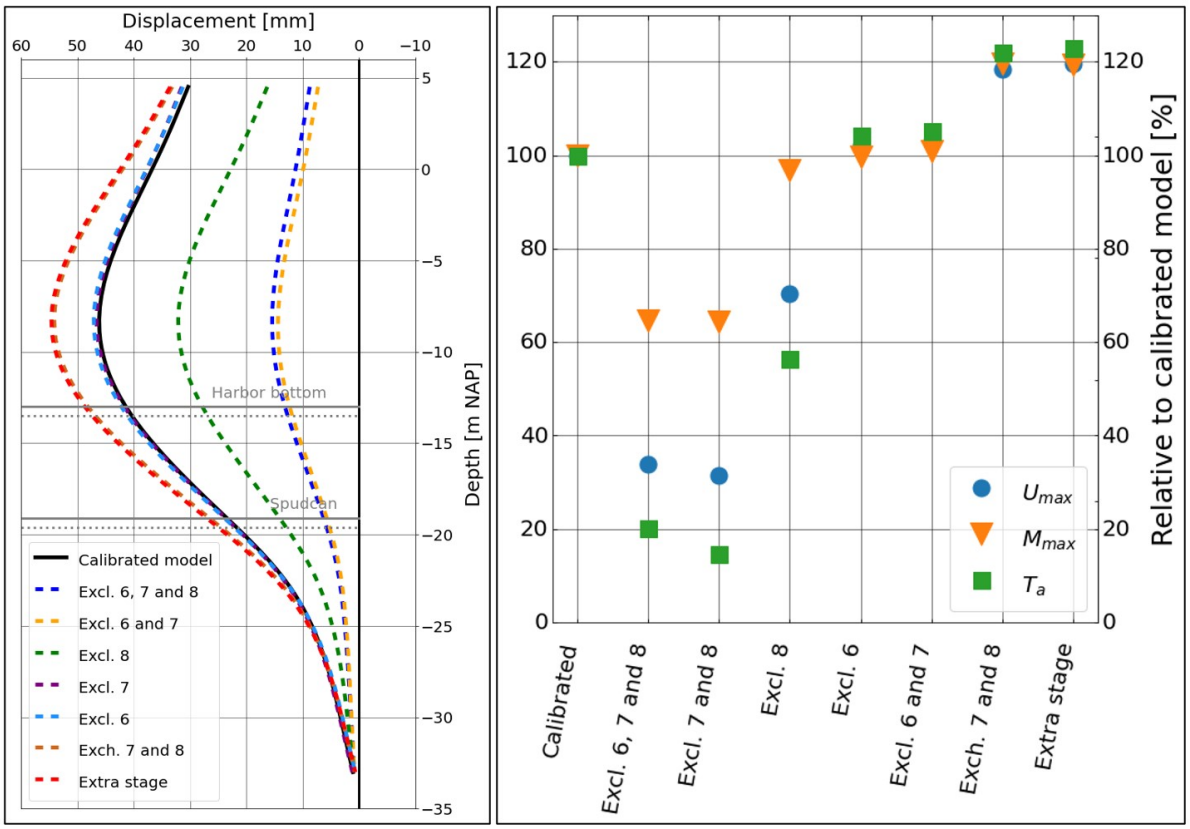

Figure 7.2: Results of variations in phasing. *Left:* Displacements vs depth. *Right:* Maximum displacement $U_{x;max}$, maximum bending moment M_{max} and anchor force T_a relative to the value of calibrated model.

The following conclusions can be drawn:

- The calculated displacement, bending moment and anchor force are in all cases lower or equal when stages are excluded from the calculation process. This is as can be expected because all three intermediate stages are stages where the applied load is larger than the previous stage.
- The graph of anchor force and maximum bending moment shows the same shape as for the displacement, which means that these quantities are also larger when more intermediate loading stages are added.
- Exchanging stages 7 and 8 results in a larger maximum displacement. Exchanging these stages means that the phase with spudcan is directly after the dry excavation of NAP -5.00 m, followed by the phase with the lowest water level. The phase with the spudcan implies a lowered bottom level, but also a load on the relieving platform. Applying the load gradually in successive stages apparently leads to smaller displacement, than when it is all applied at once.

7.2. Variation in modelling bearing piles

A large difference between D-Sheet and Plaxis is that Plaxis is able to model the bearing piles with relieving platform. The most realistic way to model these piles is by using the embedded beam in Plaxis, as is done in the calibrated model. These elements are structural elements with special interface elements that make it possible to include to the interaction of skin resistance and foot resistance. The skin friction and tip force are determined with the displacement of the embedded beam relative to the soil(Infrastructure, 2022). When the embedded beam is created in Plaxis, the line is superimposed on the soil mesh. The nodes of the embedded beams are duplicated and added to the soil mesh and connected to each other with interface elements. In this way, the soil-pile interaction is modelled and the shielding effect can be taken into account (Besseling et al., 2013).

There are other ways to model these piles that do not include this shielding effect which gives the possibility to quantify the effect of shielding on the calculated displacement. This can be relevant to know in comparing the results of Plaxis and D-Sheet as this shielding effect is one of the main differences in modelling for this type of quay wall with relieving platform. The two considered options are modelling the piles with fixed-end anchors or with node-to-node anchors.

The fixed-end anchor is a point element in Plaxis that attaches one point of the structure to a point in the 'fixed world' at a certain distance. This distance is the equivalent length that is required as input parameter. Other input parameters are the axial stiffness EA and the centre-to-centre distance in the out-of-plane direction. This element does not include the soil-structure interaction and assumes that the pile tip is not moving because this point is assumed to be fixed to the world.

The node-to-node anchor is a line element that connects two nodes of the created mesh where one node is usually part of the structure and the other node is part of a soil element. In between these nodes, no soil-structure interaction is taken into account. In this case, the first node is from the platform and the node in the soil is the pile tip. Same as with the fixed-end elements, an axial stiffness EA and centre-to-centre distance is needed as input. The difference is that the node-to-node anchor assumes that the pile tip moves with the node in the soil while the fixed-end assumes this point to be fixed to 'the world' and does not move at all.

As both of these elements do not include soil-structure interaction, also the shaft resistance of the piles is not taken into account. The real spring stiffness acting on the platform is, due to this shaft resistance, larger than the EA based on the material properties. This increase is however difficult to quantify. This is why for both types of pile modelling a calculation is done with an EA based on only the material properties as well as a calculation with infinitely large EA, showing the range between which the resulting forces and deformations can vary. The following ways of modelling the piles will thus be investigated:

1. Fixed end: The piles are modelled as fixed end anchors with an equivalent length equal to the actual pile length and the axial stiffness EA as used for the input in the embedded beam.
2. Fixed end with infinite EA: The piles are modelled as fixed end anchors, but with an infinite stiffness.
3. Node-to-node: The piles are modelled as node-to-node anchors with one node attached to the relieving platform and the other node to the soil at the pile tip. The stiffness is equal to the input in the embedded beam.
4. Node-to-node with infinite EA: The piles modelled as node-to-node anchors with infinite stiffness EA.

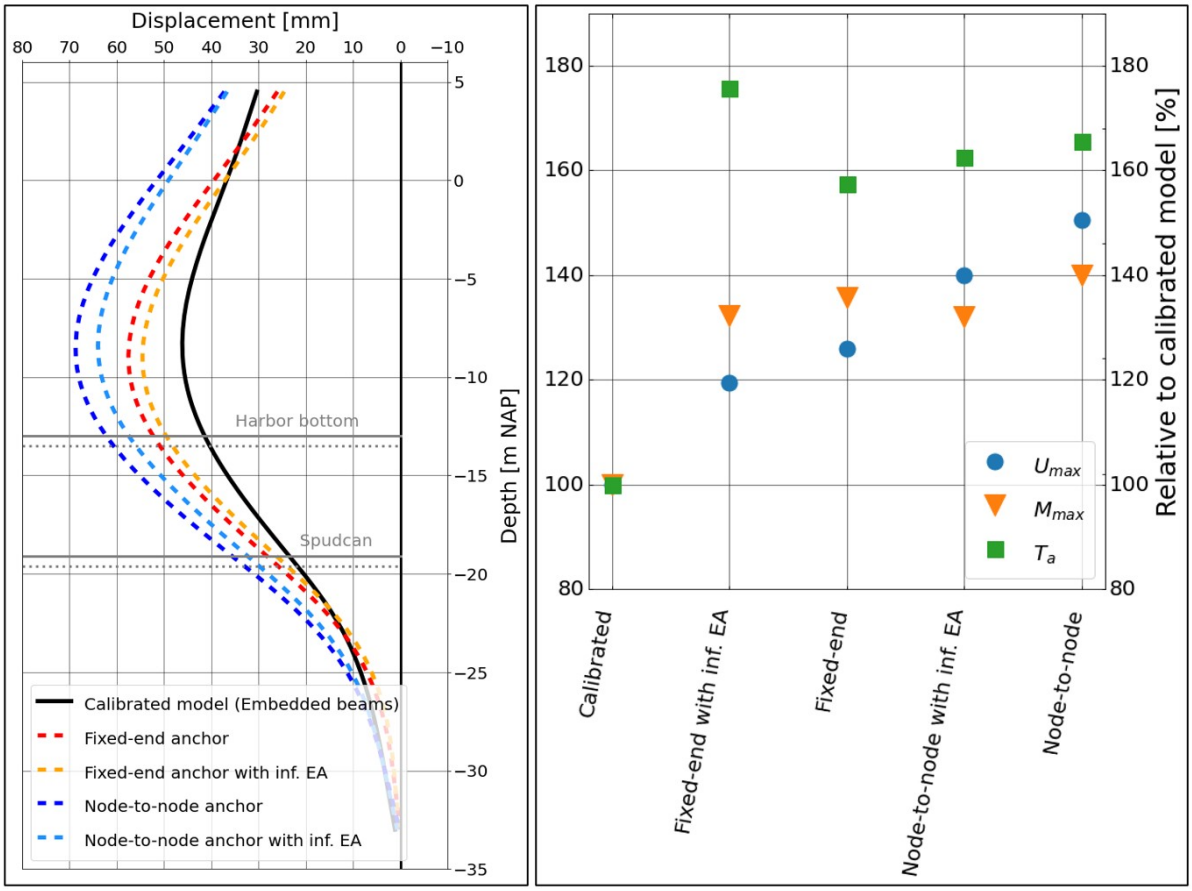

Figure 7.3: Results of variations in modelling bearing piles. *Left:* Displacements vs depth. *Right:* Maximum displacement $U_{x;max}$, maximum bending moment M_{max} and anchor force T_a relative to the value of calibrated model. See Appendix G for the graph with numerical values.

Based on these results, the following conclusions can be drawn about the different ways to model the piles:

- From the displacement graphs on the left in Figure (7.3) it can be observed that the shape is different than the calibrated model. The displacement graphs are more curved with a larger maximum displacement. This larger displacement is because the shielding effect of the piles is not included without the embedded beams resulting in larger active soil pressure on the wall. The decrease in the top displacement is probably due to the fact that the horizontal loads on the relieving platform from the piles are lower or zero when the piles are not modelled as embedded beams. The soil-pile interaction induces horizontal loads on the platform, which transfers these loads to the wall causing a larger top displacement.
- The maximum displacement is the largest for modelling the piles with node-to-node piles, with an increase of 50% compared to the calibrated model. The modelling with fixed-end piles also results in larger displacement, however lower than the case with node-to-node piles. The modelling with infinite stiffness EA results in both cases in lower maximum displacement than the case with realistic stiffness.
- The anchor force is the largest for the case that the piles are modelled as fixed-end anchors with infinite stiffness. This is presumably because the infinite EA prevents the vertical settlement of the platform and thus also partially prevents the settlement of the anchor point. This results in a larger elongation of the anchor than the calibrated model, and thus a higher anchor force. This prevention of vertical movement is lower in the case of node-to-node piles because the second node in the soil is not fully fixed but settles with the soil node. That is the reason that this increase in anchor force for node-to-node modelling is lower than for the modelling with fixed-end piles.
- The maximum bending moment is the largest for the case that the piles are modelled as fixed

end anchors with realistic stiffness. For the modelling with fixed end anchors as well as the node-to-node anchors, the M_{max} is smaller for the case when an infinite stiffness is used.

7.3. Variation of soil model

A Hardening Soil model with small strain (HSss) was used in the calibrated model resulting in the deformation that gives a good fit with the measurements. However, the model HSss is already a relatively sophisticated soil model and also more simplified models are available in Plaxis that might give also realistic results. In this sensitivity analysis, the results from a model with soil models Hardening Soil (HS), Mohr-Coulomb (MC) and Linear Elastic (LE) will be compared to the calibrated model. The influence of even more sophisticated models than the HSss is difficult to examine because this model is already very sophisticated and for other soil models more input parameters are needed that are not known based on the limited soil investigation that is available. The models that will be used in this analysis are in order of complexity:

- Linear Elastic (LE)
- Mohr Coulomb (MC)
- Hardening Soil (HS)
- Hardening Soil with increased E_{ur}: Based on the relation between the small-strain stiffness E_0 and the static stiffness E_{ur} in Figure 5.3, the G_0^{ref} as input for the Hardening Soil small-strain was determined. Table 5.1 shows that the ratio E_0/E_{ur} is approximately 2.5 for sand layers and 6 for clay layers for this particular case. In this option, the Hardening Soil will be used with an increased E_{ur} based on these ratios.

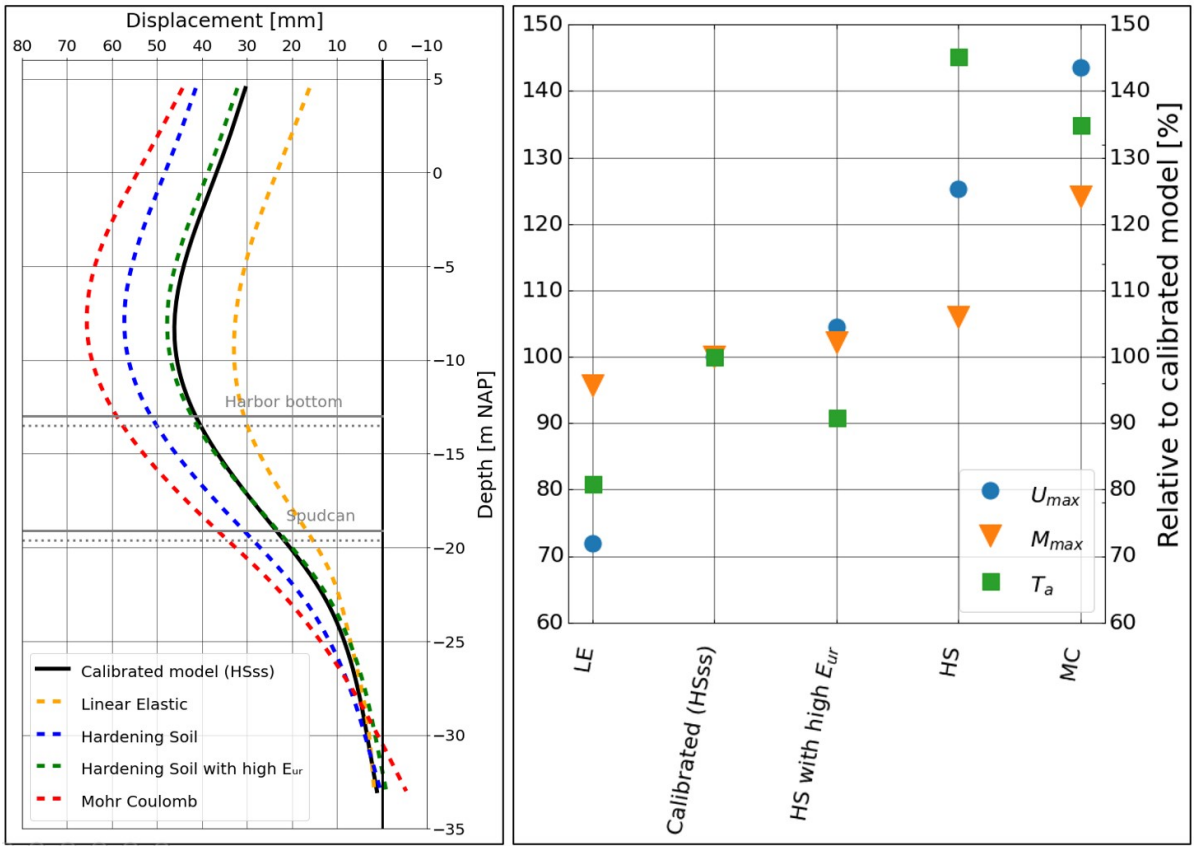

Figure 7.4: Results of variations in soil models. *Left:* Displacements vs depth. *Right:* Maximum displacement $U_{x;max}$, maximum bending moment M_{max} and anchor force T_a relative to the value of calibrated model. See Appendix G for the graph with numerical values.

The following conclusions can be drawn about the results of the different soil models

- The deformation graph on the left in Figure 7.4 shows that the shape is approximately the same, despite the significant difference in field and top displacement. The toe displacement calculated with different soil models corresponds very well, except for the Mohr-Coulomb model which also shows the largest maximum displacement
- The calculation with the Mohr-Coulomb results in the largest maximum field displacement with 140% relative to the calibrated model. For the calibrated model and models with HS, MC and HS with high E_{ur} it applies that the more complex the model, the lower the maximum displacement is. However, this does not apply to the very simple Linear Elastic model which shows an even lower displacement than the calibrated model. This is possibly due to the fact that this model is not able to include the plasticity of the soil. Output from calculation with MC shows a large number of plastic points in the active soil region behind the wall, thus a significant part of the displacement is due to the plastic behaviour of the soil. As the Linear Elastic model does not include this plastic deformation, this results in lower calculated values for the deformation.
- The change of the anchor force shows some interesting differences because it does not generally increase as the max displacement is increasing. A full explanation for this can not be given but it is possibly due to the different interactions between grout and soil for the different soil models.
- The behaviour of the maximum bending moment for the different soil models is the same as for the displacement, albeit with a smaller rate. This is expected because the bending moment is determined based on the calculated displacement.

7.3.1. Sensitivity analysis on small strain parameters

The only difference in model input between the HS and HS small-strain are the two parameters G_0^{ref} and $\gamma_{0.7}$ which were determined with empirical formulas. The G_0^{ref} was determined with the ratio of dynamic to static stiffness E_0/E_{ur} using the empirical relation in the graph in Figure 5.3. The $\gamma_{0.7}$ was determined with Equation 5.2 where the G_0^{ref} and φ' is needed as input parameter. Both parameters are therefore directly or indirectly based on an empirical relationship besides the already existing uncertainties in E_{ur} and other soil parameters. It is important to know which of those two parameters has the largest influence on the calculated deformation and in which soil type this has the largest effect. With the tool *Sensitivity Analysis* in Plaxis it is possible to calculate the sensitivity score in % for each parameter in each layer. This *Sensitivity Analysis* has the following procedure:

1. For both parameters a maximum and minimum value is needed as input. The variation coefficient according to Table 2b (NEN-EN:1997-1, 2012) is 0.10 for both E_{100} and φ, which are both input in the calculation of the two small-strain parameters. On top of that, also the uncertainty of the empirical relationships should be taken into account, so a total variation coefficient of 0.20 is used. The minimum and maximum values are thus respectively 0.80 and 1.20 times the input value used in the calibrated model.
2. A criteria need to be specified which is used to calculate the sensitivity score. In this case, the criteria used is the maximum field displacement.
3. Plaxis performs calculations with the maximum and minimum of each parameter. This means that for every maximum and minimum one calculation is performed where the other parameters are kept at their original value.
4. For each parameter a global score GS is calculated with the results from the calculation with maximum and minimum values:

$$GS_i = |f(x_{i;max}) - f(x_{i;min})| \tag{7.1}$$

   Where $f(x_{i;min})$ is the resulting field displacement with the minimum value of the considered parameter.
5. The sensitivity parameter SS in % for each parameter is determined with this global score using:

$$SS_i = 100 \cdot \frac{GS_i}{\sum_{i=1}^{n} GS_i} \tag{7.2}$$

The results from this analysis are shown in Figure 7.5. The stacked bar plot on the left shows the score per layer for both parameters. Each colour stands for one soil layer as specified in the soil profile. The right graph shows the sensitivity score over the depth together with the total displacement calculated with Plaxis.

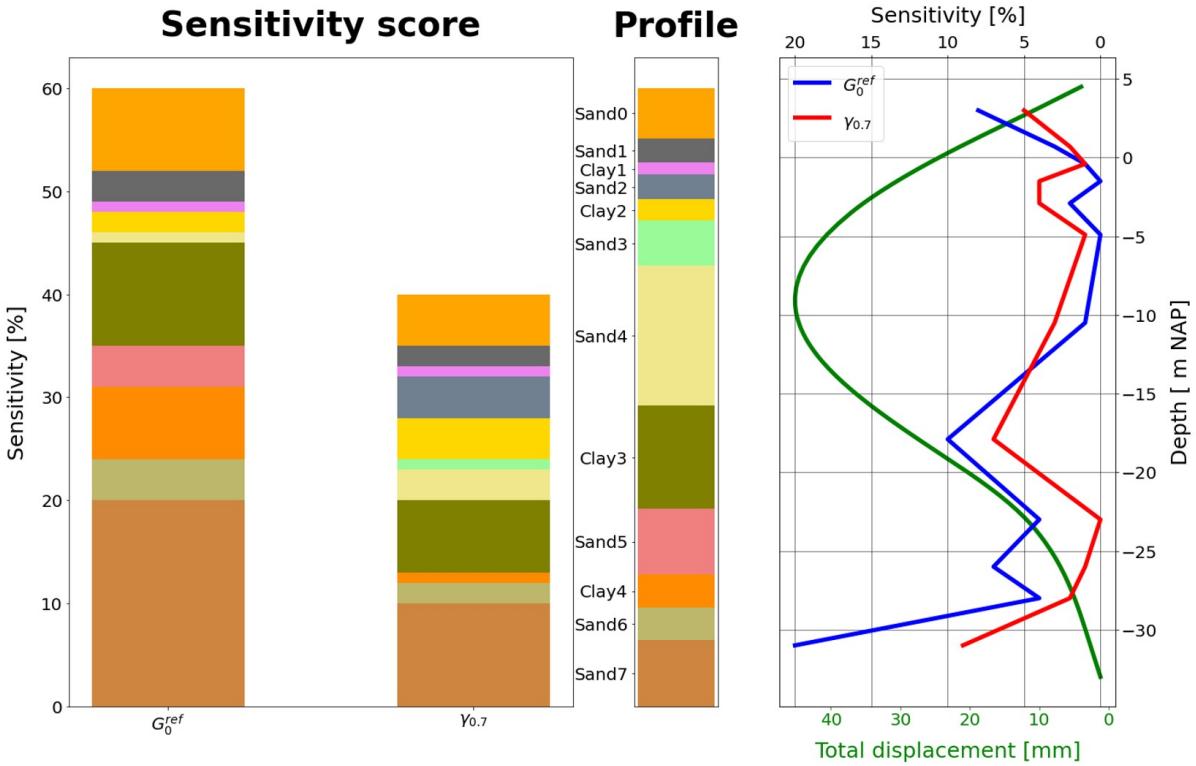

Figure 7.5: Results of sensitivity analysis in Plaxis. *Left:* Sensitivity score for the two small-strain parameters G_0^{ref} and $\gamma_{0.7}$. *Middle:* The soil profile. *Right:* The sensitivity score for both small-strain parameters plotted over depth (blue and red), together with the total displacement (green) calculated with Plaxis.

The following conclusions can be drawn:

- The total sensitivity of G_0^{ref} is 60% and 40% for $\gamma_{0.7}$. Changes and uncertainties of G_0^{ref} thus have a larger influence on the calculated deformations.
- The lowest soil layer Sand7 contributes the most to the total sensitivity score while this is certainly not the largest layer. The layer Sand4 has the largest thickness, however the contribution of this layer is very small. This can be explained by the fact that these two small-strain parameters only have an influence on the region where the soil strain is in this range, so regions where the soil displacement is small. The right figure shows the deformation of the wall together with the sensitivity scores plotted over depth. This roughly shows that the sensitivity score is larger in the region at the top and toe where the displacement is small.
- An exception to this phenomenon is the layer Clay3 which has a relatively large sensitivity score despite the large displacement at that depth. This is due to the fact that for layers of clay, the values for $\gamma_{0.7}$ are generally higher which means that a change in G_0^{ref} also has an effect on higher strain levels.

7.4. Variation of surcharge loads

Another relatively large uncertainty in the input parameters is the magnitude of the surcharge loads on the relieving platform and behind the platform. However, little is known about the duration and the location along the quay wall that is used for these projects. Besides, the loads are implemented in the 2D model as uniformly distributed loads, while they are actually local bearing pressures of the crane supports that should be implemented in a 3D model. Therefore the effect of a possible lower or higher surcharge load on the wall deformation will be examined.

The influence of the load Q on the platform and the load q behind the platform will be investigated separately because the distribution of the load to the wall is different for these loads. In theory, Q will be carried by the bearing piles and thus only have little influence on the maximum deflection of the wall, while the surcharge load q behind the platform results in a larger active soil pressure under the relieving platform and thus a larger maximum deflection of the wall.

7.4.1. Surcharge load Q on platform

In §2.6.2 the load Q on the platform was quantified based on information about the loading projects that took place over the past years. These maximum ground bearing pressures under the crane supports varied approximately from 80 to 150 kN/m^2, with one exceptional load of 176 kN/m^2. An average uniformly distributed load of 100 kN/m^2 was assumed in the Plaxis model. In this sensitivity analysis Q will be varied from 0 to 160 kN/m^2. The resulting deformations of $Q = 0$ and $Q = 160$ are given in Figure 7.6 together with the maximum displacement, bending moment and anchor force.

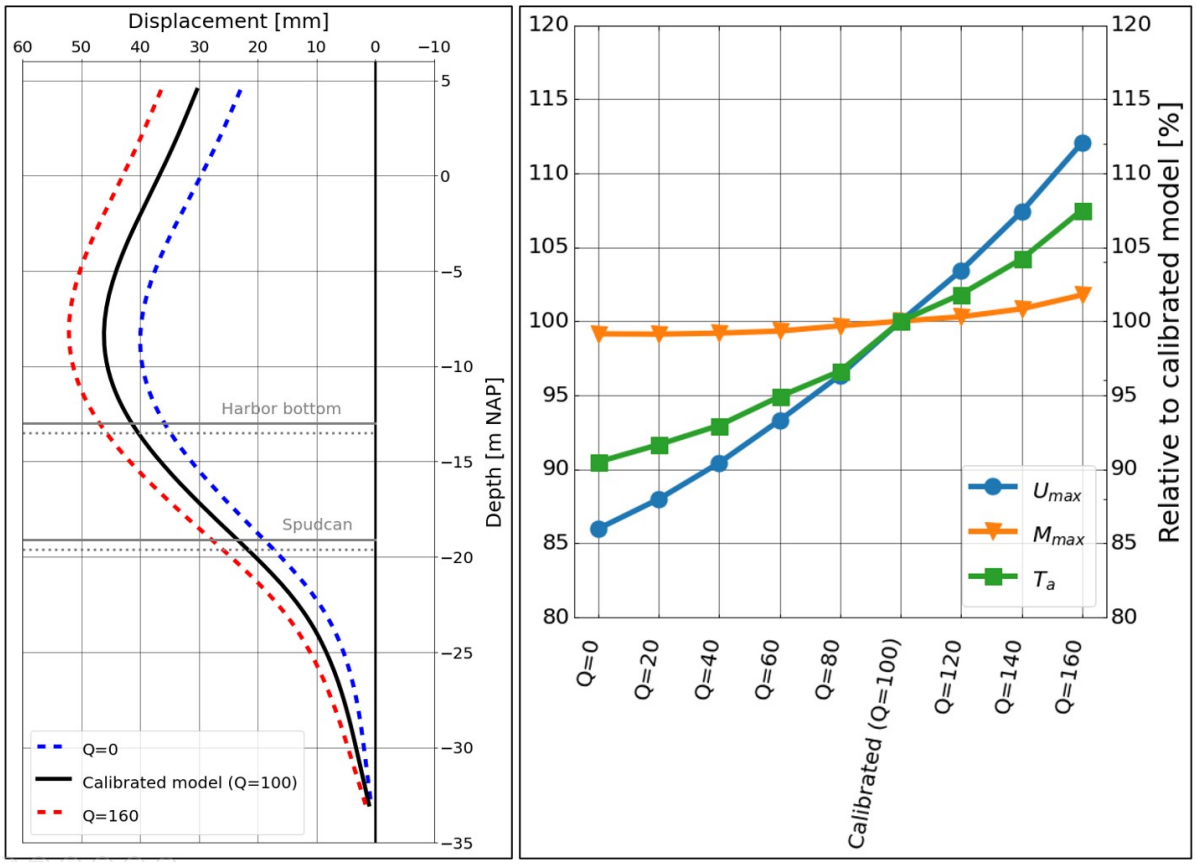

Figure 7.6: Results of variations in magnitude surcharge load Q. *Left:* Displacements vs depth. *Right:* Maximum displacement $U_{x;max}$, maximum bending moment M_{max} and anchor force T_a relative to the value of calibrated model. See Appendix G for the graph with numerical values.

Based on these results, the following conclusions can be drawn:

- Based on the deformation graph in Figure 7.6, it can be observed that Q has little influence on the toe displacement while the maximum field displacement and the top displacement are more affected. Based on the theory, it would be more logical that the toe displacement is affected more because Q is transferred via the bearing piles to the soil at the toe level causing larger horizontal soil pressure on the wall. It could be that the load Q is mainly transfered to the soil by friction between soil and pile over the whole length. This can explain the fact that the change in toe displacement is relatively small.
- The maximum displacement is increasing almost linearly with the surcharge load Q. A minor

curvature can be observed. A reduction of the load with 50% results in a reduction in the max displacement of almost 10%.

- The anchor force is increasing approximately linearly with the surcharge load Q. The relative change in anchor force is lower than that of the maximum displacement.
- The maximum bending moment slightly increases when Q is increasing, but the relative change is lower than that of the anchor force or the maximum displacement.

7.4.2. Surcharge load q behind the platform

q behind the platform was assumed to be 20 kPa. This was based on the assumption that there would be a mobile crane of 60 tons driving or standing. Also, this load was modelled as a uniform distributed load in the 2D model, while in reality it is a local force and acting at just one section of the wall. Therefore it is not known with certainty that this 20 kPa acts on the cross-section that is modelled. To investigate this uncertainty, q will be varied from 0 to 40 kPa. The results are shown in Figure 7.7.

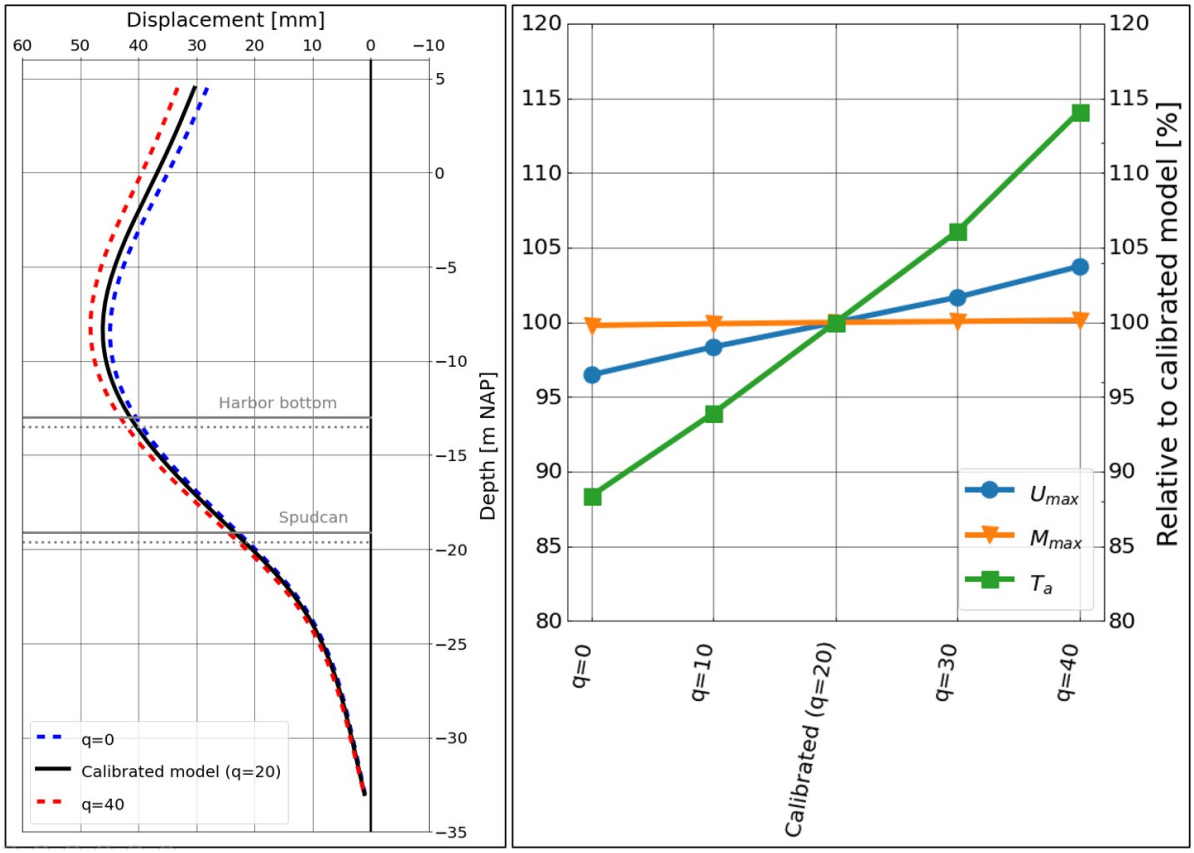

Figure 7.7: Results of variations in magnitude surcharge load q. *Left:* Displacements vs depth. *Right:* Maximum displacement $U_{x;max}$, maximum bending moment M_{max} and anchor force T_a relative to the value of calibrated model. See Appendix G for the graph with numerical values.

Based on these results, the following conclusions can be drawn:

- Like with load on the platform, it can be observed that q has little influence on the toe displacement while the maximum field displacement and the top displacement are more affected. In this case, this is as expected because q is transferred directly to the soil affecting the horizontal soil pressure on the wall.
- The maximum displacement is increasing almost linearly with the surcharge load q.
- The anchor force is also increasing approximately linearly with the surcharge load q, however with a higher rate than the displacement. This is different than for the surcharge load Q where the relative change in displacement was larger than that of the anchor force. This can be explained

by the fact that q has more effect on the load on the higher part of the wall as q is transmitted directly to the topsoil.

- The change in surcharge load q has almost no effect on the maximum bending moment. A doubling of q results in an increase of M_{max} of only a few per cent.

7.5. Variation of soil parameters

One of the main assumptions in this research is that the mean values for the soil parameters are representing the real values, see §2.3. These mean values were determined based on the low and high characteristic values from NEN-EN1997 for the parameters γ, γ_{sat}, E_{100}, φ and c. The mean values for the modulus of subgrade reaction k_h were determined based on low and high characteristics according to CUR166. Invalidity of this assumption can have a large influence on the validity of the calculated deformations. In order to investigate the possible influence, the soil parameters will be adjusted to the low and high characteristics respectively. This gives an indication of to which extent the results can vary, though there is no absolute certainty that the real values lie between the low and high characteristic values. The parameters are changed for both the Plaxis and the D-Sheet model. The parameters are divided in strength and stiffness parameters and its influence is separately:

- Strength parameters
  - D-Sheet: φ, δ and c
  - Plaxis: φ, ψ and c
- Stiffness parameters
  - D-Sheet: k_h
  - Plaxis: E_{50}^{ref}, E_{oed}^{ref}, E_{ur}^{ref}, G_0^{ref} and $\gamma_{0.7}$

The results of these variations are plotted in Figure 7.8. The dashed lines show the results after adjusting only the strength parameters. The solid blue and red lines show the results with low or high strength and stiffness parameters.

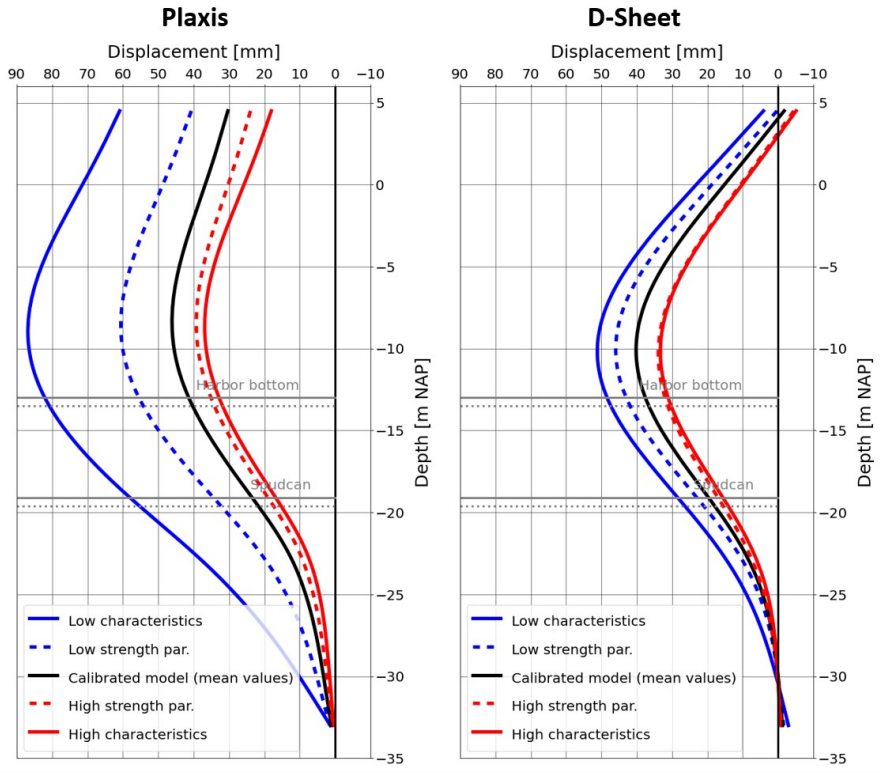

Figure 7.8: Resulting deformations of variations in soil parameters. *Left:* Plaxis *Right:* D-Sheet

The following observations can be made:

- Applying the high characteristic strength parameters results in a reduction of the maximum deformation to 80% of the calibrated value for both Plaxis and D-Sheet (red dashed line). Using the low characteristic strength parameters results in a calculated maximum displacement that is 130% and 110% of the measurement for Plaxis and D-Sheet respectively (blue dashed line).
- Using high characteristic parameters for both the strenght and stiffness parameters results in a reduction of the maximum deformation to 78% of the calibrated value for both Plaxis and D-Sheet (blue solid line). The additional reduction due to high characteristic stiffness values is thus limited to only 2%. Applying low characteristic strength and stiffness parameters results in a maximum deformation that is 209% and 127% of the measurement for Plaxis and D-Sheet respectively (blue solid line). So the change in deformation is larger for applying low stiffness parameters than for applying high stiffness parameters. A possible explanation for this can be that large parts of the soil are already in its plastic regime, where changes in stiffness have no influence on displacement. The fact that this increase in deformation with low stiffness is larger in Plaxis than in D-Sheet can be explained by the fact that the small strain parameters G_0^{ref} and $\gamma_{0.7}$ do not change linearly with the Youngs Modulus E_{50}^{ref}. The relation between the small strain stiffness and static stiffness in Figure 5.3 shows an exponential relation.

No explanation can be given for every observation, but this analysis shows that a change in values of soil parameters can lead to significant differences in results. Especially for using lower values of stiffness parameters in the Plaxis model.

7.6. Variation of water level (tidal variation)

In the calibrated model, a mean tide was assumed when the measurement of 2022 was calculated in the final stage. In this section, the effect of a normal tidal variation on the calculated displacement in the final stage is investigated. In order to do that, an average tide in Eemshaven with an amplitude of 1.3m, a period of 0.5 days and a mean water level of NAP -0.09m is used. This resulted in a change in maximum wall deformation of only 0.5 mm between the low and the high tide, which is negligible.

7.7. Conclusion

This sensitivity analysis gives an answer to the question of how sensitive the calculation models are to changes in input and modelling choices, which was limited to only the Plaxis model. Several variations are performed in this Chapter with conclusions about changes in displacements, anchor force and bending moment. In this section not all conclusions will be repeated, only some general conclusion regarding the influence on displacement for each variation is made.

Variation in phasing
Excluding intermediate phases between the construction and the stage of the measurement of 2022 results in smaller deformations. Exchanging the two intermediate stages *Spudcan (7)* and *Lowest water level (8)* however results in an increase of 20% of the maximum displacement. It is an actual option that this alternating of the stage represents reality more because it is not known which stage, in reality, happened first (§7.1).

Variation in modelling bearing piles
Replacing the embedded beams with fixed-end piles or node-to-node piles results in an increase of the maximum wall displacement of respectively 25% and 50%. The reason for this larger increase in node-to-node piles is that the fictitious pile tip is not fully fixed, but moves with the soil node at the pile tip level (§7.2).

Variation of soil model
The use of the Linear Elastic soil model results in a decrease of the displacement by 28%. The use of the Hardening Soil and the Mohr-Coulomb model increases the max displacement with respectively 125% and 140%. The decrease in displacement by using the Linear Elastic model is possibly due to the effect that this model does not include the plasticity of the soil, while the Mohr-Coulomb does take into account this effect (§7.3).

Sensitivity analysis small-strain parameters
With the tool *Sensitivity Analysis* in Plaxis, the sensitivity of the max displacement due to changes in small-strain parameters G_0^{ref} and $\gamma_{0.7}$ is calculated per soil layer. This shows that the total sensitivity score for G_0^{ref} is 60% and for $\gamma_{0.7}$ is 40%, which means that changes in G_0^{ref} have a larger effect on displacements than changes in $\gamma_{0.7}$. Generally, the sensitivity in small-strain regions is lower (§7.3.1).

Variation of surcharge loads
Both the surcharge load Q on the platform and the load q behind the platform were changed. The relationship between change in surcharge load and maximum displacement is almost linear in both cases. Halving the load Q decreases the displacement with 8% and halving the load q decreases it by only 2%. There are large uncertainties in the real magnitude of these surcharge loads, so these changes in calculated displacement are realistic (§7.4).

Variation of sea water level (tide)
Including a tidal water level variation in the final calculation stage resulted only in a change of 0.5 mm in the max wall displacement (§7.6).

From these possible changes to the model listed above, the exchange of the two intermediate phases (*Spudcan* and *Lowest water*) and a lower or higher surcharge load are factors that could represent the reality more and that should be changed in the Plaxis model. This would then lead to an increase of 20% (due to a change in phasing) and an increase or decrease in the order of 10% (due to a change in surcharge loads).

Variation of soil parameters
Calculating the deformations with low characteristic strength and stiffness parameters results in a maximum deformation that is 209% and 127% of the measurement for Plaxis and D-Sheet respectively. Applying high characteristic values for strength and stiffness results in a maximum deformation of 78% of the measurement for both Plaxis and D-Sheet.

8

Discussion

This discussion reflects on the followed methodology, assumptions made along the way and used techniques or equations. This chapter also reflects on the generalization of the findings from this case study to other quay walls.

8.1. Use of 2D or 3D model

Modelling the quay wall with a 2D program such as D-Sheet and Plaxis 2D seemed to be a valid choice because a wall is eminently a structure that has a constant cross-section in the longitudinal direction. However, for some aspects the 3D model can possibly give more realistic results:

- In the search for causes for differences between measurement and calculations with D-Sheet it was stated that the modelling of the anchor test stage before prestressing can give different deformations in the final stage. These anchor tests were not performed on each anchor simultaneously so it was not possible to model this stage in a 2D program. A 3D program can calculate the effect of adding this stage.
- The magnitude of the surcharge loads on the relieving platform was determined based on information about loading projects provided by Groningen Seaports. The largest surcharge load is due to the assembling of a Noise Mitigation System. The largest loads from other projects are mainly loads from local ground-bearing pressures under cranes. These are thus all very local loads. In the calibrated models the surcharge loads were for simplicity assumed to be uniform over the width of the relieving platform, which is not the reality. With the use of a 2D model it is also not taken into account that this load only applies to a part of the total length of the quay wall. The use of a 3D model of the whole quay wall enables the application of the load for only a small part of the wall and might result in different deformation at the considered cross-section.
- With a 3D model it is also possible to include the effect of the 'free' end of the quay near TP78, where the harbour is shallow and the wall joints with the embankment. The other end of the quay wall is connected in the corner to the quay wall perpendicular which gives a large stiffness to horizontal deformations which can be included in a 3D model.
- The shielding effect of the bearing piles can be included in the Plaxis model when using the embedded beam row, according to Besseling et al. (2013). This is however only the case when the soil load on the piles is equally distributed over the piles. This is the case for most conditions. One case where this is not the case is when the surcharge load behind the relieving platform is very local, resulting in an increase of horizontal load on only a part of the bearing piles.
  The deformation of the combined wall also increases the displacement of the bearing piles. This wall deformation is uniform over the length of the quay wall, however not in the case of the extra deformation due to the spudcan in front of the wall. This will locally increase the retaining height and thereby locally increase the wall deformation and additional displacement of bearing piles which can not be included in the 2D model.

8.2. Model input

8.2.1. Soil model selection

In choosing the soil model for the Plaxis model it was assumed that the time-dependent behaviour such as creep, settlement and relaxation would have a minor influence on the deformation. Therefore the Hardening Soil with small strain was chosen instead of the Soft Soil Creep model for the clay layers. The advantages of the Hardening Soil small strain such as the input of different stiffnesses were assumed to be more important than the ability to include time-dependent behaviour such as creep and relaxation. However, based on CUR211 (2014) this time-dependent behaviour of soft soils can result in extra horizontal deformations some time after the harbour is excavated. This can be an extra deformation of a few centimetres to sometimes more than ten centimetres for quay walls with relieving structures. Based on this information it is probably more accurate to use the Soft Soil Creep soil model for the clay layers instead of the HSsmall strain, especially for the modelled stage where the harbour is being excavated. It is however a consideration whether this advantage outweighs the possibilities of the Hardening Soil with small strain. The duration of the modelled stage and the amount of cohesion of the soil should be taken into account in this consideration.

8.2.2. Determination of plain strain φ

The first calibration step of the D-Sheet model is about adjusting the triaxial-φ to the plain strain-φ. This was done according to the graph presented by Cornforth (1964), where the triaxial and plain strain φ is related to the initial porosity for cohesionless soils. Using this method resulted in an improvement of the calculations of only one out of the three cross-sections, so no conclusions could be made. There are however other ways to determine the plain strain φ:

- In Plaxis it is possible to simulate several soil tests using the feature Soil Test. In this feature, it is possible to simulate a plain strain test and a triaxial test with a specified soil. In this research only Plaxis 2D was available, but it can be interesting to simulate a triaxial compression test and a plain strain test in Plaxis 3D, to see whether the plain strain test results in larger major principal stress before failure, when the same φ is used in both tests. By adjusting the friction angle φ in the plain strain test such that the major principle stress before failure is the same as in the triaxial test, the plain strain φ can be found for that type of soil. In this way, it is not necessary to know the initial porosity as is the case when using the graph in Figure 4.5.
- In NEN9997-1 it is advised to increase the φ with a factor 9/8 to get from triaxial to plain-strain regardless of the amount of cohesion of the soil and independent of the porosity.
- Performing a real plain strain soil test to determine the φ under plain strain conditions in the most accurate way.

There is also some investigation about the difference in friction angle φ in extension tests or compression tests. Most investigators concluded that it is the same for both cases, but some have found that the friction angle was several degrees greater for triaxial extension tests (Lambe & Whitman, 1991). In this case study both extensive and compressive stress paths occur. The soil on the land side will experience axial compression because of the lateral unloading and soil beneath the excavation will experience axial extension because of the axial unloading. Including this difference in friction angle might give different deformation results.

8.2.3. Determination of soil parameters

Part of the inaccuracy of the results lies in the assumptions in soil properties. The soil parameters in this thesis are determined with CPTs available at that site, closest to the cross-section that is considered. Subsequently, the mean or expected values are determined by averaging the low and high characteristic values presented in Table 2b from NEN-EN1997-1 (2012), assuming that this represents the real values. This way of calculating the average was performed after the calculation with the variation coefficient and low characteristic values given in Table 2b resulted in even higher mean values than the high characteristic values in Table 2b, see the calculation in Appendix C.2. This was the case for example for the angle of internal friction φ. With this calculation, the low and high characteristic values are assumed to be limits of the range of scatter, where the low and high characteristic are values 1.65 times the standard deviation σ from the mean value.

This is however only one way of interpreting the variation coefficient provided in Table 2b. Other interpretations are possible because the NEN-EN1997-1 does not explicitly state what this variation coefficient means. Bruijn et al. (2008) give two other ways of interpreting these variation coefficients. These two methods follow from the stochastic model which states that this variation coefficient can be related to the local mean value or the regional mean value. This model is illustrated in Figure 8.1.

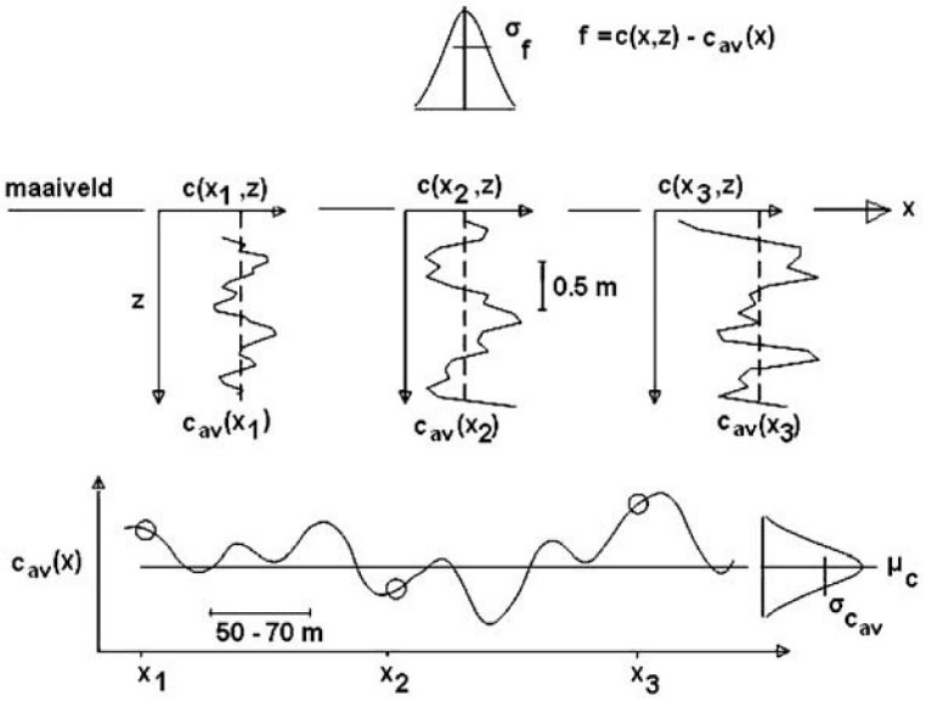

Figure 8.1: Illustration of the local and regional variation of soil parameter C (Bruijn et al., 2008)

A soil parameter C can vary over depth in the z-direction and can vary over the locations X1, X2 and X3 in the x-direction. At each location X, a mean value C_{av} with a standard deviation σ_f applies. This mean value however is different for each location X, so also a regional mean value μ_C is specified with its standard deviation σ_{Cav}. The two ways of interpreting the coefficient of variation in Table 2b is based on these two different mean values:

1. Assuming that the variation coefficient CoV of soil parameter C is the ratio of the local standard deviation σ_f to the local mean value at X $C_{av}(X)$:

$$CoV = \frac{\sigma_f}{C_{av}(X)}$$

2. Assuming that the variation coefficient CoV of soil parameter C is the ratio of the regional standard deviation σ_{Cav} to the regional mean value μ_C:

$$CoV = \frac{\sigma_{Cav}}{\mu_C}$$

Bruijn et al. (2008) provides a way to combine these two interpretations and additionally describes how this can be used with the method *Bayesian updating* to combine results from local soil investigations with the values in Table 2b of NEN-EN1997-1.

This method described above with the *Bayesian updating* could be used when more CPTs were used and when local soil investigation was available. Valuable soil investigation would be plain-strain tests, triaxial tests and oedometer tests.

8.3. Accuracy of calculation results and measurements

According to the CUR211 (2014), the inaccuracy of deformation calculations with Plaxis for quay walls is in the order of $\pm$ 30%. This range is due to deviations in schematization and assumptions in the soil properties. It is possible that the accuracy increased over the past few years, due to developments in Plaxis. However, it is expected that the accuracy will still be in this range because, among others, the features of embedded beam row and the Hardening Soil model with small strain were already available in 2012. Also the assumptions of the soil properties are still the same, so a large reduction in this accuracy range over the years is not expected. With this range of accuracy, it is questionable whether the conclusion about the correct modelling of EPS is valid. In this calibration step in Plaxis, several options in modelling the EPS were investigated resulting in a range of the top displacement from approximately 23 to 33 mm, while the measured top displacement is 30 mm. This means that the value of the measured deformation falls within the range of accuracy of the calculated deformation in Plaxis. More information about the accuracy of Plaxis calculations for especially this type of quay walls could give more certainty whether this conclusion about EPS can be made.

The general inaccuracy of calculated deformations with the method of elastic supported beam (D-Sheet) is not given in any norm or guideline. A number of studies comparing the calculated deformation with the real deformation are available for different types of quay walls, however, a general value for the inaccuracy is missing. This inaccuracy is like with Plaxis, due to deviations in schematization and assumptions in soil properties. The use of uncoupled springs in D-Sheet results in an additional cause of inaccuracy, so the inaccuracy will probably be more than the $\pm$ 30%.

Associated with this accuracy issue is the accuracy of the inclinometer measurements. In Chapter 3 a total accuracy of ± 6.27 mm over the total depth of 37.5 m was determined based on a total random error of 1.39 mm and a systematic error of 4.88 mm. This random error was determined based on literature. The systematic error consists of the bias-shift error, sensitivity drift, rotation error and depth positioning error. No information is known about the contribution of those factors separately, so a total systematic error is assumed in this case. More information about the exact measurement error might be provided by the measuring company in the future. When this accuracy range is known more precisely it is also possible to take this more into account in calibrating the models. Which was not done in this research in all cases.

Besides these possible errors in the inclinometer, it should also be noted that the toe displacement is still assumed to be zero, which is most probably not the reality. This assumption was made because the displacement of the top was not measured simultaneously with the inclinometer and only started in 2017, while the inclinometer started in 2014. With an expected toe displacement to the passive side, the total deformation graph thus shifts several mm to the passive side.

8.4. Applicability to other quay walls

The findings in this research in fact only apply to this case study and more research on other types of quay walls should be done to make more general conclusions. However, something can be said about the expectations for other types of quay walls.

It is expected that the large difference in top displacement between D-Sheet and Plaxis is also visible for quay walls with another soil characteristic but with a high relieving platform. This is based on the fact that the adjustment of the k_h in D-Sheet hardly changed the top displacement. Also applying the plain strain φ did not change the calculated top displacement significantly. It is however relevant which type of relieving platform is considered. In this case study the platform is constructed behind the wall and not directly connected to the wall. In the case of a relieving platform with a saddle point the wall is directly connected to the platform and the interaction is expected to be different than the one in this case study.

8.5. Results compared to earlier design calculations

During the design, a calculation of the governing load combination was made to provide an alarm value for the deformations in order to detect unsafe situations. This alarm value is defined as 80% of the deformation from the limit state. Where the limit state is a situation with extreme loading cases:

- Spudcan level: NAP -19.10 m
- Sea water level: NAP -3.30 m
- Groundwater: NAP -1.80 m
- Surcharge load on platform: 210 kN/m^2
- Bollard load: 34 kN/m'

This is a calculation including safety factors. Figure 8.2 shows the real measured deformation compared to this alarm and limit values. This shows that the real maximum deformation is only 50/130 = 38% of the alarm value.

The calibrated Plaxis model that simulates this measured deformation is shown with the green line in Figure 8.2. The maximum bending moment from this model is 2028 kNm/m' at NAP -8.20 m. The capacity of the combined wall system is 8842 kNm/m' at this point, so the acting bending moment is only 2028/8842 = 23% of the capacity. So the wall has a large capacity left, according to the model.

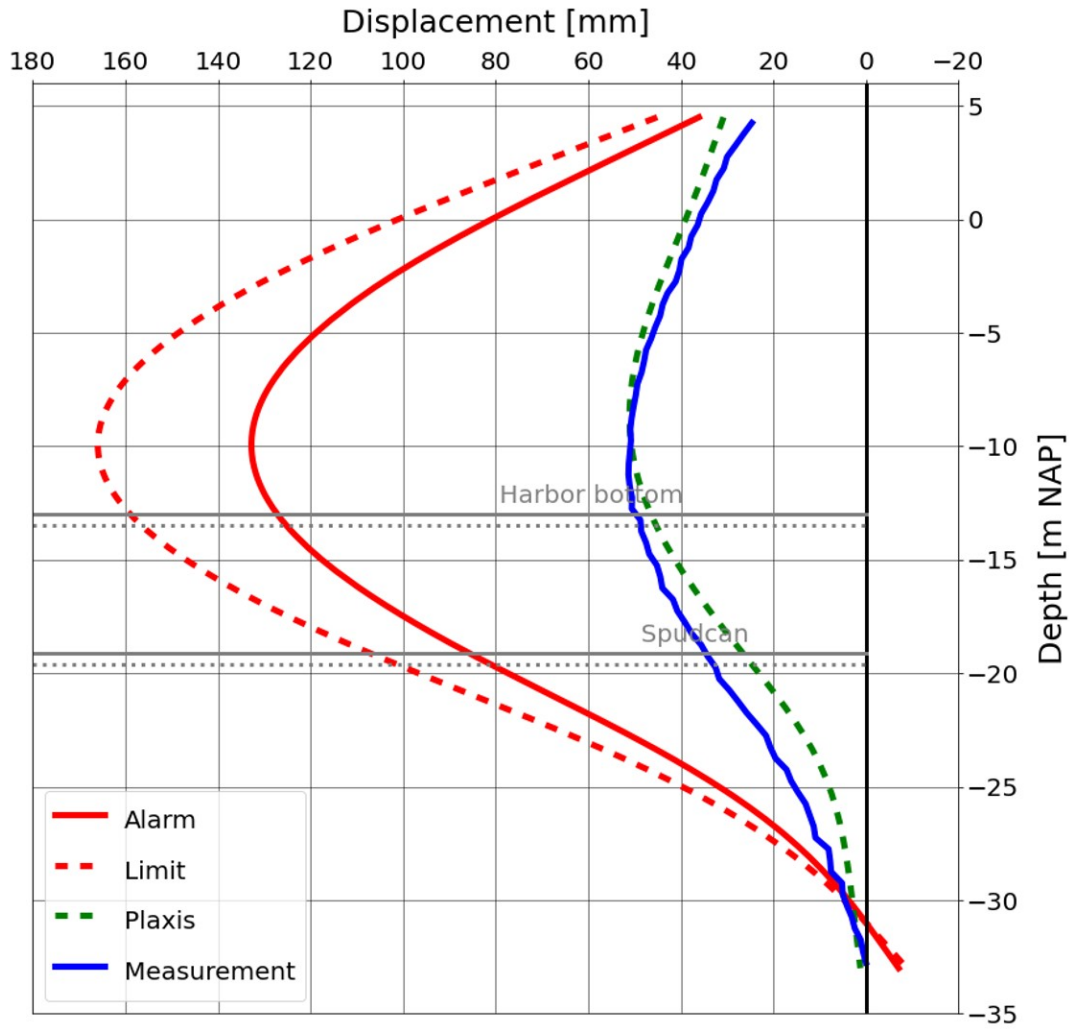

Figure 8.2: Measurement and calculated deformation compared to the alarm and limit values.

9

Conclusions and recommendations

9.1. Conclusions

The conclusions are subdivided into the sub-questions from Chapter 1. After that, the main research question is answered.

9.1.1. Answering sub-questions

The sub-questions from Chapter 1 are repeated and provided with an answer based on the research.

1. **Which modelling choices in the elastoplastic method D-Sheet lead to the best possible approximation of the measured deformation?**

   (a) Applying plain-strain-φ instead of triaxial-φ: For two out of the three cross-sections, applying plain-strain-φ increases the deviation from the measurement by approximately 3%, while for the last cross-section, the deviation decreases by 1-2%. No conclusion can be made based on these ambiguous results.
   (b) Lowering the k_h for deep excavations: This reduces the deviation in top displacement by 7-14% and reduces the deviation in maximum displacement by 11%. It is concluded that this adjusting of k_h is improving the deformation results.
   (c) Combining stages 7 and 9: Combining these leads to a reduction of the deviation of 1 to 10% for the cross-section TP38 and TP68. However, it increases the deviation of TP78 by 2.5%. This is probably because the spudcan load is not applied at the end of the quay wall near the shore where TP78 is situated, which can be observed at soundings. Based on these results it can be concluded that this adjustment improves the calculation results for the sections where the spudcan load applies.

   The model with these modelling choices gives a relative good approximation of the maximum deformation of TP38 with a relative deviation at NAP -10.70 m of 1.3%. This is not the case for TP68 and TP78 where the deviation of the maximum displacement at NAP -9.50 m is still 10 to 34%. For all three piles, the top displacement is strongly deviating from the measured one. This deviation is for all three piles from 100 to 113%.

2. **What causes the difference between measured deformation and the result of the best possible approximation with D-Sheet?**
   Possible reasons for the remaining differences are:

   - Not modelling of the anchor test stage: Each anchor is individually tested after installation to its design load. This can not be modelled in the 2D program D-Sheet.
   - Effect of pile driving on soil characteristics: Some extra CPT tests were done after installation of the combined sheet pile wall, showing a lower cone resistance in layers from NAP -21 to -24 m. This can be a reason for the smaller calculated deformations than the measured deformation.

- Not using apparent tendon length L_{app}: The apparent tendon length of the anchor was determined before the excavation started, but not after the final excavation depth was reached. Using the actual apparent tendon length in the D-Sheet model might improve the calculated deformation at the upper part of the quay wall.
- Construction of RoRo jetty: Recently, the construction of a RoRo jetty for the Holland Norway Lines started. This jetty is constructed at the end of the constructed quay wall. It is possible that the construction of this jetty made it necessary to excavate at the end of the quay wall. This then would explain the relatively large mismatch between the measurements and the calculated deformation with DSheet for TP68 and TP78.
- Disability of modelling relieving platform: The reality is that the platform does prevent movement to the land side, and does nothing when the wall is moving to the waterside because the capping beam and the platform are not connected. This disability of the model is possibly the main reason why the deformations at the top do not correspond with the measured ones.

3. **Which modelling choices in the finite element method Plaxis lead to the best possible approximation of the measured deformation?**

   (a) Connection piles-platform: The connection between bearing piles and platform is adjusted from hinged to rigid, however with no visible result on the calculated deformation. It can be concluded that this has no significant influence on the calculated deformation.
   (b) Connection platform-wall: The connection between wall and platform was adjusted by including an EPS with a thickness of 30 mm between the platform and wall. Variations with stiffnesses of this material concluded that using EPS100 with a modulus of elasticity $E = 6$ MPa and a unit weight $\gamma = 0.25$ kN/m^3 gives the best fit for the top displacement with the measurements. The modelling of the material EPS between the wall and platform thus is a good modelling choice.
   (c) The soil model Hardening Soil with small strain appears to be a good choice for this case study.

   The deviation of the top displacement for TP68 and TP78 is 1% and 6%. Only the top displacement for TP38 has a relatively large deviation of 25% from the measurements. The deviations of the maximum field displacement for the three cross-sections are 0.5 to 6%.

4. **What causes the differences between measured deformation and the result of the best possible approximation with Plaxis?**
   The remaining differences after the calibrations are a smaller calculated toe rotation than measured and a toe displacement larger than zero. The difference in toe rotation can be because of the use of incorrect soil parameters. The difference in toe displacement is because the inclinometer assumes a zero toe displacement.

5. **What are the differences between the calculated deformation in Plaxis and D-Sheet and can this be explained based on the difference in calculation procedure?**
   Comparing the resulting deformations from D-Sheet and Plaxis shows that the largest deviation occurs in the top displacement. D-Sheet calculates approximately 0 mm, while Plaxis results in a top displacement of 30 mm. The maximum wall deformation of Plaxis is in all three cross-sections equal or larger than that of D-Sheet, which is not as expected because D-Sheet is not able to take the shielding effect from piles into account.

   Two possible explanations for these differences are:

   (a) Limitations of D-Sheet: A Plaxis model without relieving platform, piles and grout body and with a fixed toe was made to investigate the influence of these limitations on the resulting deformation. It turned out that this leads to a smaller top displacement of 17 mm, but still different from D-Sheet results.
   (b) Different input of soil stiffness: Based on, among others, the relation of Ménard, the two stiffness parameters could be linked to each other. These relations are used to calculate the

k_h corresponding with the E_{50}^{ref} that was used as input in Plaxis. With these new values for k_h in D-Sheet the top displacement of D-Sheet increases with only 2 mm.

These explanations thus do not fully explain the difference in top displacement, because after adjusting both models, a difference of 15 mm in top displacement still remains.

6. **How does the calculated deformation change due to changes in model input or modelling choices?**
   The following main conclusions about the variations can be made:

   - Variation in phasing: Exchanging the two intermediate stages *Spudcan (7)* and *Lowest water level (8)* however results in an increase of 20% of the maximum displacement.
   - Variation in modelling bearing piles: Replacing the embedded beams with fixed-end piles or node-to-node piles results in an increase of the max wall displacement of respectively 25% and 50%.
   - Variation in soil model: The use of the Linear Elastic soil model results in a decrease of the displacement by 28%. The use of Hardening Soil and Mohr-Coulomb model increases the max displacement with respectively 125% and 140%.
   - Influence of small-strain parameters G_0^{ref} and $\gamma_{0.7}$: The total sensitivity score for G_0^{ref} is 60% and for $\gamma_{0.7}$ is 40%, which means that changes in G_0^{ref} have a larger effect on displacements than changes in $\gamma_{0.7}$. Generally, the sensitivity is higher in regions with low strain levels.
   - Variation of surcharge loads: Both the surcharge load Q on the platform and the load q behind the platform were changed. The relationship between change in surcharge load and maximum displacement is almost linear in both cases. Halving the load Q decreases the displacement with 8% and halving the load q decreases it by only 2%.
   - Variation of sea water level (tide): Including a tidal water level variation in the final calculation stage resulted only in a change of 0.5 mm in the max wall displacement.
   - Variation of soil parameters: Calculating the deformations with low characteristic strength and stiffness parameters results in a maximum deformation that is 209% and 127% of the measurement for Plaxis and D-Sheet respectively. Applying high characteristic values for strength and stiffness results in a maximum deformation of 78% of the measurement for both Plaxis and D-Sheet.

   From these possible changes to the model listed above, the exchange of the two intermediate phases (*Spudcan* and *Lowest water*) and a lower or higher surcharge load are factors that could represent the reality more and that could be changed in the Plaxis model. This would then lead to an increase of 20% (due to a change in phasing) and an increase or decrease in the order of 10% (due to a change in surcharge loads).

9.1.2. Answering the main research question

The main research was formulated as follows:

Which design method approximates the measured deformation best for the quay wall with relieving platform in Eemshaven Groningen, considering the elastoplastic method D-Sheet and the finite element method Plaxis?

Based on the results in this case study, it can be concluded that Plaxis results in a better approximation of the measured deformation than D-Sheet. The deviation of the calculated deformations from the measurement for the piles TP38, TP68 and TP78 are given in Table 9.1 for the maximum deformation and the deformation at the top. The Finite Element Method Plaxis thus results in a better approximation than the elastoplastic method D-Sheet, especially for the deformation at the top. This conclusion is based on the assumption that the average values for the soil properties, obtained from Table 2b of NEN-EN 1997-1, are representative of the real values.

	Top		Max	
	D-Sheet	Plaxis	D-Sheet	Plaxis
TP38	99.1	24.8	1.3	0.5
TP68	105.8	1.3	10.7	1.5
TP78	114.0	5.8	33.7	6.2

Table 9.1: Deviation in % of the calculated maximum deformation and top displacement from the measurement.

9.2. Recommendations

The recommendations are divided into recommendations for measurements, modelling and further research.

9.2.1. Recommendations related to measurements

Some recommendations for future measurements can be done based on the experience during this research.

- First of all it is recommended to perform the top displacements measure in X and Z directions simultaneously with the inclinometer measurements to have the assurance that the top position is known when the inclinometer is done.
- The inclinometer only gives a deformation relative to the reference measurement, so the top displacement is the only way to get the absolute deformation of the piles. Therefore it is also important that the top displacement is not relative to something else. The positions of the bolts should therefore be known in RD coordinates with every measurement and the exact locations of the bolts after installation should also be recorded.
- This quay wall contains a drain which reduces the water head difference. Without monitoring of the groundwater level it is however not known how fast this drain is and how effective it is after many years. It is therefore recommended to install monitoring devices already during construction that can be accessed also after construction. With the monitored water level in the harbour, the exact water head over the quay wall is known.

9.2.2. Recommendations related to modelling

Based on the results from the two used models in this research, the following recommendation can be done.

- From the calibration in D-Sheet it became clear that adjusting the modulus of subgrade reaction k_h resulted in a better agreement with the measurement. It is therefore recommended to adjust the value for k_h when the retaining height is significantly larger or smaller than the 8-10 m where the values of CUR166 apply for.
- From the sensitivity analysis it can be concluded that the modelling of intermediate loading stages is crucial to get the most realistic deformation. Excluding the intermediate phases with ship loading and lowest water levels resulted in a deformation that is only 30% of actually measured deformation. The main reason for this is that the loading in these intermediate phases caused significant plastic deformations. It is therefore recommended to model these intermediate stages as accurately as possible.
- The use of the soil model Hardening Soil with small strain is recommended for these kind of excavation problems. Also when the small strain parameters are not known, the empirical relations can give significantly better results than the Hardening Soil model.

9.2.3. Recommendation for further research

- The result of this deformation is all based on the assumption that the mean values obtained from Table 2b of NEN-EN 1997-1, are representative of the real values. This is a relatively rude assumption, so it is recommended to do more soil investigation than the CPTs in further research to quay walls.

- Adjusting the triaxial-φ to the plain-strain-φ according to tests from Cornforth (1964) did not give unambiguous results, so no conclusion could be made about this subject. This is probably because these tests were only done for cohesionless soils. The soil layers in this case study were not all cohesionless. In NEN9997-1 it is advised to increase the φ with a factor of 9/8 to get from triaxial to plain strain regardless of the amount of cohesion of the soil. In further research, it can be investigated which of these methods gives the best results for cohesionless soils. It is recommended to do this comparison for a case study with a soil characteristic which mainly consists of cohesionless layers. In this way, the difference can be observed between the two methods.
- The largest difference between the results of D-Sheet and Plaxis is in the top displacement. Even after simplifying the modelling in Plaxis this difference still remains. From this case study, it can not be said with certainty why this large difference occurs and why the top displacement in D-Sheet is almost zero. It is therefore recommended to do further research with the same type of quay wall in a different soil characteristic to investigate whether the modelling of the soil is the cause of this difference. Also a quay wall without relieving platform and bearing piles can be compared with the same type of soil characteristic to investigate whether the presence of the relieving platform is the cause for this difference.
- Based on modelling with several properties for the EPS material between platform and wall it was concluded that EPS100 gave the best fit. However, this was based on a thickness of 30 mm, which was an assumption. It can therefore not be concluded that the modelling of the material between platform and wall results in more realistic deformations in all cases. It is therefore recommended to do research with a quay wall from which the deformations are measured and where the properties of the material and the thickness are known by the design or the contractor.
- In those listed recommendations it is important to have sufficient measurements as explained in the previous section. The measurements should give certainty about the actual toe displacement and thereby also certainty about the displacement of the top. This is especially important for the research in modelling the EPS at the top of the wall.
- It is also recommended to measure the anchor force when the deformations are compared with calculation results in order to get more certainty if the anchor is modelled correctly.

References

ARBED. (1991). *Practical design of sheet pile bulkheads*. Amerlux Steel Products Corporation.

Bentley Advancing Infrastructure. (2021). *PLAXIS 3D: Geotechnical Engineering Software | Bentley Systems*. Retrieved December 14, 2021, from https://www.bentley.com/en/products/brands/plaxis

Bentley Advancing Infrastructure. (2022). *PLAXIS 2D - Material Models Manual*.

Besseling, F., Sluis, J., Lengkeek, H., & Stuurwold, P. (2013). Validation and Application of the Embedded Pile Row-Feature in Plaxis 2D. *Plaxis Bulletin*.

Blum, H. (1931). *Einspannungsverhältnisse bei Bohlwerken*. C.L.Krüger, G.m.b.H.

Boertjens, K. (2022). *The synergy partner b.v.* Retrieved November 25, 2022, from https://www.linkedin.com/posts/koos-boertjens-5082612_noordinbeeld-groningenvanboven-eemshaven-activity-6934776598957076480-ApLu?utm_source=share&utm_medium=member_desktop

Brinkgreve, D. R. (n.d.). *Materiaalmodellen voor grond en gesteente: Theorie van grondmodellen*.

Bruijn, E., Calle, E., Hannink, G., Lindenberg, J., & Vrouwenvelde, T. (2008). Representatieve waarden voor grondparameters in de Geotechniek. *GEOtechniek*, 24–29.

Clayton, C., Woods, R., & Milititsky, J. (n.d.). *Earth Pressure and Earth-Retaining Structures, Second Edition*. Taylor & Francis.

Cornforth, D. H. (1964). Some experiments on the influence of strain conditions on the strength of sand. *Géotechnique*, *14*(2), 143–167. https://doi.org/10.1680/geot.1964.14.2.143

CUR166. (2012). *CUR166 Damwandconstructies*. CUR Bouw & Infra.

De Klerk B.V. (2014). *Definitief ontwerp beatrixhaven westzijde aanleg kade fase 5* (Ontwerpnota 14A09). De Klerk BV. Werkendam.

Deltares. (2017). *Dsheet piling manual*.

DIANA. (2021). *Diana documentation*. Diana FEA. https://dianafea.com/diana-manuals

DIANA FEA. (n.d.). *Geotechnical engineering*. Retrieved December 14, 2021, from https://dianafea.com/geotechnical

D.J.Kunst. (2017). *Modelling construction phases of bored tunnels with respect to internal lining forces* (Master's thesis). Delft University of Technology. Delft.

FHWA. (1999). *Geotechnical Engineering Circular NO. 4: Ground Anchors and Anchored Systems*. Washington D.C.

Geotech Foundation Solutions. (2014). Testrapport-Controleproeven.

Gouw Dr, T.-L. (2014). Common mistakes on the application of plaxis 2d in analyzing excavation problems. *9*, 8291–8311.

Groningen Seaports. (n.d.). *Eemshaven*. Retrieved December 6, 2021, from https://www.groningen-seaports.com/havens/eemshaven/

Groningen Seaports. (2022). Peilingen Eemshaven [Raw data].

Grotegoed, D. (2010). *The Gevelco quay wall: Research into the causes of the measured displacements* (Master's thesis). Delft University of Technology. Delft.

Gumucio, J. L. (2013). *Design of quay walls using the finite element method* (Master's thesis). Delft University of Technology. Delft.

Infrastructure, B. A. (2022). *PLAXIS 2D - Reference Manual*.

Lambe, T., & Whitman, R. (1991). *Soil mechanics*. Wiley. https://books.google.nl/books?id=d-FzXyGhwcEC

Mennens Dongen B.V. (n.d.). *P14004 - berekening e-modulus vanuit trekcurve* [unpublished].

Mikkelsen, P. (2003). Advances in inclinometer data analysis. *Field Measurements in Geomechanics*. https://doi.org/10.1201/9781439833483.ch73

Mikkelsen, P. (2007). Inclinometer Data & Recognition of System Errors Recognition of System Errors [Lecture Notes]. https://www.durhamgeo.com/pdf/papers/mikkelsen-inclinometer-errors.pdf

Monaco, P., & Marchetti, S. (2004). Evaluation of the coefficient of subgrade reaction for design of multi-propped diaphragm walls from DMT moduli. *2nd International Conference on Site Characterization ISC-2At: Porto, Portugal*, 993–1002.

NEN-EN:1997-1. (2012). *Nederlandse norm, eurocode 7: Geotechnisch ontwerp - deel 1: Algemene regels.* (Standard). NEN.

Nguyen, A.-D., Kim, Y. S., Kang, G., & Kim, H.-J. (2021). Numerical analysis of static behavior of caisson-type quay wall deepened by grouting rubble-mound. *International Journal of Geo-Engineering*, *12*. https://doi.org/10.1186/s40703-020-00130-3

Notteboom, T., Pallis, A., & Rodrigue, J.-P. (2022). *Port economics, management and policy* (1st ed.). Routledge. https://doi.org/10.4324/9780429318184

SBRCURnet Publication 211E. (2014). *Quay Walls* (Second Edition). Standard. Rotterdam, SBRCURnet.

Sedran, G., Failmezger, R., & Drevininkas, A. (2019). Relationship between Menard E_M and Young's E moduli for cohesionless soils. *Proceedings of the 18th International Conference on Soil Mechanics and Geotechnical Engineering*.

SkyGeo. (2023). *Bodemdalingskaart 2.0* [https://bodemdalingskaart.portal.skygeo.com/portal/bodemdalingskaart/u2/viewers/basic/].

Stark, T., & Choi, H. (2008). Slope inclinometers for landslides. *Landslides*, *5*, 339–350. https://doi.org/10.1007/s10346-008-0126-3

Stybenex. (2007). Basisinformatie EPS [Brochure]. https://stybenex.nl/wp-content/uploads/2022/03/brochure-EPS-basisinformatie.pdf

Terracon Funderingstechniek. (n.d.). *Geboorde paalsystemen*. Retrieved December 19, 2022, from https://terracon.nl/expertise-geboorde-paalsystemen/

ThyssenKrupp GfT Bautechnik. (2008). *Sheet Piling Handbook*.

Truty, A. (2008). Hardening soil model with small strain stiffness [Lecture Notes]. https://www.zsoil.com/zsoil_day/2008/Truty_HS-model.pdf

TU Delft. (2020). *Manual hydraulic structures*. Lecture Notes.

van den Ham, G., de Groot, M., & van der Ruyt, M. (2012). *Handreiking toetsen voorland zettingsvloeiing t.b.v. het opstellen van het beheerdersoordeel in de verlengde derde toetsronde.* (Guideline). Rijkswaterstaat Ministerie van Infrastructuur en Milieu.

van der Vorm, P. (1993). *Vergelijking van berekeningsmethoden voor dukdalven* (Master's thesis). Delft University of Technology. Delft.

Vanhoutte, B., & Verstrynge, F. (2007). *Ontwerpmethodes voor damwandconstructies* (Master's thesis). KHBO. Oostende.

van Weringh, M. (2018). *Test loading of quay structures using fem* (Master's thesis). Delft University of Technology. Delft.

Visschedijk, M. (2005). *Msheet version 7.1, design of diaphragm and sheet pile walls*.

Weissenbach, A. (2001). *Baugruben Teil 3 - Berechnungsverfahren*. Ernst & Sohn.

A

Drawings

A.1. Cross section
A.2. Overview

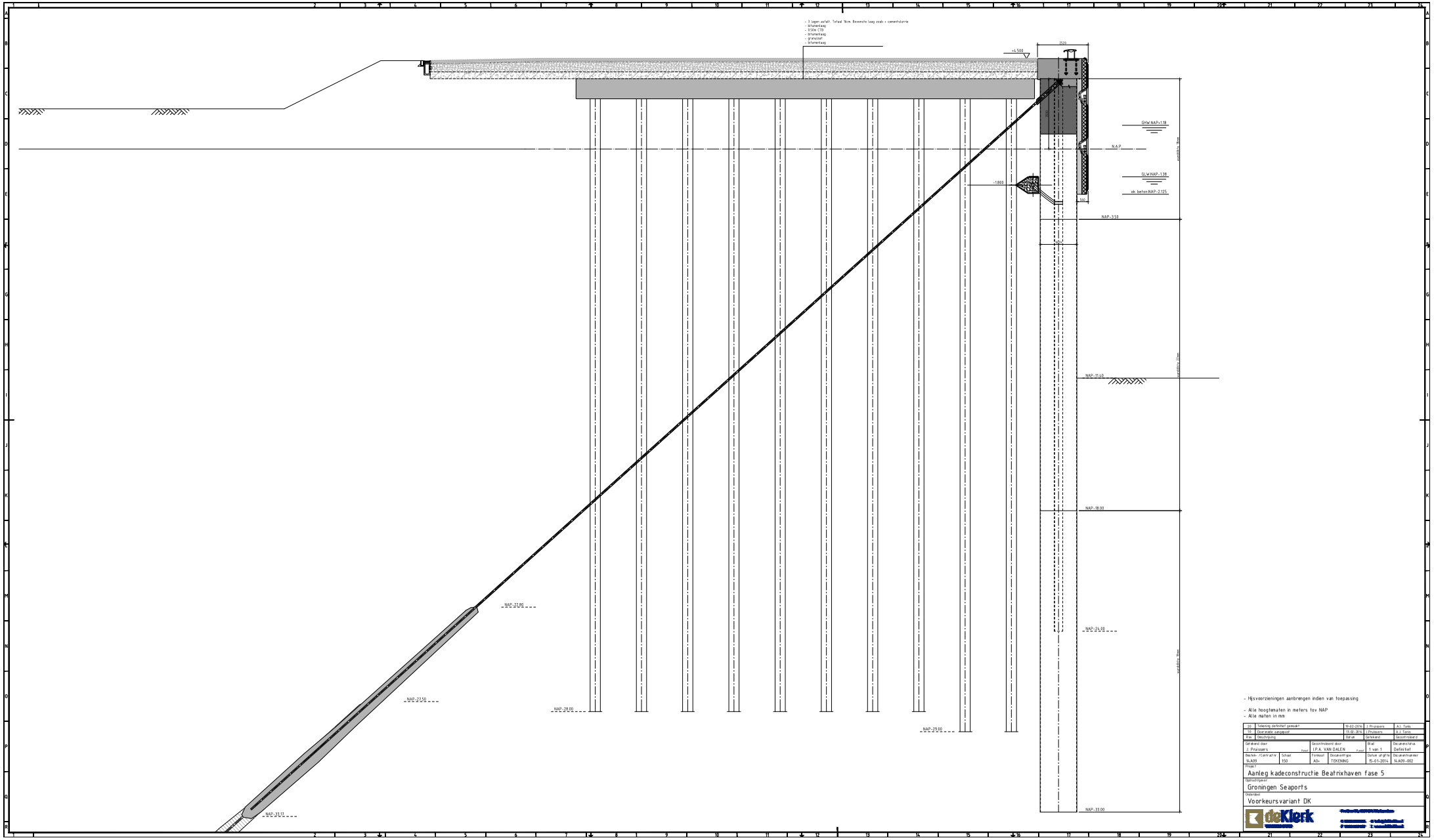
- 3 lagen asfalt. Totaal 16cm. Bovenste laag zoab + cementslurrie
- bitumenlaag
- 650m C10
- bitumenlaag
- granulaat
- bitumenlaag
+4.500
1520
GHW NAP+1.19
N.A.P.
GLW NAP-1.38
ok beton NAP-2.125
-1.900
NAP-3.50
NAP-11.40
NAP-18.00
NAP-24.90
NAP-33.00
NAP-27.00
NAP-27.50
NAP-28.00
NAP-29.00
NAP-31.11
- Hijsvoorzieningen aanbrengen indien van toepassing
- Alle hoogtenaten in meters tov NAP
- Alle maten in mm
Tekening definitief gemaakt 19-02-2014 J. Prussers A.J. Tonis
Diverse aktie opgepakt 19-02-2014 J. Prussers A.J. Tonis
Nr. Omschrijving Datum Getekend Gecontroleerd
Aanbesteding door: J. Prussers
Gecontroleerd door: I.P.A. VAN DALEN
Blad: 1 van 1
Documentsoort: Definitief
Bedrijfs- / Centraalnr.: 14.A09
Schaal: 150
Formaat: A0+
Documentgroep: TEKENING
Datum uitgifte: 15-01-2014
Documentnummer: 14.A09-002
Project
Aanleg kadeconstructie Beatrixhaven fase 5
Opdrachtgever
Groningen Seaports
Onderdeel
Voorkeursvariant OK
deKlerk

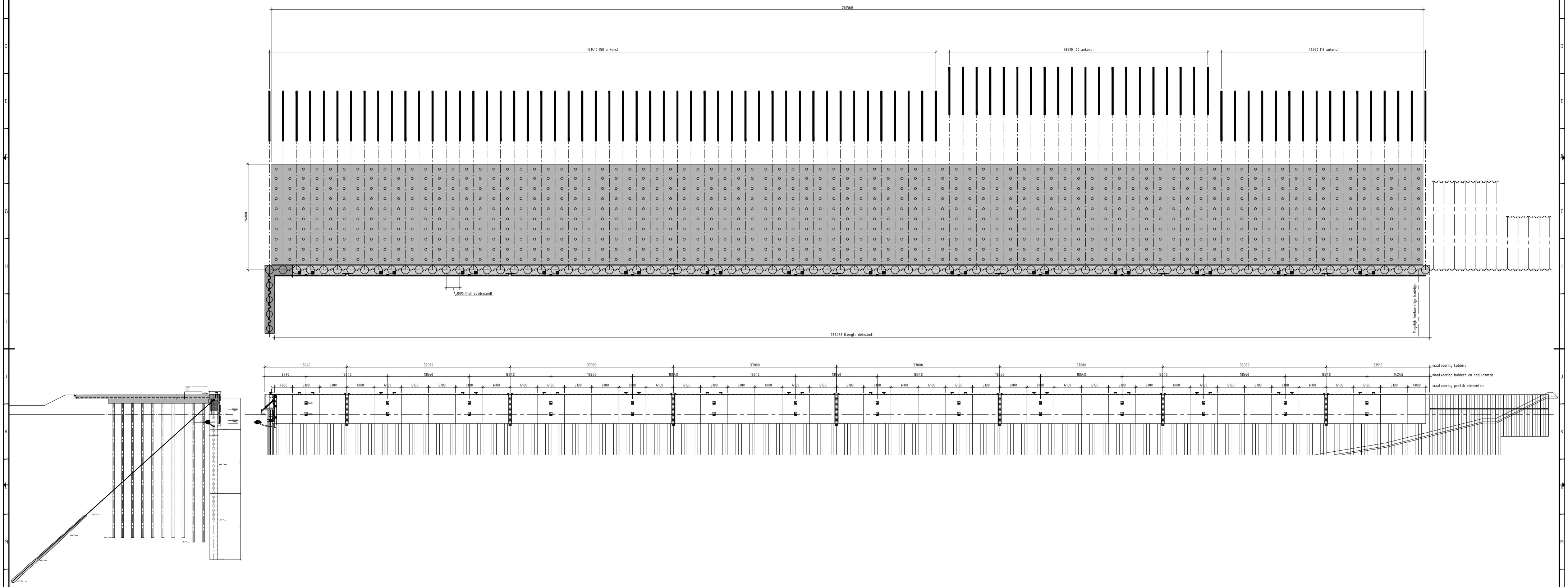

- Hijsvoorzieningen aanbrengen indien van toepassing

- Alle hoogtematen in meters tov NAP
- Alle maten in mm

Rev	Omschrijving	Datum	Getekend	Gecontroleerd
2.0	Tekening definitief gemaakt	19-02-2014	J. Pruissers	A.J. Tanis
1.0	Aanzichten aangepast	17-02-2014	J. Pruissers	A.J. Tanis

Getekend door	Gecontroleerd door	Blad	Documenstatus
J. Pruissers (Paraaf)	I.P.A. VAN DALEN (Paraaf)	1 van 1	Definitief

Bestek- /Contractnr.	Schaal	Formaat	Documenttype	Datum uitgifte	Documentnummer
14A09	1:250	A0+	TEKENING	23-01-2014	14A09-003

Project
Aanleg kadeconstructie Beatrixhaven fase 5

Opdrachtgever
Groningen Seaports

Onderdeel
Voorkeursvariant DK aanzichten

deKlerk WATERBOUW

B

Deformation measurements

This appendix provides the measurements done at the quay wall from construction until this research. appendix B.1 describes the measurements of the top displacement and appendix B.2 provides the inclinometer measurements.

B.1. XZ-top deformations

The measured displacement of the top of the quay wall are included in the file starting at the next page. The drawing gives an overview of the measured points with the reference line (Dutch = ”meetlijn”) which is used for the horizontal displacements. Points 59 and 60 are the points on the small wall perpendicular which is the joint with the consisting quay wall. The three following graphs shows:

1. Horizontal displacement with respect to the reference line.
2. Vertical position in mm with respect to NAP. A jump can be seen between the measurements of 2018 and 2019. This is because the reference bolt 0A4042 lowered apparently 17 mm that year to correct for the subsidence of 5 mm/year in that region.
3. Vertical position in mm with respect to the bolt 0A4042.

In all three graphs are the tubular piles indicated with red lines. The tabular data is added in the three following tables at the end of the file. The relative horizontal displacement at the location of the tubular piles 38, 68 and 78 are displayed in Table B.1.

	Point	**Feb 2017**	**Apr 2021**	**Relative (2021-2017)**	
TP38	66	180	188	8	9.5
	67	190	201	11	
TP68	71	183	189	6	8
	72	173	182	9	
TP78	73	171	177	6	4.7
	74	159	161	2	

Table B.1: Horizontal top displacement of 2017 and 2021 in mm. Positive = to the water

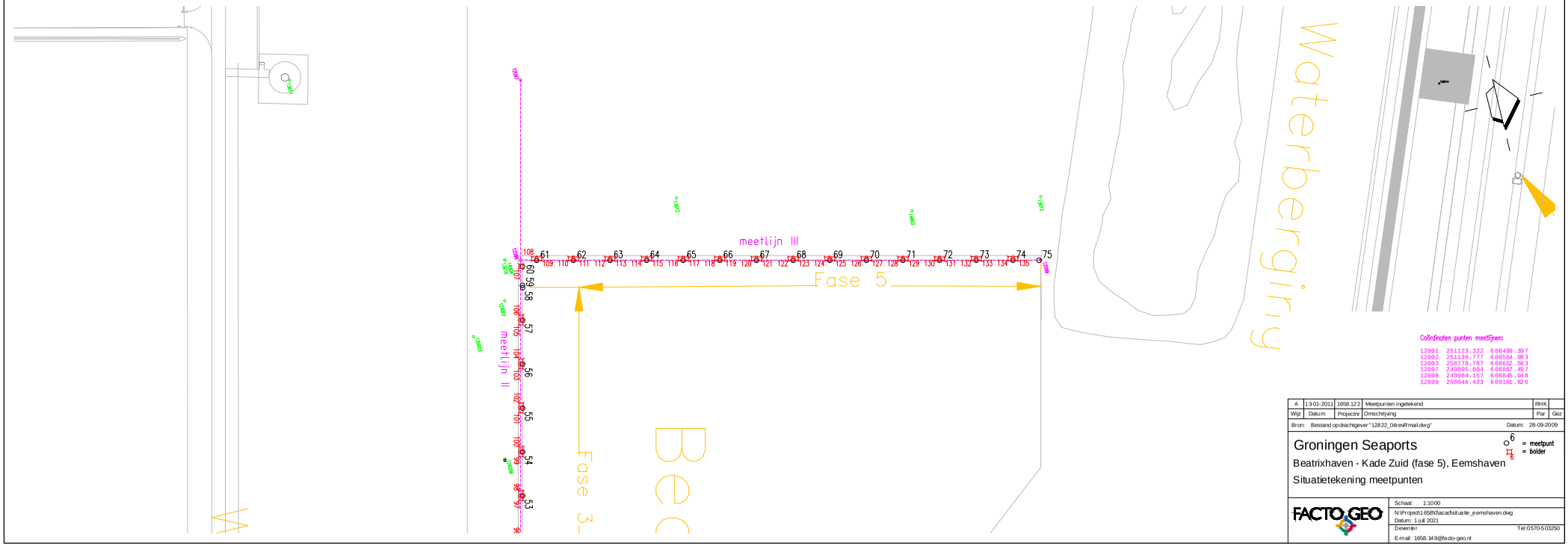

A	13-01-2011	1658.122	Meetpunten ingetekend	RHK
Wijz	Datum	Projectnr	Omschrijving	Par Gez

Bron: Bestand opdrachtgever "12822_04revRmail.dwg" Datum: 28-09-2009

Groningen Seaports

6 = meetpunt
H = bolder

Beatrixhaven - Kade Zuid (fase 5), Eemshaven

Situatietekening meetpunten

FACTO GEO

Schaal: 1:1000

N:\Project\1658\0\acadsituatie_eemshaven.dwg

Datum: 1 juli 2021

Deventer Tel.0570-503250

E-mail: 1658.149@facto-geo.nl

FACTO GEO - Postbus 2017 - 7420 AA Deventer - tel. 0570-50 32 50 - **1658.156@facto-geo.nl**

Beatrixhaven - Kade Zuid (Fase 5) - Eemshaven
Afstand t.o.v. meetlijn III per punt - Punt 61 t/m 75

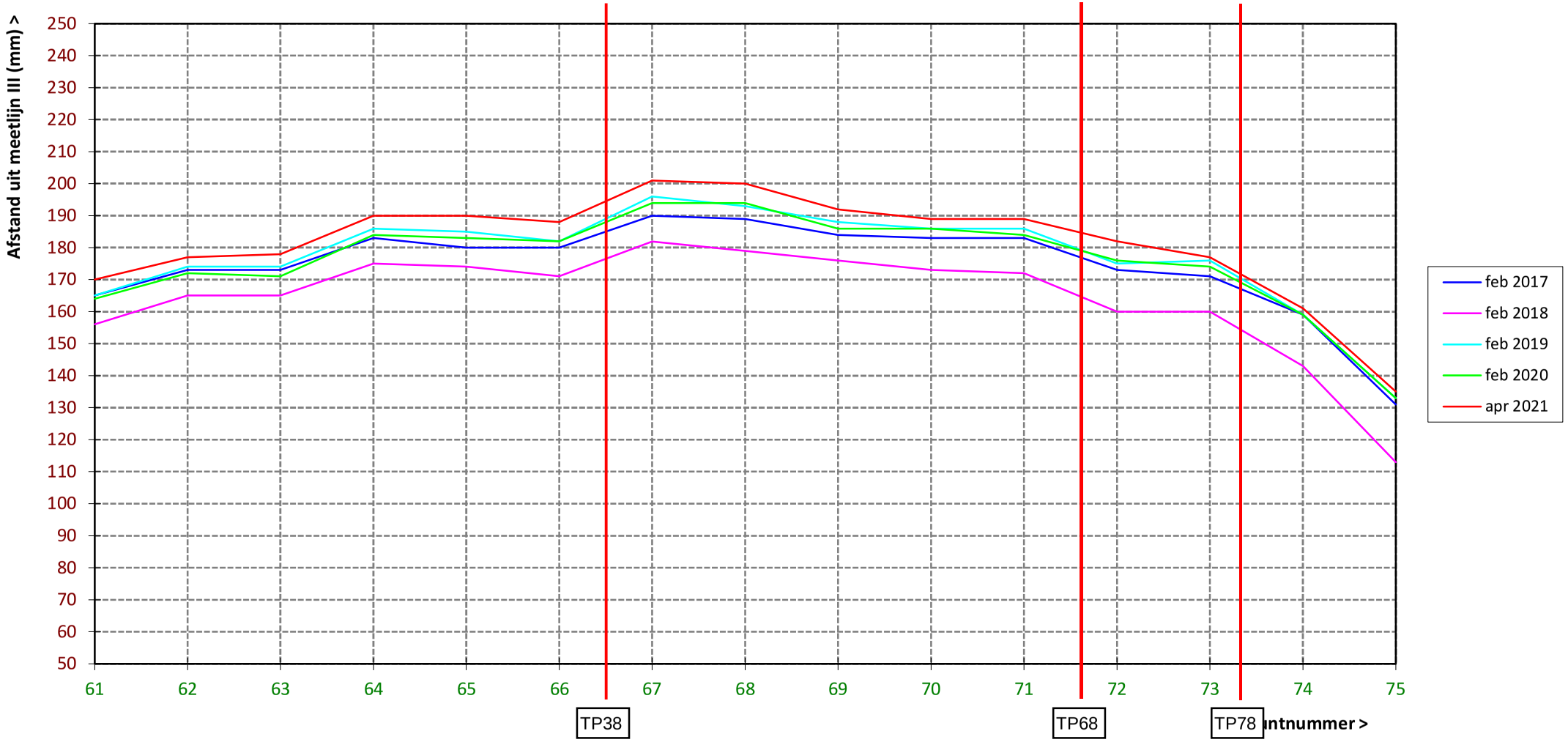

FACTO GEO - Postbus 2017 - 7420 AA Deventer - tel. 0570-50 32 50 - **1658.156@facto-geo.nl**

Beatrixhaven - Kade Zuid (Fase 5) - Eemshaven
Hoogte t.o.v. N.A.P. per punt - Punt 59 t/m 75

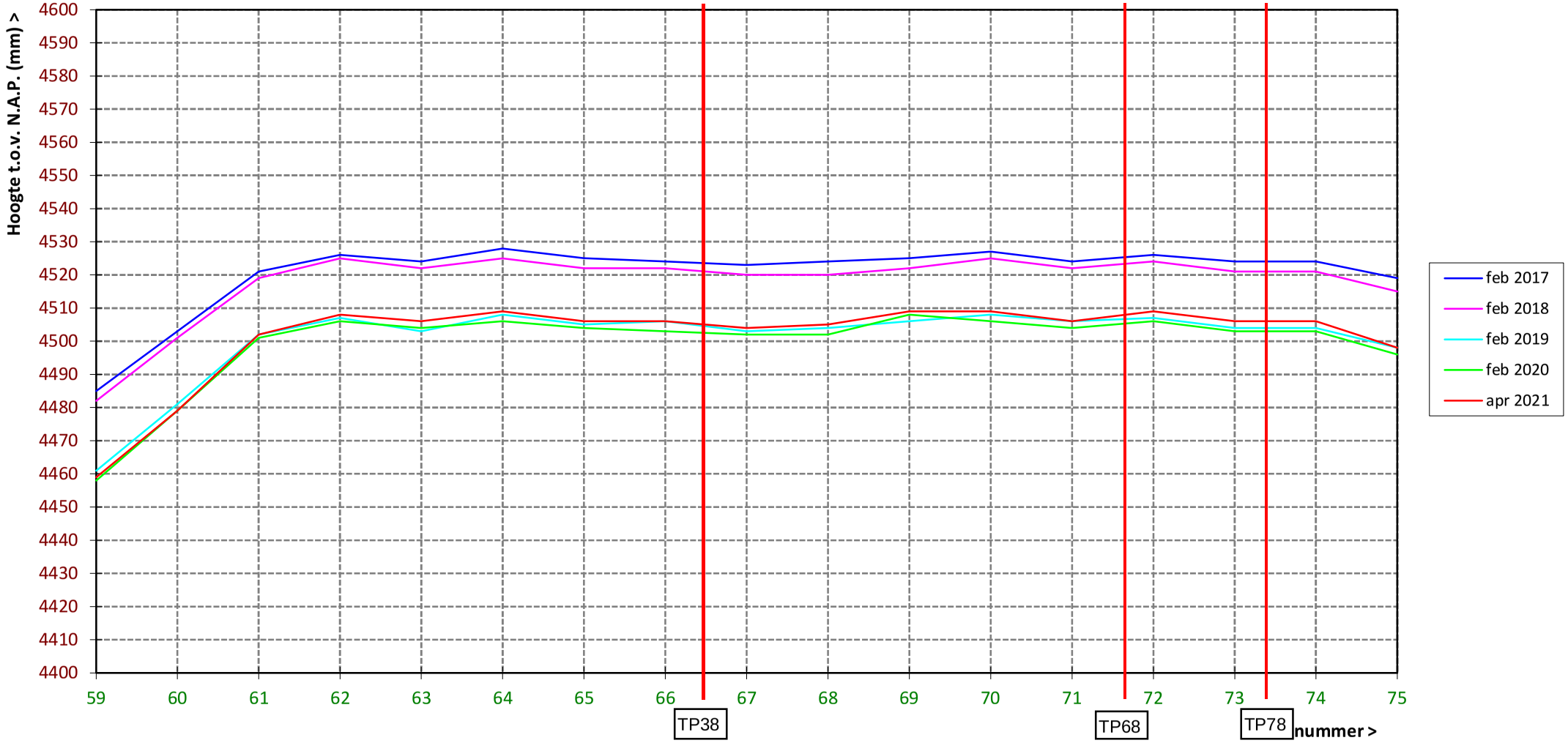

FACTO GEO - Postbus 2017 - 7420 AA Deventer - tel. 0570-50 32 50 - **1658.156@facto-geo.nl**

Beatrixhaven - Kade Zuid (Fase 5) - Eemshaven
Hoogte t.o.v. bout 0A4042 (=0.000) per punt - Punt 59 t/m 75

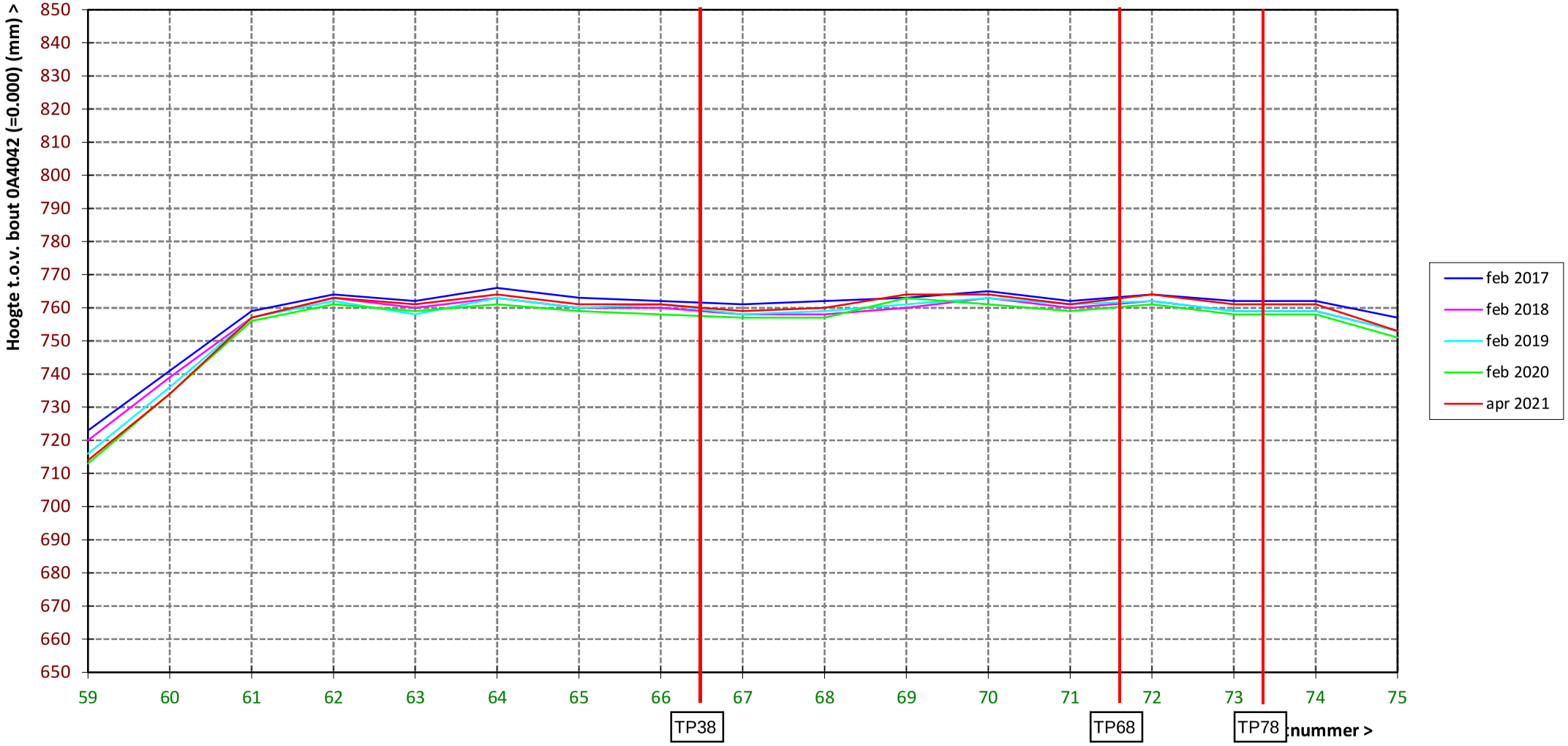

Overzicht zettingen kademuren Groningen Seaports

Plaats: ***Eemshaven***
Locatie: ***Beatrixhaven - Kade Zuid (Fase 5)***
Datum: ***April 2021***
Onderwerp: ***Horizontale zettingen t.o.v. meetlijn***

Puntnr.:	Afstand uit meetlijn *12002-12003 (meetlijn II)* (mm)					Verschil t.o.v. vorige meting (mm) *(positieve waarde = richting water)*			
	feb 2017	feb 2018	feb 2019	feb 2020	apr 2021	2018-2017	2019-2018	2020-2019	2021-2020
59	998	1002	1005	1008	1012	4	3	3	4
60	953	959	959	959	961	6	0	0	2
	Afstand uit meetlijn *12098-12099 (meetlijn III)* (mm)					Verschil t.o.v. vorige meting (mm) *(positieve waarde = richting water)*			
61	165	156	165	164	170	-9	9	-1	6
62	173	165	174	172	177	-8	9	-2	5
63	173	165	174	171	178	-8	9	-3	7
64	183	175	186	184	190	-8	11	-2	6
65	180	174	185	183	190	-6	11	-2	7
66	180	171	182	182	188	-9	11	0	6
67	190	182	196	194	201	-8	14	-2	7
68	189	179	193	194	200	-10	14	1	6
69	184	176	188	186	192	-8	12	-2	6
70	183	173	186	186	189	-10	13	0	3
71	183	172	186	184	189	-11	14	-2	5
72	173	160	175	176	182	-13	15	1	6
73	171	160	176	174	177	-11	16	-2	3
74	159	143	159	159	161	-16	16	0	2
75	131	113	133	133	135	-18	20	0	2

Overzicht zettingen kademuren Groningen Seaports

Plaats: *Eemshaven*
Locatie: *Beatrixhaven - Kade Zuid (Fase 5)*
Datum: *April 2021*
Onderwerp: *Verticale zettingen t.o.v. NAP*

Referentiepunten:	*0A4042*	*3H0092*	*3H0099*
NAP-hoogte feb '17:	*+3.762*	*+3.867*	
NAP-hoogte feb '18:	*+3.762*	*+3.867*	
NAP-hoogte feb '19:	*+3.745*	*+3.847*	
NAP-hoogte feb '20:	*+3.745*	*+3.847*	
NAP-hoogte apr '21:	*+3.745*	*+3.847*	*+4.932*

Puntnr.:	Hoogte t.o.v. NAP (mm)					Verschil t.o.v. vorige meting (mm)			
	feb 2017	feb 2018	feb 2019	feb 2020	apr 2021	2018-2017	2019-2018	2020-2019	2021-2020
59	4485	4482	4461	4458	4459	-3	-21	-3	1
60	4503	4501	4481	4479	4479	-2	-20	-2	0
61	4521	4519	4502	4501	4502	-2	-17	-1	1
62	4526	4525	4507	4506	4508	-1	-18	-1	2
63	4524	4522	4503	4504	4506	-2	-19	1	2
64	4528	4525	4508	4506	4509	-3	-17	-2	3
65	4525	4522	4505	4504	4506	-3	-17	-1	2
66	4524	4522	4506	4503	4506	-2	-16	-3	3
67	4523	4520	4503	4502	4504	-3	-17	-1	2
68	4524	4520	4504	4502	4505	-4	-16	-2	3
69	4525	4522	4506	4508	4509	-3	-16	2	1
70	4527	4525	4508	4506	4509	-2	-17	-2	3
71	4524	4522	4506	4504	4506	-2	-16	-2	2
72	4526	4524	4507	4506	4509	-2	-17	-1	3
73	4524	4521	4504	4503	4506	-3	-17	-1	3
74	4524	4521	4504	4503	4506	-3	-17	-1	3
75	4519	4515	4498	4496	4498	-4	-17	-2	2

Overzicht zettingen kademuren Groningen Seaports

Plaats: *Eemshaven*
Locatie: *Beatrixhaven - Kade Zuid (Fase 5)*
Datum: *April 2021*
Onderwerp: *Verticale zettingen t.o.v. vast hoogtemerk (= 0.000)*

Puntnr.:	Hoogte t.o.v. bout 0A4042 (=0.000) (mm)					Verschil t.o.v. vorige meting (mm)			
	feb 2017	feb 2018	feb 2019	feb 2020	apr 2021	2018-2017	2019-2018	2020-2019	2021-2020
59	723	720	716	713	714	-3	-4	-3	1
60	741	739	736	734	734	-2	-3	-2	0
61	759	757	757	756	757	-2	0	-1	1
62	764	763	762	761	763	-1	-1	-1	2
63	762	760	758	759	761	-2	-2	1	2
64	766	763	763	761	764	-3	0	-2	3
65	763	760	760	759	761	-3	0	-1	2
66	762	760	761	758	761	-2	1	-3	3
67	761	758	758	757	759	-3	0	-1	2
68	762	758	759	757	760	-4	1	-2	3
69	763	760	761	763	764	-3	1	2	1
70	765	763	763	761	764	-2	0	-2	3
71	762	760	761	759	761	-2	1	-2	2
72	764	762	762	761	764	-2	0	-1	3
73	762	759	759	758	761	-3	0	-1	3
74	762	759	759	758	761	-3	0	-1	3
75	757	753	753	751	753	-4	0	-2	2

B.2. Inclinometer

The inclinometer measurement was done at 12-11-2014 and repeated at 8-1-2015 and 11-1-2022. For the three positions, the Figures B.1, B.2 and B.3 shows three graphs per tubular pile:

- a): The raw data with the reference measurement of 2014 indicated with the black dotted line. The toe is assumed zero in all cases.
- b): The relative deformation of 2015 and 2022 by subtracting the reference measurement of 2014.

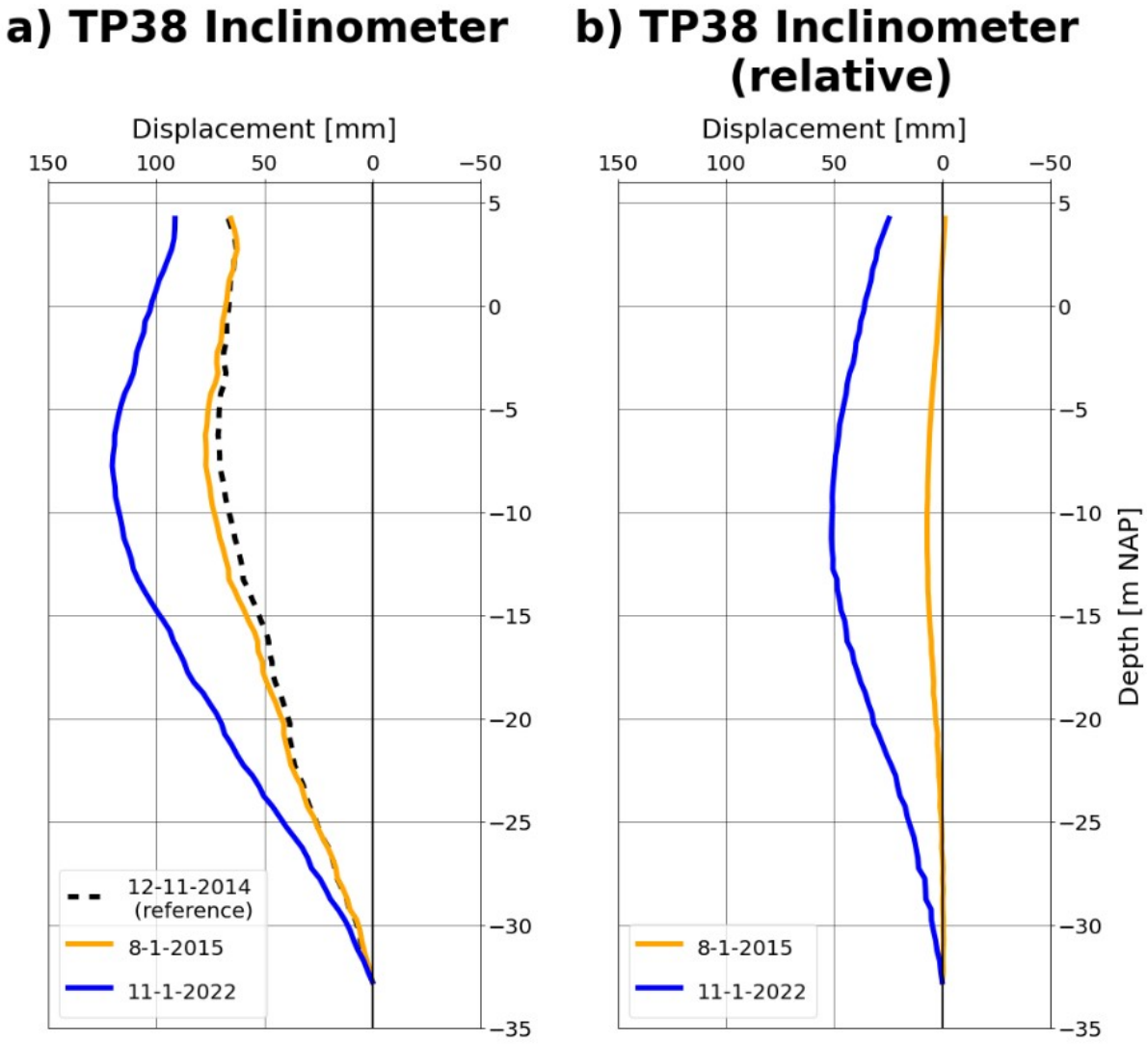

Figure B.1: Measured deformations for TP38

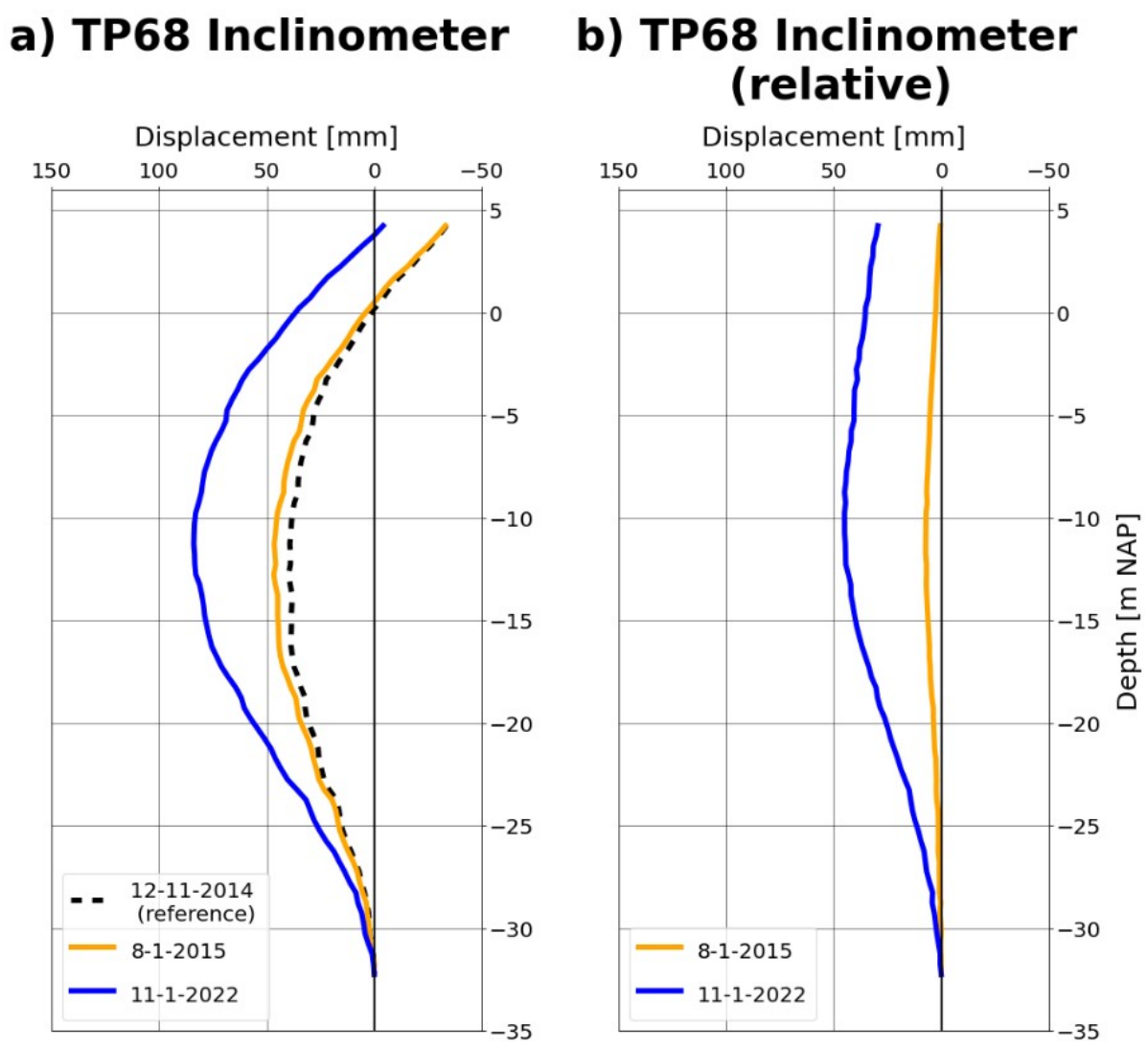

Figure B.2: Measured deformations for TP68

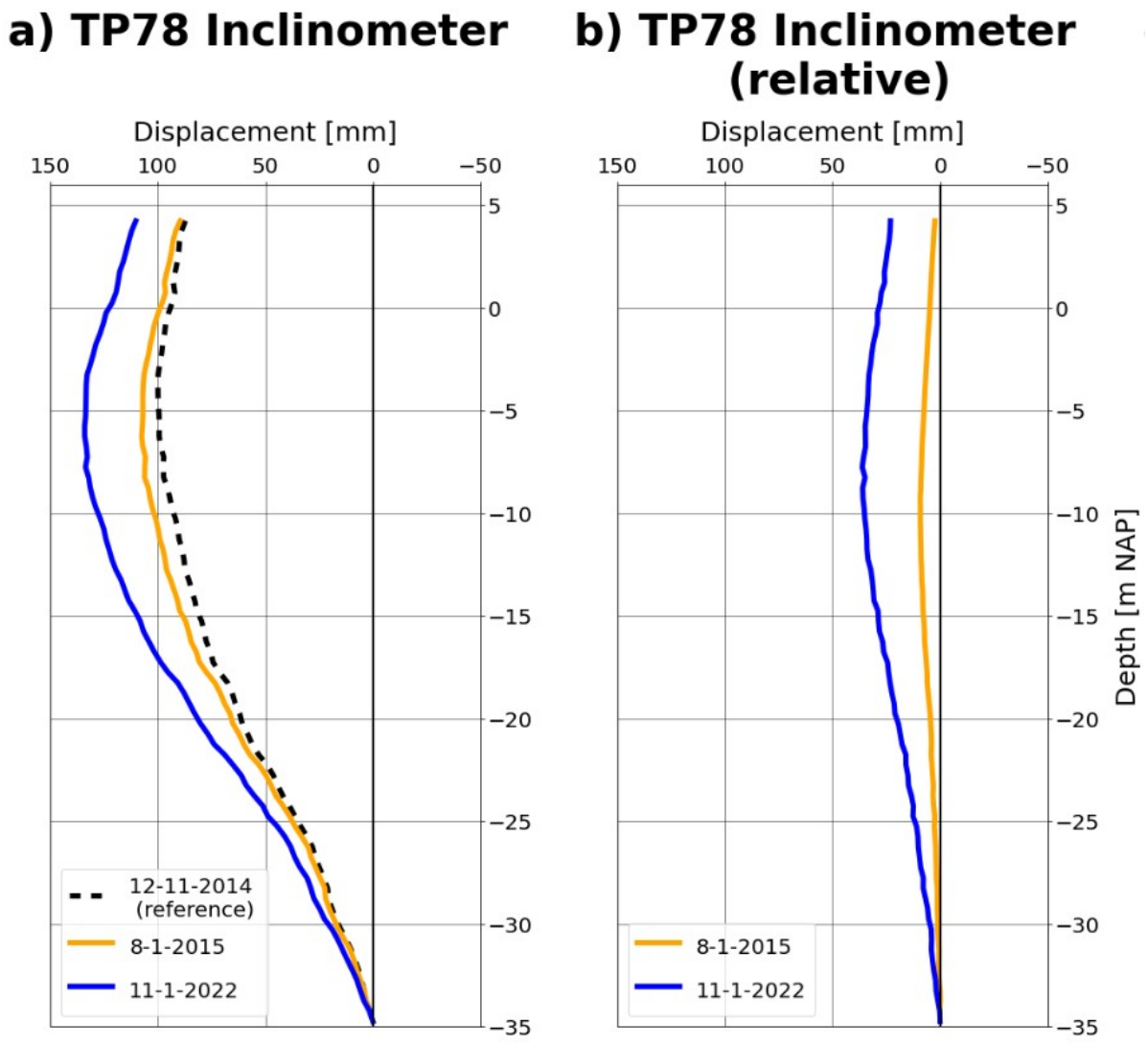

Figure B.3: Measured deformations for TP78

C

Soil characteristics

This appendix will describe the determination of soil parameters based on the available CPT's. Unfortunately, only CPT's where available and more advanced soil investigation would be to costly to perform for this research.

C.1. Selection of CPT's

Several CPT's where done during the design phase and for each TP, several CPT's can be used. Figure C.1 shows the three closest around TP38. There is little variation, so to avoid complexity, only one CPT is used for the soil interpretation.

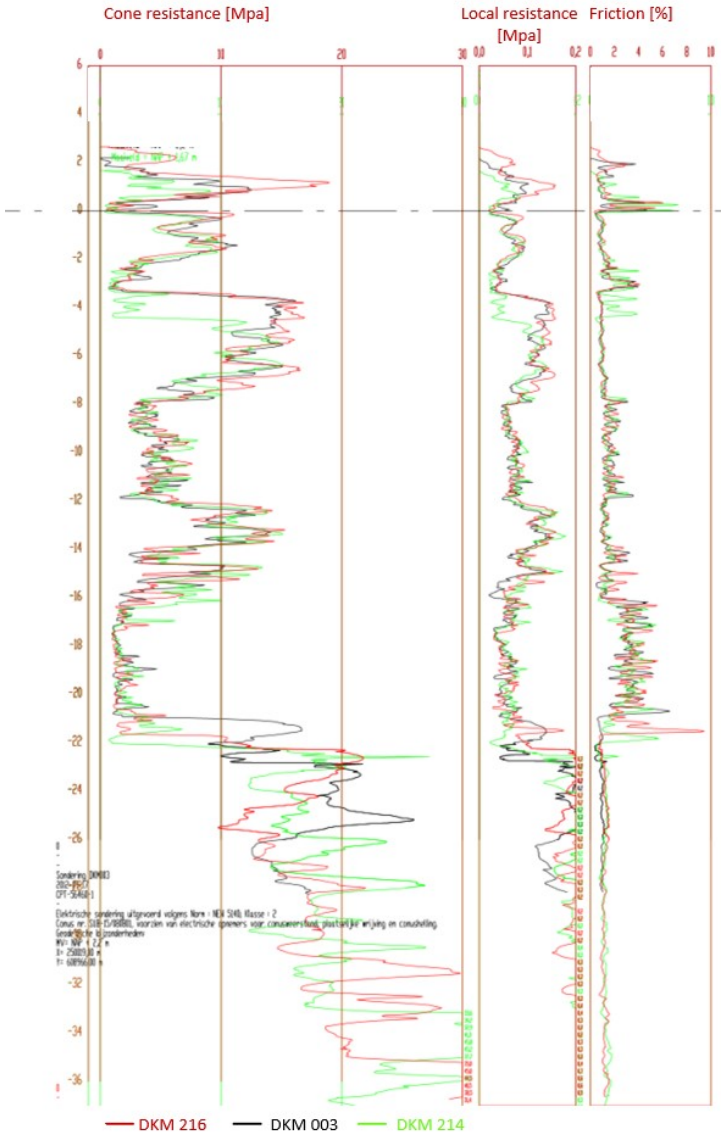

Figure C.1: Three closest CPT's plotted (DKM216, DKM214 and DKM003)

Figure C.2 shows a top view of the three tubular piles that are investigated in red. For each pile, one CPT is selected, which is circled in red.

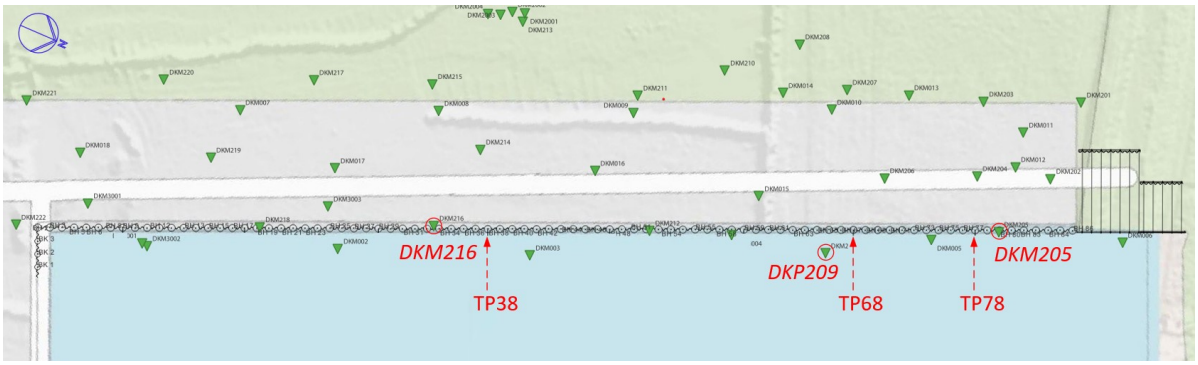

Figure C.2: Overview of CPT's with the used CPT's DKM216, DKP209 and DKM205 highlighted in red.

C.2. Determination of soil parameters

In order to distinct different layers, for each CPT, the average cone resistance and friction ratio per layer is shown in the CPT's on the next pages. It shows the average cone resistance and friction ratio in blue and red respectively per layer. The first layer is the sand fill that is placed after installing the wall and the anchors. The top of this sand fill is at NAP +3.5 m, which is the bottom of the relieving platform. Behind the relieving platform, the top of this layer is at NAP +4.5 m.

DKM216 belonging to BP38

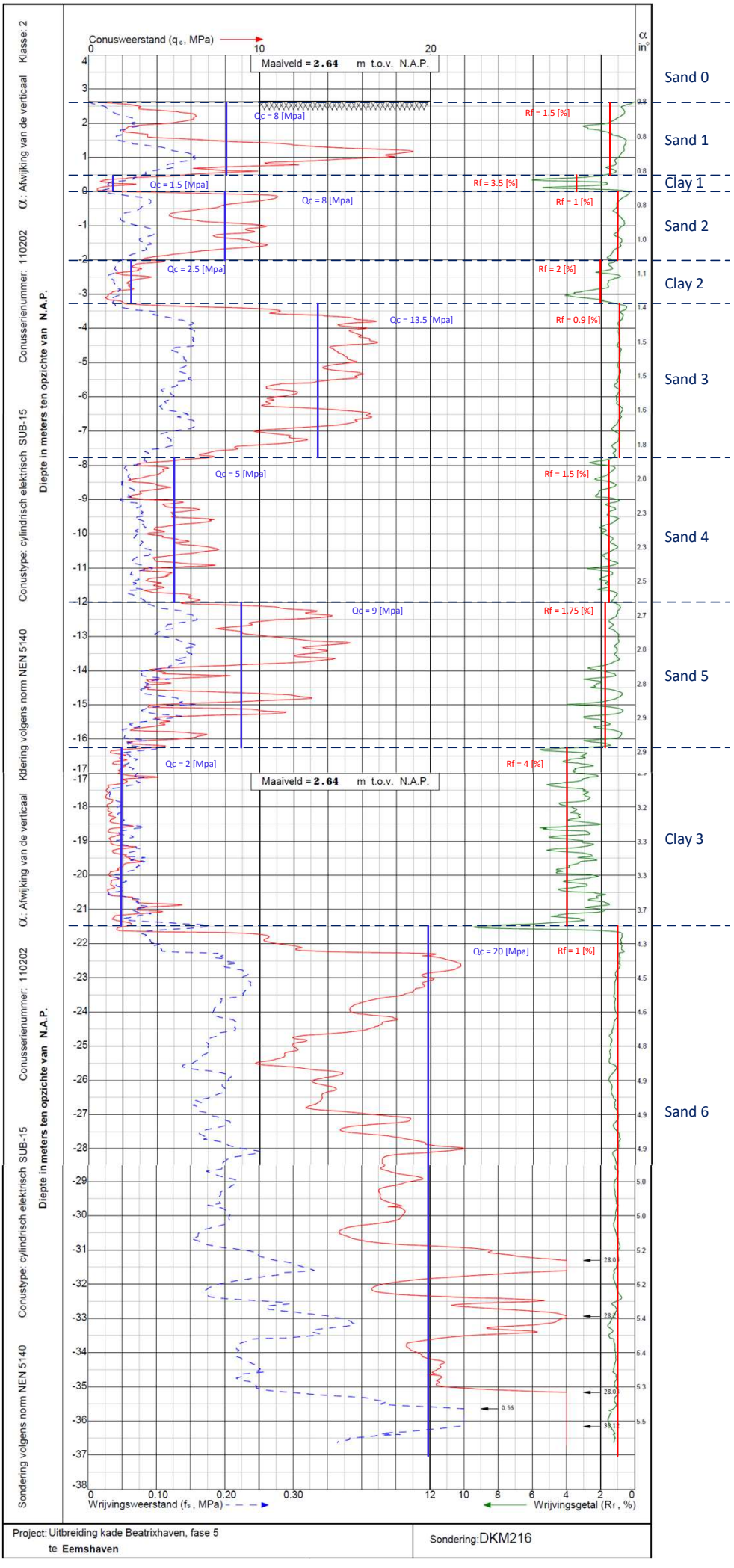

DKP209 belonging to BP68

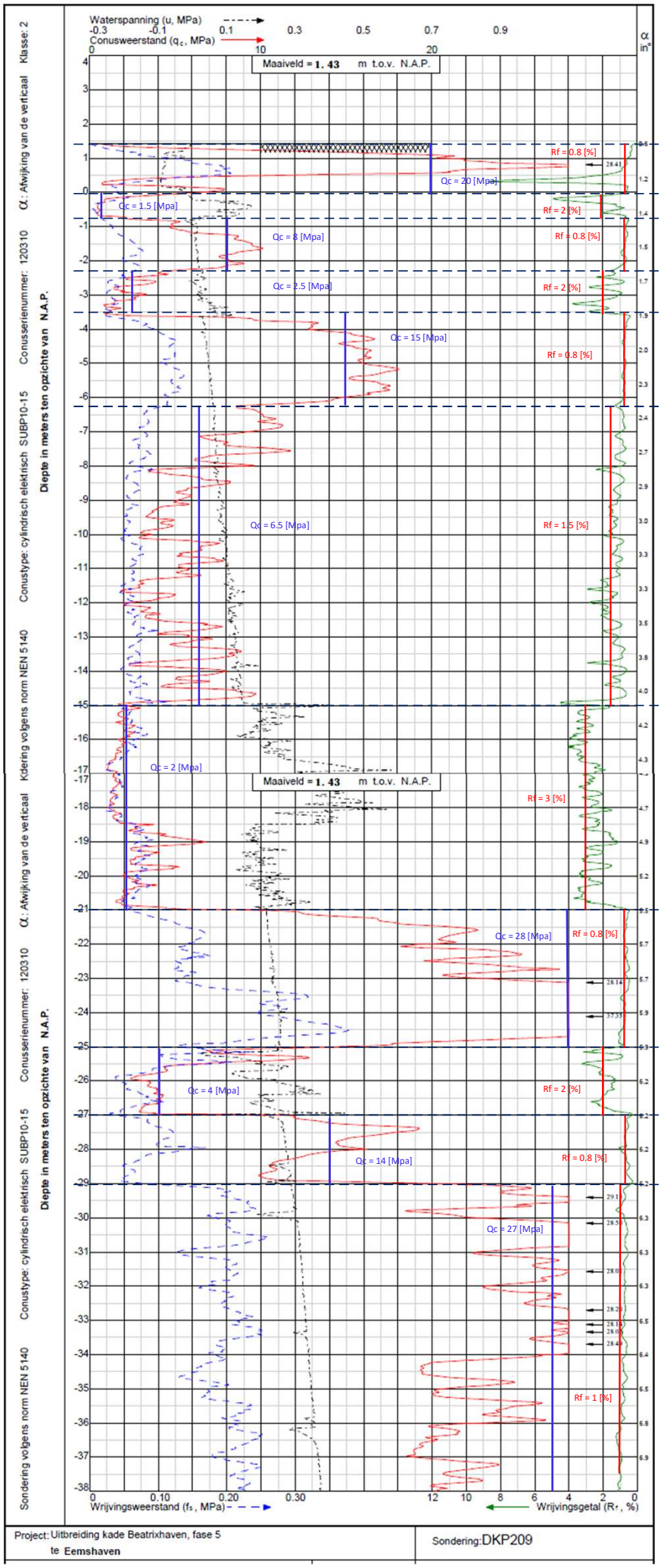

DKM205 belonging to BP78

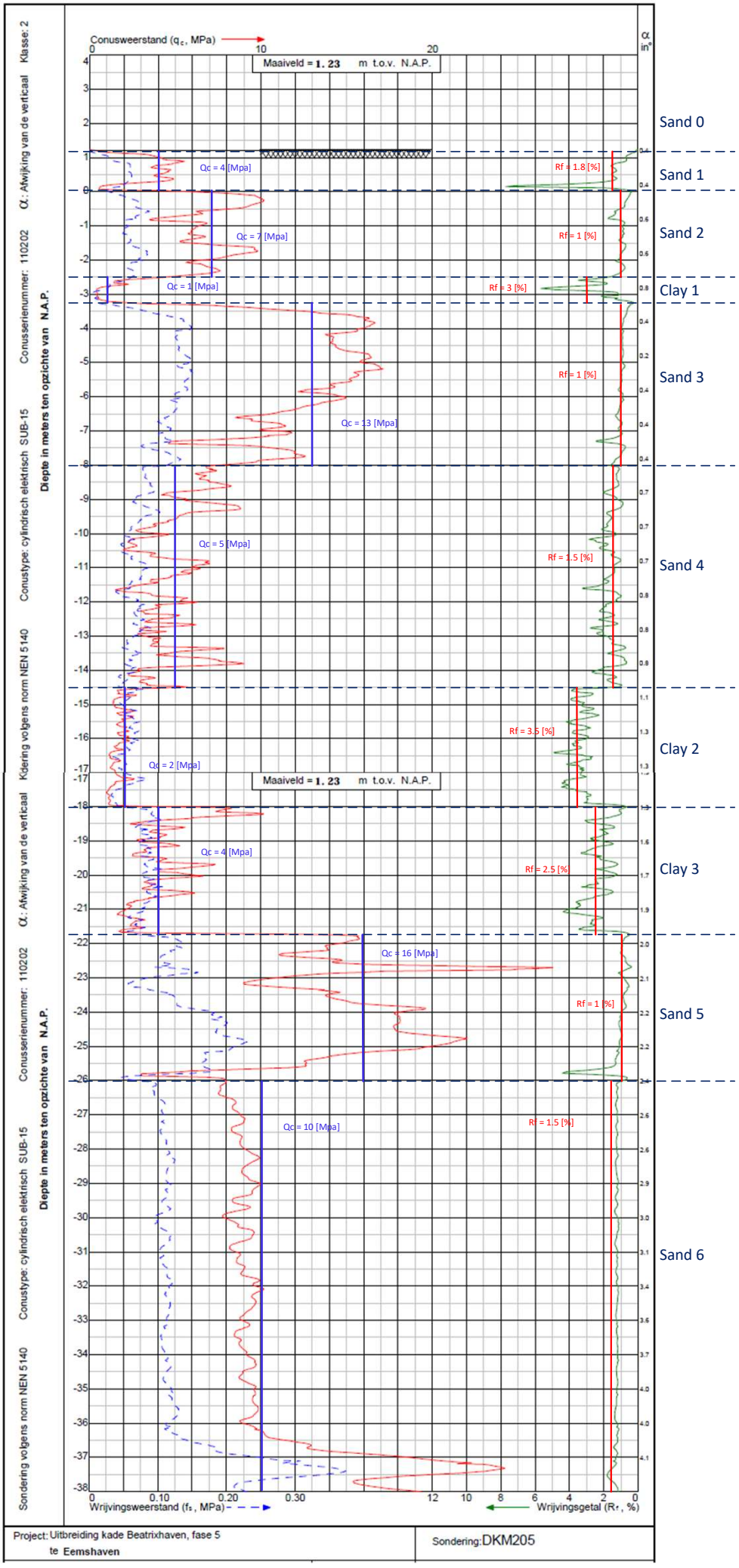

The average cone resistance Q_c and friction ratio R_f are then used in determining the type of soil. With the help of Table 2b (NEN-EN:1997-1, 2012) and Figure 3.22 (CUR166, 2012), the soil type is determined with the volumetric weights. To indicate the package density of the sandy layers, the relative density is calculated using the following equation (van den Ham et al., 2012):

$$Re = 0.4 \cdot ln(\frac{q_c}{0.14 \cdot \sigma_{eff}^{0.6}}) \tag{C.1}$$

Where:

q_c : Average measured cone resistance per layer [MPa]
σ_{eff} : Vertical effective soil stress halfway the soil layer [kPa]

A ground water level of NAP +0.0 m is assumed in calculating the effective soil stress, which is based on other CPT's in the surrounding with measured pore water pressure, for example DKP209. A volumetric weight of 10 kN/m^3 is used. The average parameters per layer from the CPT are listed in Tables C.1, C.2 and C.3.

Layer	**Soil type**	**Top** [m NAP]	q_c [MPa]	R_f [%]	γ [kN/m^3]	γ_{sat} [kN/m^3]	σ_{eff} [kPa]	Re [-]
0	Sand fill (loosely packed)	+3.5/+4.5	-	-	17	19	7.3	-
1	Sand, moderate	+2.64	8.0	1.5	18	20	33.9	0.77
2	Clay, slightly sandy	+0.50	1.5	3.5	19	19	60.4	-
3	Sand, very silty	0.00	8.0	1.0	18	20	72.6	0.59
4	Clay, slightly sandy	-2.00	2.5	2.0	20	20	88.9	-
5	Sand, moderate	-3.25	13.5	0.9	18	20	117.6	0.68
6	Sand, loosely packed	-7.75	5.0	1.5	17	19	159.3	0.21
7	Sand, very silty	-12.00	9.0	1.8	18	20	199.6	0.39
8	Clay, slightly sandy	-16.25	2.0	4.0	16.5	16.5	238.0	-
9	Sand, moderate	-21.50	20.0	1.0	18	20	337.5	0.59

Table C.1: Parameters from DKM216 for TP38

Layer	**Soil type**	**Top** [m NAP]	q_c [MPa]	R_f [%]	γ [kN/m^3]	γ_{sat} [kN/m^3]	σ_{eff} [kPa]	Re [-]
0	Sand fill (loosely packed)	+3.5/+4.5	-	-	17	19	17.6	-
1	Sand, dense	+1.43	20.0	0.8	19	21	48.8	1.05
2	Clay	0.00	1.5	2.0	19	19	65.7	-
3	Sand, slightly silty	-0.75	8.0	0.8	18	20	76.6	0.58
4	Clay, slightly sandy	-2.25	2.5	2.0	20	20	90.4	-
5	Sand, moderate	-3.50	15.0	0.8	18	20	110.4	0.74
6	Sand, loosely packed	-6.25	6.5	1.5	17	19	162.4	0.31
7	Clay, slightly sandy	-14.75	2.0	3.0	17	17	222.5	-
8	Sand, moderate	-21.00	28.0	0.8	18	20	264.4	0.78
9	Clay, slighltly sandy	-25.00	4.0	2.0	18	18	292.4	-
10	Sand, very silty	-27.00	14.0	0.8	18	20	310.4	0.47
11	Sand, moderate	-29.00	27.0	1.0	18	20	365.4	0.69

Table C.2: Parameters from DKP209 for TP68

Layer	Soil type	Top [m NAP]	q_c [MPa]	R_f [%]	γ [kN/m^3]	γ_{sat} [kN/m^3]	σ_{eff} [kPa]	Re [-]
0	Sand fill (loosely packed)	+3.5/+4.5	-	-	17	19	19.3	-
1	Sand, loose	+1.23	4.0	1.8	17	19	49.0	0.41
2	Sand, moderate	0.00	7.0	1.0	18	20	72.0	0.54
3	Clay, slightly sandy	-2.50	1.0	3.0	18	18	87.5	-
4	Sand, moderate	-3.25	13.0	1.0	18	20	114.3	0.68
5	Sand, loose	-8.00	5.0	1.5	17	19	167.3	0.20
6	Clay, slightly sandy	-14.50	2.0	3.5	18	18	210.5	-
7	Clay, slightly sandy	-18.00	4.0	2.5	20	20	243.3	-
8	Sand, very silty	-21.75	16.0	1.0	18	20	283.3	0.54
9	Sand, loose	-26.00	10.0	1.5	18	20	364.5	0.29

Table C.3: Parameters from DKM205 for TP78

For gravel and sand layers the strength parameters E_{100}, φ' and c' are normed for an effective vertical soil stress of 100 kPa. To find the right entry in Table 2b, the measured q_c should be converted to the effective stress σ'_v of 100 kPa using the following equation:

$$q_{c,100} = q_c \cdot C_{qc} \tag{C.2}$$

Where:

$q_{c,100}$	:	Cone resistance normed for effective vertical soil stress of 100 kPa	[-]
q_c	:	Average measured cone resistance per layer	[-]
C_{qc}	:	Correction parameter	[kPa]

Where the correction parameter C_{qc} is calculated with the following formula:

$$C_{qc} = (\frac{100}{\sigma_{eff}})^{0.67} \tag{C.3}$$

With the corrected cone resistance, the other soil parameters are determined. The parameters of the sand fill where prescribed by the contractor (De Klerk B.V., 2014). The angle of wall friction δ' is estimated using a relation with the angle of internal friction φ' (NEN-EN:1997-1, 2012), assuming straight sliding planes:

$$Sand : \delta' = \frac{2}{3}\varphi' \quad Clay : \delta' = \frac{1}{2}\varphi' \tag{C.4}$$

The values for the soil parameters in Table 2b of NEN-EN 1997-1 are low and high characteristic values. In order to gain the average values, the following formula should be used to go from low characteristic values to the mean values:

$$\mu = \frac{f_k}{(1 - \alpha \cdot C_v)} \tag{C.5}$$

Where:

μ	:	Average value
f_k	:	Low characteristic value
α	:	Has a value of 1.64 when the confidence of characteristic values is 95 %
C_v	:	Coëfficient of variation, given in Table 2b of NEN-EN 1997-1

However, using this formula, in many cases the calculated mean value then is even larger than the high characteristic value which should not be the case. Therefore, the mean value is calculated by averaging the low and high characteristic values from Table 2b. These mean values are listed in Tables C.4, C.5 and C.6.

Layer	Layer type	q_c [MPa]	C_{qc} [-]	$q_{c,100}$ [MPa]	γ [kN/m^3]	γ_{sat} [kN/m^3]	φ' [°]	δ' [°]	E_{100} [MPa]	c' [kPa]	c_u [kPa]
0	Sand 0	-	-	-	18.0	20.0	32.5	21.7	62.5	0.0	-
1	Sand 1	8	2.07	16.5	19.0	21.0	35.0	23.3	77.5	0.0	-
2	Clay 1	1.5	1.40	2.1	20.0	20.0	25.0	12.5	7.0	12.0	135.0
3	Sand 2	8	1.24	9.9	18.5	20.5	27.5	18.3	32.5	0.0	-
4	Clay 2	2.5	1.08	2.7	20.5	20.5	25.0	12.5	7.5	14.0	145.0
5	Sand 3	13.5	0.90	12.1	19.0	21.0	35.0	23.3	77.5	0.0	-
6	Sand 4	5	0.73	3.7	18.0	20.0	32.5	21.7	62.5	0.0	-
7	Sand 5	9	0.63	5.7	18.5	20.5	27.5	18.3	22.2	0.0	-
8	Clay 3	2	0.56	1.1	18.3	18.3	21.3	10.6	6.0	8.8	118.8
9	Sand 6	20	0.44	8.9	19.0	21.0	35.0	23.3	77.5	0.0	-

Table C.4: Mean soil parameters TP38 based on Table 2b (NEN-EN:1997-1, 2012)

Layer	Layer type	q_c [MPa]	C_{qc} [-]	$q_{c,100}$ [MPa]	γ [kN/m^3]	γ_{sat} [kN/m^3]	φ' [°]	δ' [°]	E_{100} [MPa]	c' [kPa]	c_u [kPa]
0	Sand 0	-	3.20	-	18.0	20.0	32.5	21.7	62.5	0.0	-
1	Sand 1	20	1.62	32.4	19.5	21.5	37.5	25.0	92.5	0.0	-
2	Clay 1	1.5	1.32	2.0	19.5	19.5	21.3	10.7	7.0	14.0	150.0
3	Sand 2	8	1.20	9.6	18.0	20.0	29.8	19.9	42.5	0.0	-
4	Clay 2	2.5	1.07	2.7	20.5	20.5	25.0	12.5	7.5	14.0	145.0
5	Sand 3	15	0.94	14.0	19.0	21.0	35.0	23.3	77.5	0.0	-
6	Sand 4	6.5	0.72	4.7	18.0	20.0	32.5	21.7	62.5	0.0	-
7	Clay 3	2	0.59	1.2	19.0	19.0	25.0	12.5	22.2	9.5	115.0
8	Sand 5	28	0.52	14.6	19.0	21.0	35.0	23.3	77.5	0.0	-
9	Clay 4	4	0.49	1.9	19.5	19.5	25.0	12.5	6.5	10.0	125.0
10	Sand 6	14	0.47	6.6	18.0	20.0	27.5	18.3	22.5	0.0	-
11	Sand 7	27	0.42	11.3	19.0	21.0	35.0	23.3	77.5	0.0	-

Table C.5: Mean soil parameters TP68 based on Table 2b (NEN-EN:1997-1, 2012)

Layer	Layer type	q_c [MPa]	C_{qc} [-]	$q_{c,100}$ [MPa]	γ [kN/m^3]	γ_{sat} [kN/m^3]	φ' [°]	δ' [°]	E_{100} [MPa]	c' [kPa]	c_u [kPa]
0	Sand 0	-	3.01	-	18.0	20.0	32.5	21.7	62.5	0.0	-
1	Sand 1	4	1.61	6.4	18.0	20.0	32.5	21.7	62.5	0.0	-
2	Sand 2	7	1.25	8.7	19.0	21.0	35.0	23.3	77.5	0.0	-
3	Clay 1	1	1.09	1.1	19.5	19.5	25.0	12.5	6.5	10.0	125.0
4	Sand 3	13	0.91	11.9	19.0	21.0	35.0	23.3	77.5	0.0	-
5	Sand 4	5	0.71	3.5	18.0	20.0	32.5	21.7	62.5	0.0	-
6	Clay 2	2	0.61	1.2	19.5	19.5	25.0	12.5	6.5	10.0	125.0
7	Clay 3	4	0.55	2.2	20.5	20.5	25.0	12.5	7.5	14.0	145.0
8	Sand 5	16	0.50	8.0	18.0	20.0	27.5	18.3	22.5	0.0	-
9	Sand 6	10	0.42	4.2	18.0	20.0	32.5	21.7	62.5	0.0	-

Table C.6: Mean soil parameters TP78 based on Table 2b (NEN-EN:1997-1, 2012)

C.2.1. Modulus of subgrade reaction

The modulus of subgrade reaction is determined using Table 3.10 from the CUR166 (2012), see Table C.3. A spring characteristic of three branches is assumed, with secants values at 50%, 80% and 100%. This shows for each branch the low and high characteristic values. Based on the determined q_c and c_u, the mean modulus of subgrade reaction is calculated by averaging the low and high characteristic value. The results are listed in Table C.7.

		secans-waarde k_h (kN/m³)					
		[1] $p_0<p_h<0,5p_{ea;h;p;rep}$		$0,5p_{ea;h;p;rep}\leq p_h\leq 0,8p_{ea;h;p;rep}$		$0,8p_{ea;h;p;rep}<p_h\leq p_{ea;h;p;rep}$	
		1 [2]	2 [3]	1 [2]	2 [3]	1 [2]	2 [3]
zand	q_c (MPa)						
los	5	12000	27000	6000	13500	3000	6750
matig	15	20000	45000	10000	22500	5000	11250
vast	25	40000	90000	20000	45000	10000	22500
klei	c_u (kPa)						
slap	25	2000	4500	800	1800	500	1125
matig	50	4000	9000	2000	4500	800	1800
vast	200	6000	13500	4000	9000	2000	4500
veen	c_u (kPa)						
slap	10	1000	2250	500	1125	250	560
matig	30	2000	4500	800	1800	500	1125

[1] de waarden in deze kolom te gebruiken bij actieve gronddruk $P_{ea;h;a;rep}$

Figure C.3: Table 3.10 from the CUR166 (2012)

TP38 - DKM216				TP68 - DKP209				TP78 - DKM205			
	k_{h1}	k_{h2}	k_{h3}		k_{h1}	k_{h2}	k_{h3}		k_{h1}	k_{h2}	k_{h3}
	[kN/m³]	[kN/m³]	[kN/m³]		[kN/m³]	[kN/m³]	[kN/m³]		[kN/m³]	[kN/m³]	[kN/m³]
Sand 0	19500	9750	4875	Sand 0	19500	9750	4875	Sand 0	19500	9750	4875
Sand 1	26000	13000	6500	Sand 1	65000	32500	16250	Sand 1	19500	9750	4875
Clay 1	8125	4500	2275	Clay 1	9750	6500	3250	Sand 2	32500	16250	8125
Sand 2	26000	13000	6500	Sand 2	32500	16250	8125	Clay 1	6500	3250	1300
Clay 2	9750	6500	3250	Clay 2	9750	6500	3250	Sand 3	32500	16250	8125
Sand 3	32500	16250	8125	Sand 3	32500	16250	8125	Sand 4	19500	9750	4875
Sand 4	19500	9750	4875	Sand 4	19500	9750	4875	Clay 2	6500	3250	1300
Sand 5	26000	13000	6500	Clay 3	6500	3250	1300	Clay 3	9750	6500	3250
Clay 3	4875	2275	1056	Sand 5	32500	16250	8125	Sand 5	32500	16250	8125
Sand 6	32500	16250	8125	Clay 4	6500	3250	1300	Sand 6	19500	9750	4875
				Sand 6	32500	16250	8125				
				Sand 7	32500	16250	8125				

Table C.7: Modulus of subgrade reaction

C.3. CPT's before and after driving of the piles

In the following file the CPT's can be found that were used to investigate the possible effect of pile driving on the soil, see §4.5.2. The first page shows two CPT's at location near TP38 and the second page shows the CPT's done at the location between TP68 and TP78.

TP38

Before pile installation

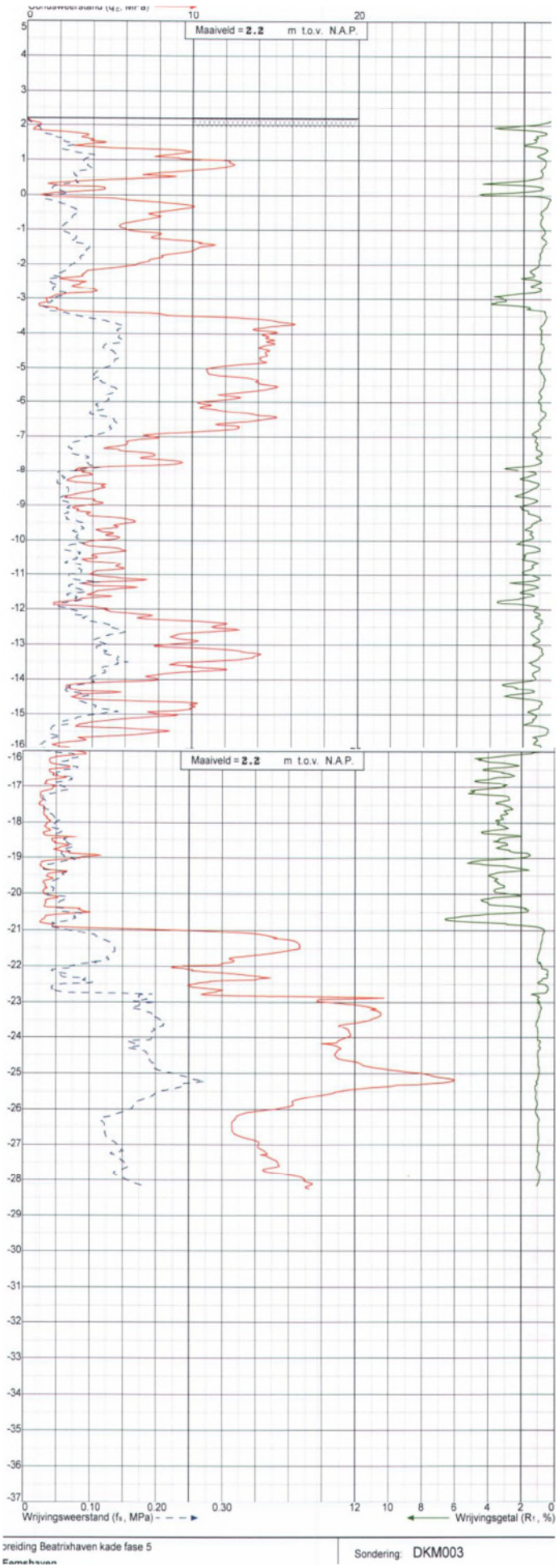

One month after pile installation

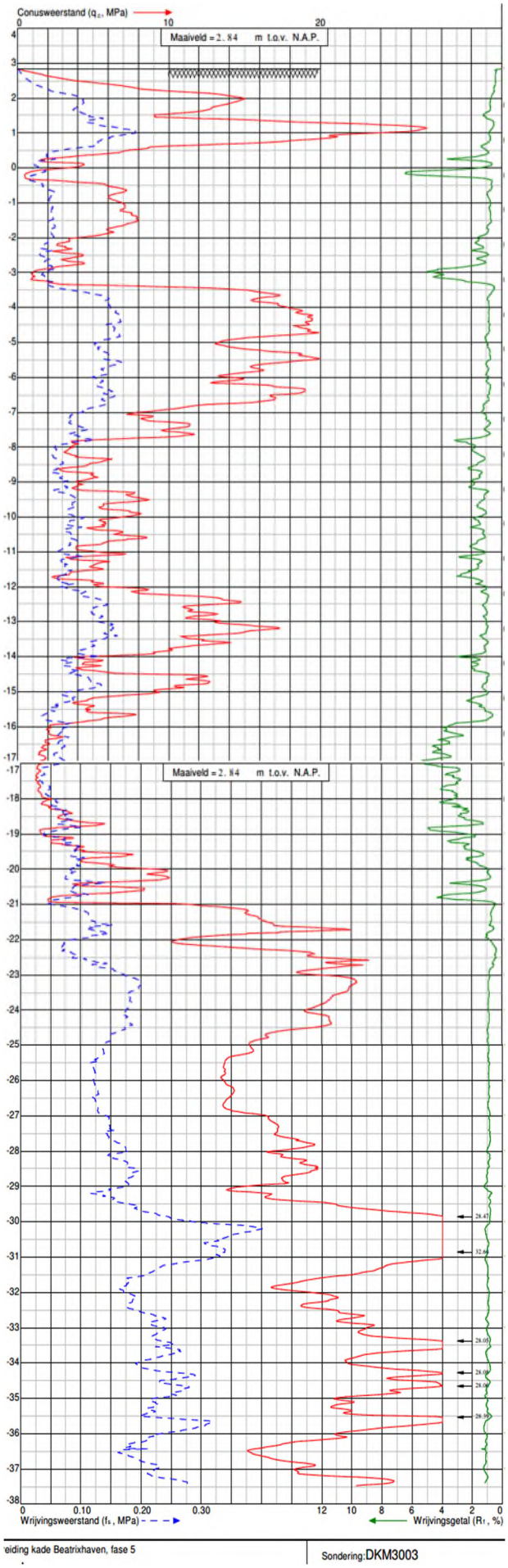

TP68 & TP78

Before pile installation

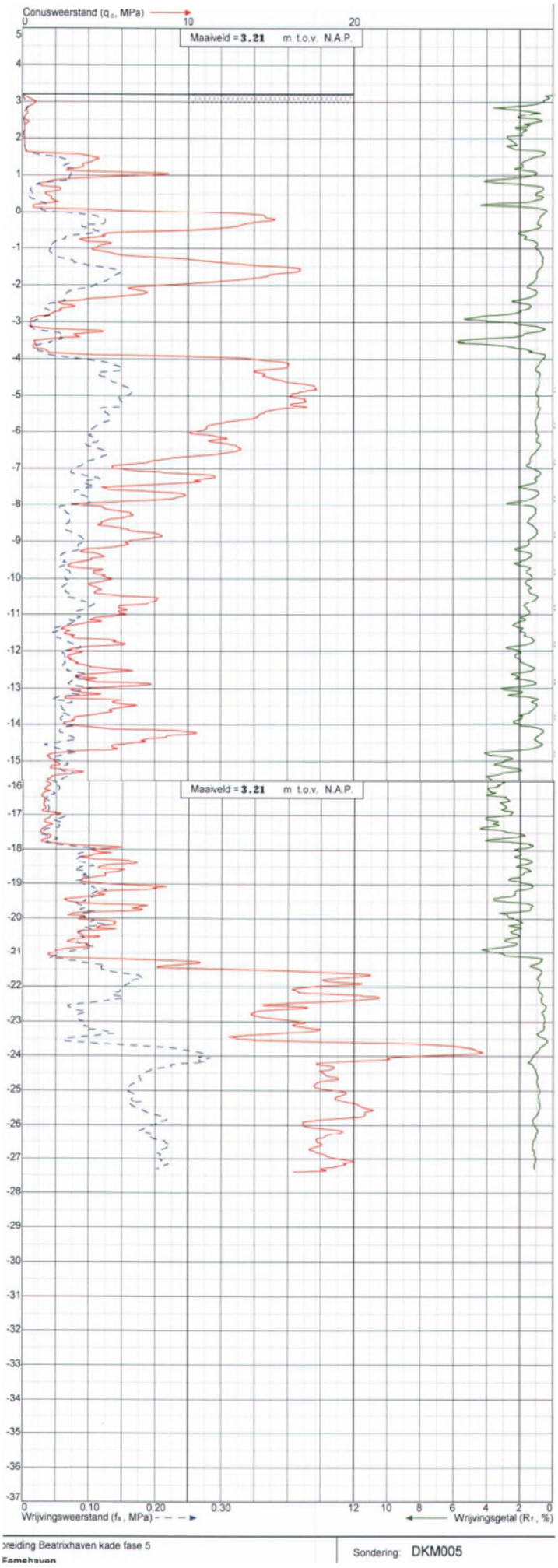

One month after pile installation

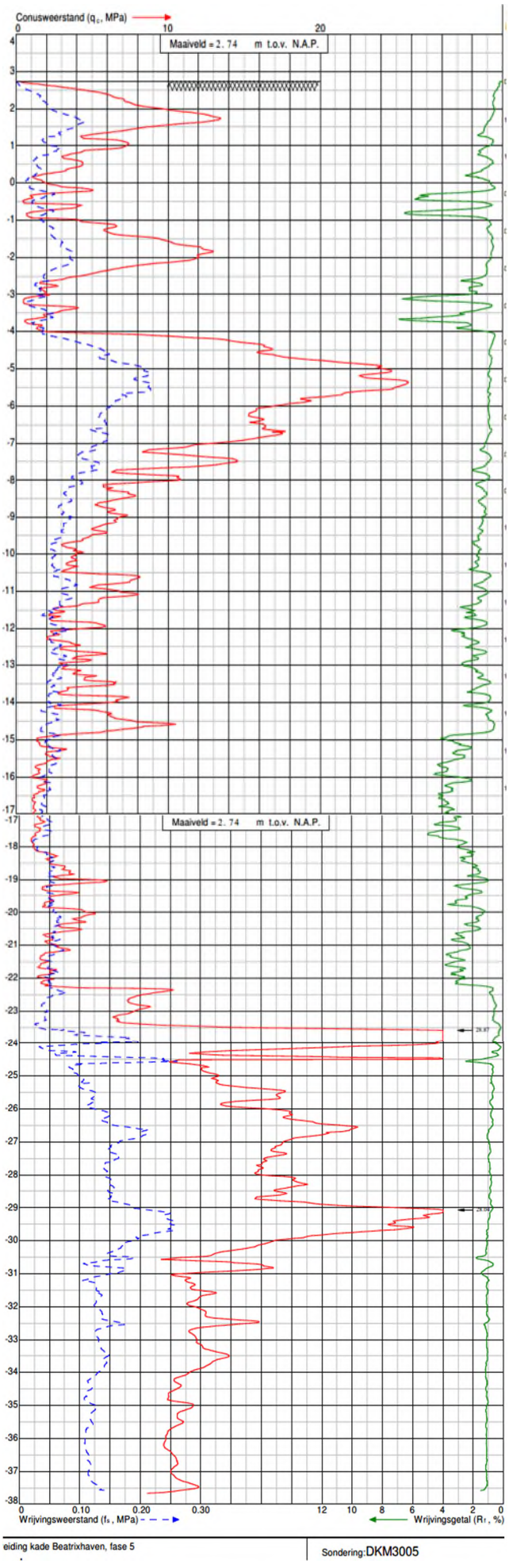

C.4. Additional soil parameters for FEM

Layer	φ [◦]	ψ [◦]	E_{oed}^{ref} [Mpa]	E_{50}^{ref} [Mpa]	E_{ur}^{ref} [Mpa]	m [-]	R_{int} [-]	E_d/E_s [-]	G_0^{ref} [Mpa]	K_0 [-]	σ' [kPa]	$\gamma_{0.7}$ [-]
Sand 0	32.5	2.5	62.5	62.5	187.5	0.5	0.7	2.3	187.5	0.46	7.31	5.7E-06
Sand 1	37.0	7.0	77.5	77.5	232.5	0.5	0.7	2.1	212.3	0.43	33.88	2.4E-05
Clay 1	25.0	0.0	5.6	7.0	21.0	1	0.5	6	54.8	0.58	60.39	2.3E-04
Sand 2	27.5	0.0	32.5	32.5	97.5	0.5	0.7	3	127.2	0.54	72.64	8.0E-05
Clay 2	25.0	0.0	6.0	7.5	22.5	1	0.5	5.6	54.8	0.58	88.89	3.1E-04
Sand 3	37.0	7.0	77.5	77.5	232.5	0.5	0.7	2.1	212.3	0.43	117.64	8.3E-05
Sand 4	32.5	2.5	62.5	62.5	187.5	0.5	0.7	2.3	187.5	0.46	159.27	1.3E-04
Sand 5	27.5	0.0	22.2	22.2	66.7	0.5	0.7	3.5	101.5	0.54	199.64	2.8E-04
Clay 3	21.3	0.0	4.8	6.0	18.0	1	0.5	6.5	50.9	0.64	237.95	6.4E-04
Sand 6	37.0	7.0	77.5	77.5	232.5	0.5	0.7	2.1	212.3	0.43	337.52	2.4E-04

Table C.8: Additional soil parameters Plaxis for TP38

Layer	φ [◦]	ψ [◦]	E_{oed}^{ref} [Mpa]	E_{50}^{ref} [Mpa]	E_{ur}^{ref} [Mpa]	m [-]	R_{int} [-]	E_d/E_s [-]	G_0^{ref} [Mpa]	K_0 [-]	σ' [kPa]	$\gamma_{0.7}$ [-]
Sand 0	32.5	2.5	62.5	62.5	187.5	0.5	0.7	2.3	187.5	0.46	17.60	1.4E-05
Sand 1	40.0	10.0	92.5	92.5	277.5	0.5	0.7	2.0	241.3	0.39	48.78	3.0E-05
Clay 1	21.3	-8.7	5.6	7.0	21.0	1	0.5	6.0	54.8	0.64	65.74	2.5E-04
Sand 2	29.8	-0.2	42.5	42.5	127.5	0.5	0.7	2.5	138.6	0.50	76.61	8.0E-05
Clay 2	25.0	-5.0	6.0	7.5	22.5	1	0.5	5.6	54.8	0.58	90.36	3.1E-04
Sand 3	37.0	7.0	77.5	77.5	232.5	0.5	0.7	2.1	212.3	0.43	110.36	7.7E-05
Sand 4	32.5	2.5	62.5	62.5	187.5	0.5	0.7	2.3	187.5	0.46	162.36	1.3E-04
Clay 3	25.0	-5.0	17.8	22.2	66.7	1	0.5	3.5	101.5	0.58	222.49	3.3E-04
Sand 5	37.0	7.0	77.5	77.5	232.5	0.5	0.7	2.1	212.3	0.43	264.36	1.9E-04
Clay 4	25.0	-5.0	5.2	6.5	19.5	1	0.5	6.0	50.9	0.58	292.36	8.4E-04
Sand 6	27.5	-2.5	22.5	22.5	67.5	0.5	0.7	3.3	96.8	0.54	310.36	4.5E-04
Sand 7	37.0	7.0	77.5	77.5	232.5	0.5	0.7	2.1	212.3	0.43	365.36	2.6E-04

Table C.9: Additional soil parameters Plaxis for TP68

Layer	φ [◦]	ψ [◦]	E_{oed}^{ref} [Mpa]	E_{50}^{ref} [Mpa]	E_{ur}^{ref} [Mpa]	m [-]	R_{int} [-]	E_d/E_s [-]	G_0^{ref} [Mpa]	K_0 [-]	σ' [kPa]	$\gamma_{0.7}$ [-]
Sand 0	32.5	2.5	62.5	62.5	187.5	0.5	0.7	2.3	187.500	0.46	19.30	1.5E-05
Sand 1	32.5	2.5	62.5	62.5	187.5	0.5	0.7	2.3	187.500	0.46	49.05	3.9E-05
Sand 2	37.0	7.0	77.5	77.5	232.5	0.5	0.7	2.1	212.283	0.40	72.00	5.0E-05
Clay 1	25.0	0.0	5.2	6.5	19.5	1	0.5	6	50.870	0.58	87.50	3.0E-04
Sand 3	37.0	7.0	77.5	77.5	232.5	0.5	0.7	2.1	212.283	0.40	114.25	7.9E-05
Sand 4	32.5	2.5	62.5	62.5	187.5	0.5	0.7	2.3	187.500	0.46	167.25	1.3E-04
Clay 2	25.0	0.0	5.2	6.5	19.5	1	0.5	6	50.870	0.58	210.50	6.3E-04
Clay 3	25.0	0.0	6.0	7.5	22.5	1	0.5	5.6	54.783	0.58	243.25	6.9E-04
Sand 5	27.5	0.0	22.5	22.5	67.5	0.5	0.7	3.3	96.848	0.54	283.25	4.1E-04
Sand 6	32.5	2.5	62.5	62.5	187.5	0.5	0.7	3.2	260.870	0.46	364.50	2.1E-04

Table C.10: Additional soil parameters Plaxis for TP78

D

Combined wall properties

This appendix gives the properties of the combined wall. This is the output of an Excel spreadsheet from De Klerk B.V. The first column shows properties of the section with a tubular wall thickness of 22 mm and the second column with a wall thickness of 18 mm. These properties are needed as input for the models in D-Sheet and Plaxis.

Project : Beatrixhaven fase 5, GSP
Date : 5-dec-'22

Input Combined wall

Tubular piles	Symbol	Unity	1829 * 22, X70 Value	1829 * 18, X70 Value	Remarks
Type of tubular pile		-	1829 * 22, X70	1829 * 18, X70	
D/t		-	83.13636364	101.6111111	
Steel quality		-	X70	X70	
Min. Yielding stress	$f_{y;d}$	N/mm²	485	485	
E-modulus	E	kN/m²	2.10E+08	2.10E+08	
Outer diameter	D_{outer}	mm	1829	1829	
Inner diameter	D_{inner}	mm	1785	1793	
Wall thickness	t_{pile}	mm	22	18	
Sectional area	A_{pile}	mm²	124891	102410	
Moment of inertia	$I_{y;pile}$	cm⁴	5098253	4198853	
Bending stiffness	Eipile	kNm²	1.07E+07	8.82E+06	
Section modulus	$W_{y;pile;LZ}$	cm³	55749	45914	
Weight	G_{pile}	kg/m¹	980	804	

Sheet piles	Symbol	Unity	1829 * 22, X70 Value	1829 * 18, X70 Value	Remarks
Type		-	2 voudige tussenplank PU 20	2 voudige tussenplank PU 20	
Quantity			2	2	
Width singular sheet pil	$B_{single\ sheet}$	mm	600	600	
Width between seet piles	B_{sheets}	mm	1200	1200	
Dikte 'wang'		mm	10	10	
Dikte 'buik'		mm	12.4	12.4	
Sectional area	A_{sheets}	mm²	21480	21480	
Moment of inertia	$I_{y;sheets}$	cm⁴	51600	51600	
Weigth		kg/m²	141	141	
Type Slot			C6	C6	
Practical width		mm	30	30	

System	Symbol	Unity	1829 * 22, X70 Value	1829 * 18, X70 Value	Remarks
System width	B_{system}	m	3.089	3.089	
Moment of inertia	$I_{y;pile}$	cm⁴/m¹	1650454	1359292	
Moment of inertia	$I_{y;sheets}$	cm⁴/m¹	16704	16704	
Moment of inertia	$I_{y;system}$	cm⁴/m¹	1667159	1375996	
Moment of inertia	$I_{y;system}$	m⁴/m¹	0.016671587	0.013759964	
Bending stiffness	Eipile	kNm²/m¹	3.4660E+06	2.8545E+06	
Bending stiffness	Eisystem	kNm²/m¹	3.5010E+06	2.8896E+06	
Section modulus	$W_{el;pile;LZ}$	cm³/m¹	18048	14864	
Section modulus	$W_{el;pile;WZ}$	cm³/m¹	18048	14864	
Section modulus	$W_{el;system;LZ}$	cm³/m¹	18230	15046	
Section modulus	$W_{el;system;WZ}$	cm³/m¹	18230	15046	
Max. bending moment	$M_{max;pile;LZ}$	kNm/m¹	8753	7209	
Max. bending moment	$M_{max;pile;WZ}$	kNm/m¹	8753	7209	
Max. bending moment	$M_{max;system;LZ}$	kNm/m¹	8842	7298	
Max. bending moment	$M_{max;system;WZ}$	kNm/m¹	8842	7298	

Weights	Symbol	Unity	1829 * 22, X70 Value	1829 * 18, X70 Value	Remarks
Length pile	L_{pile}	m	1	1	
Wieght pile	G_{pile}	kg	980	804	
Length sheet piles	L_{sheets}	m	1	1	
Weight sheet piles	G_{sheets}	kg	169	169	

Input Dsheet	Symbol	Unity	1829 * 22, X70 Value	1829 * 18, X70 Value	Remarks
Bending stiffness system	Eisystem	kNm²/m¹	3.5010E+06	2.8896E+06	
Bending stiffness tubular piles	EI_{piles}	kNm²/m¹	3.4660E+06	2.8545E+06	
Max. bending moment	$M_{max;system;LZ}$	kNm/m¹	8753	7209	

Input Plaxis	Symbol	Unity	1829 * 22, X70 Value	1829 * 18, X70 Value	Remarks
Strain stiffness system	EA_{system}	kN/m¹	9.9508E+06	8.4224E+06	
Bending stiffness system	EI_{system}	kNm²/m¹	3.5010E+06	2.8896E+06	
Weight system	w_{system}	kN/m¹/m¹	3.6509E+00	3.0904E+00	
Strain stiffness piles	EA_{piles}	kN/m¹	8.4905E+06	6.9621E+06	
Bending stiffness piles	EI_{piles}	kNm²/m¹	3.4660E+06	2.8545E+06	
Weight piles	w_{piles}	kN/m¹/m¹	3.1135E+00	2.5531E+00	

E

Anchors

The following appendix shows the calculation of the anchor elasticity modulus based on test results. Section appendix E.1 shows the displacement-load diagram from the anchor tests done after installation and prestressing. appendix E.2 shows the calculation of the anchor rod stiffness based on lab results. These properties are used as input in D-Sheet and Plaxis.

E.1. Anchor tests

The anchor test starts with an initial load P_i. After that the load is increased in steps to the design load P_d=3219 kN. After unloading to the initial load, it is raised again to the level of prestressing P_{prestr}.

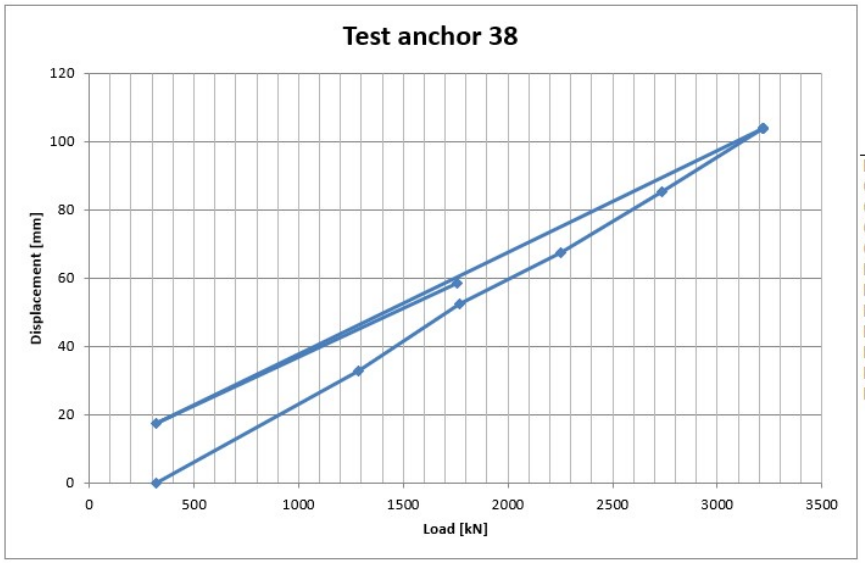

	Force [kN]	Displacement [mm]
Pi	322	0
0.4Pd	1288	32.77
0.55Pd	1770	52.3
0.7Pd	2253	67.25
0.85Pd	2736	85.12
Pd	3219	103.66
Pd	3219	103.71
Pd	3219	103.72
Pd	3219	103.74
Pd	3219	103.78
Pi	322	17.56
Pprestr.	1756	58.4

Figure E.1: Force-displacement diagram from the anchor test for anchor 38. Test performed by Geotech Foundation Solutions (2014).

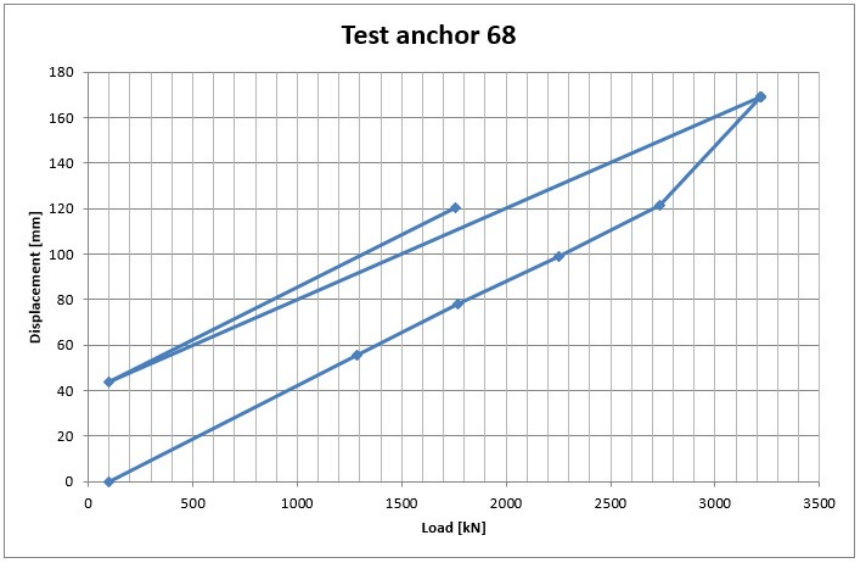

Force [kN]		Displacement [mm]
Pi	100	0
0.4Pd	1288	55.54
0.55Pd	1770	77.89
0.7Pd	2253	98.9
0.85Pd	2736	121.2
Pd	3219	168.89
Pd	3219	168.89
Pd	3219	168.89
Pd	3219	168.94
Pd	3219	169.09
Pi	100	43.54
Pprestr.	1756	120.39

Figure E.2: Force-displacement diagram from the anchor test for anchor 68. Test performed by Geotech Foundation Solutions (2014).

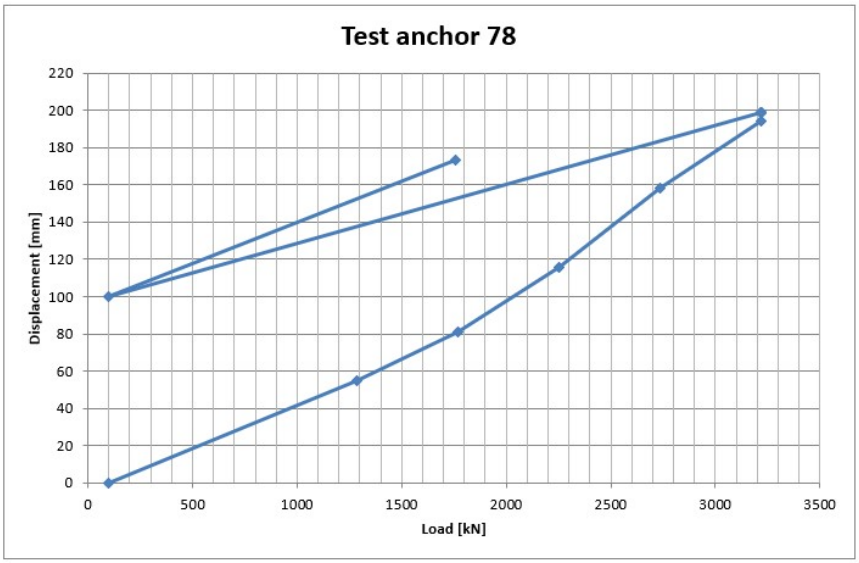

Kracht [kN]		Displacement [mm]
Pi	100	0
0.4Pd	1288	54.8
0.55Pd	1770	81.32
0.7Pd	2253	115.9
0.85Pd	2736	158.13
Pd	3219	194.26
Pd	3219	198.8
Pd	3219	198.86
Pd	3219	198.86
Pd	3219	198.88
Pi	100	99.87
Pprestr.	1756	173.56

Figure E.3: Force-displacement diagram from the anchor test for anchor 78. Test performed by Geotech Foundation Solutions (2014).

E.2. Calculation of anchor stiffness

The anchor consists of a steel rod with a grout body. The stiffness of the anchor rod is determined with a pulling test. The resulting force-elongation diagram is shown on the next page. The E-modulus is calculated with:

$$E = \frac{F \cdot L}{A \cdot \Delta l} \tag{E.1}$$

Where:

F	=	3300	[kN]	:	Highest force in elastic range
L	=	3630	[mm]	:	Length of tested anchor
A	=	6989	[mm^2]	:	Sectional area of tested anchor
Δl	=	(24-6)/2	[mm]	:	Anchor elongation divided by 2, which has something to do with the settings of the used drawbench.

This gives:

$$E = \frac{F \cdot L}{A \cdot \Delta l} = \frac{3300 \cdot 3.630}{6.989 \cdot 0.009} = 190.442\text{MPa}$$

This is taken as the mean value in modelling the anchors.

Also the yield force can be determined from this graph. The yield force is assumed to be the force where the yielding is 2%. With a length of 3630 mm, the yielding is $3630 \cdot 0.002 = 7.26$ mm. Adding the initial displacement of 6 mm, the yielding force $F_{yd} = 4450$ kN, where the total displacement is 13.26 mm. With a center to center distance of 3.09 m, this becomes 4450/3.09 = 1440 kN/m'.

MENNENS
staalkabel-, hijs- en heftechniek
Mennens Dongen B.V.
Tel. 0162 383800

Klant / Customer	**Geotech Metals**	Omschrijving / Description	
Order / Order	**735939**	**breekproef stang 117/64**	
Object / Object	**ankerstang**	Opmerkingen / Remarks	
Serie nr. / Serial No.			
Proeftype / Type of test	**Breekproef**		
Proef / Test	**0** van / of **0**	Starttijd /Time started	**4/15/2014 9:17:33 AM**
Datum / Date	**15.04.2014**	Stoptijd /Time stopped	**4/15/2014 9:26:55 AM**

Hoogste Kracht / Highest Force	**5455**	**kN**	Stijgtijd / Rising time	**500**	kN/Min
Hoogste Rek/ Highest Elasticity	**282**	**mm**			

F-E Diagram

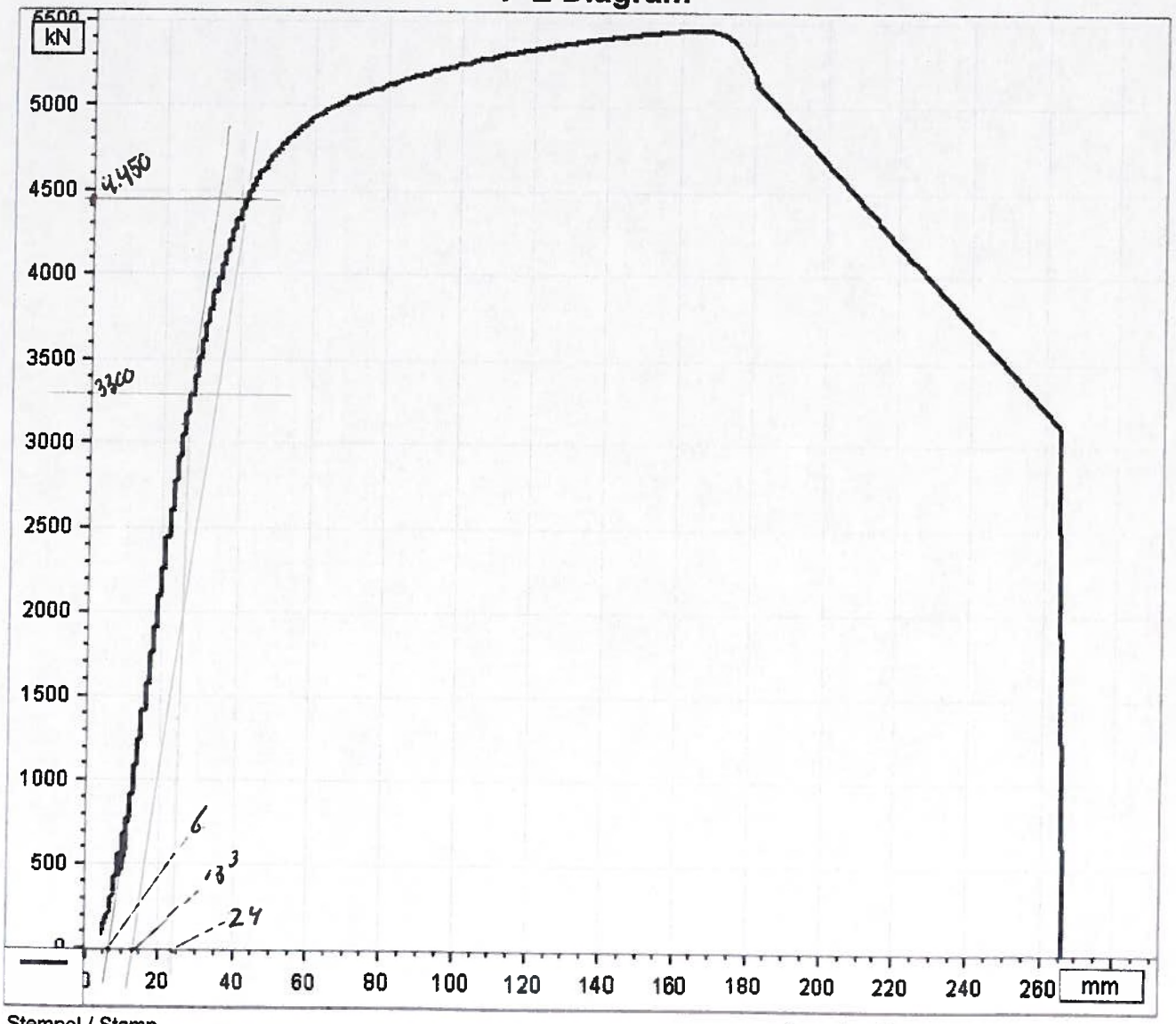

Stempel / Stamp

MENNENS DONGEN B.V.
Metaalstraat 5
5107 ND DONGEN
Tel. 0162 - 383800
MHSips

Stempel / Stamp

F

Results of D-Sheet and Plaxis

This appendix gives an overview of the results from the D-Sheet and Plaxis model. appendix F.1 shows the deformation results from D-Sheet, followed by the results from Plaxis in appendix F.2. appendix F.3 shows the distribution of bending moment M and shear force Q for both models.

F.1. Deformation results D-Sheet Piling

F.1.1. Version 1

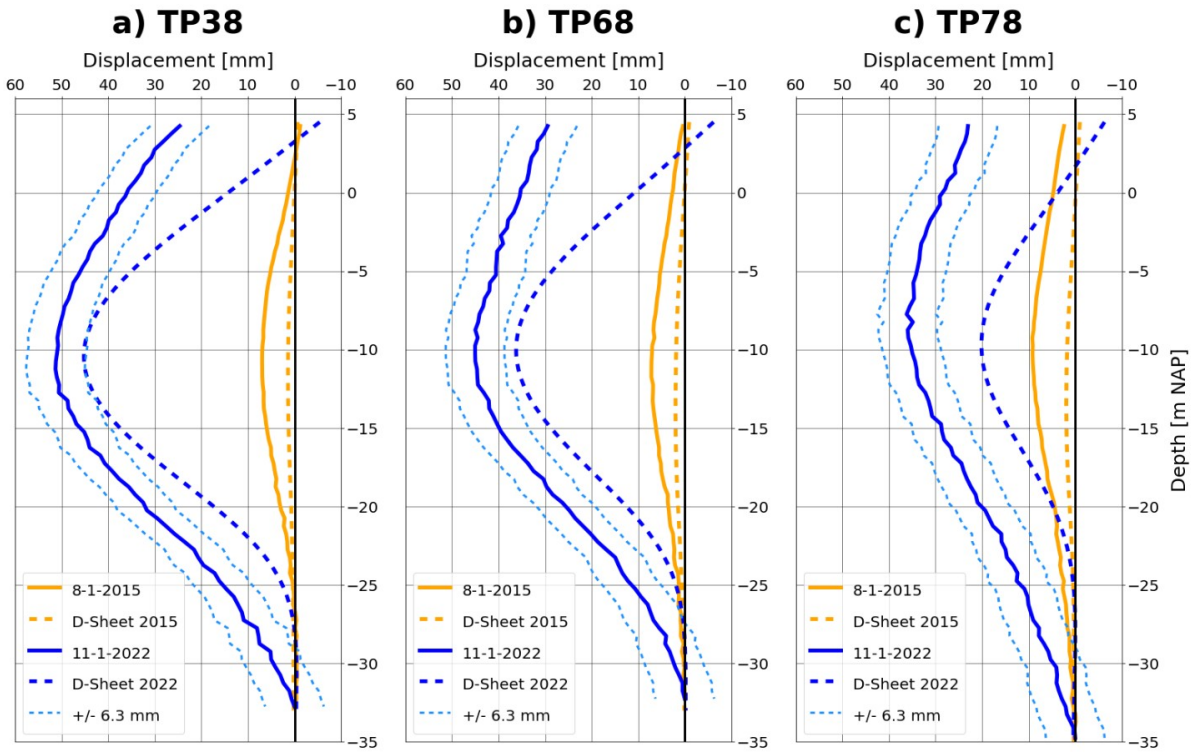

Figure F.1: DSheet results

F.1.2. Version 2

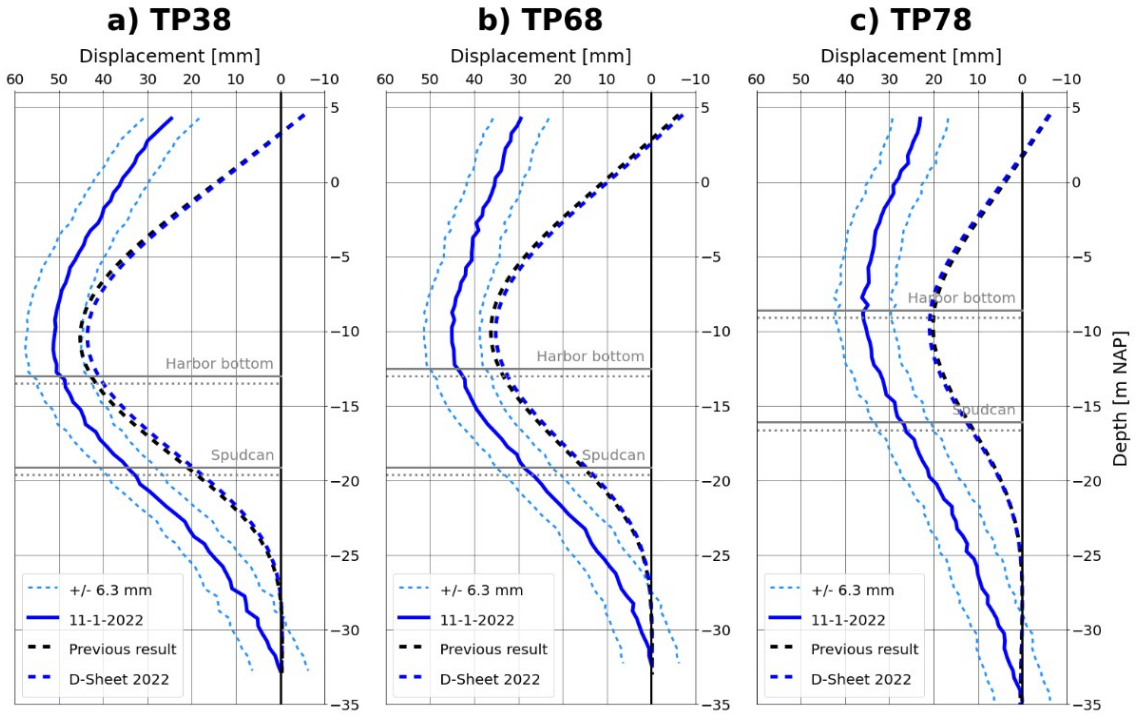

Figure F.2: DSheet results version 2: After adapting the internal friction angle

F.1.3. Version 3

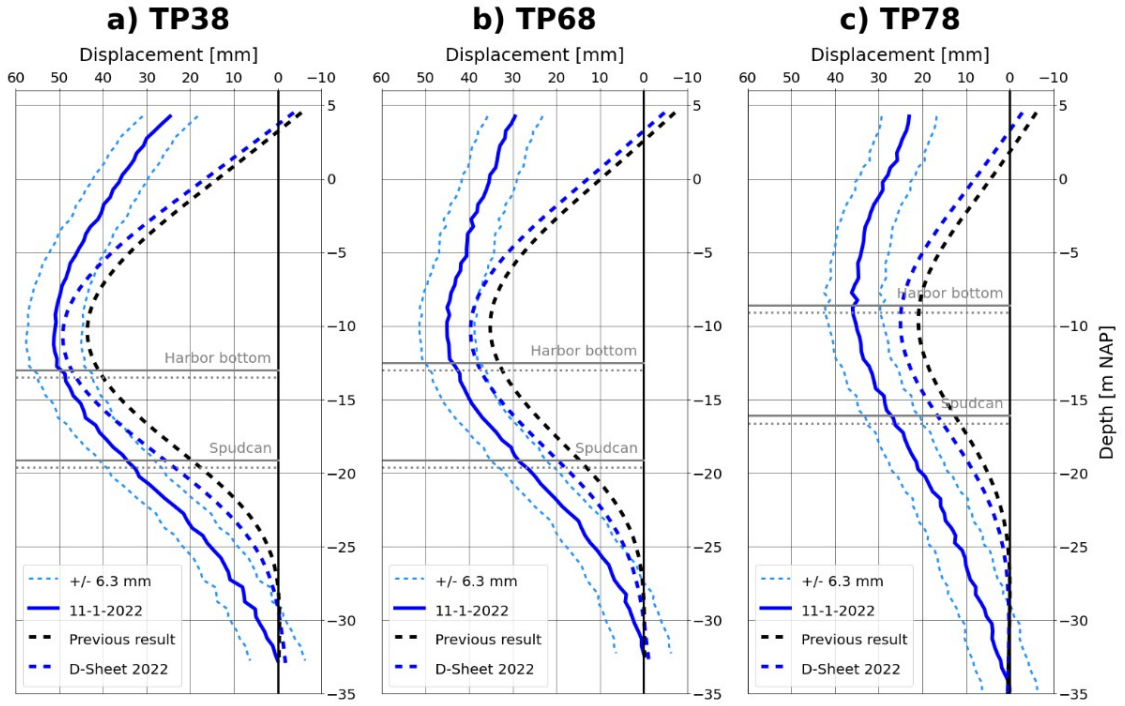

Figure F.3: DSheet results version 3: After adding the extra stage for anchor tests.

F.1.4. Version 4

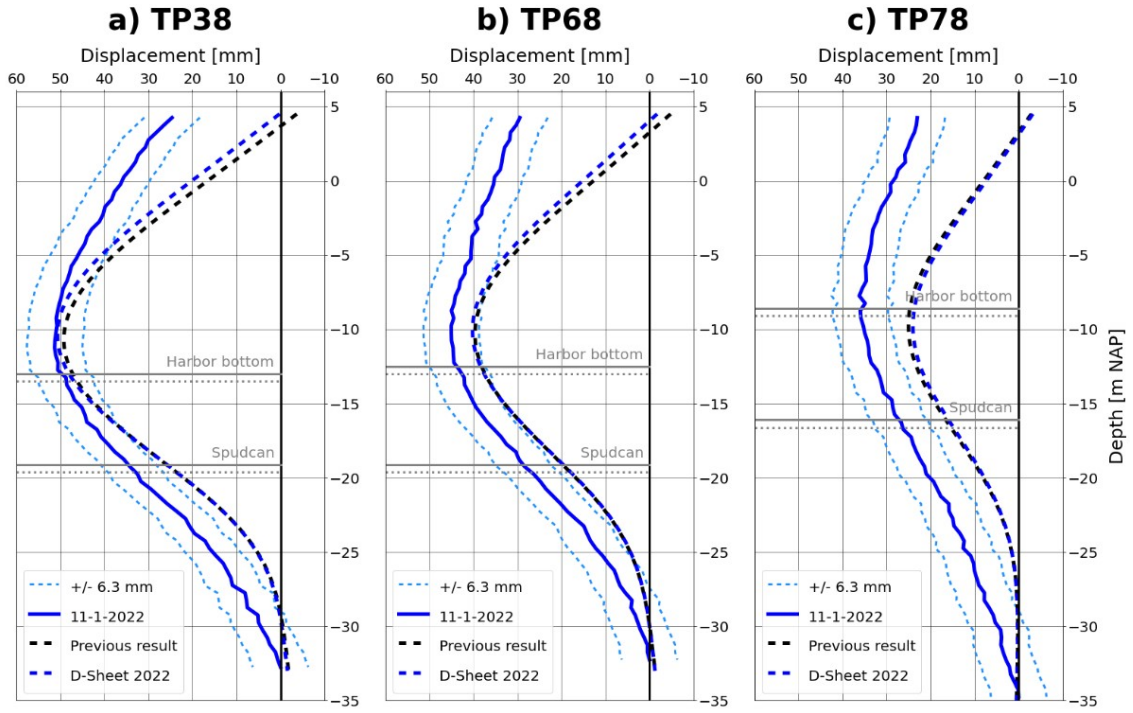

Figure F.4: DSheet results version 4: After combining the stages of the ship loads with the stage of spudcans

F.2. Deformation results Plaxis

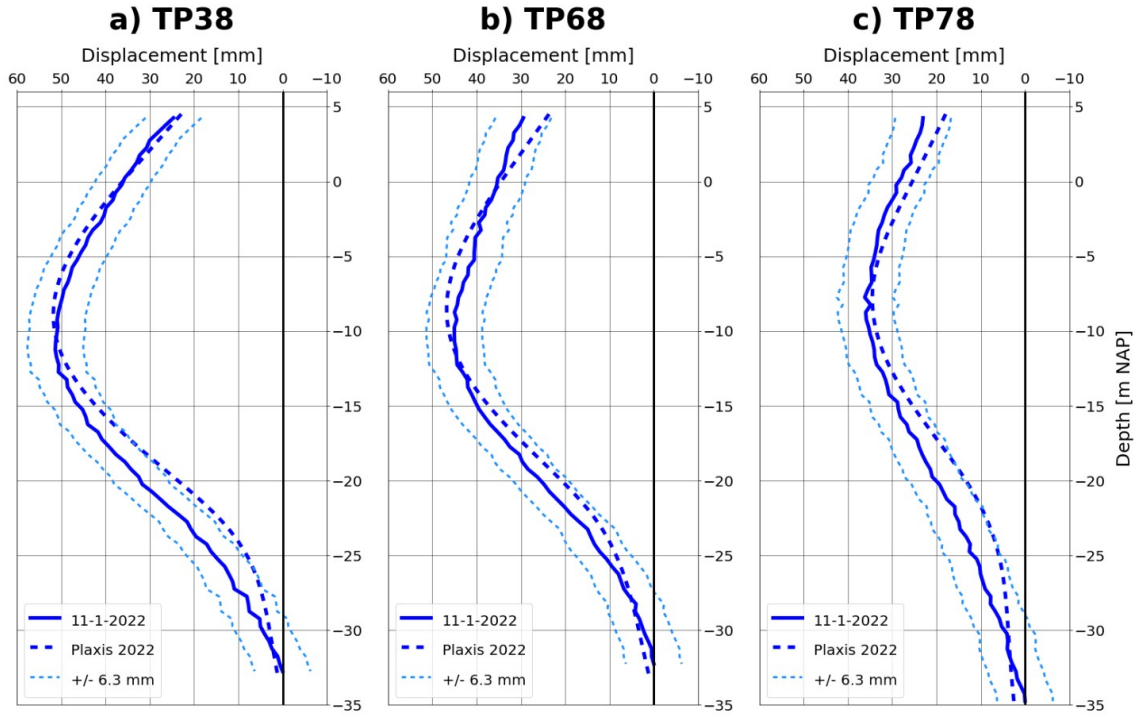

Figure F.5: Plaxis deformation results of all three piles

F.3. Bending moment, shear force and displacement in final stage

F.3.1. TP38

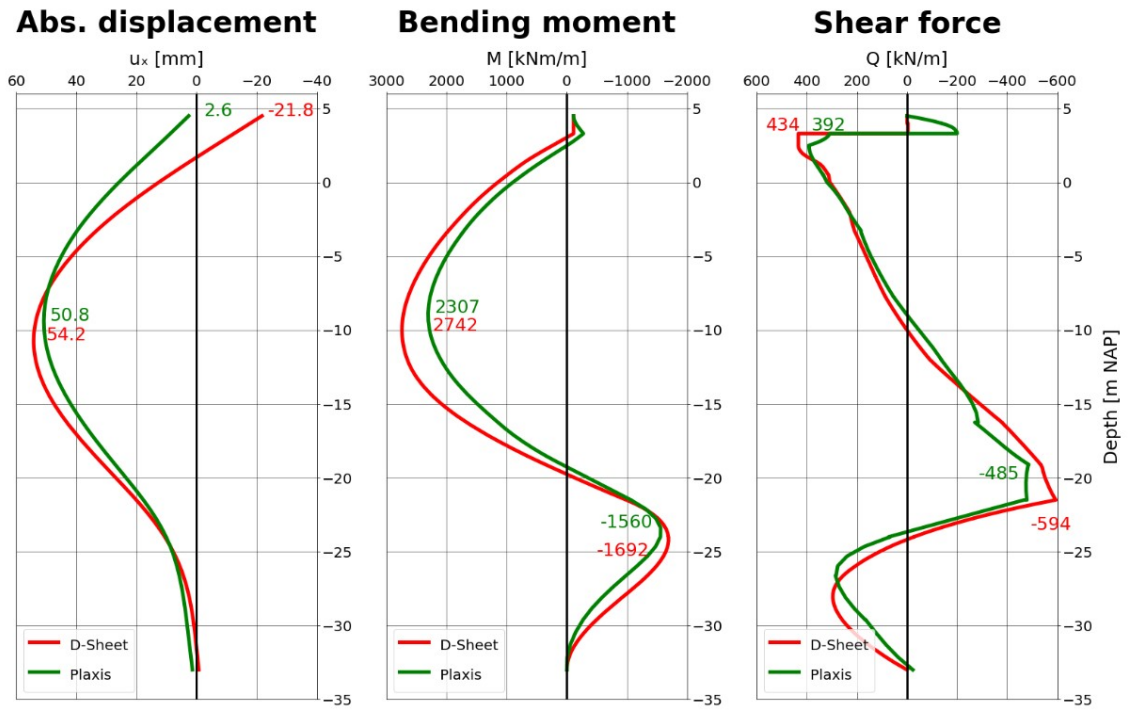

Figure F.6: Moment, Shear force and displacement graphs of TP38 in final stage. Displacement is the absolute displacement.

F.3.2. TP68

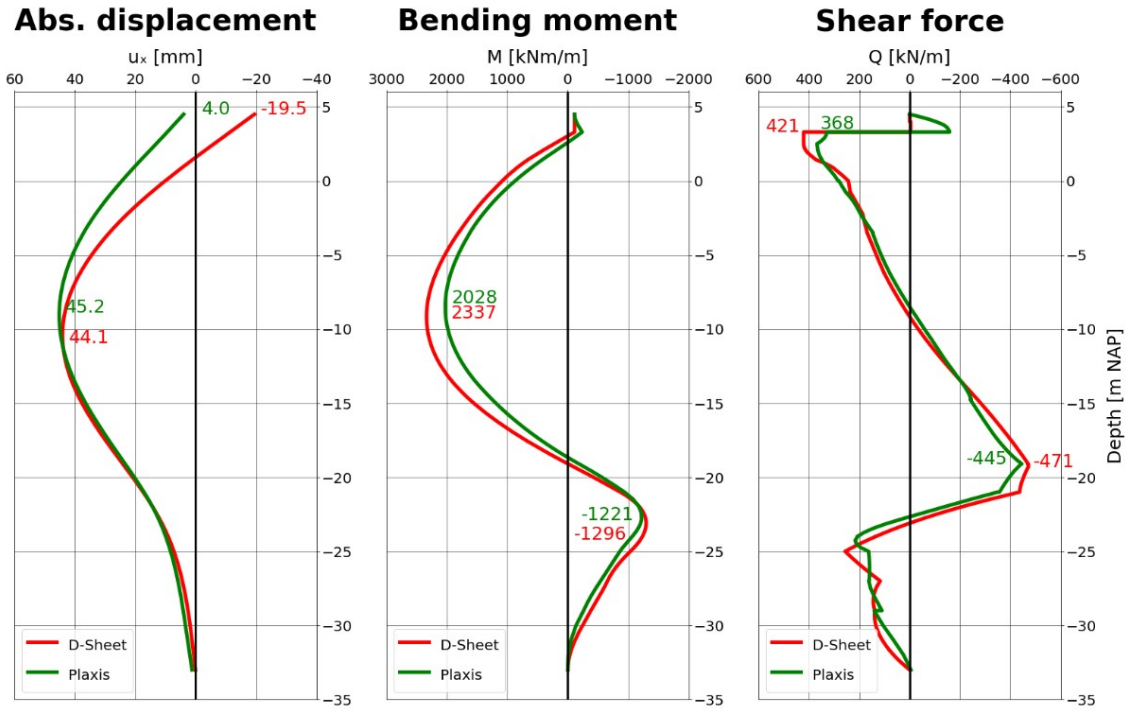

Figure F.7: Moment, Shear force and displacement graphs of TP68 in final stage. Displacement is the absolute displacement.

F.3.3. TP78

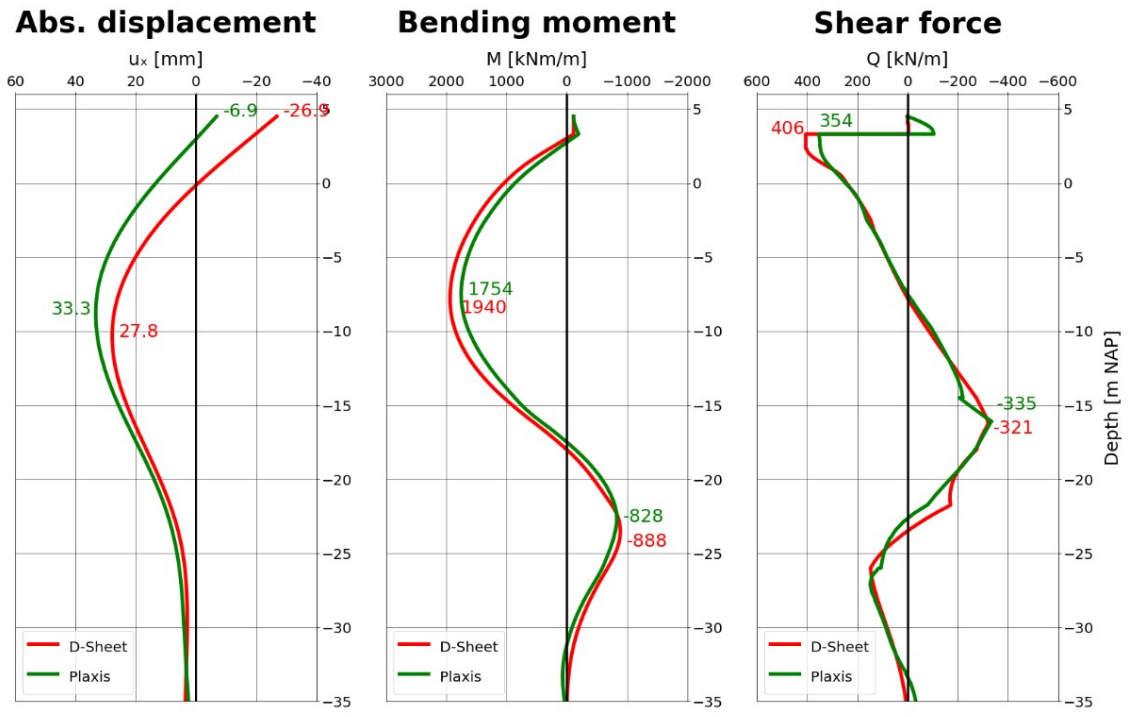

Figure F.8: Moment, Shear force and displacement graphs of TP78 in final stage. Displacement is the absolute displacement.

G

Results of sensitivity analysis

This appendix gives an overview of the results from the sensitivity analysis. Each result of one variation is given in a separate section with the numerical values in the first graph on the right. The values relative to the ones in the calibrated model are plotted in the right graph below. The displacement graph is shown on the left.

G.0.1. Variation in phasing

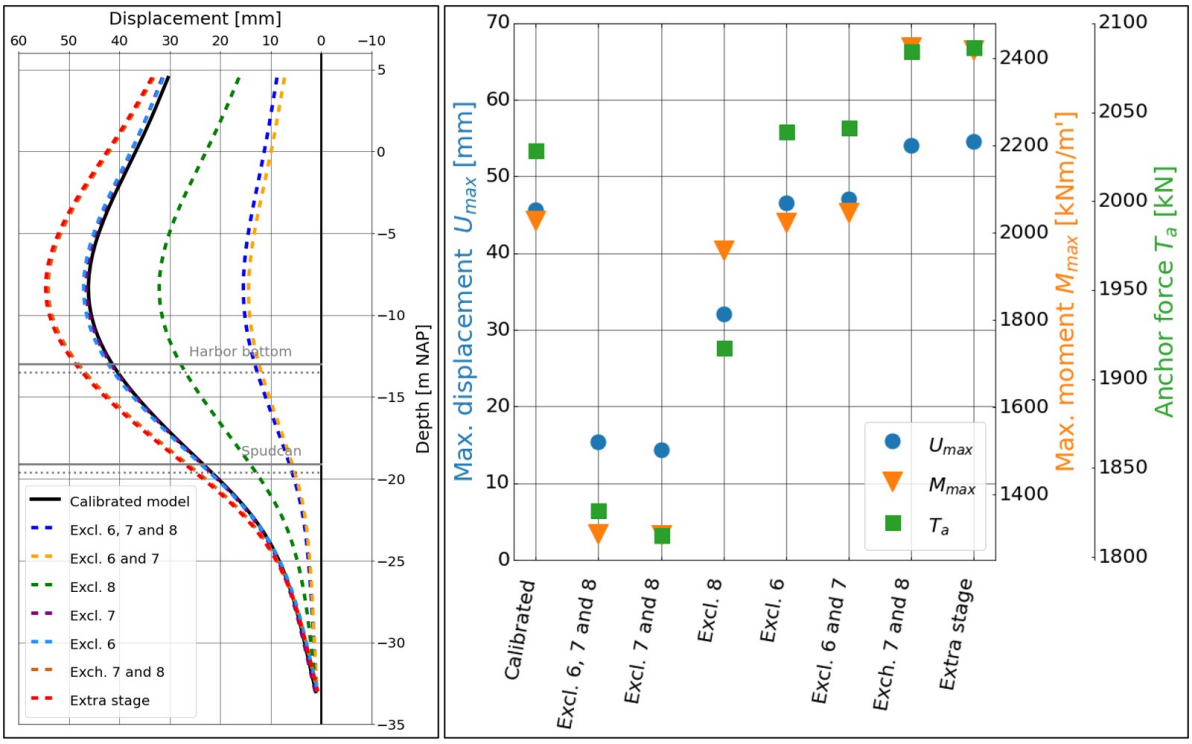

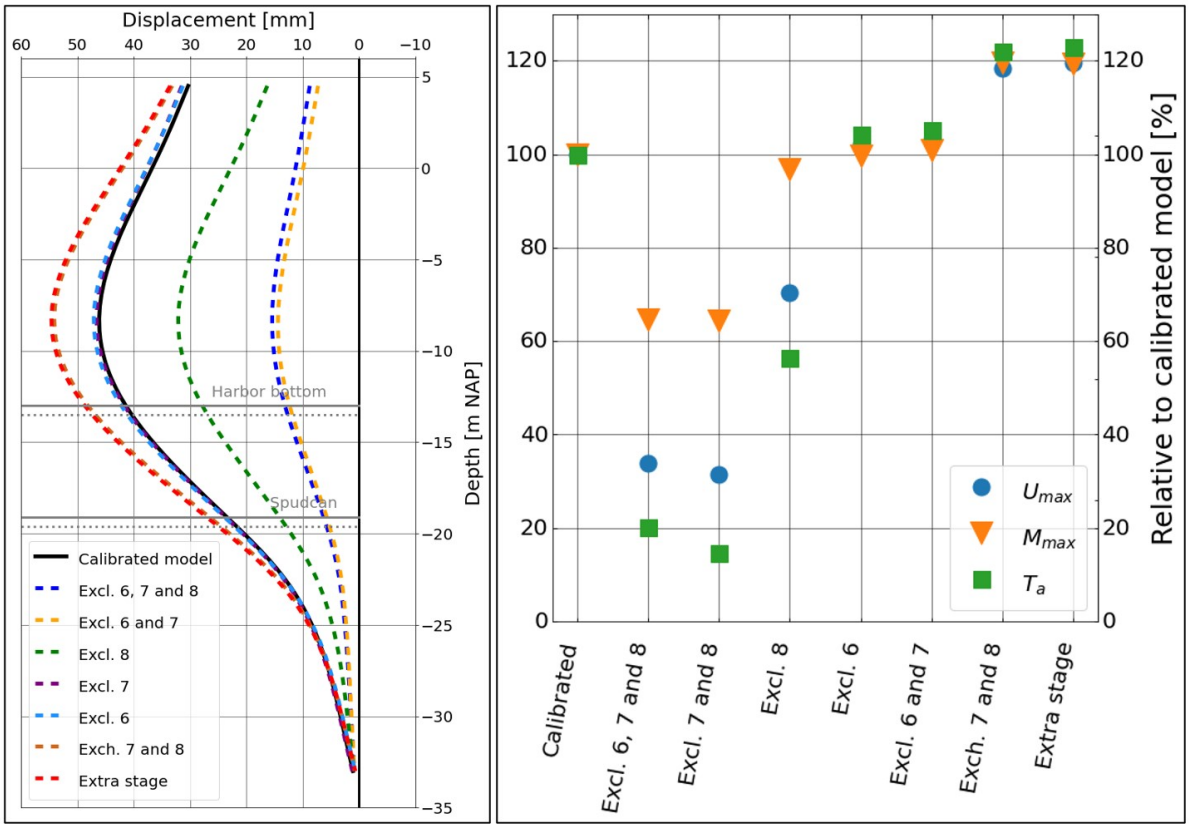

G.0.2. Variation in modelling bearing piles

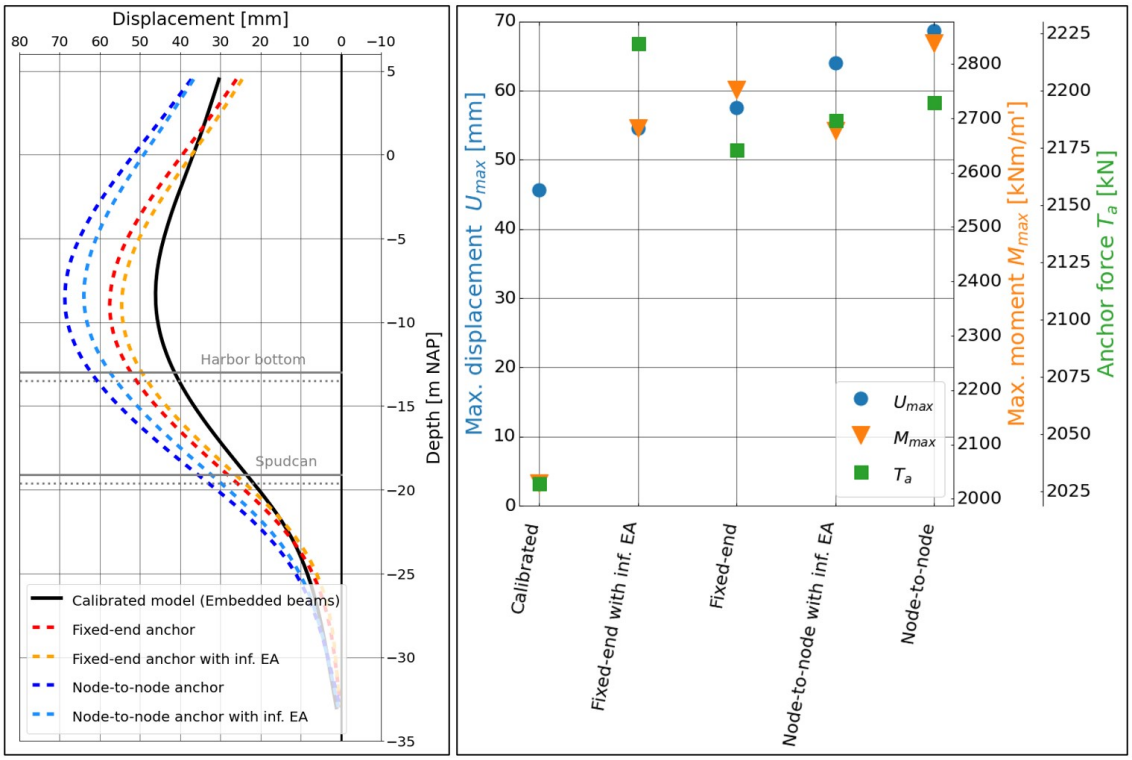

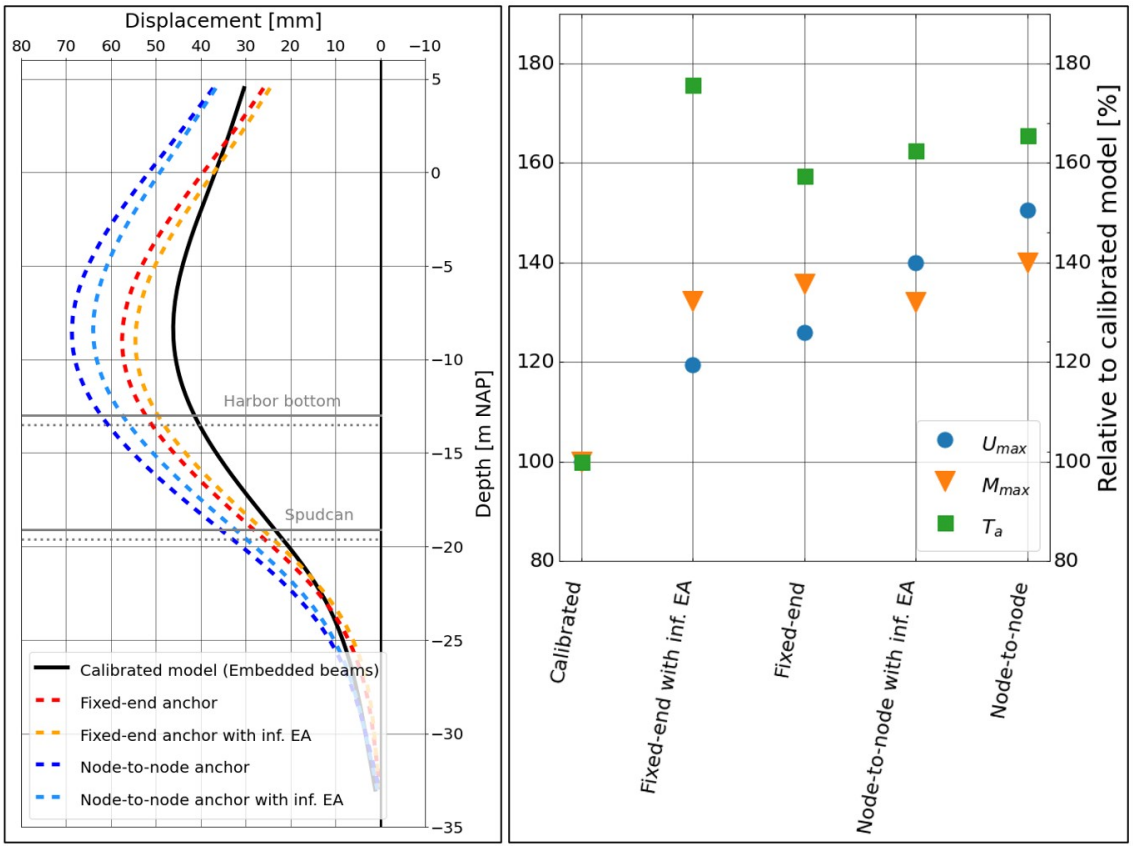

G.0.3. Variation of soil model

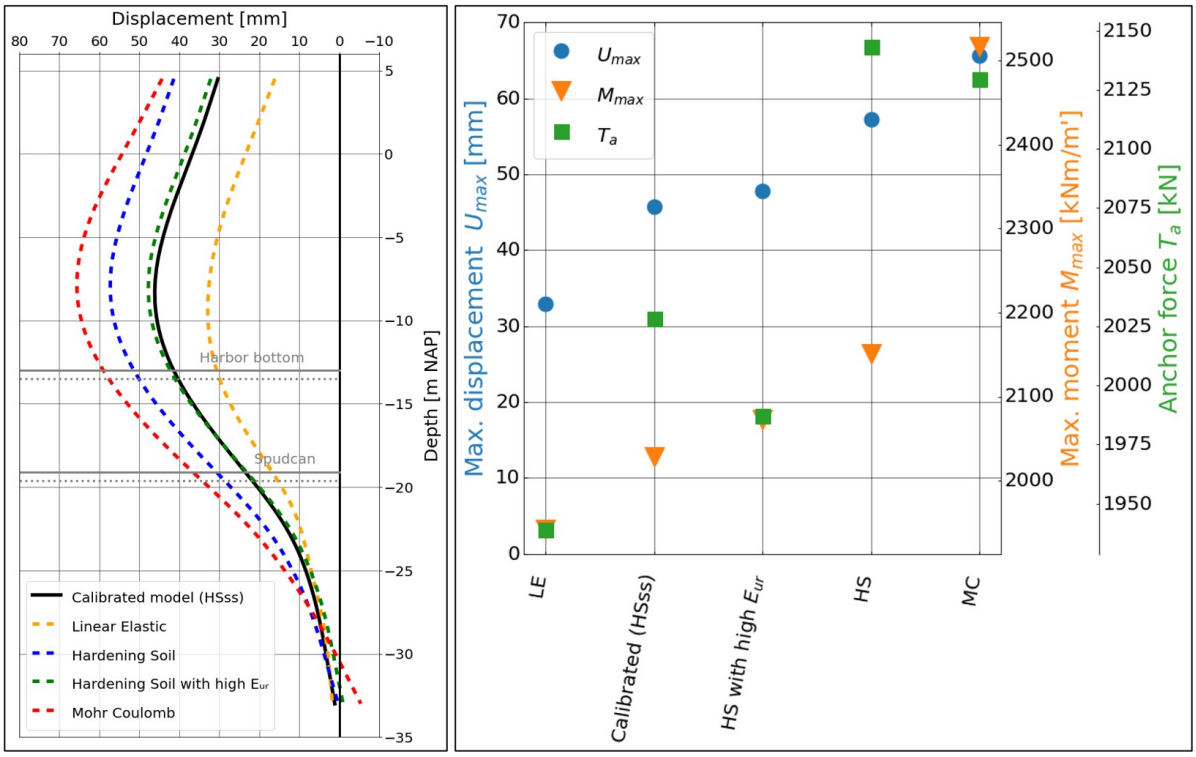

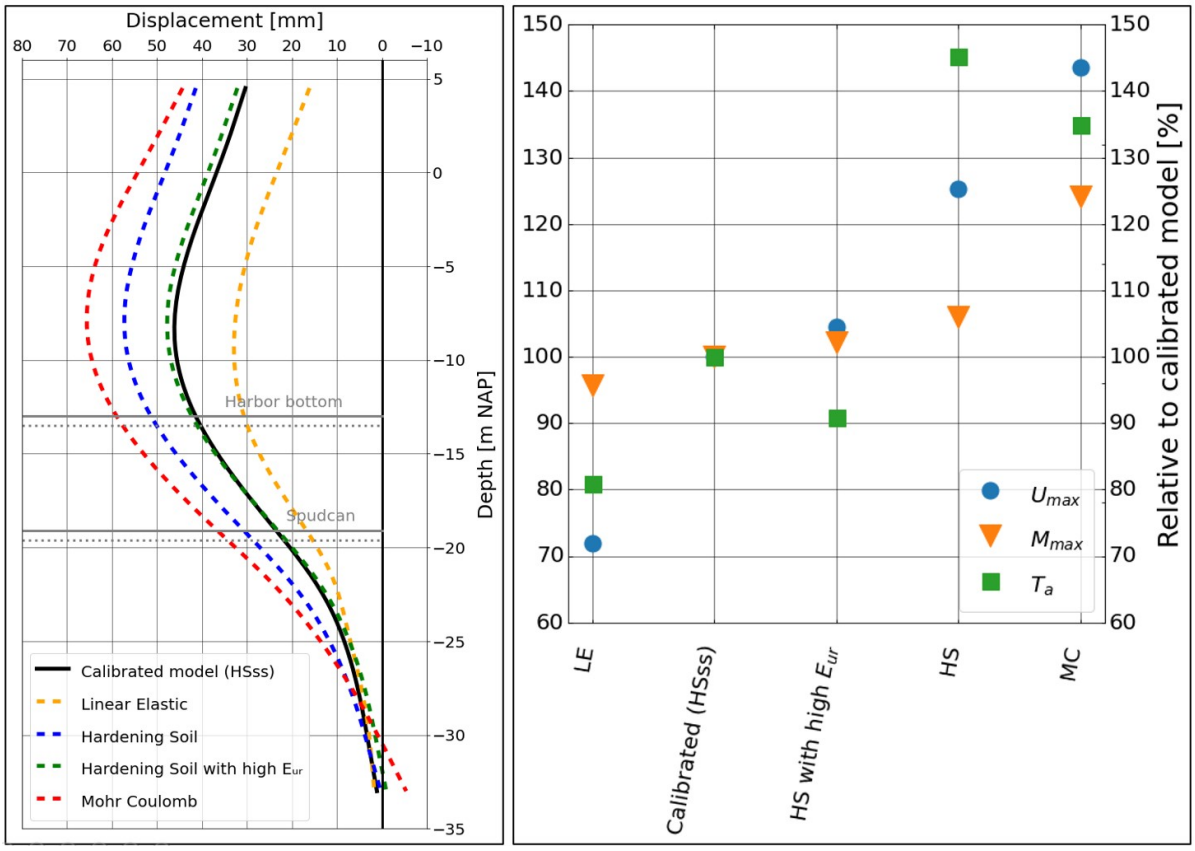

G.0.4. Variation of surcharge loads

The surcharge load is divided in a part acting on the relieving platform which is called Q. The part of surcharge behind the platform is acting directly on the soil and is called q.

Surcharge load Q on platform

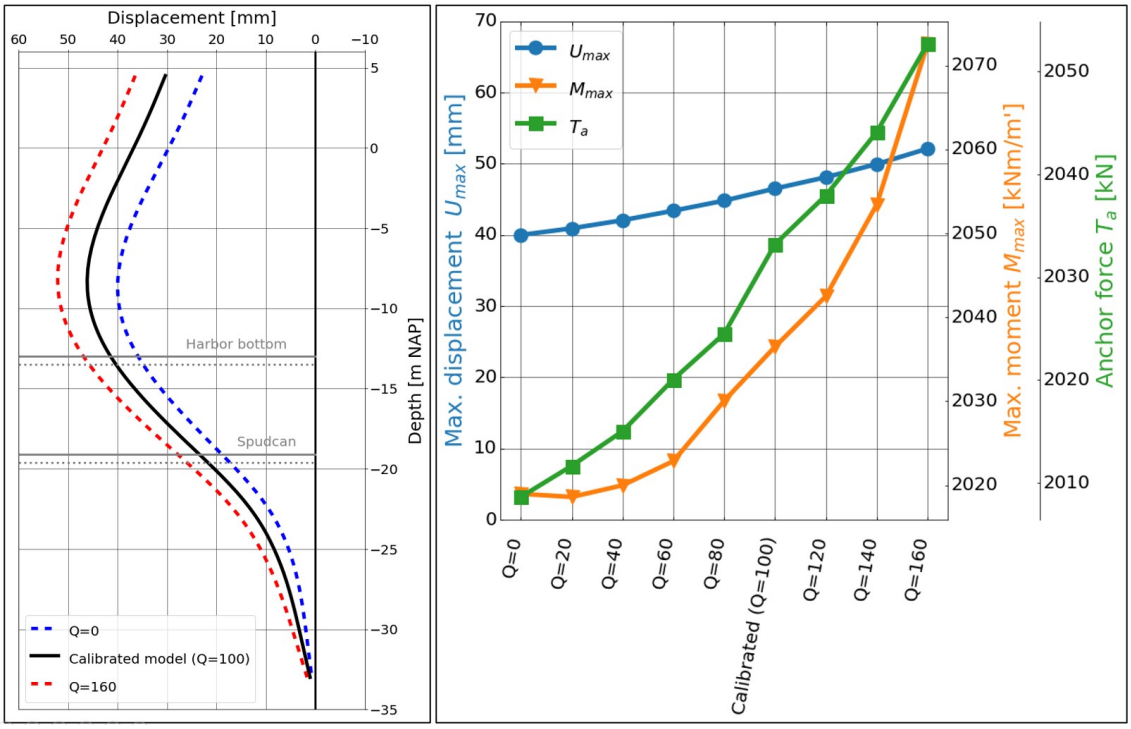

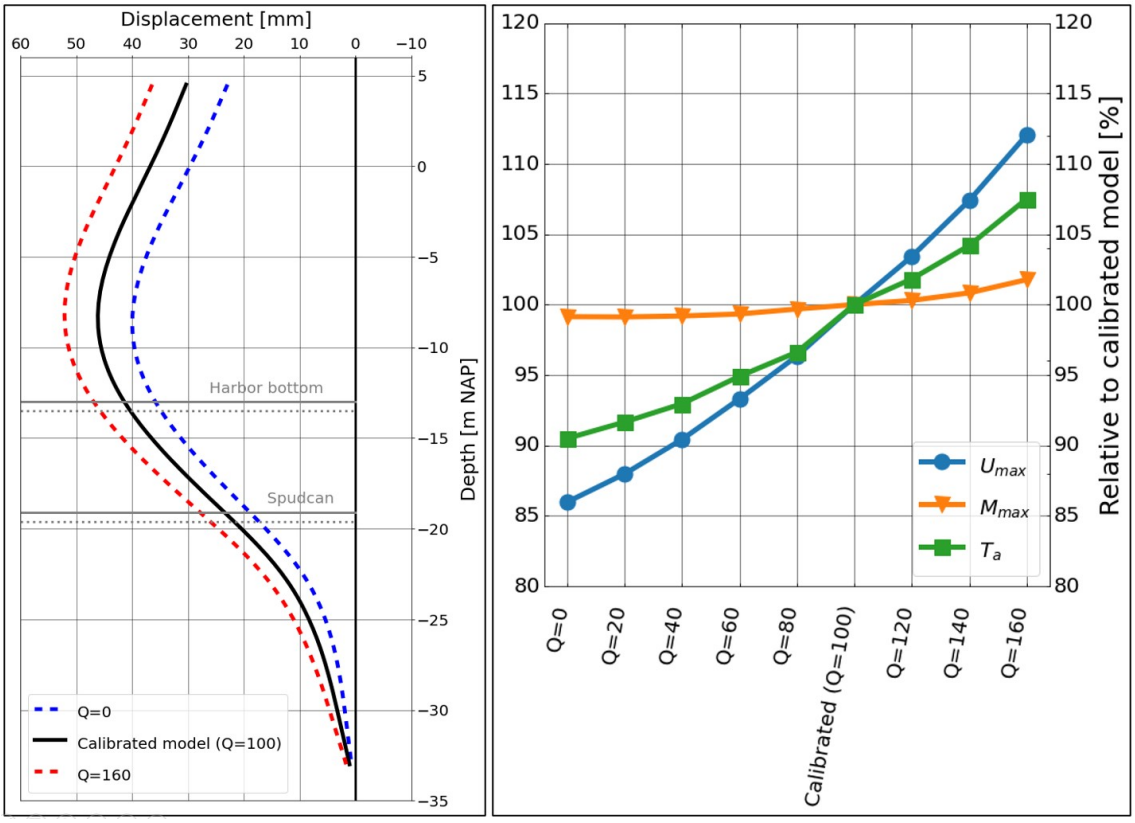

Surcharge load q behind platform